STUDY OF THE BASIS OF THE STRENGTH OF THE PULMONARY BLOOD-GAS BARRIER OF THE DOMESTIC FOWL, *Gallus gallus* variant *domesticus*

Sikiru Adekunle Jimoh

A thesis submitted to the Faculty of Science, University of the Witwatersrand, in fulfillment of the requirements for the degree

of

Doctor of Philosophy

Johannesburg, 2012

DECLARATION

I Sikiru Adekunle Jimoh declare that this thesis is my own work. It is being submitted for the degree of Doctor of Philosophy in the University of the Witwatersrand, Johannesburg. It has not been submitted before for any degree or examination at this or any other University

……day of …….2012

DEDICATION

In memory of my mother

Ramatallah Dufai

1943-1987

PUBLICATIONS AND PRESENTATIONS

Publication in a Journal:

Maina JN, Jimoh SA, Hosie M. Implicit mechanistic role of the collagen, smooth muscle, and elastic tissue components in strengthening the air and blood capillaries of the avian lung. Journal of Anatomy 2010; 217: 597-608.

Presentations at conferences:

10th Annual conference of the Anatomical Society of Nigeria 2010:

Jimoh SA, Hosie M, Maina JN. Implicit mechanistic role of the collagen-, smooth muscle, and elastic tissue components in strengthening the air- and the blood capillaries of the avian lung

39th Annual conference of the Anatomical Society of Southern Africa 2011:

Jimoh SA, Maina JN. Structural failure of the pulmonary blood-gas barrier at rest and during exercise in the lung of the domestic fowl, *Gallus gallus* variant *domesticus*

Jimoh SA, Maina JN. Demonstration of collagen connective tissues scaffold in the exchange tissue of the lung of the domestic fowl, *Gallus gallus* variant *domesticus*

“While knowledge defines all we currently know and understand, imagination points to all we might yet discover and create”.

ALBERT EINSTEIN

(*wisdomquotes.com*)

ABSTRACT

In spite of the extreme thinness of the avian pulmonary blood-gas barrier (PBGB), it is remarkably strong. To understand the basis of the remarkable strength of the avian PBGB, network of collagen connective tissue that form the lung's parabronchial fibrous framework and type-IV collagen, a principal component of the basement membrane was investigated in the BGB and in the epithelial-epithelial contacts between the air capillaries in the domestic fowl, *Gallus gallus* variant *domesticus*. Techniques of discriminatory staining, selective alkali digestion, vascular casting followed by alkali digestion and immunoelectron microscopy were used. Abundant collagen fibers of the interparabronchial septa, which form part of the tunica adventitia of the interparbronchial vessels, firmly interconnect adjacent parabronchi directly and indirectly (via intraparabronchial vessels). Peripherally, the intraparabronchial artery, with its tunic of collagen fibers, enters and penetrates the exchange tissue mantle. The collagen fibers around the vessel decrease in quantity as it divides into blood capillaries. From the luminal side, the projection of the parabronchial lumen into the exchange tissue mantle as the atria, the infundibulae and the air capillaries, in this order, carry collagen covering which reduces in quantity with each division. The three-dimensional interactions between blood capillaries from the peripheral part and air capillaries from the central lumen allow contact formation between blood capillaries, air capillaries and between air- and blood capillaries. Collagen fiber continuum starting from the interparabronchial septa runs through the exchange tissue by following the three contacts sites and terminates at the parabronchial lumen. At the periphery, the collagen fibers constitute a conspicuous bundle. Within the exchange tissue mantle, the collagen forms diffuse complex interconnections of thin fibers. Towards the parabronchial lumen and within interatrial septa, the thinner collagen fibers of the exchange

tissue mantle aggregate to form thick bundles which bind to the connective tissues surrounding the parabronchial muscles. Based on the structural arrangements and function of the smooth muscle, the collagen- and the elastic tissue fibers, and structures like the interparabronchial septa and their associated blood vessels, it was envisaged that: dynamic-tension and compressive forces exist in a parabronchus to form a tensegrity (tension integrity) system. The tensegrity arrangement imparts rigidity to a parabronchus while strengthening the air and the blood capillaries. Mechanical interdependence between parabronchi and between air- and blood capillaries allows efficient transmission and redistribution of tension. The tortuous course of the collagen fiber continuum that follows the three-dimensional intertwining of the gas exchange units- from septa to the lumen- ensures that tension does not travel a straight course and as such, any extrinsic or intrinsic force applied to the structure is transmitted away from the point of origin.

Graded exercise intensities and perfusion at different pressures on the integrity of the BGB were used to determine the condition under which the blood-gas barrier in the avian lungs fails. Number of red blood cells and protein concentration in the harvested lung lavage fluid were estimated in the exercised chickens. For histological analysis, numbers of epithelial-epithelial (E-E) breaks and blood-gas barrier (BGB) breaks were counted in each of the four vascular regions of the lung in both the exercised and the perfused lungs. Post exercise blood lactate analysis showed a 4-fold increase between rest and maximal exercise (2.95 m/s) while the numbers of red blood cells and protein concentration increased steadily with increasing exercise intensity, however, the degree of increments appeared to decrease at higher workloads. The two kinds of breaks occurred at all levels of exercise and in the resting birds

but at any exercise intensity, there were more E-E breaks than BGB breaks. The numbers of breaks increased with increasing exercise intensity and the difference between the two types of breaks decreased with increasing exercise intensity. In resting birds, there were no breaks in the area of the lung supplied by the cranial branch of the PA. In the exercised birds, differences in number of blood-gas barrier breaks among the four vascular territories only occurred at 0.66 m/s where the lowest and highest counts occurred in the cranial- and caudomedial regions respectively, whereas at all other levels of exercise, the numbers of breaks were comparable. Presence of red blood cells in the lungs of resting birds indicated that failure of the blood-gas barrier might be a common but inconsequential event in the avian lung. A positive linear relationship exists between the perfusion pressure and the numbers of both E-E and blood-gas barrier breaks. At all perfusion pressures, there are more E-E breaks than BGB breaks. The difference between the two types of breaks decreased with increasing pressure. At any perfusion pressure, more breaks occurred in the regions supplied by the accessory- and caudomedial branches of the PA than in the regions supplied by the cranial- and the caudomedial ones. This could be because the pressures in the two blood vessels may be higher since the caudomedial branch is the most direct continuation of the PA while the accessory branch is the narrowest and the first to originate from the PA. Because of the extreme thinness of the blood-gas barrier and unavoidable puncturing of air sac when the thorax is accessed to cannulate the pulmonary vessels, the exact pressure at which the BGB fails could not be ascertained since both types of failure occurred at all perfusion pressures. However, separation of the epithelial-epithelial contacts, caused by distension of the blood capillaries, started appearing at the perfusion pressure of 2.89kPa. This may represent the pressure at which the blood-gas barrier starts to fail.

ACKNOWLEDGEMENTS

This doctoral thesis would not have been successful without the help and support of kind people around me. It is possible to mention only a few here.

First and foremost, I offer my sincerest gratitude to my supervisor, Professor JN Maina. Your steadfast, thorough and consistent guidance whilst allowing room for my self-evolution throughout the period of the study is deeply appreciated.

I was assisted over the years in the various laboratories in running different equipments and getting acquainted with different techniques. I am especially grateful to all the technical staff of the School of Anatomical Sciences, the University of Witwatersrand. I am equally grateful to Mr. Chris van der Merwe of University of Pretoria for sacrificing his time to assist with scanning electron microscopy.

I am most grateful to Dr. Virginia Meskenaite for giving her precious time to teach me the techniques of immune-electron microscopy, even during weekends.

I would like to thank all the staff of the Central Animal Service (CAS) Unit of the University of the Witwatersrand for their tolerance and the friendship. These include Dr. Leith, Patrick Selahle, Mary Ann, Loraine, Amelia, Keshne and all others - you are a family to me!

My stay in South Africa would have been a hell on earth save the generous friends who were always willing to help. Mooi, you are a wonderful person. Dr. Olatayo Oladejo, you

are a God send. There is nothing I can offer to repay your kind generosities but to you all, I am most indebted.

I am heartily thankful for the loving encouragements that never cease to rain on me from my lovely wife, a gentle heart in a beautiful body, Dr. Bolarinwa Azeezah Modupeola.

I thank my father, Mr. Ajibaye Jimoh Ajani, and my siblings for supporting me throughout my stay in South Africa

Finally, I offer my most sincere gratitude to all of those that I have not mentioned who supported and encouraged me during the course of this research.

Sikiru Adekunle

Johannesburg

2012

TABLE OF CONTENT

TABLE OF FIGURES

LIST OF TABLES

CHAPTER I

1. INTRODUCTION

1.1 PULMONARY STRUCTURAL AND FUNCTIONAL CHALLENGES

Mammals and birds are the only two extant groups/taxa of vertebrates capable of sustained high oxygen consumption (e.g. Schmidt-Nielsen, 1972; Taylor *et al*., 1982; Ellerby *et al*., 2003). Higher oxygen demand obligated complex lungs with smaller gas exchange units (e.g. Powell and Hopkins, 2004) and extremely thin blood-gas (tissue) barrier (BGB) (e.g. Dubach, 1981; Gehr *et al.,* 1981; Maina, 1998). Smaller gas exchange units achieved through intense partitioning of the exchange tissues offer greater respiratory surface area (Maina, 2000a) while thinness of the BGB increases the diffusing capacity of the lung for oxygen (Maina, 1998). Combination of large surface area and extreme thinness of pulmonary BGB promote the transfer of respiratory gases by passive diffusion (e.g. Tenney and Remmers, 1963; Maina and West, 2005) optimizing respiratory performance (e.g. Gehr *et al.*, 1978; Maina and West, 2005). However, the need for extreme thinness and expansive surface area for higher gas exchange efficiency impose a challenge of maintaining the structural integrity of a well-perfused lung (Maina and West, 2005). Several studies (e.g. Schoene *et al.,* 1986; Tsukimoto *et al*., 1991; West *et al*., 1991; Birks *et al*., 1994) have shown that respiratory mechanics continuously challenge the integrity of the extremely thin pulmonary BGB. Large fluctuations in the pulmonary intramural pressures between rest and different levels of activities as well as presence of surface tension that exists at the air-tissue interface (e.g. Tsukimoto *et al*., 1991; West *et al*., 1991) are the foremost challenges that threaten the mechanical integrity of the BGB. Additionally, pulmonary capillaries, unlike those of the other organs, are not supported by surrounding tissues (e.g. Weibel, 1984); rather, they are suspended in air: the weight of the blood contained in the lung is borne by the BGB (Fig. 1.1).

There is evidence that the continuous basement membrane that is sandwiched between the endothelial- and the epithelial- cells is responsible for the strength of the BGB (e.g. Williamson *et al*., 1971; Welling and Grantham, 1972; Swayne *et al*. 1989). Specifically, rather than the entire thickness of the basement membrane, only the 50 nm thin lamina densa, located between the lamina rara interna and the lamina rara externa and compose mainly of type-IV collagen, is responsible for the strength of the BGB (Crouch *et al*., 1997; West and Mathieu-Costello, 1999). Type-IV collagen is a unique basement membrane type: it belongs to a protein family of triple helical isoforms that form two-dimensional planar network of fibers (e.g. Hudson *et al.*, 1993). Because of the functional significance of the BGB, questions concerning the basis of its strength, why, when and how it fails under extreme conditions of exercise and pathologies (e.g. emphysema) are important to morphologists, physiologists, and clinicians.

Figure 1. 1: Challenges imposed by pulmonary function on the mechanical integrity of the blood-gas barrier

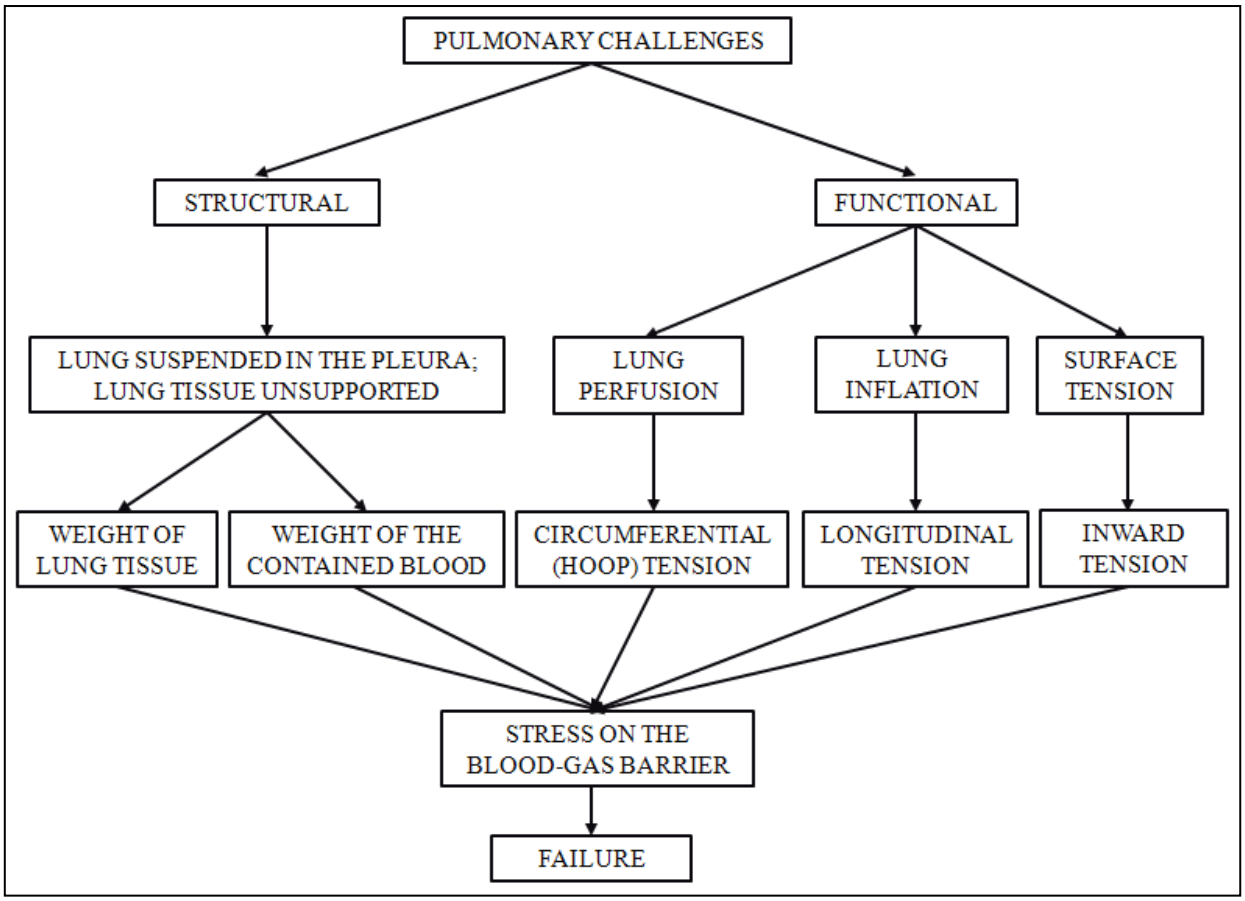

1.2 **OVERCOMING PULMONARY STRUCTURAL AND FUNCTIONAL CHALLENGES – STRATEGIES**

The unique structural design imposed by respiratory functional demands necessitates that the pulmonary BGB meets various conflicting requirements (West and Mathieu-Costello, 1999; West, 2000a; Maina and West, 2005): the BGB must be exceptionally thin over a large operating surface area and must be extraordinarily strong to maintain integrity at all physiological levels (Maina and West, 2005). In the air-breathing vertebrates, the BGB must be strong because the barrier separates two media of different densities – air and blood. Furthermore, the media exist at different pressures that subject the BGB to differences in tension on both sides. The denser blood in its compartment pushes the barrier because of greater and changing intramural pressure when the capillary pressure rises, e.g., during intense activity (Birks *et al*., 1994; West and Mathieu-Costello, 1995, 1999; West, 2000a, b). In fish gills, there is significant connective tissue between endothelial and epithelial cells of the water-blood barrier (e.g. Hughes, 1966; Hughes, 1978): pillar cells containing abundant intracytoplasmic microfibrillar elements (Hughes and Grimstone, 1965; Bettex-Galland and Hughes, 1973; Smith and Chamley-Campbell, 1981) and two parallel sheets of epithelial cells (Hughes and Wright, 1970) contribute to maintaining the integrity of the water-blood barrier. Thick septa in the lungs of lungfishes and amphibians (e.g. Meban, 1980) strengthen the barrier. In the mammalian lung, the BGB is structurally and functionally divisible into two parts - the thick and the thin side (e.g. Gehr *et al*., 1978; Weibel, 1984; West and Mathieu-Costello, 1999). The thin side, with a thickness of only 0.2-0.3μm and covering about half of the alveolar surface area (Gehr *et al*., 1978), serves the role of gas exchange. In human beings the thick side of the BGB, about 1μm or more in thickness, contains type- I collagen and

interstitial cells (Weibel, 1984; Weibel, 2009) which strengthen and give support to the exchange tissue (parenchyma). However, in the avian lung, the pulmonary BGB is uniformly thin (e.g. Maina and King, 1982; Maina *et al*., 1989; Maina and West, 2005; Watson *et al*., 2007): it lacks the 'strong' supporting thick side found in the mammalian BGB (Maina and West, 2005; Maina, 2005; Maina, 2007a). The avian BGB is 56-67% thinner than the thin side of the mammalian BGB (Maina *et al.,* 1989) and the harmonic mean thickness is thirty times smaller than in a mammal of comparable body mass (Gehr *et al*., 1981). The basement membrane, reported to be responsible for the strength of the BGB (e.g. Maina and West, 2005), is even thinner in the avian BGB (e.g. Maina and King, 1982; Watson *et al*., 2008). For example, the harmonic mean thickness of the BGB in a non-flying vertebrate like Etruscan shrew, *Suncus etruscus*, with a body mass (BM) of 0.02 kg is 0.340 µm (Gehr *et al.*, 1981) and in naked mole rat, *Heterocephalus glaber* (BM, 0.031 kg) is 0.243 µm (Maina *et al.,* 1992). In birds of comparable body-mass, e.g., the Klaa's cuckoo, *Chrysococcyx klaas* (BM, 0.027 kg) (Maina, 1989; Maina *et al.,* 1989) and the house sparrow, *Passer domesticus* (BM, 0.026 kg) (Maina, 1984, 1989; Maina *et al.,* 1989), the harmonic mean thickness of the BGB is only 0.157 µm and 0.096 µm, respectively.

The deceptively weak avian BGB functionally withstands blood delivered at apparently higher pressure (e.g. Seymour and Blaylock, 2000) by evidently relatively larger and more powerful hearts (Hartman, 1955; Berger and Hart, 1974) than that of mammals. For example, a bird like the turkey, *Meleagris gallopavo*, with a BM of 4.77 kg has a higher systolic blood pressure of 19.95 kPa (149.6 mmHg) compared to 12.64 kPa (94.8 mmHg) in a mammal like the cynomologus monkey, *Macaca fascularis*, with a BM of 4.60 kg (Seymour and Blaylock, 2000). Based on thickness, it is generally assumed that the more vulnerable part of the

mammalian BGB is the thin side (Maina and West, 2005) while the thick side, which accommodates type- I collagen fibers (e.g. Weibel, 1984, 2009), is assumed to be stronger. If the structural elements of the BGB provide equal strength for a given thickness irrespective of species, then the mechanical strength will depend on the particular structural characteristics of the BGB (Birks *et al.*, 1994). It has been reported that failure of the BGB occurs in lungs of animals with thicker interstitium under intense activity (West *et al*., 1993) despite presence of supporting and contractile elements such as collagen, elastic tissue, smooth muscle, and fibroblast (e.g. Weibel, 1984; Maina 2005). The extremely thin avian BGB (e.g. Maina and King, 1982; Maina *et al*., 1989; Maina and West, 2005) is reported to be remarkably strong. About three decades ago, Macklem *et al*. (1979) observed that air capillaries in the parabronchial lung of a duck did not collapse after applying a positive pressure of 20 cm H_2O (~2 kPa = 15 mmHg) on it. Half a decade later, Powell *et al*. (1985) reported that avian pulmonary blood capillaries behave like a rigid tube: the vascular resistance remained unchanged when blood flow to one of the lungs was doubled. Resistance of the blood capillaries to distension and the unyielding of the air capillaries from compression have been corroborated by other investigators (e.g. Wideman, 2001; West *et al*., 2006, 2007a; Wideman *et al*., 2007; Watson *et al*., 2007). Taking into account the large respiratory surface area (e.g. Maina, 2000a, b), high systolic pressure (e.g. Seymour and Blaylock, 2000) and the highly energetically demanding lifestyle (flight) that birds generally lead (e.g. Tucker, 1972a, b), the BGB of the avian lung is exceptionally strong. However, the basis of the strength of the apparently structurally fragile avian BGB remains unclear.

1.3 THE DESIGN OF THE AVIAN BLOOD-GAS BARRIER: THE PARADOX - DECEPTIVELY FRAGILE, REMARKABLY STRONG

During the last decade, there has been upsurge of investigations aimed at explaining the basis of the remarkable strength of the avian lung and that of the terminal respiratory units – the air- and the blood capillaries (e.g. Scheuermann *et al*., 1997; Klika *et al*., 1997; Maina 2007a, b; West, 2009; West *et al*., 2006, 2007a; Watson *et al*., 2007, 2008). The basis of the strength of the avian gas exchanger, however, remains unclear and controversial (see Maina, 2005, 2008 for reviews). The different ideas that have been put forward to explain the strength of the avian BGB can be grouped into two - *structural* and *mechanistic* ones. Investigators holding *structural view* look for demonstrable structural component(s)/features to explain the remarkable strength. For instance, Scheuermann *et al*. (1997) assumed that the lipoproteinaceous trilaminar substance and pairs of epithelial cell processes (retinacula) strengthen and support the air capillaries; Klika *et al*. (1997) opined that the presence of lipoproteinaceous trilaminar substance between blood capillaries and within the squamous epithelial cell, which form a three dimensional web-like system, serves to anchor and support the air- and the blood-capillaries; West *et al*. (2006) suggested that the close packing of the air capillaries around the blood capillaries in a 'honeycomb-like arrangement' provide mechanical "rigidity"; and West *et al*. (2007a), Watson *et al*. (2007, 2008), and West (2009), envisaged that the strength is provided by the presence of back to back plates of epithelial bridges ('struts') that bridge (connect) two blood capillaries. On the other hand, the *mechanistic* view advanced by Maina (2007a, b) asserted that shape and strength of the air- and blood capillaries and indeed the entire avian lung are imparted by finitely continuous tensional and compressional adjustments between the integral elements of the system. In such assemblages, he argued that structural components form an integrated hierarchical network of tension and

compression that dissipate tension. In Maina *et al.* (2010), an integrated system of collagen fibers (tension components) was shown to connect the presumably rigid central and peripheral parts (compressional components) of a parabronchus, forming what was presumed to be a tensegrity state.

The structural and/or mechanistic factors that strengthen the avian pulmonary BGB, (Maina and King, 1982; Klika *et al.*, 1997; Scheuermann *et al*., 1997; Watson *et al*., 2007) are not mutually exclusive. Experimental data abound on the strength and the basis of the strength of the mammalian BGB of the mammalian lung (e.g. West *et al.*, 1991, 1993; West and Mathieu-Costello, 1992) but corresponding data on the BGB of the avian lung is scanty. Here, on the domestic fowl, *Gallus gallus* variant *domesticus*, a network of collagen connective tissue fibers that form the lung's parabronchial skeletal framework and type-IV collagen, a principal component of the basement membrane (Crouch *et al*., 1997) was investigated in the BGB and in the epithelial-epithelial contacts between the air capillaries. The effects of graded exercise intensities and perfusion at different pressures on the integrity of the BGB were experimentally assessed to determine the condition under which the barrier fails.

1.4 STRUCTURE AND FUNCTION OF THE LUNG-AIR SAC SYSTEM OF BIRDS

The complex design of the avian respiratory system is not a prerequisite for flight (e.g. Farmer, 2006; Maina, 2000a). Bats, the only other extant vertebrate group capable of powered flight, use a fundamentally mammalian respiratory system (Yalden and Morris, 1975) though a highly specialized one (e.g. Maina and Nicholson, 1982; Maina and King, 1984; Maina, 1986). Flight is a highly metabolically demanding form of locomotion (e.g. Pennycuick, 1972;

Tucker, 1972a, b; Berger and Hart, 1974; Carpenter, 1975; Thomas, 1975). It is the unique avian pulmonary morphology with its exceptional functional efficiency (e.g. Schmidt-Nielsen, 1975; Scheid, 1979; Maina, 1996) that has enables birds to fly nonstop for hours (e.g. Berger, 1961; Lasiewski, 1962) at high altitude (e.g. Laybourne, 1974; Richardson, 1976; Elkins, 1983) even without acclimatization, (e.g. Swan, 1961, 1970; Black *et al*., 1978; Black and Tenney, 1980). At high altitude, birds breathe in hypoxic- (e.g. West, 1983), hypothermic- (e.g. Torre-Bueno, 1985), hypobaric- (e.g. Swan, 1961; Laybourne, 1974) desiccating air. During a controlled dive on a prey, a speed of 403 km h^{-1} has been reported for falcons (Tucker, 1998) and during their annual migration, some hummingbirds (Lasiewski, 1962) and the Arctic tern, *Sterna paradise pontoppidan* (Salomonsen, 1967) are reported to cover huge distances. All these remarkable achievements have attracted and sustained fascination and interest in the forms and functions of birds and specifically their respiratory system (e.g. Maina, 2005). The ease of escape from terrestrial (earth-bound) predators and opportunity to secure vast food resources with little competition very likely imposed on the primitive theropod dinosaurs enough selective survival pressure for development of powered flight (Welty, 1982; Farmer, 2006). Evolution of flight as means of locomotion has compelled major modifications in virtually all organ systems in birds (Maina, 2000a), especially the respiratory system. In the lung-air sac system, the gas exchanger is completely separated from the ventilator (Maina, 2005). The lung which is compact and inexpansible (Jones *et al.,* 1985) is ventilated unidirectionally and continuously by coordinated bellows-like action of the air sacs (Scheid, 1979). Because the lung is firmly attached to the body wall (e.g. Duncker, 1971; McLelland, 1989) and compliance of the lung has been relegated to the air sacs (Jones *et al.,* 1985), strict limitation is not imposed on the ultimate size of the air capillaries by surface tension force. Thus, the air capillaries are extremely small, 3-20 µm in diameter (e.g. Duncker,

1972; Maina and Nathaniel, 2001; Woodward and Maina, 2008) compared to more than 50 µm alveolar diameter of the mammalian lung (Tenney and Remmers, 1963; Weibel, 1963; Ochs *et al*., 2004). Confounding structural complexity and exceptional functional efficiency lead Peter Scheid (1990) to remark, "It cannot yet be decided whether the complexity of the avian lung evolved out of functional needs or simply out of structural constraints with no significance for the higher efficiency". However, Farmer (2006) thought the separation of the exchanger from the ventilator was a prescription for major body reorganization necessary for evolution of flight: air sacs were selected for flight because they enhanced balance and agility. On the other hand, Figueroa *et al*. (2007) thought that energetic requirements of flight as a means of locomotion compelled the adaptation that lead to development of novel avian pulmonary morphometric parameters.

1.4.1 Functional design of the lung-air sac system

Powered flight is an exceptionally highly energetically expensive mode of locomotion (Pennycuick, 1972; Tucker, 1972a, b; Berger and Hart, 1974; Carpenter, 1975; Thomas, 1975). The aerodynamic and energetic demands for flight are so extreme that only four groups of animals have ever evolved it: these are insects, the now extinct pterosaurs, birds, and bats, chronologically in that order. Flight as a single adaptive feature has compelled major modifications in birds and bats. For example, the chiropteran (bat) respiratory system, which is structurally mammalian (Maina, 1985), is remarkably highly morphometrically refined (Maina and Nicholson, 1982; Maina and King, 1984; Maina, 1986, Maina *et al.*, 1991). The highly metabolically demanding lifestyle adopted by the class aves has resulted in a unique and more specialized pulmonary system characterized by the following features:

a. The gas exchanger is completely *separated* from the ventilator (Maina, 2005)
b. *Minutialization* of the air capillaries (Maina, 2007a) - a determinant of surface area per unit volume of parenchyma and a measure of degree of partitioning of the gas exchange tissue hence the sizes of the terminal gas exchange units (Maina, 2000a, b). Among the air breathers, the degree of partitioning increases from simple sac like structures (ediculae and faveoli) in amphibians and reptiles (Perry, 1989) to complex branching structures in the bronchioalveolar lungs of mammals and the parabronchial lungs of birds (Duncker, 1978; Piiper and Scheid, 1999; Powell and Hopkins, 2004).
c. Extreme *attenuation* of the pulmonary BGB gives rise to a higher diffusing capacity of the lung for oxygen (Maina, 1998). Animals with higher metabolic rates and greater oxygen demands have thinner BGB (e.g. Dubach, 1981; Gehr *et al.*, 1981).
d. *Multicapillary serial arterialization* arrangement of the blood capillaries relative to the parabronchial lengths maximizes oxygen extraction in the gas exchange tissues (Abdalla and King, 1976a). The design is so efficient that under some conditions the partial pressure of oxygen (PO_2) in the arterial blood exceeds that in the expired air (Lasiewski and Calder, 1971; Scheid and Piiper, 1972; Bernstein and Schmidt-Nielsen, 1974). and
e. *Large heart with a huge cardiac output* (Hartman, 1955; Snyder, 1976; Jurgens *et al.*, 1981) delivers more blood to the lungs.

1.4.2. The lung

The avian lung is small, compact, and about a flattened quadrilateral in longitudinal profile, and is wedge-shaped in cross section (e.g. McLelland, 1989). It has three surfaces (coastal,

vertebral and septal) which are separated by five borders (coastovertebral, coastoseptal, vertebroseptal, cranial and caudal) (e.g. King and Molony, 1971; McLelland, 1989; Maina, 2005). Air passages are visible on most of the surfaces. On the coastal surface, which is in contact with the ribs, small transparent areas largely representing parabronchi with missing exchange tissue of the outer walls are visible (e.g. King and Cowie, 1969). The septal surface is covered by the horizontal septum and scattered on this surface are openings (ostia) that connect the bronchi to the air sacs (King and Molony, 1971; McLelland, 1989; Maina, 2005). The vertebral surface is related to the cranial aspect of the thoracic wall where it fits snugly in the paravertebral gutters and deeply embedded in the vertebral ribs. One-fifth to one third of the dorsal part of the lung is tucked between the ribs (King and Molony, 1971). The lungs are not divided into lobes but carry six deep impressions (coastal sulci) made by the vertebral ribs (King, 1966; King and Molony, 1971). Craniocaudally, the lung extends from the first cervical rib to the cranial margin of the ilium (Maina, 2005). Ventrally, the lung, at its thickest portion (junction between cranial and middle thirds), extends almost as far as the level of the joints between the second and third vertebral and sternal ribs (King and Molony, 1971; McLelland, 1989; Maina, 2005).

1.4.3 The airways

The regular pattern of dichotomous branching bronchial system characteristic of mammalian lungs (Weibel, 1984; Maina and van Gils, 2001) is completely absent in the avian lung. The bronchial system in the bird lung shows extensive anastomoses and extrapulmonary extensions which connect to the air sacs (e.g. McLelland, 1989, Maina, 2005). The trachea

bifurcates at the syrinx to give rise to the two primary bronchi, one to each lung. The two bronchi travel a short distance as extrapulmonary segments before they enter the lungs as the intrapulmonary parts. Account of the intrapulmonary airways is not yet firmly established and the names and numbers of secondary bronchi arising from the intrapulmonary primary bronchus are still controversial (e.g. McLelland, 1989, Maina, 2005). In the domestic fowl, *Gallus gallus* variant *domesticus*, Duncker (1974) reported four medioventral-, 7-10 laterodorsal-, and an indeterminate numbers of lateral secondary bronchi. Lopez *et al.* (1992) described four dorsomedial-, four dorsal- and three lateral secondary bronchi. Recently, Makanya and Djonov (2008) identified four mediovental-, 7-10 laterodorsal-, 1-3 lateroventral- and up to 60 posterior secondary bronchi. In all cases, each of the secondary bronchi gives rise to large numbers of parabronchi (tertiary bronchi). In cross-sectional view, in some species of birds, the parabronchi are conspicuously hexagonal in shape, with a lumen surrounded by a mantle of exchange tissue. Parabronchial diameter is constant for each species (Duncker, 1971) and ranges from 0.5 mm to 2.0 mm, except in penguins where the parabronchi lying close to the primary bronchus are much narrower than parabronchi at the periphery of the lung (Duncker, 1971). The diameter of the lumen of a parabronchus is about one-half its total diameter (Maina *et al*., 1982). The parabronchi are not blind ending but join end to end to form long hoop-like bronchial circuits which connect groups of secondary parabronchi. The parabronchi associated with the mediodorsal and the lateroventral secondary bronchi terminate by joining end-to-end with the parabronchi of the medioventral bronchi at the planum anastomosticum, visible on the vertebral surface and cranial end of the coastal surface as a line, the so-called linea anastomostica (McLelland, 1989). The parabronchi are arranged into well-defined medial and lateral groups. The medial group arises from the deep surfaces of the medioventral-, mediodorsal- and lateroventral secondary bronchi and is

directed towards the interior of the lung. This group of parabronchi, approximately 150-200 in number, form curved parallel bronchial circuits running layer upon layer about 4 cm in length between the mediodorsal-, lateroventral- and medioventral aspects of the lung (McLelland, 1989). These curved stacks form the bulk of the lung and are named the *paleopulmo* (Duncker, 1971). The lateral group of parabronchi (*neopulmo*) is variably developed in different species. The neopulmonic parabronchi arise from the outer surfaces of the lateroventral-, laterodorsal- and mediodorsal secondary bronchi. This group, absent in penguins (*Spheniscidae*) and in birds like the kiwi (*Apteryx*), is superficial in position in the lateral part of the lung where they form anastomosing network of parabronchi with different lengths and degrees of branching (McLelland, 1989). However, it is difficult to distinguish the lateroventral secondary bronchi from the parabronchi due to their small size (Maina, 2005)

1.4.4 The gas exchange tissue of the avian lung

The profusely anastomosing, three dimensionally arranged and intimately interdigitating air - and blood capillaries of the parenchyma of the avian lung develop from days 18 and 21 of incubation period in the chicken (e.g. Maina, 2003). The development of the air passages, which start with the appearance of the lung bud on the ventral aspect of the primordial foregut on day 3, continue after hatching (Maina, 2003): the atria and the infundibulae are formed on days 15 and 16 respectively after which air capillaries start projecting into the surrounding mesenchymal tissue on day 18. The perikarya of the epithelial cells are located at the atria and initial parts of the infundibulae, with their processes continuing into the air- and blood capillaries. Thinning of the closely approximated epithelial-endothelial contacts is effected by

continuous projection of the epithelial cell into the mesenchyme tissue which latter disintegrate (undergo apoptosis). Mesenchymal tissues are quickly replaced by deposition of intercellular matrix to form the laminated, tripartite cytoarchitectural design of the blood-gas barrier (Maina, 2004). The exchange tissue (mantle) which is formed in the process surrounds the parabronchial lumen and some similar sized secondary parabronchi.

In the lungs of mainly the galliform birds, the outer most part of the exchange tissue is limited by the interparabronchial septum within which are blood vessels (e.g. King and Molony, 1971; McLelland, 1989; Maina, 2005). Lungs of many species of birds, however, lack interparabronchial septum (Maina *et al.,* 1982; Maina, 2005). The thickness of the exchange tissue mantle is species dependent and ranges between 200 – 500 µm (Duncker, 1974). In cross-section, the interparabronchi septa, where present, separate and give a roughly hexagonal outline to the parabronchi. The thickness of the interparabronchial septa is also species dependent (e.g. King, 1966; Duncker, 1971). A relationship, noted by Duncker (1971), exists between the size of the parabronchi, the thickness of the interparabronchi septa and the relative proportion of the atria and the exchange tissue: poor flyers, e.g., the *galliform* species, have large parabronchial diameters with thick interparabronchial septa, deep atria, and thin exchange tissue mantle. Strong flyers, e.g., the *passerine* species, have reduced parabronchi diameter, increased proportion of exchange tissue and thinner or no interparabronchial septa (Maina *et al*., 1982)

The atria, which are supported by atrial muscles, lead from the parabronchial lumen to the exchange tissue. The atrial muscles consist of large spiral bands and small irregular bundles of smooth muscles: small irregular bundles join the large spiral bands to surround the atrial openings (King and Cowie, 1969). Atrial walls are formed by connective tissues that

constitute the interatrial septa (Maina, 2005). The atrial dimensions are species dependent (Duncker, 1974; West *et al*., 1977; Maina *et al*., 1982). The atrial floor leads into 3 - 8 funnel shaped infundibula, which in turn lead into air capillaries. Infundibular diameter ranges between 25 – 40 µm and penetrate the exchange tissue mantle for about 100 -150 µm (West *et al*., 1977). The air capillaries are not *culs de sacs* like mammalian alveoli: they form anastomosing three-dimensional networks which profusely and intimately interdigitate with blood capillaries (Maina, 1982; Woodward and Maina, 2005; Woodward and Maina, 2008; Maina and Woodward, 2009). The air capillaries have diameters that range between 3 – 20 µm (Duncker, 1972; Maina and Nathaniel, 2001). Within the exchange tissue, they show abrupt difference in size and unlike the blood capillaries, they are more tortuous, larger, and anastomose more irregularly (Maina, 1982).

1.4.5 Innervation of the bronchial muscles

Bundles of axons have been reported in the smooth muscles of the parabronchi, though more of them are said to be present in the secondary bronchi (Cook and King, 1970). Because muscle cells in parabronchi have fewer close neuromuscular junctions but highly developed intercellular couplings, King and Molony (1971) suggested that complex, slow graded local tension changes and spontaneous rhythmicity are possible. Contractions of these bands of muscle tissue may narrow the parabronchial lumina and atrial openings. King and Cowie (1969) made *in vivo* observations of the contraction of parabronchial smooth muscle cells through the small transparent areas of some parabronchi on the lateral aspect of the lung. Contractions by cholinergic drugs blocked by atropine and relaxation by adrenergic drugs

confirm an intrinsic tone maintained by the muscles (King and Cowie, 1969). Complex integration of smooth muscle action and elastic forces has been reported to be possible because of close association or continuity between muscle- and elastic tissue fibers (King and Molony, 1971). Because of presence of elastic fibers in the atrial walls along with atria muscles, King and Cowie (1969) suggested that the atrial part of a parabronchus is the most mobile. When the muscle contracts to narrow the lumen, the elastic fibers store energy to oppose the tone of the muscle when it relaxes.

1.4.6 The vascular system

The organization of the pulmonary arterial vasculature in the avian lung is significantly different from the mammalian tree-branching pattern (Maina and van Gils, 2001). The arterial supply does not accompany the airways and venous drainage system. The following accounts of the avian vascular anatomy summarize works of Abdalla and King (1975, 1976a, b, 1977), and Abdalla (1989) on the domestic fowl. The vascular system starts as the pulmonary trunk. The trunk in the chicken is ~0.7 cm in diameter and is 1-1.5 cm long. The trunk originates at the infundibulum of the right ventricle and terminates where it bifurcates into right and left arteries each of which is 0.4 cm in diameter. Within the lung, the pulmonary artery divides into four main branches which divide the lung into cranial and caudal vascular territories, with the dividing line roughly passing through the third coastal sulcus. The vascular supply to the two territories usually overlaps but the blood vessels do not anastomose. The accessory- and the cranial branches supply the cranial territory while the caudomedial and caudolateral branches supply the caudal territory. The accessory branch, which is missing in some species, is the smallest branch that supplies a small area ventral to the hilum. The cranial branch

supplies the craniodorsal part anterior to the third sulcus. The caudomedial branch is the most direct continuation of the pulmonary artery: it courses along the longitudinal axis of the lung and supplies the greatest part of the lung. The caudolateral branch supplies the ventral-, the ventrolateral- and the caudoventral part of the lung caudal to the third coastal sulcus. Each of the four branches gives several orders of interparabronchial branches that run longitudinal or transverse to the parabronchi. The short terminal branches encircle the parabronchi at right angles to give rise to intraparabronchial branches (20 - 40 µm diameter) that enter radially into adjacent parabronchi to supply the exchange tissues with blood. Intraparbronchial arterioles give rise to blood capillaries, which are typically 6µm in diameter. Blood capillaries anastomose freely with each other and with those from adjacent arterioles but no anastomosis occur in the arterial pathway from the pulmonary artery to the level of arterioles. Blood capillaries extend centripetally from the peripheral part of the exchange tissue mantle, anastomose profusely and intertwine intimately with the air capillaries that project from the infundibulae.

The blood capillaries in the exchange tissue drain either into intraparabronchial venules, atria veins or into septal venules. The intraparabronchial venules drain towards the parabronchial lumen and empty into the atrial veins. The atrial veins lying in the floor of the interatrial septa either pass radially through the exchange tissue to interparabronchial vein or empty into the septal venules. The septal venules ascend in the septa just beneath the atria muscles where they anastomose with other septal venules to form the intraparabronchial vein. The intraparabronchial veins emerge at regular intervals along the length of the parabronchus and empty into the interparabronchial veins. The interparabronchial veins from the caudal region of the lung form the caudal radices while those from the cranial region form the cranial radices

of the pulmonary venous system. The cranial and caudal radices join to form the pulmonary vein which is 0.4 cm in diameter.

1.4.7 The blood-gas (tissue) barrier

The pulmonary blood-gas (tissue) barrier (BGB) is a composite structure which separates two fluid media (e.g. Weibel, 1973) - air and blood within the lung. In the mammalian lung, it consists of a single layer of alveolar epithelium, separated from a single layer of capillary endothelium by a common basement membrane (Weibel, 1973; Gehr *et al.,* 1978) (Fig. 1.2). An interstitial space with smooth muscle and connective tissue elements such as collagen and elastic tissue occur in the amphibian and the reptilian lungs as well as in the thick (supportive) parts of the tissue barrier in the mammalian lung (Weibel, 1973; Meban, 1980). Such interstitial connective tissue elements are completely absent in the avian BGB (e.g. Maina and King, 1982; Maina *et al.,* 1989; Maina, 2002a). In most mammals, the common basement membrane constitutes about 40 % of the barrier while the endothelium and the epithelium account for about 30 % each (Weibel, 1973; Meban, 1980). In birds, the endothelium, the basement membrane, and the epithelium constitute 67 %, 21 % and 12 % of the BGB respectively (Maina and King, 1982); however, Watson *et al*. (2007) reported slightly different values from those of Maina and King (1982). The low volume density of the basement membrane confers a smaller arithmetic mean thickness of the BGB for birds (1.060 μm) (Maina and King, 1982) compared to values reported for mammals (1.50 μm) (Weibel, 1972, 1973; Meban, 1980; Gehr and Erni, 1980), reptiles (2.02 μm) (Meban, 1980) and amphibians (2.22 μm) (Meban, 1980). Measurement of the thickness of the BGB is commonly expressed

as either the arithmetic mean thickness (τt), which reflects the mass of tissue (volume density) that forms the barrier or the harmonic mean thickness (τht), which is more indicative of the resistance (or its reciprocal, the conductance) of the barrier to gas (oxygen) diffusion (Weibel and Knight, 1964; Weibel, 1973). The ratio of τt to τht shows the degree of the corrugation of the BGB (Weibel, 1973; Meban, 1980; Maina and King, 1982). This ratio increases from amphibians (1.3:1), reptiles (2.0:1) (Meban, 1980), mammals (3.0:1) (Weibel, 1970, 1972, 1973; Meban, 1980) to birds (7.0:1) (Maina and King, 1982; Maina *et al.*, 1989). Corrugation (sporadic attenuation) of the BGB is a compromise for efficient flux of respiratory gases across the barrier and maintenance of mechanical stability of the barrier: the thick parts confer strength while the thin ones promote gas exchange (Weibel, 1973; Meban, 1980). The high ratio determined in the avian lung suggests that the BGB is the most corrugated among the air-breathing vertebrates. Firm attachment of the avian lung to the sturdy body trunk and to the oblique - and horizontal septa ensures extreme attenuation of the BGB (Duncker, 1971; McLelland, 1989): in a noncompliant (rigid) lung, the air capillaries are not subjected to rhythmic inflation and deflation as is the case for the alveoli of the compliant mammalian lung. The avian BGB has therefore attained stability while improving respiratory efficiency.

Figure 1. 2: Comparison of mean arithmetic mean thicknesses of the blood-gas barrier between mammals and birds

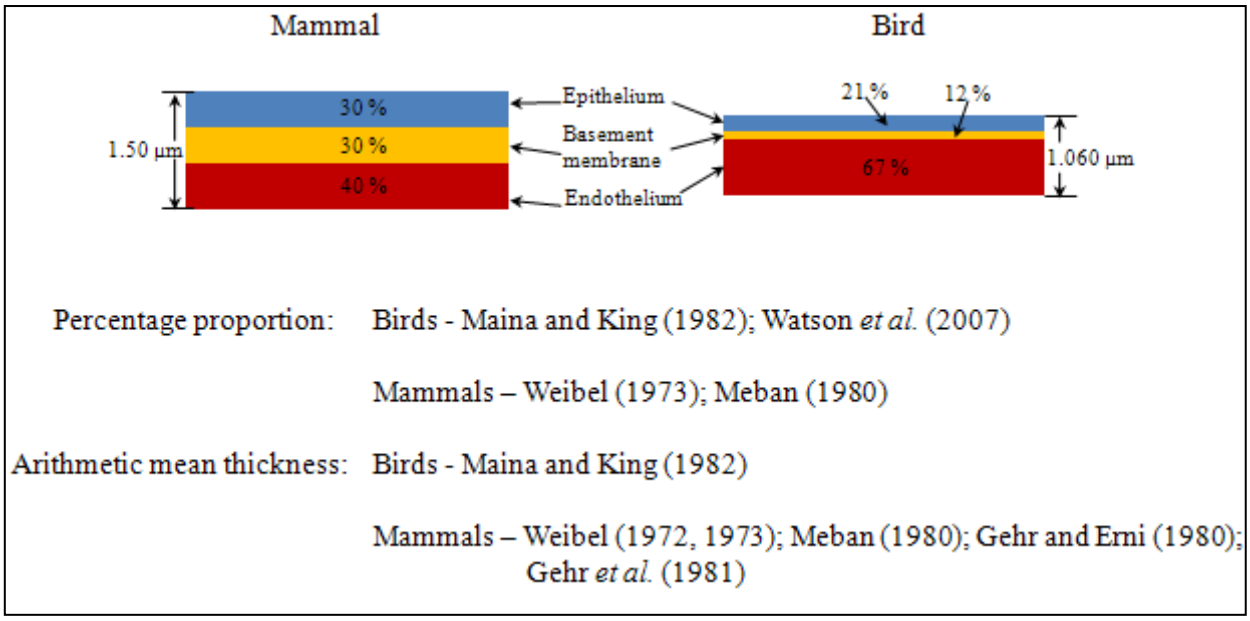

1.4.7.1 Alveolar epithelium

Within the exchange tissue, the part of the pulmonary BGB facing the air is the extremely thin and extensive epithelial cell process. Out of the 20 different cells that populate the pulmonary exchange area (e.g. Burri, 1985), alveolar type- I cells constitute only 10% yet this type of cell covers 96% of the alveolar surface (Crapo *et al.*, 1983). With a volume of 1,764 µm^3, the alveolar type- I cell is also the largest. It is thinly spread over an area of 5,098 µm^2 (Crapo *et al.*, 1982). To make the barrier very thin and enhance gas exchange, in the avian lung, the alveolar type- I perikarya are commonly located at the corners of the BGB, mostly outside of the air capillaries (Maina, 2005): a thin cytoplasmic extension that contains the sparse organelles extends to form the epithelial part of the BGB.

1.4.7.2 Basement membrane

Generally, the basement membranes are characteristic products of overlying epithelial cells (e.g. Dodson and Hay, 1971; Banerjee *et al*., 1977). However, there is evidence showing that mesenchymal cells also produce basement membrane components (e.g. Kuhl *et al*., 1984; Sanderson *et al*., 1986; Simon-Assmann *et al*., 1988). The basement membrane comprises of polysaccharides and proteins secreted locally and assembled into a specialized felt-like meshwork of continuous sheets (Alberts *et al.,* 1989; Crouch *et al.,* 1997). In general, a basement membrane separates parenchymal cells or cell sheets from the underlying or surrounding connective tissue. In a unique location, such as the pulmonary BGB, the basement membrane lies between two sheets of cells (Alberts *et al*., 1989): the sandwiched basement membrane of the pulmonary BGB exists as an extremely thin but tough extracellular matrix material that separates pulmonary epithelium from capillary endothelium (Martin *et al*., 1988, Timpl *et al*., 1989; Leblond and Inoue, 1989). Because the basement membrane frequently remains intact while capillary endothelium and alveolar epithelium show ultrastructural signs of ultrastructural disruptions, Tsukimoto *et al*. (1991) suggested that the strongest component of the barrier is the basement membrane. Several experimental evidences support the fact that the basement membrane is the strength-bearing component of the BGB. For example, by removing the single sheet of epithelial layer of an isolated rabbit renal tubule with detergent, Welling and Grantham (1972) demonstrated that the relationship between transmural pressure and diameter of the tubule remained unchanged. Swayne *et al*. (1989) showed that distension of blood capillaries from frog and rat mesentery was consistent with the Young's modulus of the basement membrane. The relationship between the thickness of the basement membrane and the need for stronger capillaries in the leg of humans and the giraffe (e.g. Williamson *et*

al., 1971) and in long-standing cases of pulmonary venous hypertension (e.g. Haworth *et al*., 1988) also affirm that the basement membrane is the strength-bearing component of a blood vessel.

The basement membrane appears as a single unit under the light microscope but under the high-resolution power of the electron microscope, it is divisible into three parts, i.e., the middle lamina densa is flanked by lamina rara externa adjacent to the alveolar epithelial cell and lamina rara interna adjacent to the capillary endothelial cell (e.g. Vaccaro and Brody, 1981). Type-IV collagen, laminin, entactin/nidogen and heparan sulphate proteoglycans are the four principal molecules that make up the basement membrane (Crouch *et al*., 1997). Composition and organization of these macromolecules within the basement membrane varies with location and function (Widnell and Pfenninger, 1990). While detailed organization of the basement membrane is unclear, Crouch *et al*. (1997) used purified antibodies to demonstrate that the lamina densa is composed mainly of type-IV collagen while proteoglycan molecules are located on either sides of the lamina densa within the lamina rara interna and externa.

Type-IV collagen, found exclusively in the basement membrane, shares the characteristic stiff, triple helical structure of all collagen (Alberts *et al*., 1989) but uniquely contain a flexible region and non-collagenous domains at each end of the triple helix (Widnell and Pfenninger, 1990). Because of the unique structural features, instead of forming fibrils, type-IV collagen assembles into a two-dimensional sheet-like meshwork (Alberts *et al*., 1989; Widnell and Pfenninger, 1990) which can lengthen in one direction when pulled (Timpl *et al*., 1989; West and Mathieu-Costello, 1999). The lengthening associated with distortion of type-IV collagen two-dimensional matrix when stress is applied and its recovery when stress is removed form

the basis of explanation made by West *et al*. (1991). They suggested that when the pulmonary intramural pressure is increased, the flexible collagen in the basement membrane stretches beyond the cells to accommodate the increase in pressure but capillary endothelial and alveolar epithelial cells may show micro disruptions. However, if the pressure is reduced and the basement membrane remains intact, the original arrangement is restored and the disruptions reunite. However, failure of the BGB becomes observable when the basement membrane is stretched beyond its elastic limit (West *et al*., 1991).

Heparan sulphate proteoglycans is another major component of the basement membrane found in the laminae rara externa and interna. Negatively charged heparan sulphate proteoglycans (Widnell and Pfenninger, 1990) form both mechanical and electrical barriers that regulate permeability (Negrini *et al.,* 1996). By forming a highly hydrated gel-like ground substance, heparan sulphate proteoglycans also anchor other components of the basement membrane (Alberts *et al*., 1989). Adhesive proteins are other components of the basement membrane that are dispersed within the laminae: they attach cells to the basement membrane. One of the adhesive proteins is laminin: it consists of two subunits held by disulfide cross-links and is organized into distinct functional domains that bind to collagen type-IV, heparan sulfate proteoglycan, and plasma membrane receptors (Alberts *et al*., 1989; Widnell and Pfenninger, 1990; Lallemand *et al.*, 1995). Another adhesive protein is entactin, a sulfated glycoprotein (Widnell and Pfenninger, 1990), which binds laminin to type-IV collagen (Senior *et al.,* 1996).

1.4.7.3 Capillary endothelium

The pulmonary capillary, like other blood capillaries, consists of an endothelial cell rolled-up to surround a cylindrical space (Junqueira and Carneiro 2003). In cross section, endothelial cells have a characteristic nucleus that follows the curvature of the lumen it surrounds. The cells, which are elongated in the direction of blood flow, are, in longitudinal section, polygonal in shape (Junqueira and Carneiro 2003). Intermediate filaments are found in the perinuclear region of the endothelial cells. Because of abundance of microfilaments in their cytoplasm, endothelial cells are presumed to contract (Fishman, 1982). Presence of numerous micropinocytic vesicles is indicative of transport of macromolecules across the cell (Junqueira and Carneiro 2003). Contrary to the commonly held view that vascular endothelial cells are homogenous, evidence is growing that these cells exhibit structural and functional heterogeneity (Aird, 2006, 2007a, b). Endothelial cell diversity is apparent in different organs, along a single vascular segment within an organ, and even between two adjacent cells (Stevens *et al*., 2008). Within the exchange tissue, some capillary endothelial cells are exclusively in contact with other endothelial cells, others share contact with only alveolar epithelium while others are in contact with both epithelial and other endothelial cells. Because the composition and organization of the macromolecules of the basement membrane vary depending on the cells being separated (Widnell and Pfenninger, 1990), there may be molecular variations between the cells and within the same cell.

1.4.8 Forces acting on the blood-gas barrier

The lung, unlike the heart, is not visibly mechanically active (Maina and West, 2005) but its operational dynamics (ventilation and perfusion) are purely mechanical. These mechanical events are associated with a number of forces that act directly on the pulmonary parenchyma (Fig. 1.3). Expansion induced by volume change associated with pulmonary function in humans cause 12,000 liters of air to ventilate and 6,000 liters of blood to perfuse the lung per day (Burri, 1985). At any point in time, approximately 9% of the total blood volume in the body is contained in the lung (Dock *et al*., 1961). Ventilation is an active process produced by muscular (*cranial and hypobranchial musculature for* buccal pump *and axial musculature for* aspiration pump) contraction (e.g. Brainerd, 1999). The rhythmic contraction of the heart delivers blood in a pulsatile flow through the pulmonary vascular bed (Milnor, 1982; Maarek and Chang, 1991); however, the pulsatile wave is dampened at the capillary bed (Wienner *et al*., 1966). In mammals, lung ventilation creates longitudinal stress on the BGB while the effect of perfusion causes circumferential stress (West *et al*., 1991). Longitudinal tension is associated with lung inflation which creates tension in the tissue elements of the alveolar wall. Since pulmonary blood capillaries form most of the alveolar wall, the longitudinal tension is transmitted to the capillary walls (West and Mathieu-Costello, 1999; Maina and West, 2005). Ultrastructural changes in the walls of the blood capillaries at high state of lung inflation (Fu *et al.,* 1992) have confirmed transmission of longitudinal tension to the capillary walls. Circumferential (hoop) tension is the result of transmural pressure difference acting across the curved capillary wall (West and Mathieu-Costello, 1999; Maina and West, 2005). Surface tension force also acts on the BGB. At the alveolar liquid-air interface, the pull generated by surface tension tends to make the alveoli collapse but the intricate network of fiber system in

the alveolar walls stretches to prevent the collapse (e.g. Weibel, 1984). According to the Laplace's equation, the pressure (*P*) needed to balance the collapsing force of surface tension (γ) in an alveolus of radius *r* is expressed as: $P = 2\gamma/r$. The smaller the radius of an alveolus the higher the pressure needed to balance the collapsing force of surface tension. In other words, surface tensional force acting on the barrier will be greater in an animal with extremely small respiratory units. By extrapolation, surface tension should be very high in the relatively small (3-20 μm in diameter) air capillaries of the avian lung (Duncker, 1971; Maina, 1982) which are on average one-tenth the size of the mammalian alveoli (Maina, 2005). Interestingly, besides lamellated osmiophilic bodies, which are also found in the mammalian lungs, the avian pulmonary cells also secrete unique material, the trilaminar substance (Pattle, 1978). Pattle (1978) and Fedde (1980), however, challenged its role as a 'surface tension diffuser' in bird's lungs. Other functions such as serving as boundary lubricator (Hills *et al*., 1982) and anti-adhesive that decreases the work needed to separate apposed epithelial surfaces (Sanderson *et al*., 1976; Reinfenrath, 1983; Daniels and Orgeig, 2003) have been proposed.

Figure 1. 3: Comparison of mean arithmetic mean thicknesses of the blood-gas barrier between mammals and birds

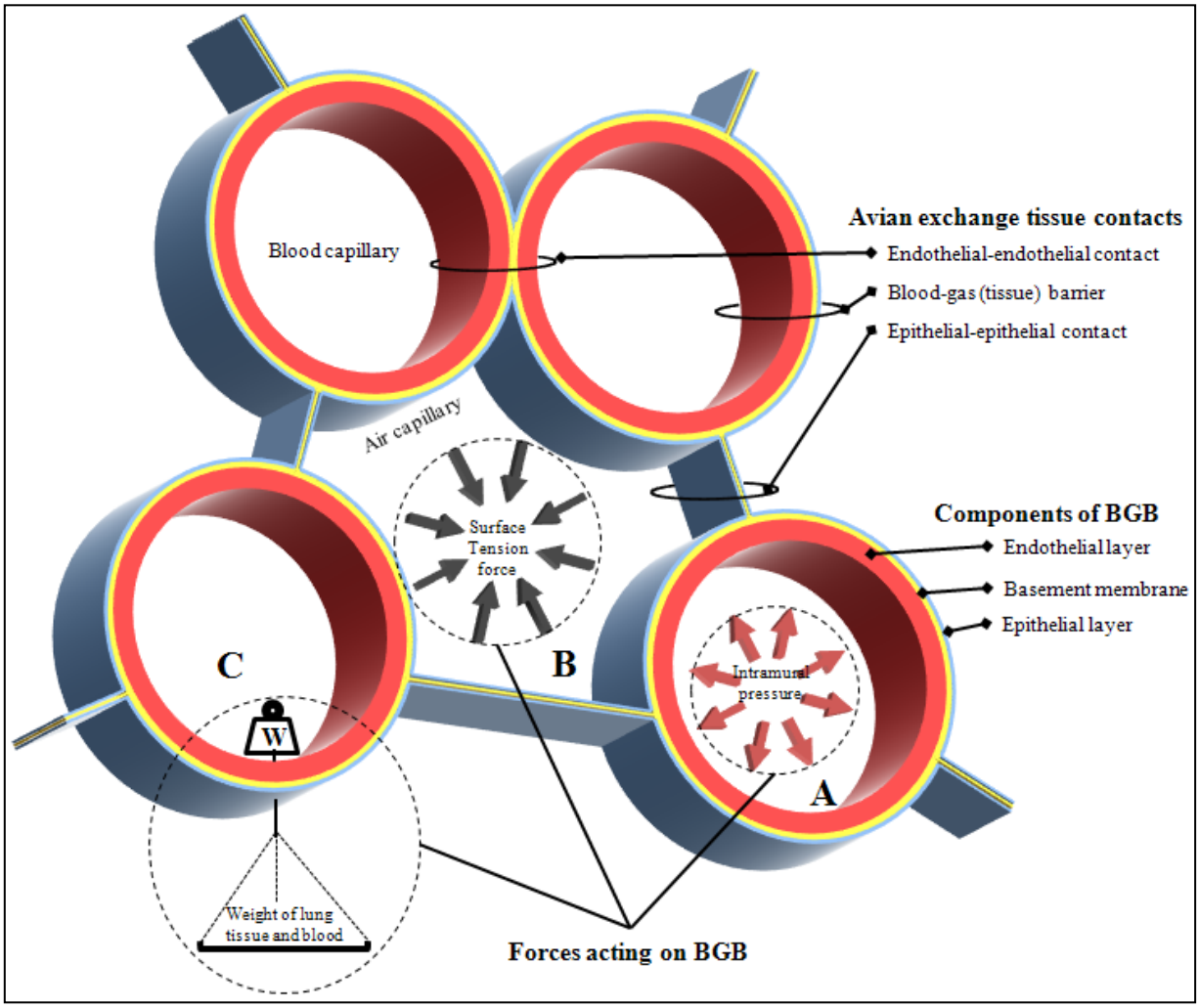

A. Blood within the capillary is under pressure, outward push caused by the blood pressure creates circumferential tension that acts on the BGB.

B. Intermolecular forces at the air-liquid interface produces surface tension, which exerts an inward pull on the barrier toward the air space. This effect further stretches the barrier adding to the effect of circumferential tension.

C. Weight of lung tissue and the contained blood tense the BGB

1.4.9 Structural failure of pulmonary blood-gas (tissue) barrier

Study of structural failure of the BGB probably started in earnest with the observation by Schoene and colleagues. While they were studying the pathophysiology of high altitude pulmonary edema (HAPE), they noted that pulmonary lavage fluid from patient suffering from HAPE is high in protein and cells (Schoene *et al.,* 1986). They suspected leakage from pulmonary capillaries and envisaged that it arose from changes in capillary permeability. Later, Tsukimoto *et al*. (1991) and West *et al*. (1991) suspected damage of the blood capillary walls, a feature that they confirmed microscopically. West and Mathieu-Costello (1999) characterized the extents and forms of failure as:

a. Disruptions of the capillary endothelial and alveolar epithelial layers.
b. Extensive collections of red blood cells and proteinaceous fluid in the alveolar spaces.
c. Interstitial edema and fluid-filled protrusions of the endothelium into the capillary lumen.

Because the strength of the wall must be overcome before failure can occur, West *et al.* (1991) asserted that any physiological and pathophysiological conditions that excessively raise pulmonary capillary wall tension would cause structural failure of the BGB. HAPE is a well-studied example (e.g. Schoene *et al.,* 1986; Kobayashi *et al*., 1987; Koitzumi *et al*., 1994) in which excessive wall tension is caused by increase in pressure in some capillaries consequent to uneven hypoxic pulmonary venous constriction (Hultgren, 1969). The increase in pressure causes high-permeability alveolar edema (Schoene *et al.,* 1986). Similarly, increased pulmonary capillary pressure associated with heart diseases such as mitral stenosis and left ventricular failure (causing excessive increases in wall tension of the BGB) can result in stress failure (West and Mathieu-Costello, 1995). A relationship also exists between stress failure

and abnormally high states of lung inflation (Dreyfuss *et al.,* 1985), especially when the geometry of the pulmonary capillary in relation to the alveolar wall allows increase in longitudinal tension to be translated into increase in circumferential tension in the capillary wall (Fu *et al.,* 1992).

Stress failure of the BGB became a more interesting area of research when its occurrence was associated with intense activities (e.g. Tsukimoto *et al.,* 1991; West *et al.,* 1991) which includes activities such as chasing a prey, escaping predation, and even during recreational exercises (West, 2004; Wagner, 2005; Eldridge *et al.,* 2006; Zavorsky *et al.,* 2006; Ludwig *et al.,* 2006). Intense activity, generally tasks all systems of the body especially the cardiopulmonary system (e.g. Rowell, 1974). In line with suspicion of stress failure being associated with normal activities, Hopkins *et al*. (1997) reported higher concentrations of red blood cells and protein in bronchioalveolar lavage, which lack pro-inflammatory pathways indicators except leukotreine B4 in lungs of elite human athletes: they suggested mechanical cause of failure. Racehorses selectively bred for very high levels of exercise, recorded to raise pulmonary arterial and left atria pressures to as high as 16 kPa (120 mmHg) and 9.3 kPa (70 mmHg) respectively (Erickson *et al*., 1990; Jones *et al*., 1992; Manohar, 1993), commonly bleed into their alveolar spaces on exercise (Whitwell and Greet, 1984). Exacting requirements imposed on the lung, which requires extreme thinness, a very large surface area for adequate and efficient flux of respiratory gases (Gehr *et al*., 1978) renders the BGB vulnerable, and its integrity challenged during intense exercise. In spite of the already vulnerable design of the BGB (thin and devoid of significant connective tissue elements), the two media it separates in the air-breathing vertebrates are of different densities and operate at different pressures. The operational (respiratory) dynamics of the two fluids constantly challenge the structural

integrity of the BGB. For instance, high fluctuations in the pulmonary intramural pressure (West and Mathieu-Costello, 1995) and different levels of lung inflation (Dreyfuss *et al*., 1985; Fu *et al*., 1992) between rest and different level of activities, which produces huge pressure difference in the two media, stretch (tense) the BGB. Furthermore, the pulmonary capillaries are not supported by surrounding tissues like the systemic capillaries (Fung *et al*., 1966). Tensional forces created by the weight of lung tissue, the weight of the contained blood (~9%) (Dock *et al.*, 1961), the effect of changing intramural pressure, different state of lung inflation and surface tensional force that exists at the air tissue interface (Fig. 1.3) directly impinges on the physical integrity of the BGB. Although, the combined effect of intramural pressure, surface tension, and lung inflation may be negligible in resting state (Hopkins *et al*., 1998), during intense activity, the effects become significant (West *et al*., 1991; Hopkins *et al*., 1997).

1.4.9.1 Mechanisms of structural failure

Although very little is known about the micromechanics that lead to failure of the BGB, much of what is known came from comprehensive works and insightful thoughts of Dr. John West and his associates (e.g. West *et al*., 1991; Birks *et al*., 1994; West and Mathieu-Costello, 1999). When tension in the BGB is raised to unphysiologically high level, ultrastructural changes in the BGB, identifiable under electron microscope, start to appear (West *et al*., 1991; Birks *et al*., 1994; West and Mathieu-Costello, 1999, West, 2000a; Maina and West, 2005). Three different principal forces act on the BGB (West and Mathieu-Costello, 1999) (Fig. 1.3). These forces act in concert (West *et al*., 1991) to balance tension across the barrier. Failure of

the BGB occurs when the balance that exists among these forces is disturbed. The probable events that lead to failure of the avian BGB are highlighted in Fig. 1.4.

Figure 1. 4: Envisaged mechanism of stress failure of the blood-gas barrier of the avian lung

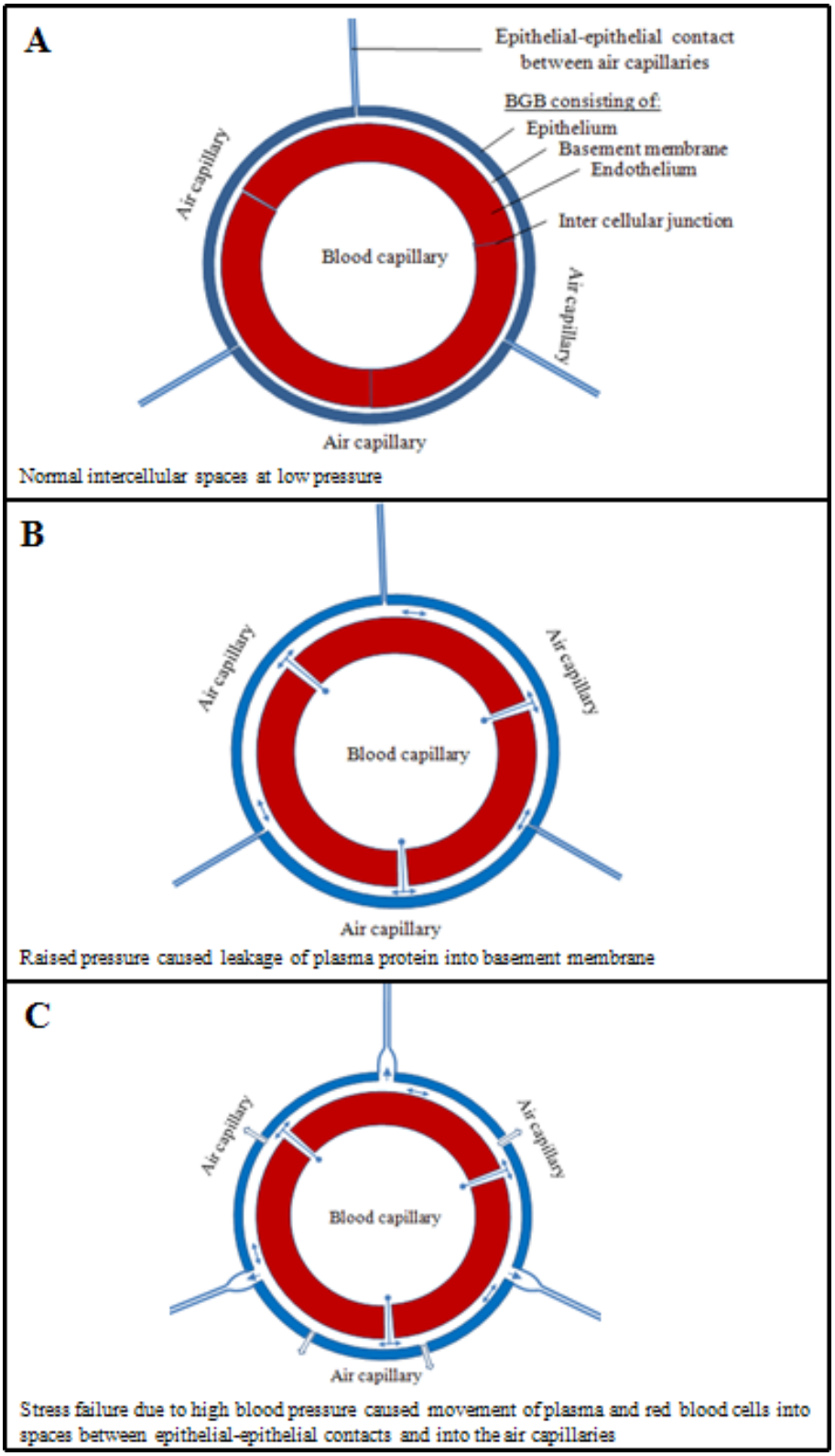

Adapted from West *et al.* (1991)

Figure 1.4 legend:

A: At low pressures, the blood capillary shows normal morphology with normal intercellular spaces**. B:** When blood capillary pressure is raised, intercellular spaces are stretched; this state is associated with low-protein hydrostatic edema, increased permeability, and leakage of plasma protein into basement membrane (thin arrow) causing it to swell; at this stage, epithelium may remain intact**. C:** Further increase in pressure causes blood capillary to acquire a circular shape because the basement membranes does not allow further distension. The basement membrane at this point may remain intact but endothelial- (red) and epithelial cell (blue) disruption caused by stress failure lead to movement of plasma and red blood cells through the basement membrane (thin arrow) into spaces between epithelial-epithelial contacts and into the air capillaries (open arrow).

1.5 RESEARCH QUESTIONS AND STATEMENT OF THE PROBLEM

1. ***How is the structural integrity of the extremely thin blood-gas barrier of the avian lung maintained under high intravascular blood pressure?***

It is interesting that the avian BGB which is 56-67% thinner than that of mammals of comparable body mass (Maina *et al.,* 1989) can withstand comparatively much higher blood pressure (Seymour and Blaylock, 2000). In spite of thicker interstitium galloping race horses still break their BGB (West *et al.,* 1993), structural characteristics or arrangement of the constituent elements of the avian BGB that provide greater strength per unit thickness need to be investigated in order to gain insight into the basis of the reported exceptional strength of the avian BGB. Connective tissue collagen of a parabronchus and basement membrane collagen type-IV were investigated in an attempt to elucidate this paradox.

2. ***Is the blood-gas barrier susceptible to structural failure at rest and especially during exercise?***

Minimum harmonic mean thickness of the avian BGB (Maina and King, 1982), high blood pressure (Seymour and Blaylock, 2000), and avian energetic lifestyle (Tucker, 1972a, b) should predispose the BGB of the avian lung to failure. While presence of red blood cells is frequently reported to occur in the lavage fluid of resting birds (e.g. Maina and Cowley, 1998; Nganpiep and Maina, 2002), it is necessary to find out how vulnerable or pervious (leaky) the avian BGB is at rest and during intense activity.

3. At what intramural capillary pressure does the blood-gas barrier of the avian lung structurally fail?

The morphological design and operational dynamics of the avian gas exchanger is remarkably different from the mammalian one (e.g. Duncker, 1972; Maina, 1982, 2005; McLelland, 1989). Intramural pressures at which BGBs fail in mammals have been experimentally determined by intravascular perfusion at different head pressures (e.g. West *et al.,* 1991; West and Mathieu-Costello, 1992; West *et al.,* 1993). It is necessary to find out how different the value is in the avian lung which has a 'flow through' ventilatory system and miniscule air capillaries separated from blood capillaries by an extremely thin BGB (e.g. Maina *et al.,* 1989; Maina and West, 2005).

In this investigation, the following features of structural failure were investigated and where possible quantified:

1. Presence of red blood cells in the air capillaries.
2. Presence of blood proteins in the air spaces, and
3. Disruptions of the capillary endothelial and alveolar epithelial layers.
4. Complete failure of the BGB

Identification of any of these features within the exchange tissue indicated some degree of failure of the BGB.

1.6 SIGNIFICANCE OF THE STUDY

Research into understanding the relationship between pulmonary functional demands and mechanical challenges on structural integrity of the BGB has focused primarily on mammalian lung. While experimental studies have confirmed the intramural pressures at which BGB fail in mammals (rabbit, dog and horse) (West *et al.*, 1991; West and Mathieu-Costello, 1992; West *et al*., 1993), comparable data are totally lacking on birds. Besides being endothermic and homeothermic, birds operate at a relatively higher body temperature (Aschoff and Pohl, 1970) and they have adopted a form of locomotion (flight) which exerts comparatively higher metabolic demands (Tucker, 1972b; Tatner and Bryant, 1986; Banzett *et al*., 1992; Voigt and Winter, 1999). The avian respiratory morphology is characterized by extreme morphometric refinements (e.g. Maina *et al*., 1989). It should be challenged differently. For example, a bird like the turkey, *Meleagris gallopavo* and generally fast growing broiler chickens frequently suffer hypertensive complications that translate into high myocardial stress resulting in complications such as aortic aneurysm and ascites (e.g. Speckman and Ringer, 1963; Krista *et al*., 1970; Julian and Wilson, 1986; Currie, 1999). Due to more cost efficient production methods, compared with beef production, poultry meat now forms an important source of protein for the increasing human population. Better feeding regimen and genetic manipulation of birds for fast weight gain and egg production has caused a mismatch between the growth rate and organ development (Timmwood *et al*., 1987; Gyles, 1989; Silversides *et al*., 1997; Mohammed *et al*., 2005), in most cases leading to serious complications which result in high mortality. In the United States of America, the annual cost of deaths (fatalities) in the broiler industry runs into billions of dollars (e.g. Currie, 1999). The number of birds that directly succumb because of failure of the BGB and consequent intrapulmonary hemorrhage is

presently unknown. An understanding of the occurrence of the structural failure of the BGB in the lungs of birds may help in the formulation of management and preventive measures to avert economic losses from deaths of domestic/commercial birds. Moreover, investigating a structure that has been extremely refined like the BGB offers an understanding of nature's remarkable innovativeness.

CHAPTER II

2. MATERIALS AND METHODS

The University of the Witwatersrand's (Wits) Animal Ethics Committee granted approval for this research with clearance number 2007/53/01.

2.1 MATERIALS

2.1.1 Experimental animals

For easy pulmonary vascular manipulation, the experiment was designed to use large bird like pure breed turkey (*Meleagris gallopavo*). Large blood vessels are much easier to identify and cannulate for the purpose of intravascular perfusion and fixation of the lungs. Unfortunately, most of the turkeys that were readily available were quite heavy and could not run at all on the treadmill, even after trying all the different methods reported in the literature (e.g. Boulianne *et al.,* 1993; Seymour *et al.,* 2004) for stimulating birds to run on a treadmill. Following failure of the turkeys (to run on the treadmill), pure breed chickens (white leghorn breed) were procured. It was thought that chickens were smaller and less encumbered by body mass and should therefore be able to run on the treadmill. Disappointedly, they too were frustratingly indolent. After a trial run and satisfactory results with mature free range, mixed breed of domestic chickens, *Gallus gallus* variant *domesticus*, fifty-seven (57) were procured for the study from a reliable breeder. The chickens weighed between 1,392 and 2,838 gm (SD ±409.23). They were kept in a holding unit of the Central Animal Service (CAS) facility of the University of the Witwatersrand for three weeks to acclimatize, get used to handling, and for their health to be properly assessed. They were kept in a well-ventilated room with a controlled temperature of 22^{o}C and were exposed to twelve-hour light and twelve-hour darkness cycles. The birds were fed on commercial food ration and occasional green vegetable. Water was provided *ad libitum.*

In summary, the following studies were done; the arrangement of collagen fibres in the general connective tissue was investigated using Van Gieson's (collagen) discriminative staining and alkali digestion that removes all tissue components except collagen. Type-IV collagen in the basement membrane of the BGB was immuno-localized. Susceptibility of the avian pulmonary BGB to structural failure was investigated at different level of treadmill exercise and at different perfusion pressures. Failure of the BGB was assessed in rested and exercised birds while attempt was also made to determine the pressure at which the BGB starts to fail.

The experimental animals (domestic chickens) were divided into four groups (I- IV) (Figs. 2.1- 2.4). The group I experiment (Fig. 2.1) comprised of six (6) resting (unperturbed) birds. The experiment with this group was designed to check for occurrence of failure of the BGB in resting birds. The group II experiment (Fig. 2.2), with 30 birds, was designed to determine failure of the BGB in relation to exercise intensity. The group III experiment (Fig. 2.3), with 15 birds, determined the perfusion pressure at which the blood gas-barrier fails. Except for the perfusion experiment to establish the pressure at which blood gas barrier fails, all vascular perfusion fixation of the lungs was done at 1.2 kPa (12 cmH_2O = 9 mmHg) inflow pressure and 0.8 kPa (8 cmH_2O = 6 mmHg) outflow pressure. These inflow and outflow pressures were established in a pilot study as the pressures that did not cause failure of the BGB. The group IV experiment (Fig. 2.4) with six (6) birds, was divided into three sets. Presence of collagen connective tissue fibers was demonstrated in the exchange tissue of birds in this group using different techniques. The first set (with two birds) was used to show presence of type-IV collagen within the BGB and between air capillaries (i.e., in the epithelial-epithelial contacts) by immunoelectron microscopy. In the second set (two birds), all cellular and non-cellular

components of the exchange tissue of the lung were selectively digested except, collagen fibers, using an alkali (NaOH). Alkali digestion of all tissue components left the undigested collagen fiber without support, leading to loss of form. To show the undigested collagen fibers in their more natural location, pulmonary intravascular latex casting followed by selective alkali digestion was carried out on the third set of two birds. Samples for van Gieson's (collagen) discriminative staining were taken from lungs of non-exercised resting chicken.

2.1.2 Experimental set-up

Figure 2. 1: A flow diagram of the experimental setup on resting birds to determine failure of BGB

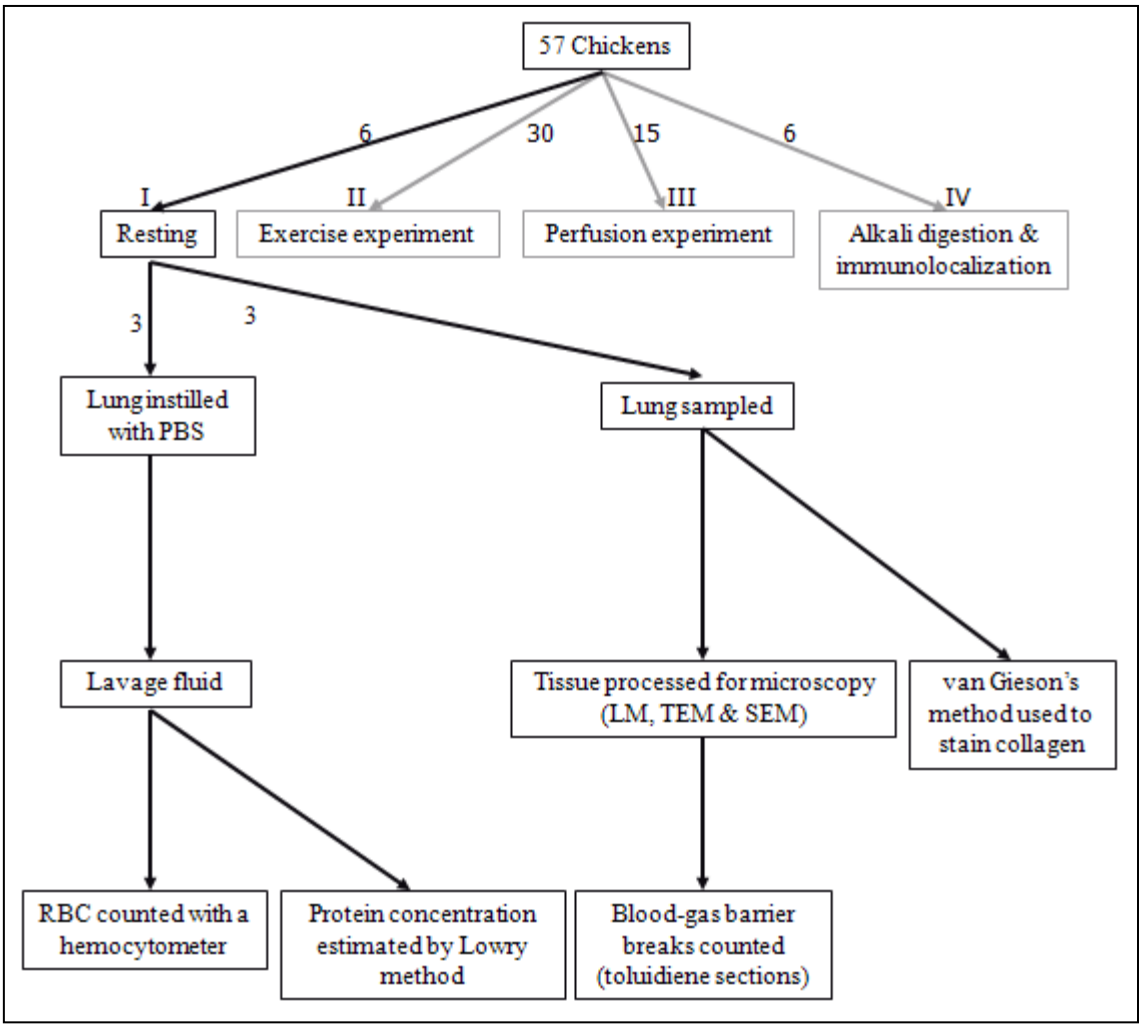

LM: Light microscopy

TEM: transmission electron microscopy

SEM: scanning electron microscopy

Figure 2. 2: A flow diagram of the experimental setup for treadmill exercise at different speeds to determine failure of the BGB in exercising birds

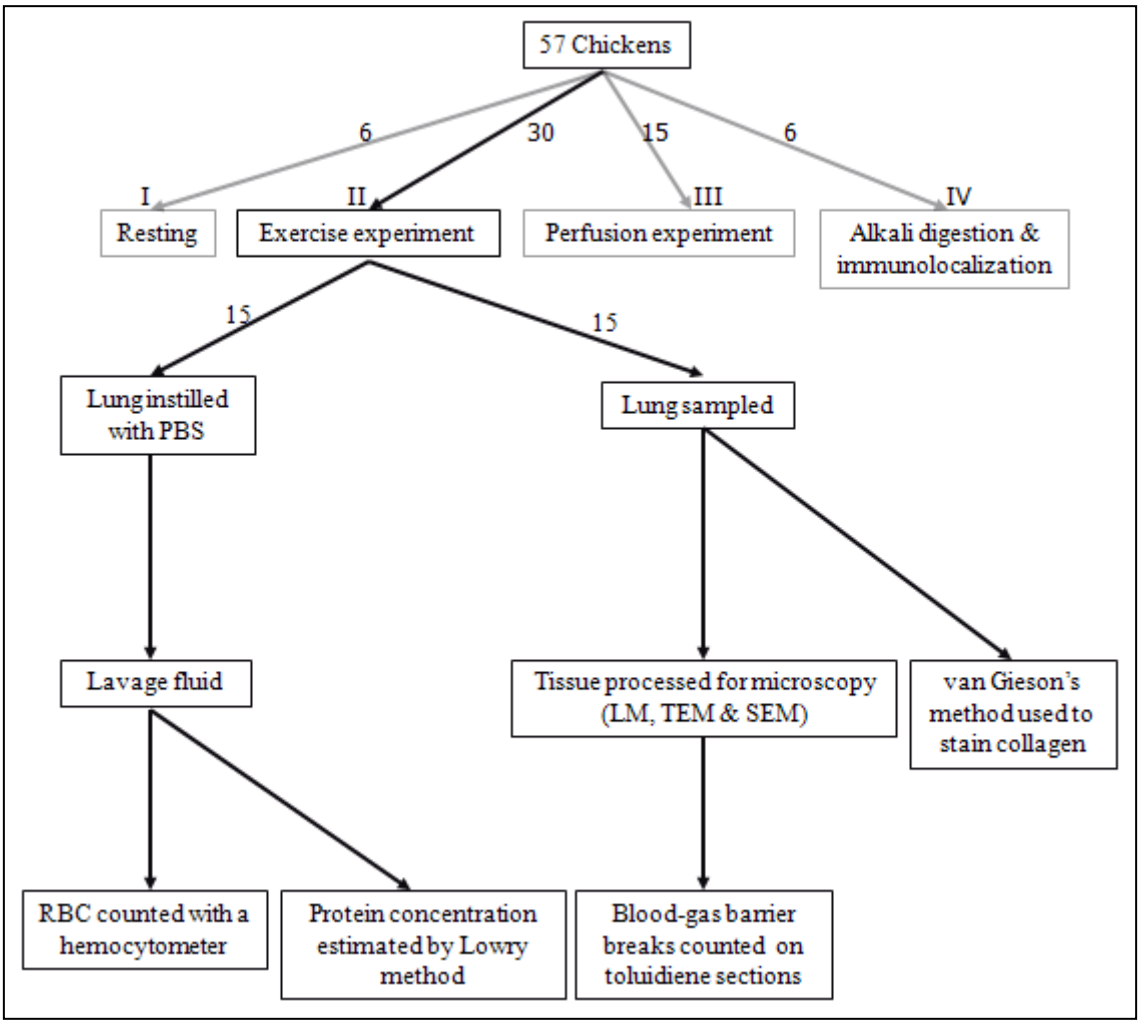

LM: Light microscopy

TEM: transmission electron microscopy

SEM: scanning electron microscopy

Figure 2. 3: A flow diagram of the experimental setup for perfusion at different pressures to determine the pressure at which the BGB starts to fail

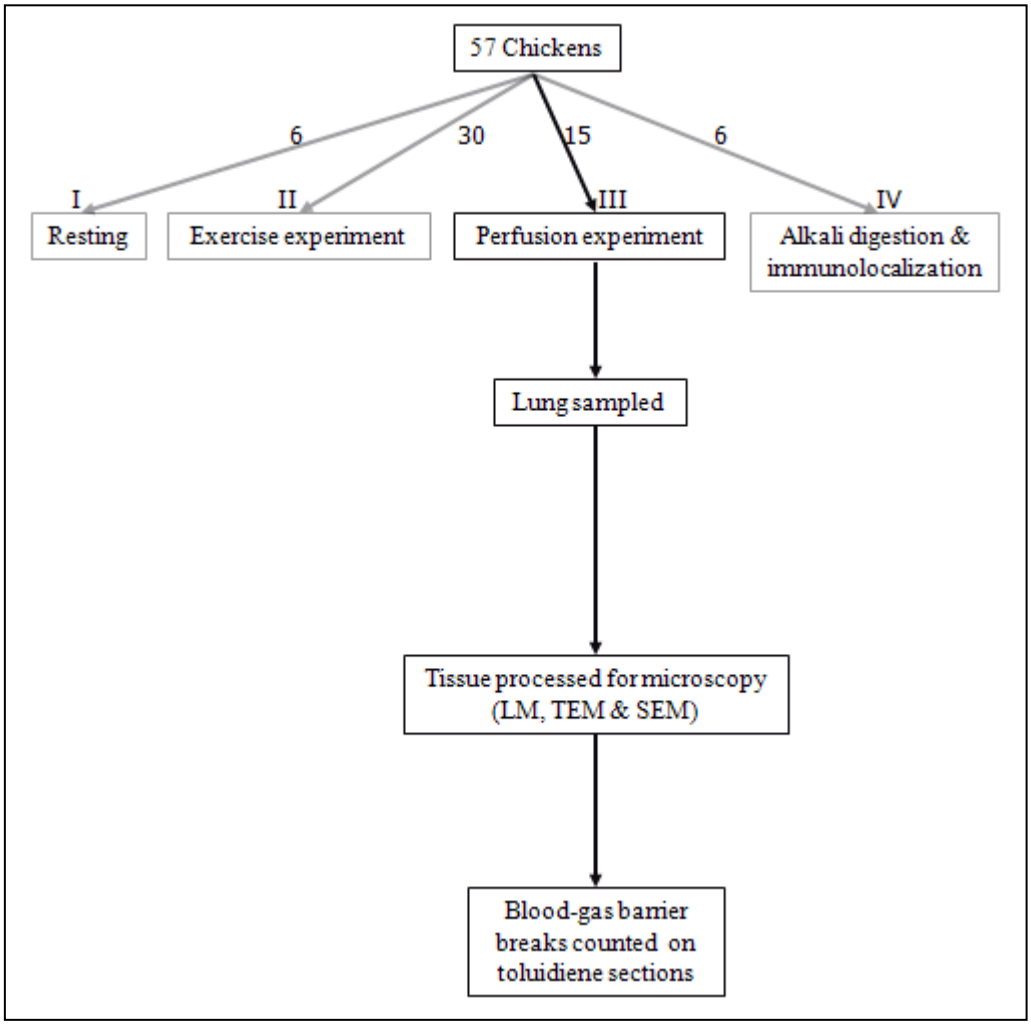

LM: Light microscopy

TEM: transmission electron microscopy

SEM: scanning electron microscopy

Figure 2. 4: A flow diagram of the experimental setup on selective digestion of lung tissue and immuno-localization of type- IV collagen

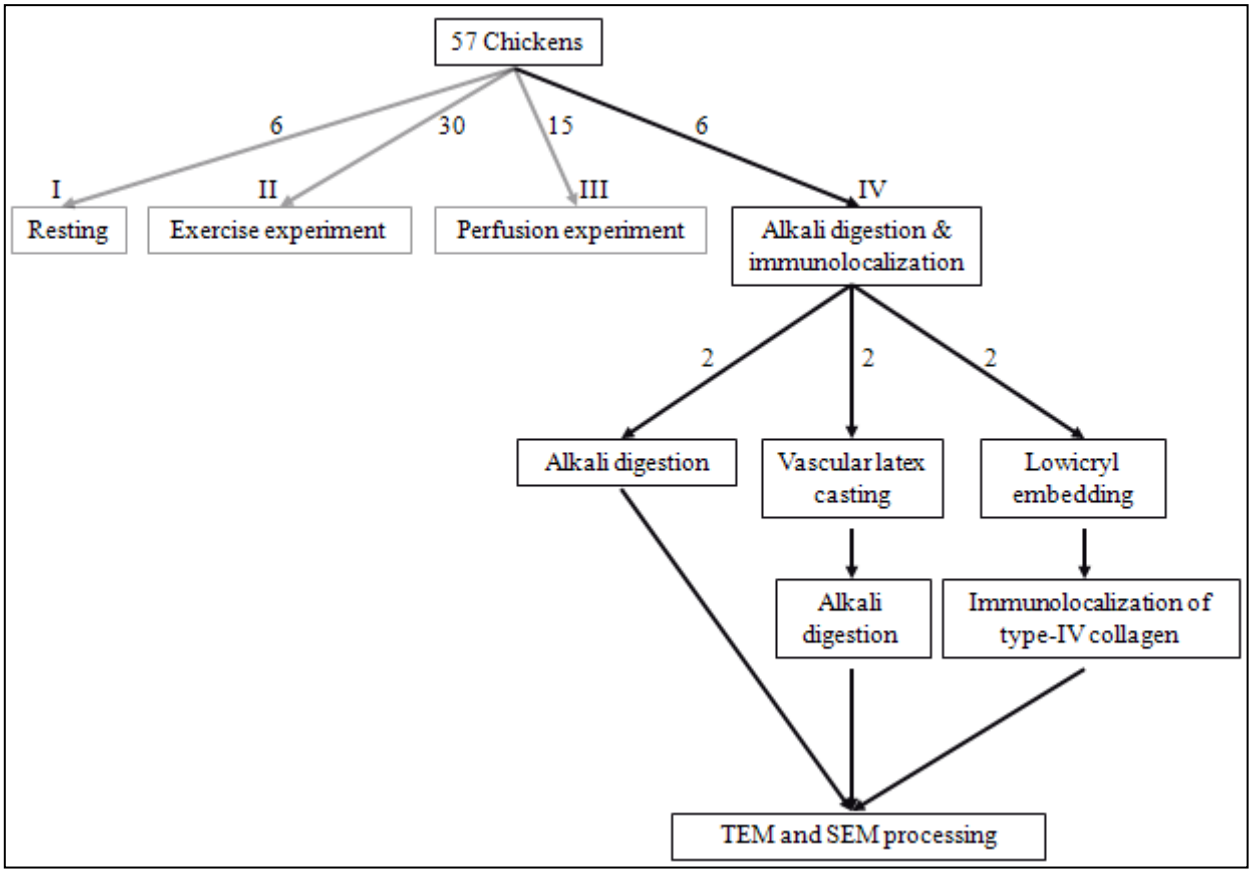

TEM: transmission electron microscopy

SEM: scanning electron microscopy

2.1.3 Summary of the experiments performed and procedures followed

Experiment 1

To answer the question: – *what is the basis of the reported strength of the avian exchange tissue?* The following experiments were carried out:

- Direct collagen staining
- Alkali digestion to reveal collagen fibers
- Casting combined with alkali digestion to reveal collagen fibers
- Immuno-gold localization of type-IV collagen

Experiment 2

To answer the question: - *How susceptible to structural failure is the avian pulmonary blood-gas barrier at rest and during exercise?*

- Treadmill exercise at different speeds
- Measurement of blood lactate concentration
- Lung lavage and determination of:
    - RBC numbers
    - Protein concentration
- Examination of semi-thin Toluidine-blue sections; ultrathin TEM sections, and SEM images

Experiment 3

To answer the question: - *At what intramural pressure does the blood-gas barrier of the avian lung structurally fail?*

- Perfusion at different pressures
- Examination of semi-thin Toluidine-blue stained sections, ultrathin TEM sections, and SEM images

2.2 METHODS

2.2.1 Staining collagen fibers by van Gieson's method

Lungs from the resting (unperturbed) chickens (Fig. 2.1, I) were fixed by intravascular perfusion with 2.5% glutaraldhyde in phosphate buffer solution (pH 7.4) at 1.2 kPa (12 cmH_2O = 9 mmHg) inflow pressure and 0.8 kPa (8 cmH_2O = 6 mmHg) outflow pressure. Tissue samples measuring about 3 x 3 x 6 mm were obtained from a slice of tissue in the region of the third costal sulcus of the right lung. The tissue samples were processed for light microscopy. Standard laboratory methods for paraffin wax embedding (e.g. Bancroft and Steven, 1996) were employed. Sections were cut on a Jung Biocut 2035 rotary microtome at 5-µm thickness. After deparafinization, sections were placed in Weigert's iron hematoxylin solution for 5 minutes and washed briefly in running tap water before rinsing in two changes of distilled water. Subsequently, the sections were placed in van Gieson's solution for three minutes. This was followed by dehydration in three changes of 95% alcohol and three changes of absolute alcohol. After clearing, the sections were put in three changes of xylene, mounted with entellen and cover-slipped. The staining imparted sharp contrast between collagen fibers, which stained red, cell nuclei blue-black, and other tissues yellow.

2.2.2 Revealing lung tissue collagen by alkali digestion

The pulmonary vascular bed was perfused with phosphate buffered saline solution (pH 7.4). The perfusion was quickly followed by intravascular fixation with 2.5% glutaraldhyde buffered in phosphate buffer solution (pH 7.4) at 1.2 kPa (12 cmH_2O = 9 mmHg) inflow

pressure and 0.8 kPa (8 cmH_2O = 6 mmHg) outflow pressure (Fig. 2.4, IV). Tissues samples measuring 5 x 5 x 5 mm were taken from the middle part of the right lung in the region of the third costal sulcus. Lung tissue samples were digested to remove all tissue components except collagen. This procedure was carried out according to the methods described by Ohtani (1987, 1992) and Toshima *et al*. (2004). Briefly, the tissues were placed in 10M solution of sodium hydroxide (NaOH) for a maximum period of six days at room temperature (20^oC). This was followed by washing in distilled water for another four days. When tissues turned whitish and semi-translucent, they were treated with 1% tannic acid solution overnight. After rinsing in distilled water for 4 hours, the tissues were post-fixed in 1% aqueous solution of osmium tetroxide (OsO_4) for 2 hours. The specimens were then dehydrated in a series of graded concentration of ethanol. After critical point drying with liquid carbon dioxide, the samples were freeze-cracked in liquid nitrogen, mounted on aluminum stubs, and observed on a JEOL 840 SEM under an accelerating voltage of 15 kV. Some of the digested tissue samples were processed for TEM after days 3, 4, 5, and 6 of digestion.

2.2.3 Exposing collagen fibers in their normal position by intravascular casting followed by alkali digestion

To effectively reveal the normal, i.e., in-life arrangement of collagen fibers around the blood- and air capillaries, intravascular latex rubber casting of the lung was performed (Fig. 2.4, IV). The setup consists of a reservoir containing phosphate buffered saline (pH 7.4) and 10 cm^3 syringe containing latex rubber. The reservoir and the syringe were connected to the limbs of a Y-tube. The stem of the Y-tube was connected to a tube that was inserted into the pulmonary trunk: the tube was ligated just few millimeters to the bifurcation of the trunk. The pulmonary

vascular bed was thoroughly flushed with phosphate buffered saline after which the vasculature was infused with latex rubber. Once the latex set, it provided a scaffold that preserved the natural spatial arrangement of the collagen fibers: in uncast preparations, during digestion, collagen fibers folded, curled, and collapsed once the supporting lung tissues were removed. The procedure of combining casting and digestion was successfully used by, Gonçalves *et al*. (1995) to study the organization of the elastic fibers in the rat lung. Here, a 10-cm3 syringe was used to inject the latex rubber through the pulmonary trunk until moderate resistance developed in the plunger of the syringe. At that point, the blood vessel was ligated to maintain the intravascular pressure. The bird was put in a cold room (4^{o}C) and continually assessed for progress in the setting of the latex rubber for 1 week. When this was satisfactory, the lung was carefully removed from the body and samples taken for digestion in 10M solution of NaOH as described above. After digestion, the tissues were left in running tap water for about 6 hours before they were processed and viewed on a JEOL 840 SEM.

2.2.4 Immuno-electron staining of type-IV collagen fibers

After vascular perfusion-fixation with 4% paraformaldehyde and 0.025% glutaraldehyde in 0.05% saturated solution of picric acid in phosphate buffer pH (7.4), 1 mm^3 lung tissue samples were taken from the middle part of a transverse slices acquired from the region of the third costal sulcus (Fig. 2.4, IV). Samples were washed in 0.1 M phosphate buffer for 6 hrs. Thereafter, the samples were dehydrated in graded strength of ethanol as follow: 30% methanol for 5 min at 4^{0}C; 50% methanol for 10 min at -10^{0}C; 75% methanol for 10 min at -10^{0}C; 90% methanol for 15 min at -20^{0}C; 90% methanol for 15 min at -20^{0}C. Infiltration of

the dehydrated tissue samples with Lowicryl was carried out as follows: 1:1 lowicryl: 90% methanol at -20^{0}C for 1 hr; 2:1 lowicryl: 90% methanol at -20^{0}C for 1 hr; 100% lowicryl at -20^{0}C for 1 hr. After infiltration, tissue samples were placed in beam capsules already pre-cooled in a freezer set at -35^{0}C. The capsules were filled with fresh 100% lowicryl and polymerized under UV light at 30 cm distance for 3 days at 4^{0}C. Thin sections were cut on Reichert Jung Ultracut® and sections were mounted on gold grids. Immuno-staining of the sections followed the method of Lemanski *et al*. (1985). Briefly, sections mounted on gold grids were placed in a drop of phosphate buffered saline (PBS) for 15 minutes. The grids were then transferred to a drop of 100% goat serum for 30 minutes. Without rinsing, the grids were transferred to a drop of primary antibody (50% strength, type-IV collagen ABCAM®) for 90 minutes. The grids were then rinsed in PBS 3 x 20 minutes and afterwards placed in a drop of 100% goat serum for 30 minutes. Without rinsing, the grids were placed in gold conjugated secondary antibody (50% strength, ABCAM®) for 45 minutes. Afterwards, the grids were rinsed in PBS 3 x 20 minutes then in water and blotted dry. The grids were then counterstained in lead citrate and uranyl acetate. The sections were viewed on JEOL100S electron microscope at 80 kV.

2.2.5 Appropriateness of the antibodies

Type IV collagen is an evolutionary constant that is represented in all animal phyla (Boute *et al*., 1996; Exposito *et al*., 2002). It is the most abundant protein within all basement membranes (Kalluri, 2003). In the basement membrane, type IV collagen forms a network, to which other basement membrane molecules attached or within which they are sequestered

(Hudson *et al*., 1993; Kalluri, 2003). Type IV collagen is described as the only known ubiquitous collagen that has at least two different alpha chains in all the species where it has been characterized (Boute *et al*., 1996). Structure of type IV collagen has been conserved from nematodes to mammals (Kramer, 1994; Kuhn, 1994). Immunohistochemical study of reactivity to same antibody against type IV collagen in the sections of the integument from vertebrate connective tissue, gastropod, bivalve and cephalopod confirmed that the structure and composition of basement membrane have remained constant throughout the evolution of all animal phyla (Corbetta *et al*., 2002). It is against this firm establishment of sequence homology that polyclonal primary antibody raised against type IV collagen in rabbit (ABCAM ®) was used to localised type IV collagen in the avian blood gas barrier and in the contacts between the air capillaries. The gold conjugated polyclonal secondary antibody specifically raised in goat against rabbit bind to the primary antibody which binds to type IV collagen and rendered it visible.

2.2.6 Lung lavage

After killing by injection of 5 ml of thiopentone sodium (25 $mg.cm^{-3}$) into the right brachial vein, the birds were placed in a supine position in a dissecting tray, the skin around the neck was incised, reflected, and the trachea were exteriorized. The trachea was cannulated using a Tygon® tubing inserted through a slit made between cartilages of the exposed trachea. The other end of the tube was connected to a funnel. With the funnel held 30 cm above the sternum (e.g. Nganpiep and Maina, 2002) phosphate buffered saline (pH 7.4) warmed to 40^0C was instilled into the respiratory system. During instillation, the birds were gently rocked from side

to side to displace air in the pulmonary system. The fluid was left in the respiratory system for 10 minutes after which it was collected by gravity.

2.2.6.1 Red blood cell counts

A standard hemocytometer with Neubauer markings (chambers) and its special cover slip were thoroughly cleaned. After the collected lavage fluid was well stirred up, a drop of the liquid was gently introduced into the V-shaped well of the hemocytometer underneath the coverslip with a pipette. Enough fluid was introduced so that the mirror surface under the cover slip was completely filled by capillary action. At 400X magnification, RBCs were counted in the four squares at the corners plus the square in the center. Cells that overlapped the top or right boundary of the counting area were counted as "in" while those that overlapped the bottom or left boundary of the counting area were counted as "out". Since each square counted had an area of 1/25 mm^2 (0.04 mm^2) and a depth of 0.1 mm, the volume of liquid over each square was 0.004 mm^3. The combined volume of the five squares used in the counting was 0.02 mm^3. The number of RBCs counted in the five squares divided by the combined volume gives the total number of RBC in one mm^3. This number was then multiplied by 1000 to give the number of RBC in one cubic centimeter (1 ml) of the liquid.

2.2.6.2 Total protein estimation by Lowry's method

The Lowry method of total protein estimation is based on Biuret and Folin-Ciocalteau reactions (Lowry *et al.,* 1951). In Biuret reaction, peptide bonds of proteins react with copper under alkaline conditions to produce copper ions. Copper ions in turn react with the Folin

reagent. Folin-Ciocalteau reaction involves phosphomolybdotungstate reduction to a blue heteropolymolybdenum by copper catalyzed oxidation of aromatic amino acids (Lowry *et al.*, 1951). Lowry method is sensitive down to about 0.01 mg of protein/ml and is accurate on solution with protein concentrations in the range 0.01–1.0 mg/ml.

Method: One-milliliter eppendoff tubes were used for the test. A triplicate of 50 µl each of the serial diluted working solution of BSA (Appendix I) were put in eppendoff tubes. The collected lavage fluid was also prepared in triplicate. Two hundred micro liters of reagent A (Appendix I) was added to the contents of each eppendoff tubes. The mixtures were left on a mechanical shaker for 10 minutes at room temperature. Fifty micro liters of reagent B (Appendix I) was added to the content of each tube. They were left on the shaker for another 30 minutes. Absorbance of each of the solutions in a microtiter well were read at 690 nm using Labsystems Multiskan Ascent (Amersham Pharmacia, Buckinghamshire, UK). Absorbance values of the BSA standards were plotted against concentrations to create a standard curve. Protein concentration of the lavage fluid sample was calculated using the derived mathematical equation relating the absorbance of the BSA standard to concentration obtained from the graph (see appendix II).

2.3 THE EXPERIMENTS

2.3.1 Resting chickens

Six mature chickens were used for this experiment (Fig. 2.1, I). Pulmonary lavage was done on three of the chickens and lungs from the remaining three were fixed and processed for electron microscopy. To avoid agitating the birds, at the commencement of the experiment, each bird was held in isolation in a small holding cage for two hours. With extra care not to perturb the calmed bird, they were in turn gently taken out of the cage. Each of the birds were carefully handled and injected with 2.5 cm^3 heparin (1000 IU) through the left brachial vein. After 10 minutes of heparin circulation, the birds were euthanized by injection of 5 ml of thiopentone sodium (25 $mg.cm^{-3}$) into the right brachial vein. The first three of the six chickens were placed in a supine position in a dissecting tray (Figs. 2.2, II and 2.5) and the trachea exteriorized. Tygon® tubing connected to a funnel was inserted through a slit made in the exposed part of the trachea. After tracheal instillation with warm phosphate buffered saline (PBS), the number of red blood cells in the recovered fluid was counted with a hemocytometer (Section 2.2.5.1) while protein concentration was determined by the Lowry method (Lowry *et al.*, 1951) (section 2.2.5.2). After opening the thorax and exposing the pulmonary artery and vein, the lungs of the three remaining chickens were first perfused with warmed (40^oC) phosphate buffered saline (pH 7.4) for 2-3 minutes then fixed *in situ* by perfusion with warmed (40^oC) 2.5% glutaraldehyde buffered in phosphate solution (pH 7.4) at an inflow pressure of 12 cmH_2O (1.2 kPa = 8.8 mmHg). The outflow tube was placed at the level of the sternum to register 0 cmH_2O (0.0 kPa = 0.0 mmHg) on the outflow manometer. Thereafter, the

lungs were removed from the thorax, immersed in the same fixative, and stored at 4^0C before processing for electron microscopy.

2.3.2 Exercise experiment

Thirty healthy adult chickens of both sexes weighing between 1,500 and 2,500 grams were used for this experiment (Fig. 2.2, II). Pulmonary lavage was carried out on 15 of the chickens and lungs from the remaining 15 processed for transmission- and scanning electron microscopy after *in situ* perfusion fixation.

2.3.2.1 The treadmill

Collins treadmill® machine (Fig. 2.5) powered by a single electric motor with a variable speed of between 0.5 and 3.0 ms^{-1} was used for this experiment. The 45 cm wide and 350 cm long belt has a rough surface which gave good traction. About 150 cm of the total belt length is available to the exercising animal. Steel wire mesh walls built over the machine provided side enclosure while a perspex sheet supported just above the running bird prevent them from jumping off the running surface. The exercise schedule is as presented in Table 1.

Figure 2. 5: Collins treadmill® machine

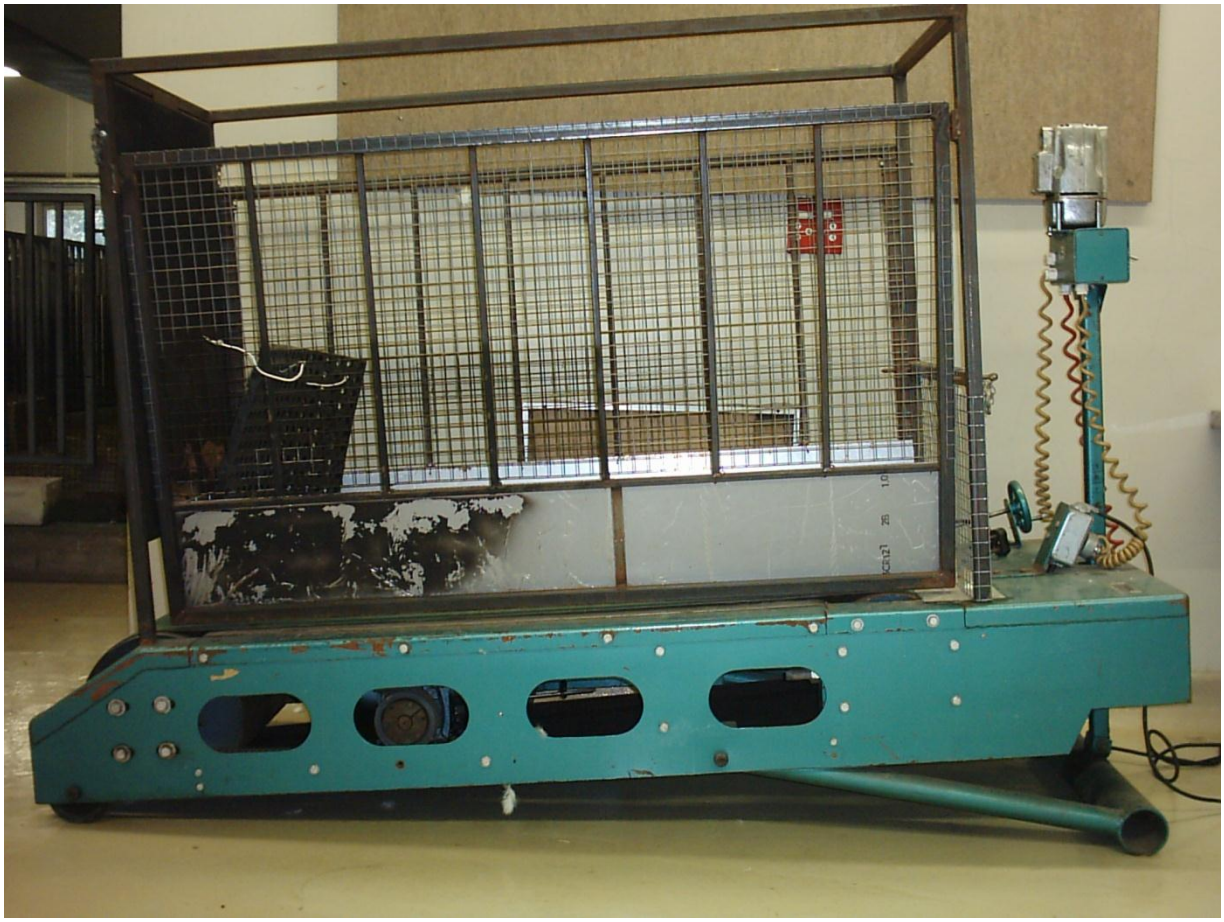

Figure 2.5 legend:

Collins treadmill® machine with a variable speed of between 0.5 and 3.0 ms^{-1}. A steel cage built over the machine enclosed 45 cm by 350 cm belt area which is available to the bird during exercise.

Table 1: Running exercise schedule and post exercise handling of birds

Number of birds	Treadmill speed* (m/s)	Duration of exercise (min)	Post exercise handling	
			Number of birds for protein estimation and RBC count	Number of birds for BGB failure determination
6	Resting chicken	0	3	3
6	0.66	10	3	3
6	0.98	10	3	3
6	1.97	10	3	3
6	2.53	10	3	3
6	2.95	10	3	3

* Running speed was arbitrarily chosen within the range achievable on the treadmill machine used for the experiment. However, the interval between speeds was systematised to reflect discrete increases. The birds were not run on the machine prior to the experiment to avoid any physiological or morphological changes in the lung that may affect the outcome of the intervention.

2.3.2.2 Preparation of the birds for exercise

Before the start of the experiment, the birds were familiarized with the surroundings and the sound of the machine by placing them close to the treadmill machine in the morning for 1hr every day for two weeks. They were also allowed to play, peck, and perch on the machine. The birds were, however, not run on the machine prior to the experiment to avoid any unaccounted for physiological or morphological changes in the body and the lung in particular. The experiment was carried out in the morning within the animal holding facility of the University of Witwatersrand's Central Animal Services at room temperature of 20^{o}C.

Although it was practically impossible not to agitate the birds, every care was taken to minimize disturbances that could raise their heart and respiratory rates. For instance, the birds were kept in small holding cages for two hours before the experiment. They were quietly approached and gently placed legs first on the treadmill while the machine was running at the lowest speed. When the bird started walking, the speed of the belt was slowly increased to the desired level. Sedation of the birds was considered but avoided because of possible effect it might have on the outcome of the experiment. Before the start of exercise and immediately after exercise, blood lactate concentration was measured with Lactate Plus®. The comb was gently pricked with a thin lancet. One end of the test strip was inserted into the meter and the other end was brought close enough to just touch a drop of blood. After approximately 10 seconds, the lactate meter displayed blood lactate value on its screen. Three such readings were taken before and after exercise for each bird (Appendix III). Following exercise, three chickens out of the six in an exercise protocol were euthanized by injecting 5 cm^{3} of thiopentone sodium (25 mg cm^{-3}) into the brachial vein. Lavage of the lung was carried out by

instilling between 200 and 300 ml (depending on the size of the bird) of freshly prepared warm (40^{o}C) PBS into the trachea. Instillation was done with a funnel held 30 cm above the sternum. After 10 minutes in the pulmonary system, the instilled fluid was recovered by gravity: The numbers of RBC in the recovered fluid (Appendix IV) was determined using a hemocytometer (see Section 2.2.5.1) and protein concentrations were estimated (Appendix V) using Lowry method (see section 2.2.5.2). The remaining three birds in the same exercise plan were first injected with 2.5 cm^3 heparin (1000 IU) through the left brachial vein. After 10 minutes of circulation in the blood, the birds were euthanized by injecting 5 ml of thiopentone sodium (25 $mg.cm^{-3}$) into the right brachial vein. The thorax was opened and the pulmonary artery and vein exposed. After 2-3 minutes of flushing the pulmonary circulation with warmed phosphate buffered saline (pH 7.4), the lungs were fixed *in situ* by vascular perfusion with warmed 2.5% glutaraldehyde buffered in phosphate solution (pH 7.4) at an inflow pressure of 12 cmH_2O (1.2 kPa = 8.8 mmHg). The outflow tube was placed at the level of the sternum (7 cmH_2O (0.7 kPa = 5.3 mmHg)). Thereafter, the lungs were removed from the thorax, immersed in the same fixative, and stored at 4^{0}C before processing for electron microscopy.

2.3.3 Perfusion experiment

Fifteen healthy adult chickens of both sexes, weighing between 1,500 and 2,500 grams, were used for this experiment (Fig. 2.3, III). The birds were first injected with 2.5 cm^3 heparin (1000 IU) through the left brachial vein and after 10 minutes of circulation in the blood, the birds were euthanized by injecting 5 cm^3 of thiopentone sodium (25 $mg.cm^{-3}$) through the right brachial vein. The perfusion plan is shown in table 2 (below).

Table 2: Perfusion schedule

	Number of birds	Inflow pressure (kPa)	Outflow pressure (kPa)	Capillary pressure* (kPa)
Resting chicken	3	1.18	0.69	0.93
Expt. 1	3	1.67	1.18	1.42
Expt. 2	3	2.16	1.67	1.91
Expt. 3	3	2.65	2.16	2.4
Expt. 4	3	3.14	2.65	2.89
Expt. 5	3	3.63	3.14	3.38

*****The mean pulmonary capillary pressure was calculated as the average of the inflow pressure (pressure in the pulmonary artery) and the outflow pressure (pressure in the pulmonary vein) (e.g. Bhattacharya *et al*., 1982). Starting from the pressure established during pilot study to cause least number of failures, the perfusion pressure was raised by 5-unit interval up to the highest pressure in this experiment. The idea behind this study was to determine the pressure at which the blood gas barrier will start to fail with no intention to reproduce natural fluid dynamics.

2.3.3.1 Surgical preparation of the birds

With the bird in a supine position, the thorax was opened by cutting away the flight muscles and their attachment to the sternum and the coracoids, the pericardial sac was incised and the adipose tissue around the root of the pulmonary trunk was cleared up to where the vessel bifurcates. Slits were made on the right ventricle and the tip of the left ventricle to access the cavities. The inflow tube was inserted through the slit in the right ventricle and pushed up to rest in the pulmonary trunk. Outflow tube was inserted through the opening at the apex of the heart and pushed past atrioventicular valve into the left atrium. The connections were held in place by ligatures. This arrangement isolates the pulmonary circulation from systemic circulation (Fig. 2.6A). Pressure in the pulmonary capillary bed was taken as the average of the pressures registered by the inflow and outflow manometers (Bhattacharya *et al*., 1982).

2.3.3.2 Perfusion set-up

Two glass funnels clamped at a determined height on a retort stand (Fig. 2.6B) served as inflow reservoir for fixative and PBS. Through a system of connected Tygon® tubing, the funnels were connected to a three-way valve which was in turn connected via a T-tube to a glass tube (0.5 cm internal diameter and 50 cm in height) that served as a manometer for the inflow pressure. The third end of the T-tube was connected to another tube that was passed into the heart through a slit in the right ventricle. A ligature (in the pulmonary trunk) just before it bifurcated into right and left branches was used to hold the tube place. Another manometer, which measured the outflow pressure, connected the outflow tube to a collecting reservoir. The two manometers were graduated in centimeters. Adjustment of the inflow

pressure was done by changing the height of the inflow reservoir while the outflow pressure was adjusted by changing the height of the collecting reservoir. The perfusates (PBS and fixative) were maintained at 40 ^{0}C in a water bath. The whole set-up was thoroughly checked for presence of air bubbles and if any was noticed, care was taken to remove the bubble before the start of experiment. By turning the three-way valve, the PBS reservoir was opened and run for a maximum of three minutes to flush out RBC within the pulmonary circuit. Immediately after PBS flushing, the three-way valve was turned to open the reservoir for the fixative. Perfusion fixation was allowed to run until 400–500 ml of fixative passed through the pulmonary vascular bed. After perfusion fixation, the lung was gently removed from its vertebrocoastal insertions, placed in fresh fixative, and stored at 4 ^{0}C.

Figure 2. 6: A: Isolation of the pulmonary circulation. B: Perfusion setup

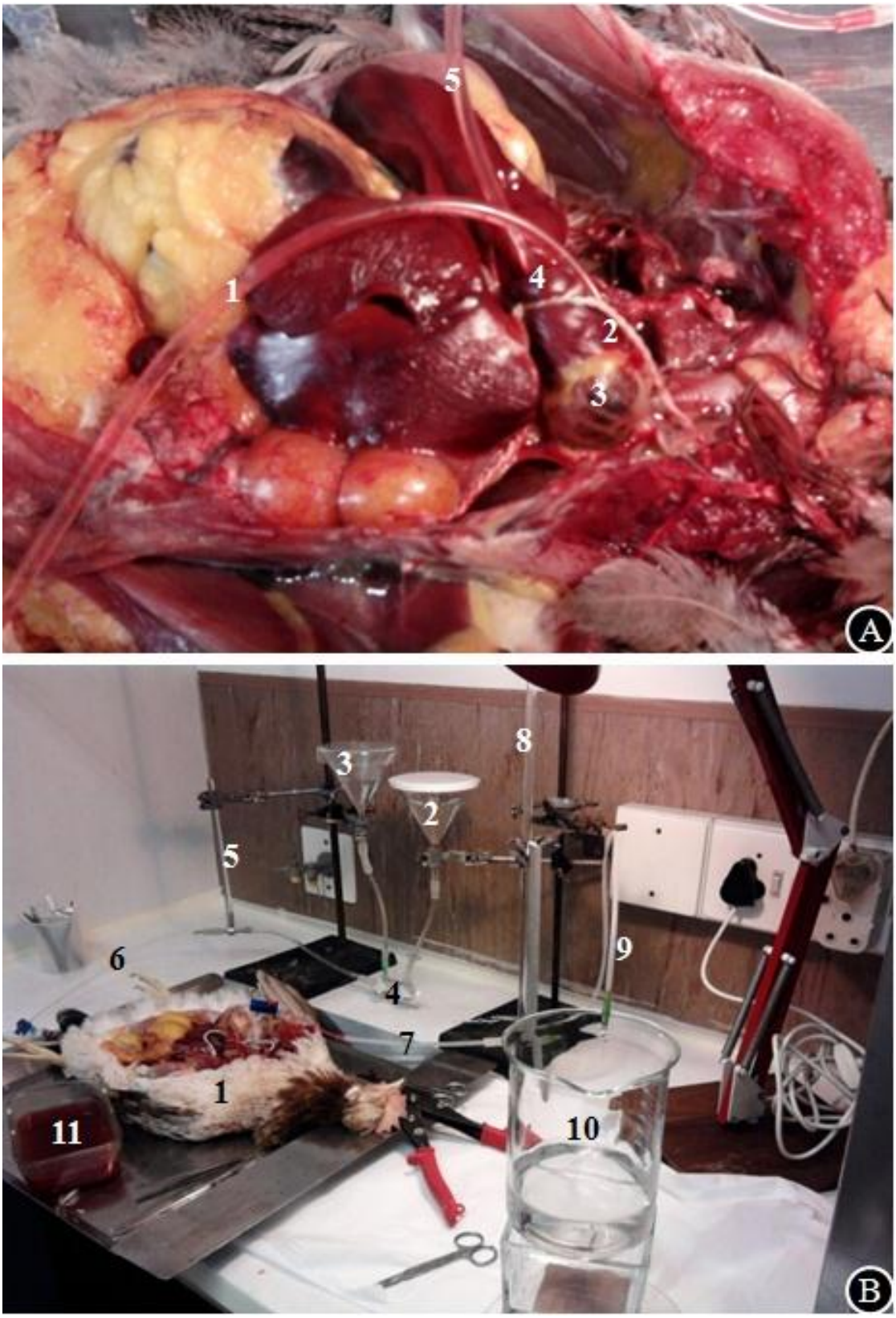

Figure 2.6 legend:

A. Close up of the connections of the heart to the perfusion apparatus. The connections isolated the pulmonary circulation from the systemic circulation. The inflow tube (1) passed through a slit in the right ventricle (2) and into the pulmonary trunk. The left atrium (3) collected the perfusate after passing through the pulmonary vascular bed. Inserted through the left ventricle (4), an outflow tube (5) which terminated in the left atrium drained the lungs.

B. Pulmonary perfusion in set-up: - **1**: Chicken in a supine position with thorax opened and the pulmonary circulation isolated and coupled to inflow and outflow tubes of the perfusion apparatus. **2:** PBS inflow reservoir to flush the pulmonary vascular bed. **3**: Fixative inflow reservoir for intravascular fixation of the lung. **4**: Three-way valve for controlling fluid flow in the perfusion circuit. **5**: Glass-tube manometer to register inflow pressure. **6**: Inflow tube to carry fluid through the right ventricle into the pulmonary trunk. **7**: Outflow tube carries fluid from the left atrium through the left ventricle out of the pulmonary circuit. **8**: Glass-tube manometer for registering outflow pressure. **9**: Adjustable outflow tube from the manometer empties into the outflow reservoir: the height of this tube determines the outflow pressure. **10**: Outflow reservoir containing used fixative. **11:** Glass bowl containing flushed out blood.

Figure 2. 7: Two different views of an exercising birds

Figure 2.7 legend:

Two different views (A, rear view; B, side view) of a chicken exercising on a treadmill. The steel cage wall and the Perspex slab at the back confined the bird to the treadmill.

2.3.4 Tissue sampling

Transverse slices of the lung were cut along the costal sulci. Tissue samples were taken from the regions perfused by the four main branches of the pulmonary artery (the cranial-, the accessory-, the caudomedial- and the caudolateral branches) (Abdalla, 1989) (Fig. 2.8). An acetate paper with six-millimeter by six-millimeter areas drawn on it and divided into 1 mm by 1 mm squares was placed on the surface of a lung slice. Random numbers were generated using random number generator (free software) and samples (four) were taken from sites corresponding to the generated number. The tissue samples were processed for electron microscopy.

Figure 2. 8: Process of lung tissue sampling for microscopy

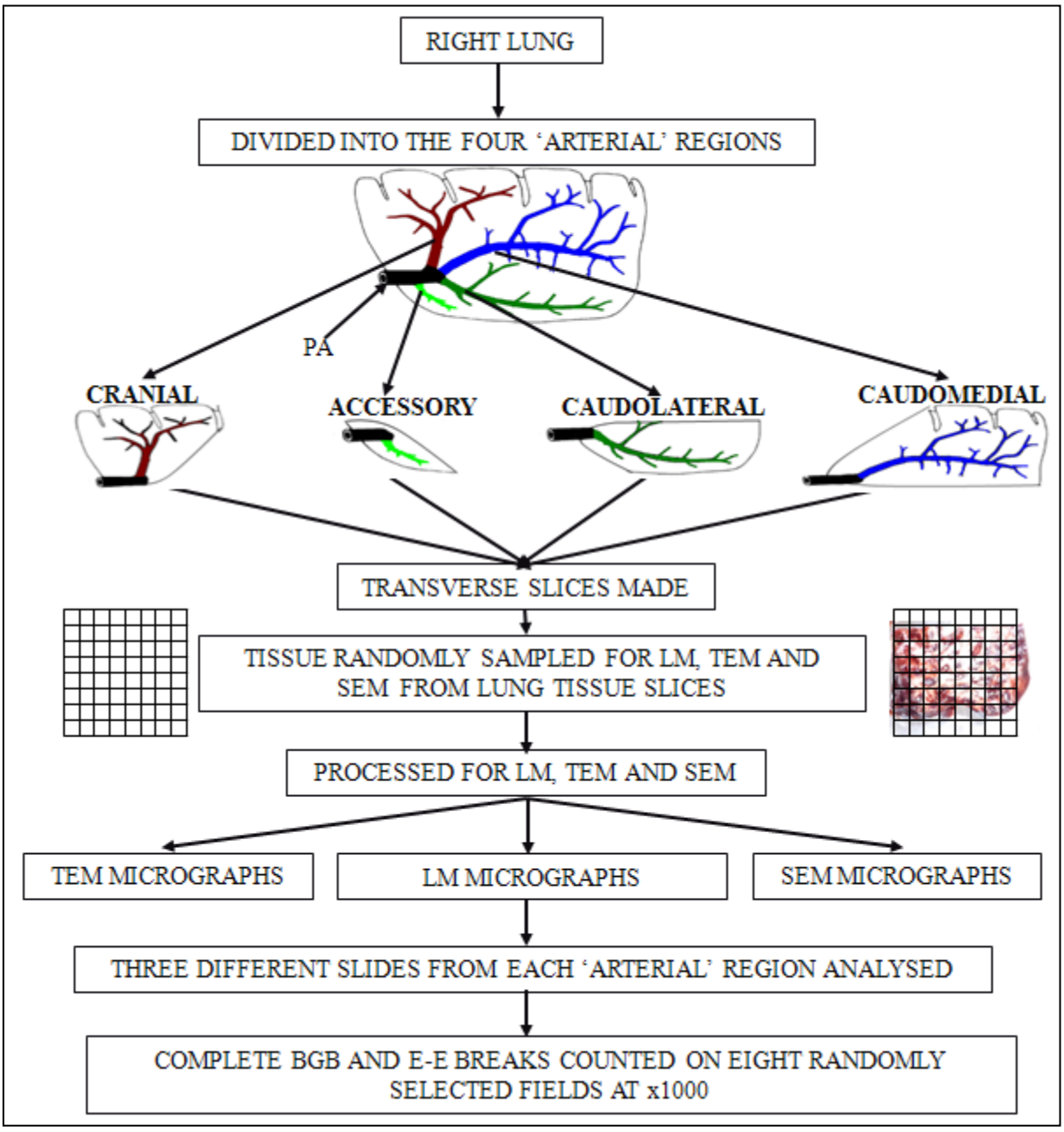

LM: Light microscopy

BGB: blood-gas barrier

PA: Pulmonary artery

SEM: scanning electron microscopy

TEM: transmission electron microscopy

E-E: epithelial-epithelial contact

2.3.5 Tissue processing for transmission- (TEM) and scanning electron microscopy (SEM)

Fixed tissues were processed for TEM and SEM by standard laboratory techniques. Tissue samples were postfixed for 2hr in 1% osmium tetraoxide, rinsed in two changes of phosphate buffer, dehydrated in increasing concentrations of ethanol, rinse in two changes of propylene oxide and embedded in epoxy resin. Randomly selected blocks were sectioned on a Reichert-Jung ultra microtome. Semi-thin sections were stained with 0.1% aqueous solution of Toluidine blue and examined under a light microscope. Ultrathin sections were cut, collected on copper grids, and stained with uranyl acetate and lead citrate before viewing with a JEOL100S transmission electron microscope. Captured images were edited using photoshopelement® 8.0.

Figure 2. 9: Non-biased lung tissue sampling based on vascular supply territories of the pulmonary artery

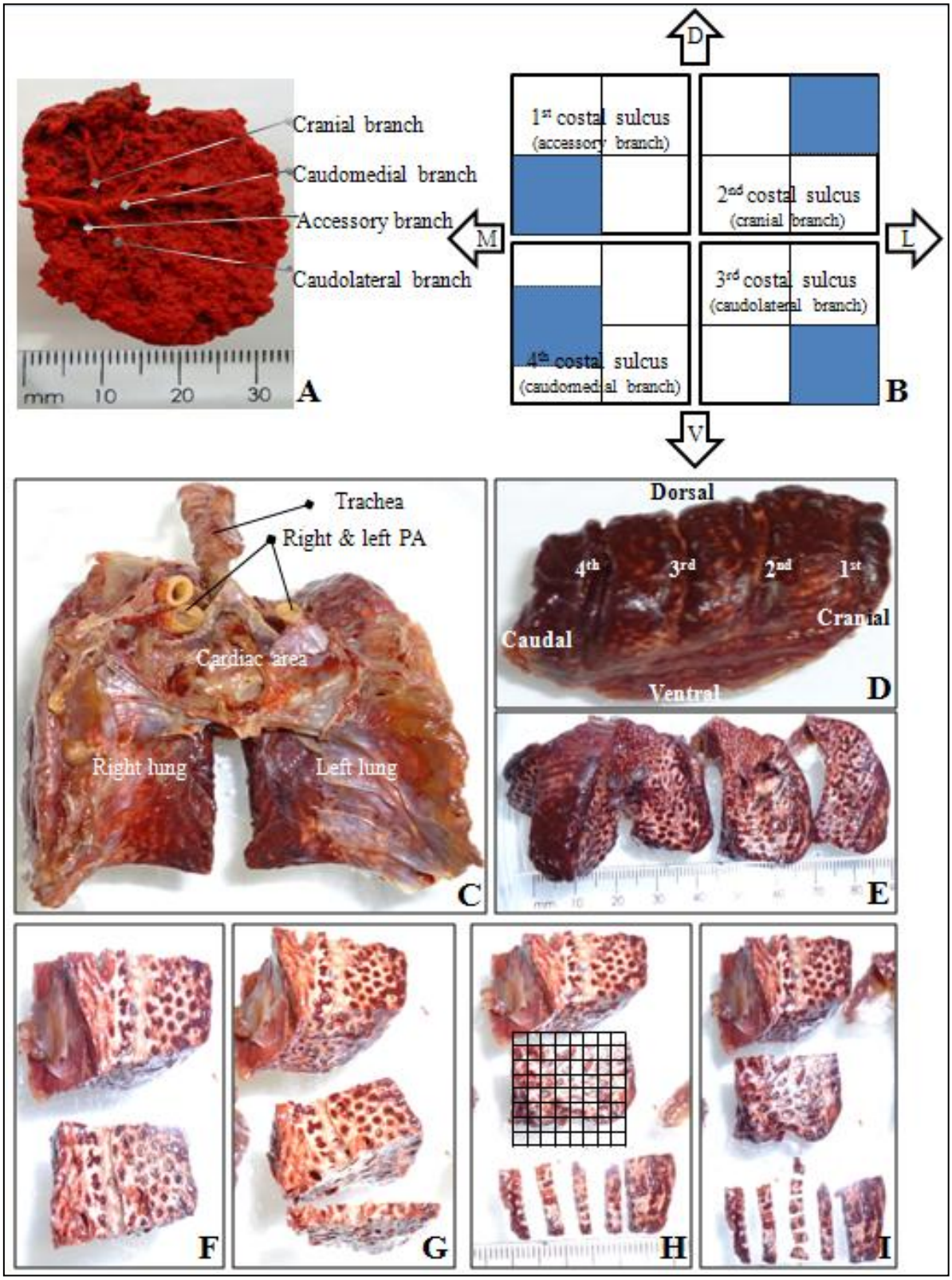

Figure 2.9 legend:

A: Based on the four branches of the pulmonary artery described by Abdalla (1989) the lung was divided into the four vascular areas: the *accessory*, the *cranial*, the *caudomedial* and the *caudolateral* territories. The lungs were sliced along the costal sulci and an approximate vascular area was mapped out for each of the four branches. **B**: The ventromedial quadrant of the posterior surface of the first slice is the exclusive vascular area of *accessory* branch. The dorsolateral quadrant of the anterior surface of the second slice is the exclusive vascular area of *cranial* branch. The ventrolateral quadrant of the anterior surface of the third slice is the exclusive vascular area of *caudolateral* branch. An area straddling both the dorsal– and ventral - medial quadrant of the anterior surface of the fourth slice is the exclusive vascular area of *caudomedial* branch. After removing the lung (**C**) from the thoracic cage, the right lung was divided along the costal sulci (**D-E**). Except for the first slice, anterior surface of each slice were randomly sampled using a 1 x 1 mm numbered grids drawn on a transparent paper. **F**: Each slice was divided into upper and lower halves along the plain of the primary parabronchus. **G.** 1mm thick slice was cut from either half depending on the vascular territory. **H**: One millimeter by one millimeter numbered grid on an acetate paper was placed on the flat surface of the slice to cover most of the area of interest. Random number between 1 and 36 is generated. **I**: Area of lung tissue corresponding to the generated number was cut out and samples were taken for microscopy as follow:

5 x 5 x 6 mm lung tissue were cut out for light microscopy

1 x 1 x 2 mm lung tissue were cut out for transmission electron microscopy

3 x 4 x 6 mm lung tissue were cut out for scanning electron microscopy

2.3.6 Statistical Method

Data were expressed as means ± SE. The SE of the estimates of number of failures in an area that covers 100 μm^2 at 1000x indicates the variability between individual measurements. The variability between micrographs was obtained by pooling the data of the micrographs from eight randomly selected areas per tissue block. The variability between blocks was obtained by pooling the data from four blocks per each of the four branches of the pulmonary artery. Group means were compared by Student's *t*-test. Differences were taken as significant for $P < 0.05$. Statistical analysis was performed using Microsoft Excel®.

CHAPTER III

3. RESULTS

3.1 COLLAGEN FIBERS

3.1.1 van Gieson's staining

In cross-sectional view, thick bands of collagen connective tissue, which make up the inter-parabronchi septa, conspicuously take up red color. The color provided sharp contrast between red color of the fibers and cell nuclei which were stained blue black and other tissues which stained light yellow (Fig. 3.1). In spite of wide spaces caused by tissue shrinkage, the rough hexagonal outlines of the interparabronchi septa that delimit the exchange tissue (mantle) of the parabronchi (Fig. 3.1A) were conspicuous. The parabronchi, the third level of airways of the avian lung were closely packed. A thick band of connective tissue, the interparabronchial septum, separated the parabronchi. In cross-section, the parabronchi had roughly a hexagonal shape (Fig. 3.1A). The interparabronchial blood vessels with their collagen-rich tunica adventitia (Figs. 3.1B, D) gave out fibers that run into the exchange tissues of adjacent parabronchi. The intraparabronchial arteries branched off from the interparabronchial arteries and entered the exchange tissue (Fig. 3.1B). The intraparabronchial arteries were also invested with collagen connective tissue, tunica adventitia (Fig. 3.1A, B). Collagen connective tissue fibers (forming the tunica adventitial of the vessels) are given out as the blood vessels branched into smaller vessels within the exchange tissue (Fig. 3.1D). At the capillary level, the connective tissue sheet was reduced to thin strands of collagen fibers that were sandwiched between the endothelial- and the epithelial cells (Fig. 3.1E). Although most fibers from the interparabronchial septa entered the exchange tissue indirectly by following the blood vessel, some fibers, however, entered the exchange tissue directly (Fig. 3.1D). Even though, the histological sections are in two-dimension, continuous collagen cable could be followed from the peripheral part (interparabronchial septum) of the parabronchus to the interatrial septum.

Thick bundles of collagen fibers (Figs 3.1A-C.) surrounded atrial openings, which connect the exchange tissue to the parabronchial lumen. Bordering the parabronchial lumen and surrounding the entrances into atria were prominent atrial muscles (Figs. 3.1A-D, F). Collagen connective tissue fibers surrounded and interconnected with the atrial smooth muscles and extended into the atrial septa (Fig. 3.1F). Collagen fibers, together with other connective tissues, formed the core of the interatrial septa (Fig. 3.1F-H). Prominent interatrial septa and its core of connective tissue separated the atria (Fig. 3.1F-H). Collagen-rich cores of the atrial wall thinned-out as they projected into the exchange tissue where they became part of the infundibular wall and ultimately became the basement membrane collagen fibers that were sandwiched between the endothelial- and epithelial cells of the BGB (Fig. 3.1E). The fibers, though scarce, followed the division of the atria into infundibulae and ultimately, the air capillaries (Fig 3.1E).

The high density of collagen fibers at the peripheral and luminal parts of the parabronchus imparted an intense red color to these regions at low magnification (Figs. 3.1B; C). At higher magnification, branches of collagen fibers were seen to enter the peripheral part of the exchange tissue from the collagen fibers around blood vessels located within the interparabronchial septa (Fig. 3.1D). The branches run the whole thickness of the exchange tissue and as they left the exchange tissue and run towards the parabronchial lumen (Figs. 3.1B, C, F, H), they converged on the inter-atrial septa where they interfaced with elastic tissues and smooth muscle cells (Figs. 3.1F, H). The spatial distribution of the collagen fibers divides a parabronchus into three parts: the peripheral, the intermediate and the central parts.

Figure 3. 1: Exchange tissue of the domestic fowl stained for collagen fibers by van Gieson method

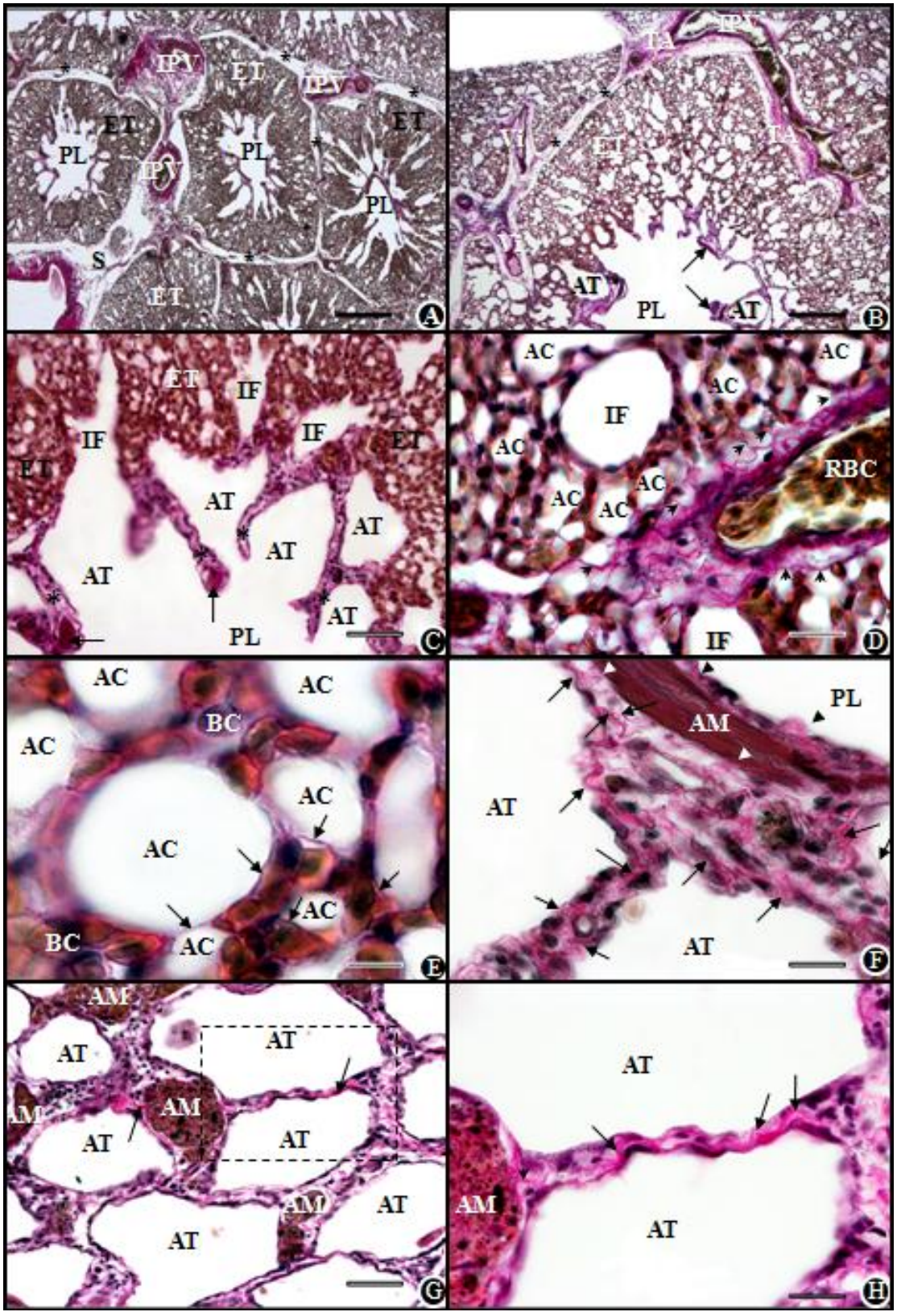

Figure 3.1 legend:

A: Interparabronchi septa (*) which contain interparabronchial vessels (IPV) separated the roughly hexagonal shaped parabronchi. Wide spaces (S) between parabronchi are caused by tissue shrinkage. A parabronchus comprises of an exchange tissue (ET) mantle which surrounds a lumen (PL). Scale bar, 400µm. **B**: Close-up of a part of a parabronchus. Interparabronchial vessel (IPV) on the outer border of the exchange tissue (ET) mantle gave rise to intraparabronchial vessels (Vi) which carried collagen fibers into the exchange tissue. Collagen rich tunica adventitial (TA) of the interparabronchial vessel (IPV) as well as atrial walls (AT) are intensely red. Parabronchial and atrial smooth muscles (arrows) bordered the parabronchial lumen (PL). Graded colour intensity in these stained sections divides parabronchus into three parts: the peripheral, the intermediate and the central parts. Scale bar, 200µm. **C**: Close-up of parabronchial lumen (PL) and part of the exchange tissue (ET) mantle. The atrial muscles (arrow) guarded entrances from the parabronchial lumen (PL) into the atria (AT). Atrial septa (*) walled the atrium. Atrium continued into the infundibulum (IF) which in turn communicated with air capillaries of the exchange tissue (ET). Scale bar, 100µm. **D**: Interparabronchial vessel (IPV) with its connective tissue gave out collagen fibers (arrowheads) that entered exchange tissues directly. Infundibulum (IF) are continuation of the atrium into the exchange tissue. Infundibulum gave rise to air capillaries (AC) which are the terminal units that interact with blood capillaries. Fibers of collagen entering the exchange tissue are sandwiched between the terminal exchange units – the air and the blood capillaries. RBCs are seen in the lumen of the interparabronchial vessel Scale bar, 50µm. **E:** Air capillaries (AC) without luminal content are separated from other air capillaries by thin septa containing few strands of collagen fibers (arrows). RBCs are contained in the blood

capillaries. Scale bar, 10µm. **F:** Teased out strands of collagen fibers entered the exchange tissue at the periphery coursed through it towards the parabronchial lumen (PL), the teased out collagen fibers converged into collagen bundles (arrows) within atrial septa and ran towards atrial muscle (AM) blending with its connective tissue (arrow head). Scale bar, 20µm. **G:** Close-up (longitudinal view) of atria (AT) of a parabronchus. Collagen bundled (arrows) within the septal are attached to the atrial muscles (AM). Scale bar = 50µm. Boxed area is enlarged in H. **H:** Collagen bundles (arrows) formed part of the atrial septa. The collagen fibers are attached to the connective tissues surrounding atria smooth muscles (arrowhead). The characteristic collagen wavy appearance is apparent in this section. Scale bar, 10µm.

3.1.2 Alkali digestion of the exchange tissue (I) – scanning electron microscopy

Alkali digestion of the cellular component of the exchange tissue showed intricate three-dimensional arrangement of collagen tissue fibers (Fig. 3.2 A-D). 'Removal' of cellular and other connective tissue component allowed a matrix wall of collagen fibers to be observed. For unclear reason, some RBCs were not digested. Fortuitously, their presence allowed the location of the blood capillaries relative to the air capillaries to be more accurately resolved. Undigested RBCs surrounded by dense network of interwoven collagen fibers represent the blood capillaries (Figs. 3.2B, C). Air capillaries (without luminal content) are seen as empty spaces bordered and separated by network of collagen fibers (Figs. 3.2A - D). Epithelial-epithelial separations of two air capillaries were, however, difficult to identify, presumably because of the thinness and/or the scarcity of collagen fibers there. A rim of collagen bundles surrounded the openings to the infundibulae (Fig. 3.2A). The infundibulae opened into the air capillaries (Fig. 3.2A).

Figure 3. 2: Scanning electron micrographs of the exchange tissue of the lung of the domestic fowl digested to show the spatial arrangement of collagen fibers

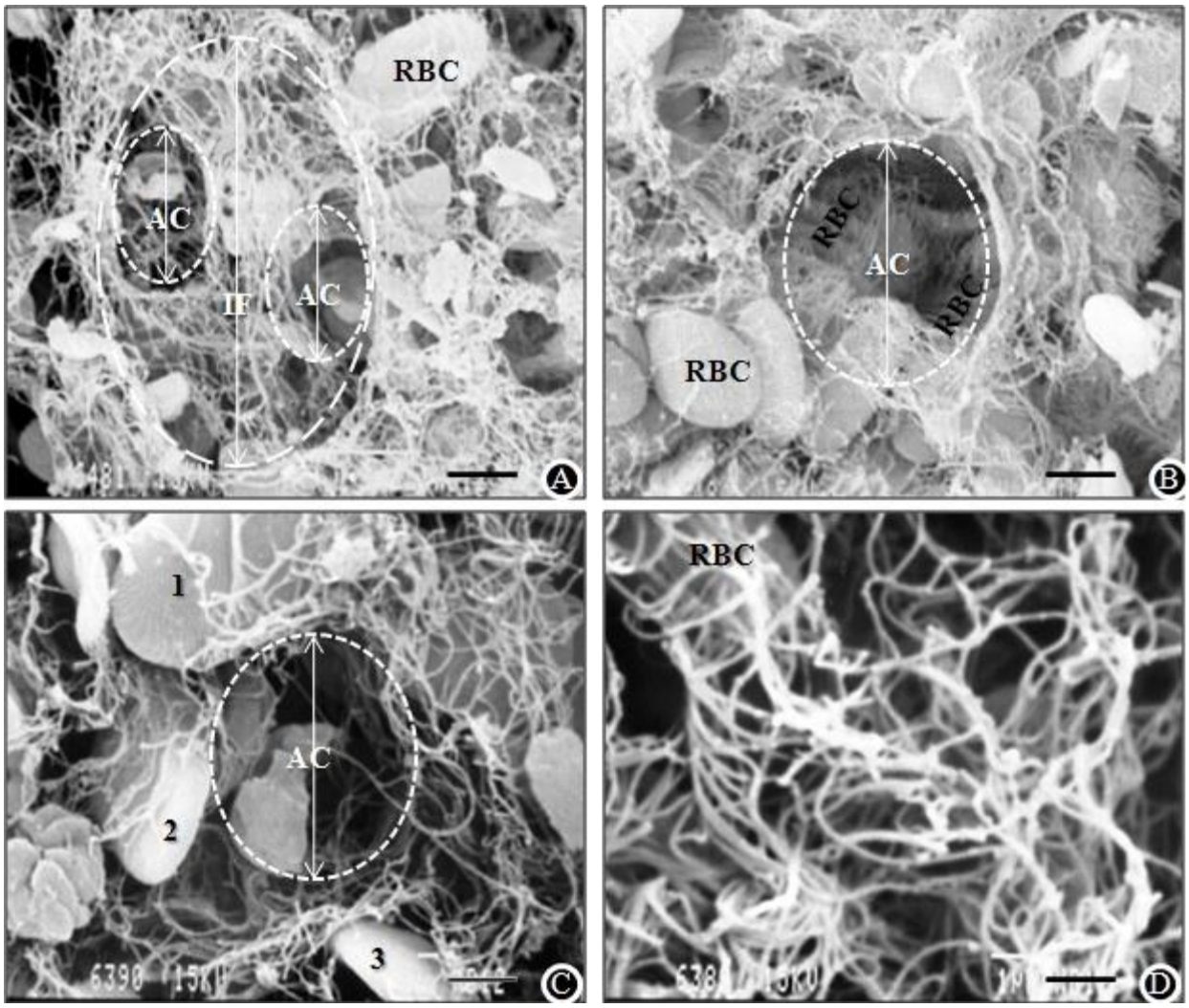

Figure 3.2 legend:

A: Bundle of collagen fibers rimmed the entrance (longer dashed circle) into an infundibulum (IF). Deep into the infundibulum are openings (smaller dashed circles) into two air capillaries (AC). Red blood cells (RBCs) are seen through the air capillaries. Scale bar, 10µm. **B:** Rows of RBCs covered by collagen fibers seen through an opening (dashed circle) into an air capillary (AC) delimited by collagen fibers surrounding blood capillaries containing RBCs. Scale bar = 5µm. **C:** Three differently disposed blood capillaries containing undigested (RBCs) surrounded an air capillary (AC). Scale bar = 5µm. **D:** intricately arranged network of collagen fibers of a blood capillary wrapped around undigested RBC. The complex network of collagen fibers are interconnected in three-dimension in this micrograph. Scale bar = 5µm.

3.1.3 Alkali digestion of the exchange tissue (II) - transmission electron microscopy

TEM micrographs of alkali digestion of the exchange tissue from day 3 to day 6 show gradual removal of tissue components which finally leave out only collagen fibers and undigested RBCs (Fig 3.3). Even though normal morphology was lost early in the digestion process, outlines of the blood- and air capillaries are discernable. TEM micrographs of the sequential digestion of the exchange tissue revealed gradual removal of the component of the BGB and complex disposition of the collagen fibers. The process of digestion started with tissue swelling which caused separation of epithelial cell processes from endothelial cell (Fig 3.3). Following swelling and separation of cells processes, disintegration of epithelial cells, which preceded that of endothelial cells, commences. Late digestion of endothelial cells may be due to its thickness or due to certain properties of the cell. Ghost or trail of endothelial cell process is probably indicative of slower digestion of this cell compared to the extremely thin epithelial cells. The common basement membrane between the two cell processes is probably more firmly attached to the endothelial cell than epithelial cell because the collagen fibers of the basement membrane is not revealed with the disintegration of the epithelial cells but became noticeable with dissolution of the endothelial cells. In addition, the wavy course of the revealed collagen appears to follow the outline of the disintegrating endothelial cells and not that of the epithelial ones.

Figure 3. 3: Selective alkali (10M NaOH) digestion of chicken lung's gas exchange tissue

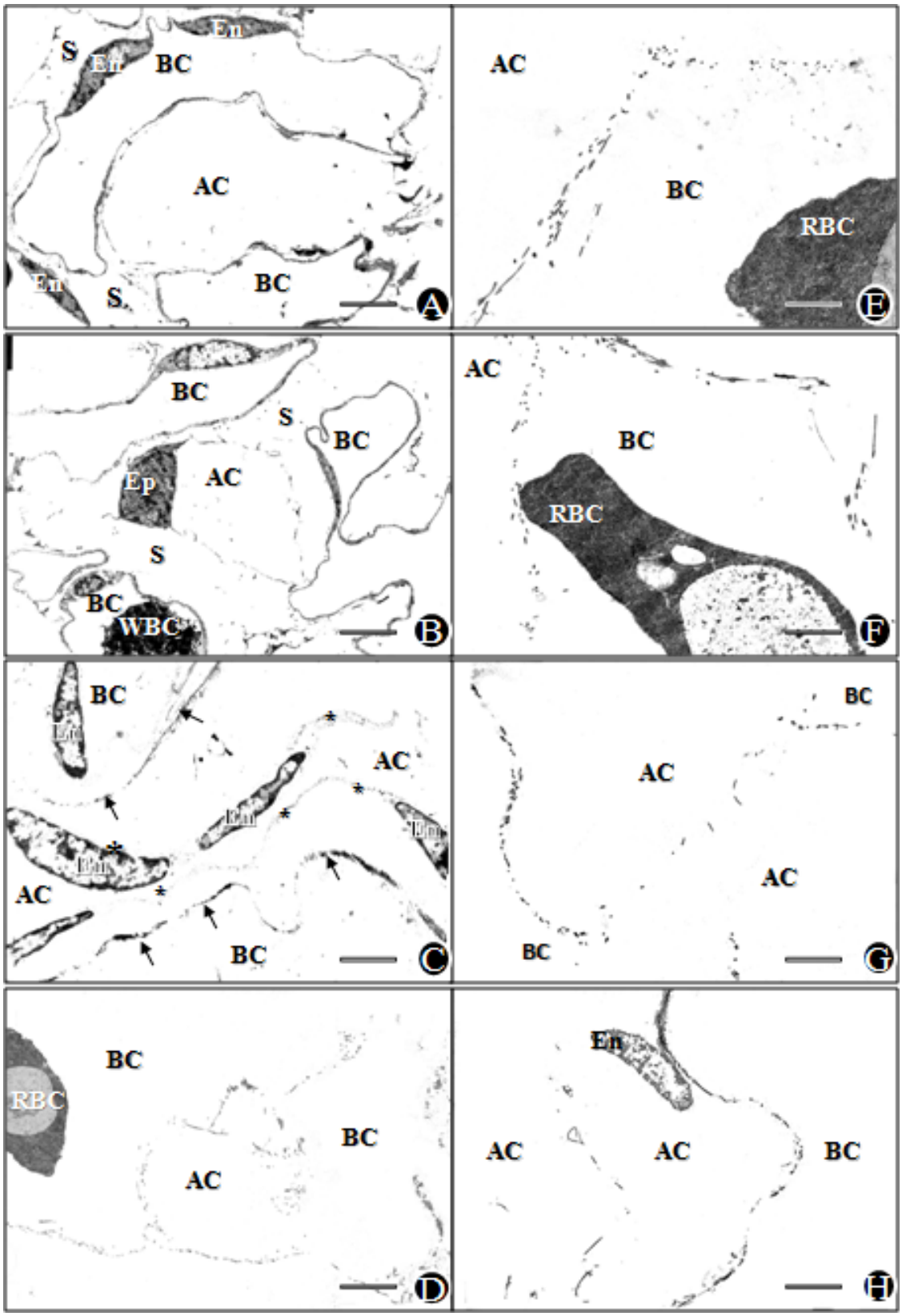

Figure 3.3 legend:

Figures A to C are respectively at days 3, 4, and 5 of the alkali digestion process of the exchange tissue while figures D to H are at day 6. **A:** Wide spaces (S) represent sites where epithelial cell processes lining an air capillary (AC) pulled away from an endothelial cell ones of a blood capillary (BC). The degenerating endothelial cell processes linked endothelial cell nuclei (En). Scale bar, 5µm. **B:** Epithelial cell nucleus (Ep) with its disintegrating cytoplasmic processes surrounding an air capillary (AC) has completely pulled away from endothelial cells (En) and their processes. The two cell processes are separated by wider spaces (S). White blood cell (WBC) within a blood capillary is seen close to an endothelial cell nucleus. Scale bar, 5µm. **C:** As the endothelial cells nuclei (En) are been digested away, remnant of the cell processes (*) linked the nuclei while network of collagen fibers (arrows) are revealed. Lumina of the air- (AC) and blood capillaries (BC) are still discernable. Scale bar, 2µm. Figures D to F are showing collagen fibers of the blood-gas barrier. Scale bar, 2µm. **D:** Blood capillaries (BC) surrounding an air capillary (AC). One of the blood capillaries has an undigested red blood cell (RBC). Scale bar, 2µm. **E:** Close-up of the collagen in the blood-gas barrier. The collagen fibers are differently orientated. The undigested collagen fibers separates the undigested red blood cell (RBC) within a blood capillary (BC) from the air capillary. Scale bar, 1µm. **F:** Undigested red blood cell (RBC) inside a blood capillary (BC) is separated from an air capillary (AC) by the collagen fibers in the BGB after digestion of the cellular components. The RBC just touched the collagen fibers, i.e., the endothelial side of the BGB. Scale bar, 1µm. **G and H:** Two adjacent air capillaries (AC). Presence of collagen fibers are seen here between two air capillaries but the fibers are not tightly packed like in the BGB, they consist of few widely spaced fibers. Scale bar, 1µm.

3.1.4 Alkali digestion of the cast of the exchange tissue (III) - scanning electron microscopy

Combination of intravascular latex rubber casting and alkali digestion of lung preparations revealed a network of collagen fibers in the blood-gas barrier that approximate to natural topographical arrangement (Fig. 3.4). While the cellular and other structural components of the parenchyma were digested away, the unmistakable morphologies of the air- and the blood capillaries together with the associated collagen fibers were clearly observed. The latex rubber provides a support framework. A network of collagen fibers formed sleeves around the latex filled capillaries.

Figure 3. 4: Cast of the blood vessels of the exchange tissue followed by alkali digestion (SEM)

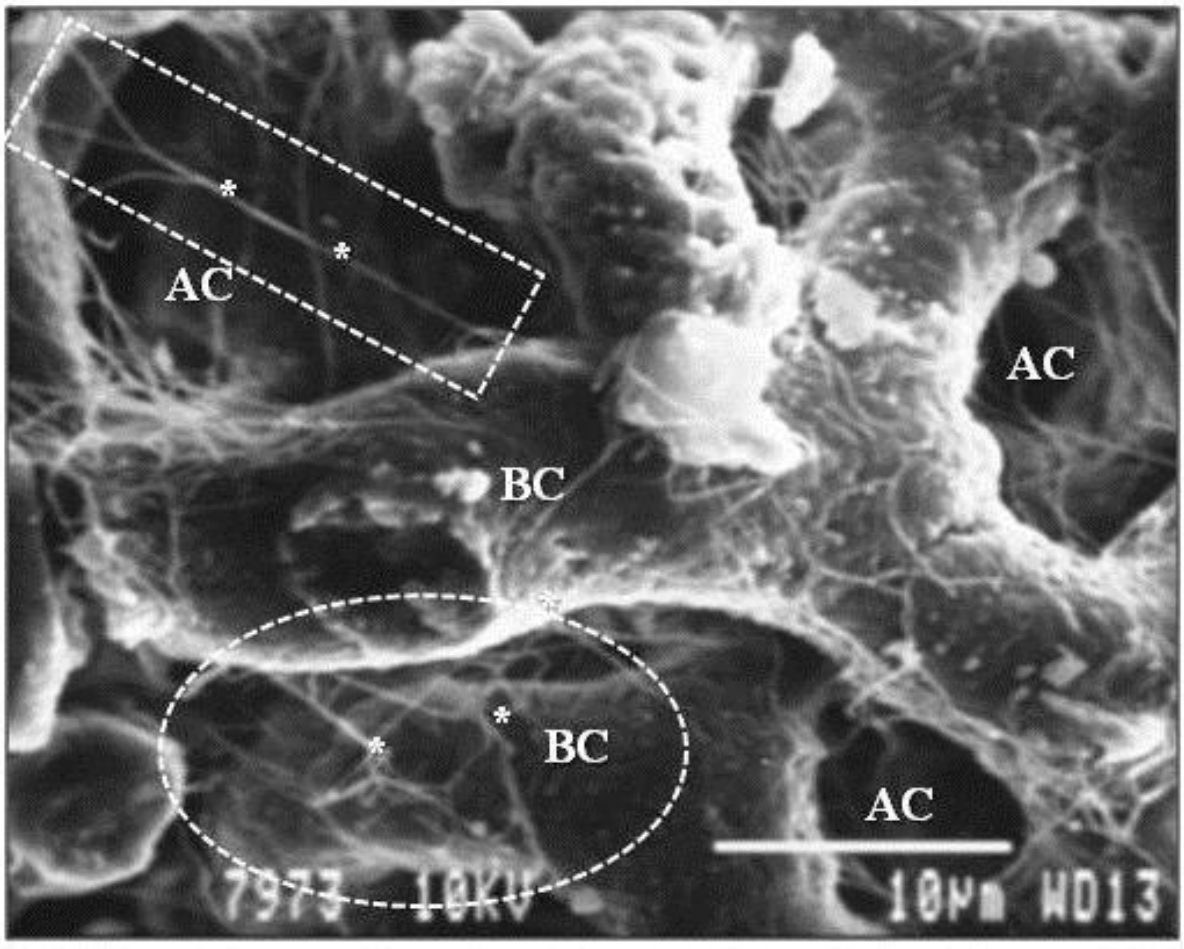

Figure 3.4 legend:

A scanning electron micrograph of a digested exchange tissues of the lung of the domestic fowl after intravascular latex cast. Networks of collagen fibers (e.g. enclosed dashed area) in their natural position surround a cast of blood capillary (BC). Air capillaries (AC) occupy spaces between blood capillary cast. Few collagen fibers (*) are seen here. Scale bar = 10µm.

3.1.5 Immuno-gold localization of type-IV collagen fibers

In the gas exchange tissue treated with polyclonal primary antibodies raised against type-IV collagen, the gold particles conjugated secondary antibodies, which bound to primary antibodies, were found within the thickness of the basement membrane (Fig. 3.5A-F). Rows of three to four gold particles were seen across the thickness of the basement membrane (Figs. 3.5A, B). Gold particles were seen separating endothelial cell nuclei from the thin cytoplasmic extension of the epithelial cell (Figs. 3.5E, F). They were also seen where two air capillaries are in contact (Figs. 3.5C, D). However, compared to the numbers of gold particles across the thickness of the BGB, gold particles were usually one or at most two particles across the thickness of epithelial-epithelial contacts (Figs. 3.5C, D). Exchange tissue sections treated with only PBS and secondary antibody but without the primary antibody (controls) did not bind any gold particles (Figs 3.5G, H).

Figure 3. 5: Exchange tissues treated with gold conjugated secondary antibodies raised against primary antibodies that bind to collagen type-IV

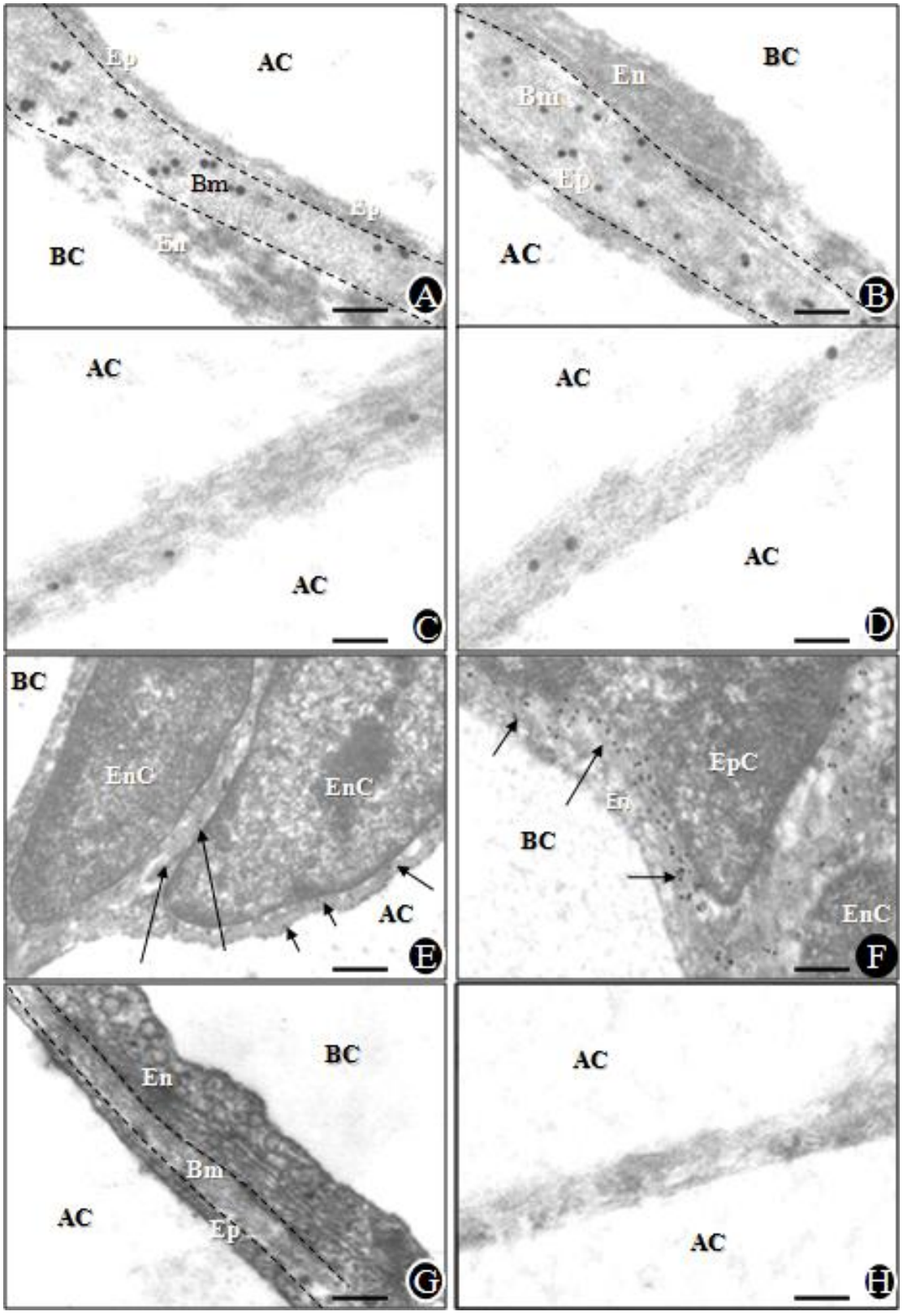

Figure 3.5 legend:

A, B: In the laminated structure of the blood-gas barrier, three to four rows of closely packed gold particles are seen across the thickness of the basement membrane. The basement membrane is sandwiched between the endothelial cell process (En) that lines the blood capillary (BC) and the epithelial cell (Ep) that lines the air capillary (AC). Scale bar, 0.1µm. **C, D:** Contact between two air capillaries (AC) shows only a single row of widely spaced gold particles. Scale bar = 0.1µm. **E:** Extracellular matrix between two endothelial cell bodies (EnC) in the exchange tissues shows presence of type-IV collagen by binding to gold particles. Scale bar = 1µm. **F:** Extracellular matrix between endothelial cell nucleus (En) and epithelial cell nucleus (EpC) also show presence of type-IV collagen by binding to gold particles (arrows). Scale bar = 0.5µm. **G, H:** Exchange tissue treated with normal goat serum and gold conjugated secondary antibody without the primary antibody did not bind any gold particles. Scale bars: G, 0.15µm; H, 0.1µm.

3.1.6 Transmission electron micrographs of epithelial-epithelial contacts

Without any special treatment of the gas exchange tissue of lung of the domestic fowl, the following important anatomical features that have never been reported in the literatures before were observed in the epithelial-epithelial (E-E) cells contacts in this study (Figs 3.6 A-L). Intercellular material occurred between contacting epithelial cells that form bridge between two blood capillaries. A clearly defined area, which is here termed the triple point of the exchange tissue, occurred at the junction of the epithelial cells plate with a blood capillary. This area which was often triangular, has sides that are bounded by the diverging epithelial cells as they approached the blood capillary, which formed the base. The extremely thin epithelia cells are widest at this area and contain abundant intracellular components. The contacting epithelia cells, which are firmly apposed and attached by the basement membrane, diverge as they approached the blood capillary. As the apposed epithelia cells diverged, each with a part of the shared basement membrane, continued with the BGB basement membrane. The continuity of the basement membrane between E-E and BGB, most likely, constituted the skeletal frameworks that strengthened and joined the extremely thin plates of epithelial cells to the blood capillary.

Figure 3. 6: Transmission electron micrograph of epithelial-epithelial contacts

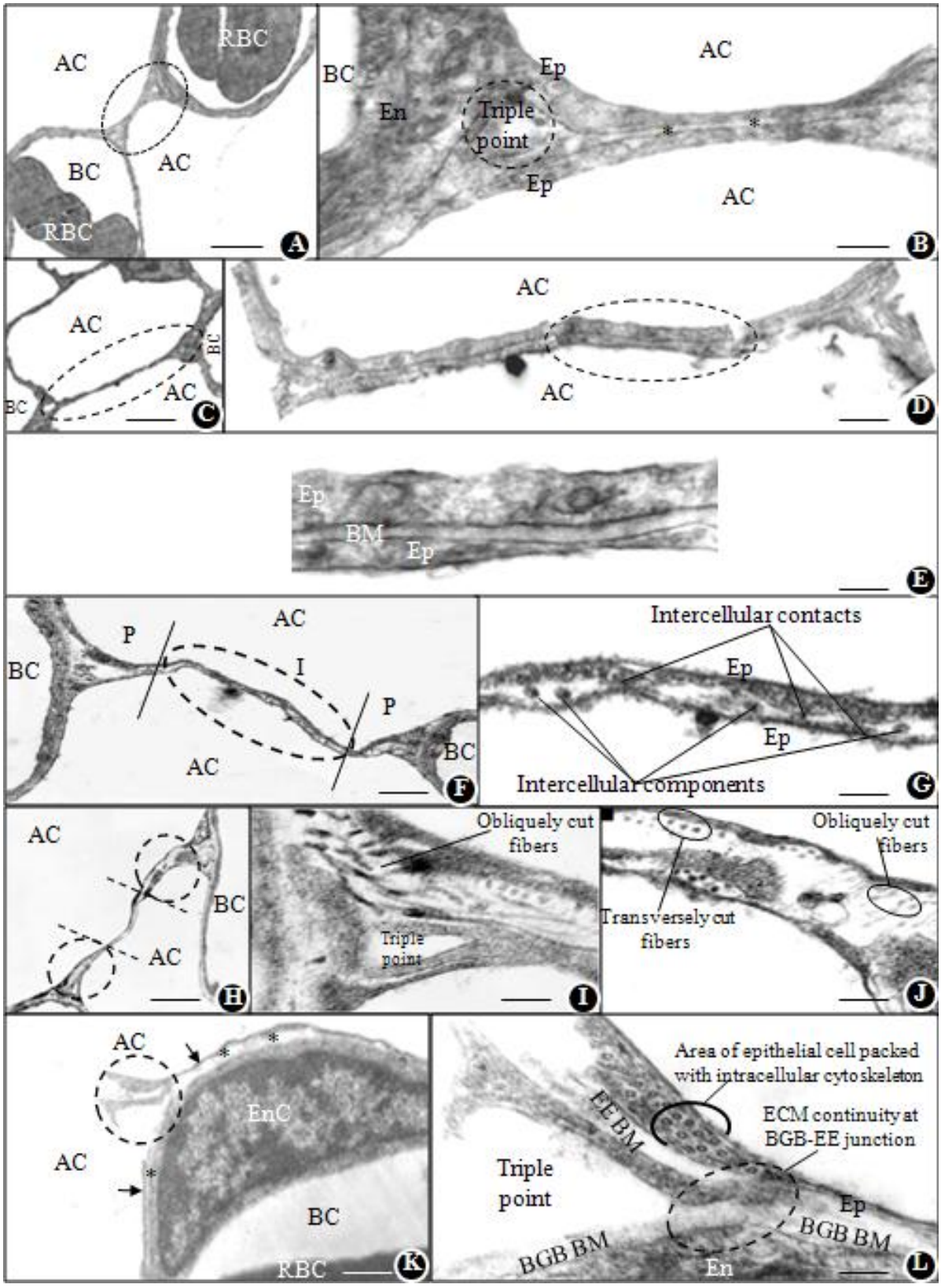

Figure 3.6 legend:

A: Short epithelial-epithelial (E-E) cell plates are seen here separating two air capillaries (AC) and connecting two blood capillaries (BC) containing red blood cells (RBC). The encircled area is enlarged in B. Scale bar, 5µm. **B:** Higher magnification of the encircled area in A showed two plates of epithelial cells (Ep) separated by a distinct material (*) - the basement membrane. The plate of epithelial cells separate two air capillaries (AC). At the junction of the plates with the endothelial cell (En) of the blood capillary (BC) is the triple point of the avian exchanges tissue where there is continuity of blood-gas barrier (BGB) and E-E basement membranes. The triple point is a definite anatomical structure with distinct boundaries. Scale bar, 1µm. **C:** Long epithelial-epithelial (E-E) cell plates are seen here separating two air capillaries (AC) and connecting two blood capillaries (BC). The encircled area is enlarged in D. Scale bar, 5µm. **D:** Montage of the whole length of the E-E cell contact at higher magnification revealed that the contact (encircled area) which appears to be a unit in C comprises of two epithelial cells separated by a distinct basement membrane. Scale bar, 0.5µm. **E:** Higher magnification of the area circled in D showed that a definite basement membrane joined the two epithelial cells together. Scale bar, 0.1µm. **F:** Epithelial cell plates which separate two air capillaries (AC) and bridged two blood capillaries (BC) can, ordinarily, be divided into three parts: *proximal third* (P) near the blood capillaries and an *intermediate third* (I) in between the proximal parts. Higher magnification of the intermediate third (encircled area) is shown in G. Scale bar, 2µm. **G**: Intercellular components between E-E cells that appeared to be collagen fibers cut transversely and intercellular contacts that actually connect the two plates of epithelial cells are seen here. These components appear as dense round structures and are alternating with areas where the two epithelial cells processes are in

actual contact or bridged by intercellular materials (intercellular contacts). Scale bar, 0.1µm. **H:** Compare to the middle third, proximal third of E-E cell processes close to the BC (encircled areas) are wider and contain intercellular materials. Scale bar 5 µm. **I:** Higher magnification of one of the proximal part (lower encircled area in H) revealed differently oriented (oblique and transverse) intercellular fibrillary structures. Triple point of exchange tissue where BGB and E-E basement membrane are in continuity is clearly demarcated. Scale bar, 0.1µm. **J:** Higher magnification of one of the proximal part (upper encircled area in H) also revealed differently oriented (oblique and transverse) intercellular fibrillary structures and amorphous materials between the cell plates. Scale bar, 0.1µm. **K**: Junction of fused E-E cells plates with BGB in the region of an endothelial cell nucleus. Dashed circle is enlarged in L. Epithelial cell process (arrows) lining the air capillary is separated from the endothelial cell nucleus (EnC) by the common basement membrane (*). Part of red blood cell (RBC) is seen within the blood capillary (BC). Scale bar, 0.5µm. **L**: Junction of epithelial cell plates with blood capillary. Abundant intracellular cytoskeletons (microtubule) are seen contained in the expanded part of an epithelial cell plate close to the endothelial cell. Dashed circle shows area of basement membrane continuity between epithelial-epithelial basement membrane (EEBM)- and blood-gas barrier basement membrane (BGBBM). One side of the triple point of exchange tissue formed by the diverging epithelial cell plates (Ep) and the base formed by the endothelium (En) of blood capillary is seen here. Scale bar, 0.1µm.

3.2 RESTING (NON-EXERCISE) AND EXERCISE EXPERIMENTS

All the chicken in the exercised group ran (Fig. 2.7) very well for the full 10 minutes except at the lowest treadmill speed (0.66 m/s) during which some of the birds tried to jump off the treadmill. The highest treadmill speed in the experiment corresponded with the highest tolerable exercise intensity by the chicken in this experiment. Most of the chickens tolerated the exercise but at the speed of 2.53 m/s and above, the chickens were noticeably exhausted by the last quarter of the 10 minute duration. The chickens were prodded away from the edge of treadmill while they complete the full 10 minutes of exercise on the treadmill. This maneuver was necessary; it prevented the birds from collapsing on the belt and becoming trapped between the revolving belt and the stationary cage.

3.2.1 Lactate measurement

Pre-exercise blood lactate concentration recorded in all the chickens were not different. Post exercise lactate concentration steadily increased with increasing exercise intensity (Fig. 3.7). The fall in lactate reading in the resting birds between the first and the second reading, 10 minutes after, was not expected but understandable. Birds in this group were never exercised on the treadmill and the second reading only represent blood lactate concentration 10 minutes after the first reading was taken while they were left undisturbed. Blood lactate concentration rose from a resting value of 1.27 mmol/L to 3.14 mmol/L in the group subjected to the lowest exercise regime (0.66 m/s). The difference represents 147% increase above resting value. However, the differences between one exercised level and the next, calculated as percentage

value, decreased with increasing exercise intensity. This indicated that blood lactate concentration approached the maximum possible concentration this species of bird could tolerate and may imply that the birds were pushed to near maximal exercise endurance limit. The huge difference in blood lactate concentration between resting chicken and those subjected to lowest exercise regimen could be explained by the lag that existed between lactate accumulation and release of lactate dehydrogenase.

Figure 3. 7: Measurement of the blood lactate concentrations with increasing exercise

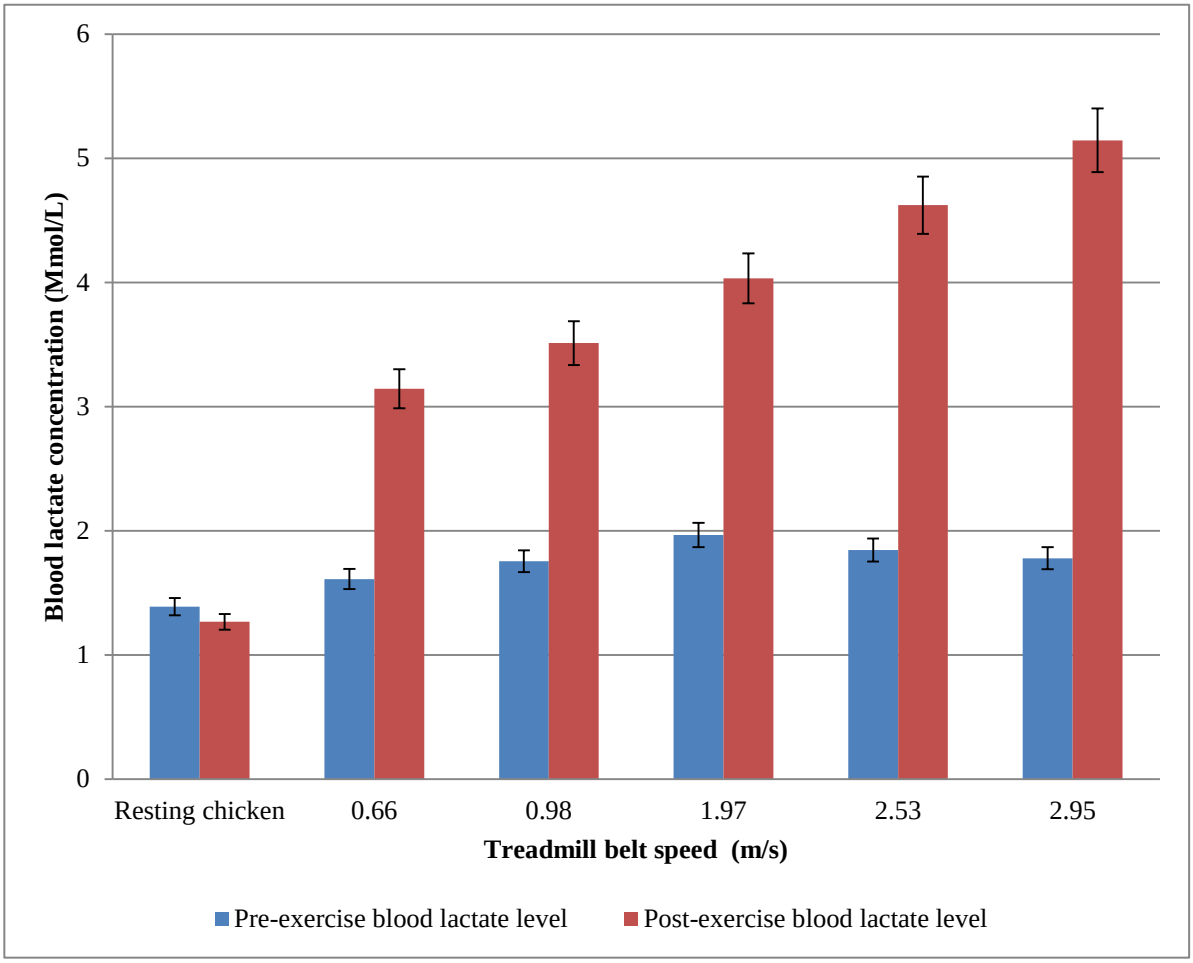

Figure 3.7 legend:

Blood lactate concentration measured before and after 10 minutes of exercise on the treadmill. In the resting bird, the second measurement was taken 10 minutes after the first reading without running the birds on the treadmill. Pre-exercise lactate values in all the birds are similar while post-exercise values increase linearly with increasing exercise intensity. Data are expressed as means ± SE (see appendix III).

3.2.2 Red blood cell counts in the lavage fluid

Large numbers of red blood cells (RBC) were found in the lavage fluid of all the exercised birds and even in the unperturbed (resting) ones. Large differences in the number of RBCs, which steadily increased were observed in the pulmonary lavage fluid between chickens subjected to increasing exercise intensity until belt speed of 1.97 m/s (Fig. 3.8): subsequently, the difference became progressively smaller. At speeds greater than 1.97 m/s, it became difficult for some of the birds to complete the 10 minutes exercise schedule. Although, these bird were prodded to complete the 10 minutes time they were visibly exhausted at the end of the exercise.

Figure 3. 8: Counts of red blood cells in the pulmonary lavage fluid of resting chickens and at increasing exercise intensity

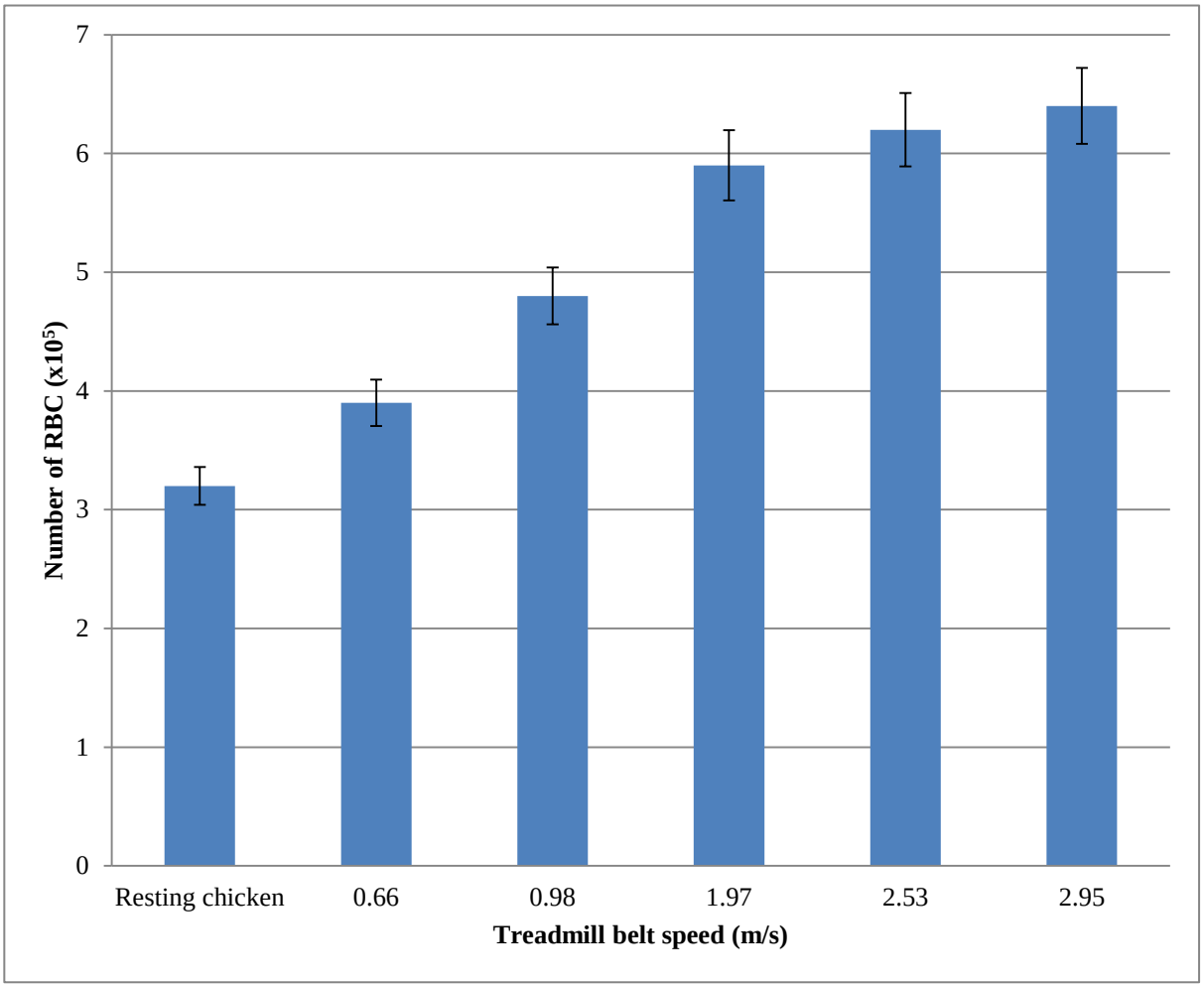

Figure 3.8 legend:

Number of red blood cells in the lavage fluid of the exercised birds increased with increasing exercise intensity. While the red blood cell counts increased greatly at lower exercise intensity, as exercise intensity increased the differences in RBC counts decreased. Data are expressed as means ± SE (see appendix IV).

3.2.3 Total protein concentration in the lavage fluid

Result of the total protein concentration in the lavage fluid in resting to exercising chickens is as shown in figure 3.9. There were large differences in protein concentrations, which increased progressively with increase in exercise intensity. Differences in concentration between one level of exercise and the next higher level were larger at treadmill speeds below 1.97 m/s while at higher speeds the change was less. The total protein concentrations in the lavage fluid from the exercised chickens were significantly greater ($P<0.05$) than the concentration from the unperturbed birds.

Figure 3. 9: Protein concentration in the respiratory system of chickens at rest and at increasing exercise intensity

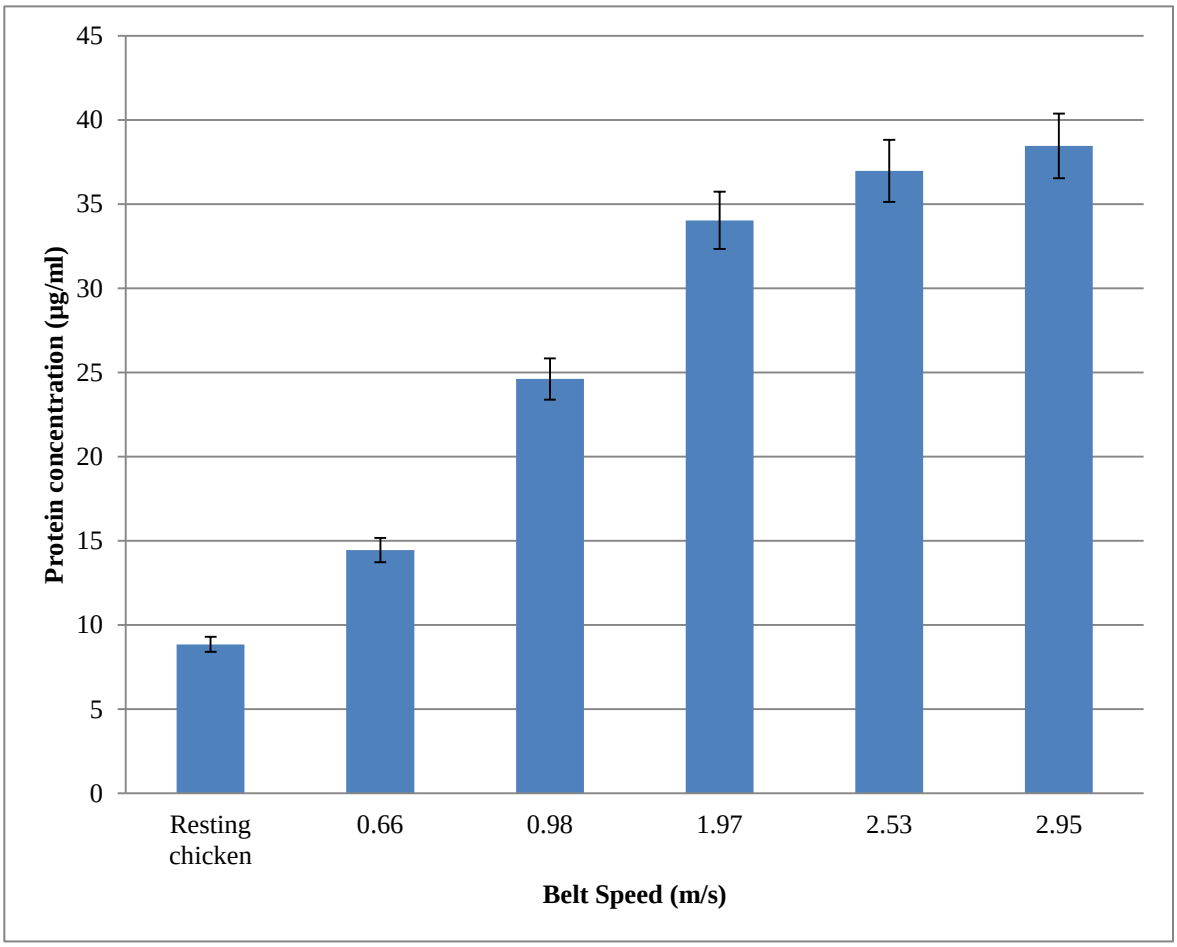

Figure 3.9 legend:

Protein concentration in the lavage fluid from the respiratory system of resting birds and exercised ones estimated using Lowry's method. The values increased progressively with increasing exercise intensity. Large difference in protein concentration between one level of exercise intensity and the next higher one occurred up to the treadmill speed of 1.97m/s. Beyond the treadmill speed of 1.97m/s the difference between one exercise intensity and the next were less. Data are expressed as means ± SE (see appendix II).

3.2.4 Number of complete blood-gas barrier and epithelial-epithelial breaks in the terminal gas exchange units

An example of Toluidine blue micrograph used in estimating number of BGB and E-E breaks in the areas supplied by the four principal branches of the pulmonary artery (Fig. 3.10) of the lung is as shown in figure 3.11. Complete BGB- (dashed circles) and E-E (square circles) breaks were counted in eight randomly selected fields of view per histological section at x1000. Four randomly selected slides from vascular areas supplied by each of the four principal branches of the pulmonary artery were analyzed this way. The total numbers of complete BGB – and E-E – breaks were pooled and the average numbers of the two types of breaks were calculated (see appendices VI-VIII). The two types of breaks were seen in all the exercised birds as well as in the resting unperturbed birds. In all the lungs analyzed, the numbers of E-E breaks were significantly greater than the BGB breaks (Fig. 3.11).

Figure 3. 10: Complete blood-gas barrier- and epithelial-epithelial breaks in the terminal exchange units seen with light microscope

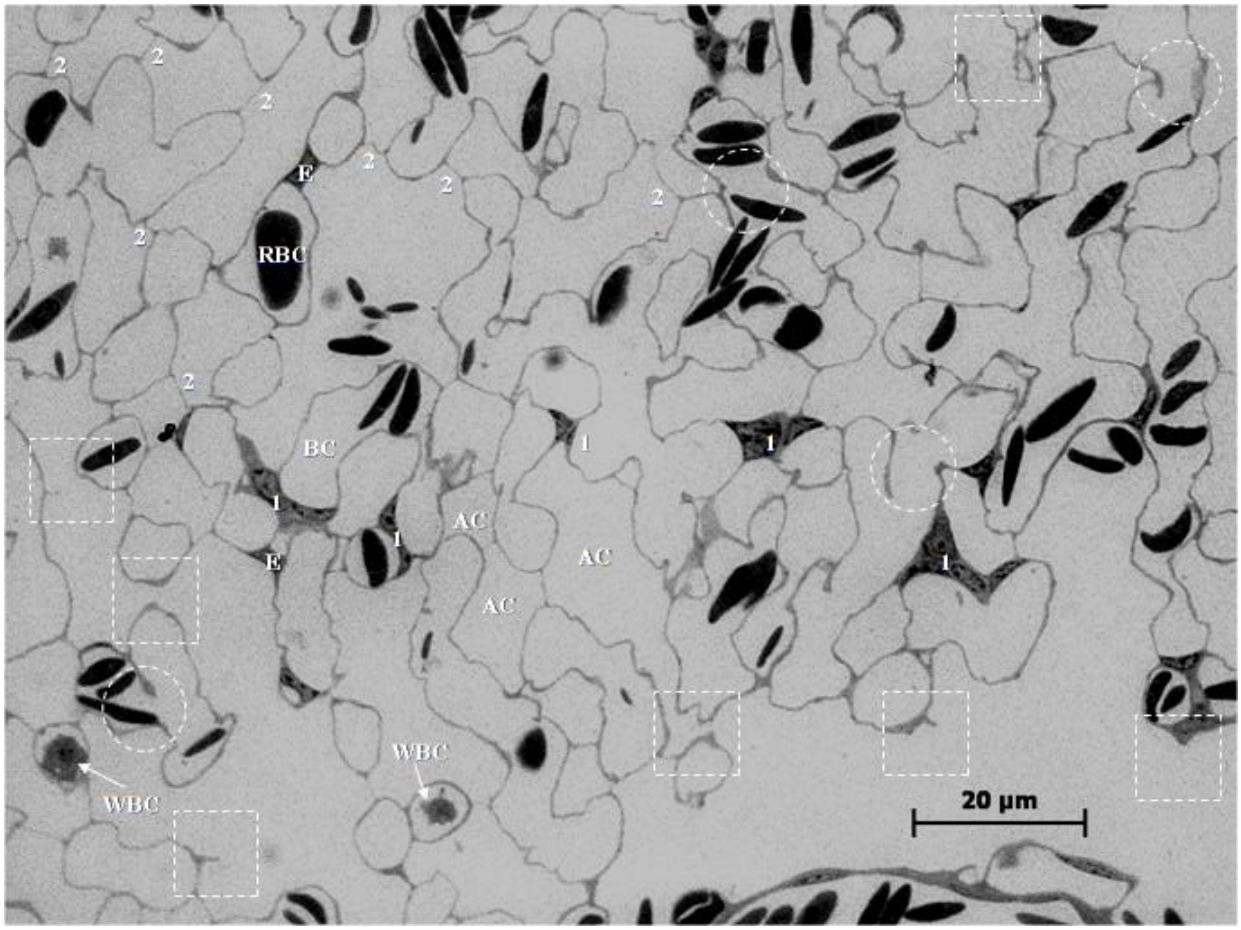

Figure 3.10 legend:

Example of Toluidine blue stained picture used in the estimation of number of blood-gas barrier (BGB) breaks (circles) and epithelial-epithelial (E-E) breaks (rectangle) in each of the four 'arterial' regions of the lung. Counting was done at x1000 magnification within an area of 100 μm^2. WBC, white blood cell; RBC, red blood cell; EnC, endothelial cell nucleus; EpC, epithelial cell nucleus; IrPV, intraparabronchial vessel. Besides BGB, other contacts found within avian gas exchange tissue are endothelial-endothelial (1) and epithelial- epithelial (2) contacts. These contacts, which do not serve exchange function, probably provide support for the extremely thin BGB.

Figure 3. 11: Average number of blood-gas barrier- and epithelial-epithelial breaks at different speeds

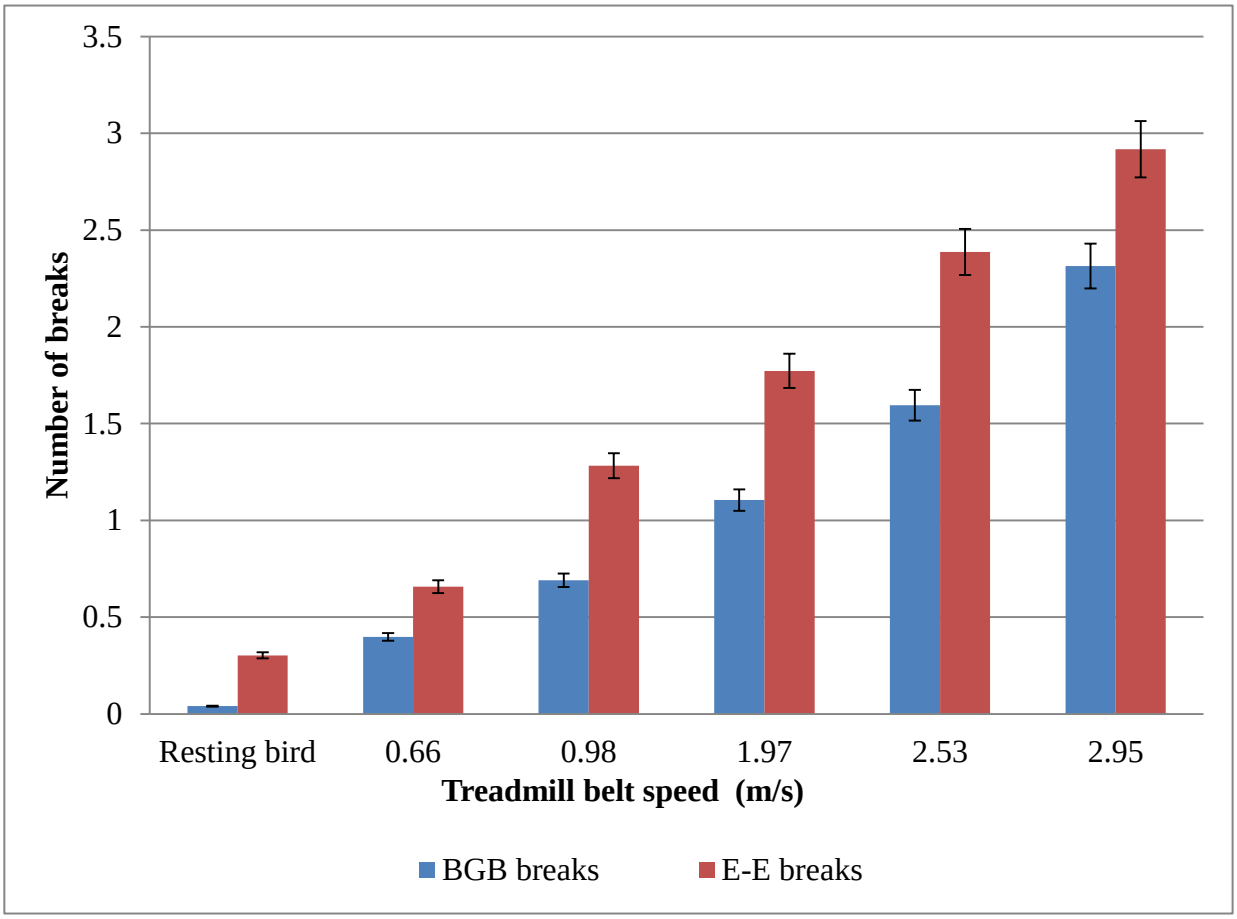

Figure 3.11 legend:

Numbers of blood-gas barrier- and epithelial-epithelial breaks counted in the whole lung at each level of exercise and in the resting chicken. While the number of breaks in the resting chicken is small, both types of breaks are present. The two types of breaks increased with increasing exercise intensity and at any level of intensity there were more epithelial-epithelial breaks than blood-gas barrier ones. Data are expressed as means ± SE (see appendix V - VII).

3.2.5 Difference between epithelial-epithelial and blood-gas barrier breaks

For the purpose of comparison, the difference between numbers of BGB- and E-E breaks were calculated as a percentage of the total number of breaks in each area of blood supply by the main branches of the pulmonary artery (Fig. 3.12). The difference between the E-E- and the BGB breaks, which gives the relative proportion of each type of breaks in an area perfused by each of the four branches of the pulmonary artery indicate the most frequent type of break and how the two types of breaks compare at different levels of exercise. The difference at a particular level of exercise intensity in a given vascular region was calculated as follows:

> *The difference between the E-E- and the BGB breaks in a vascular region divided by the total E-E- and the BGB breaks in the same vascular area multiply by one hundred (100).*

In the resting chicken, the E-E breaks were the most common type of breaks and in this group; the area supplied by the cranial branch of the pulmonary artery is the only area with 100% E-E breaks. The areas supplied by the other vascular branches show some degree of BGB breaks. In the area supplied by the caudomedial branch of pulmonary artery, the number of E-E breaks is 55% higher than BGB. The differences in the areas supplied by the accessory- and caudolateral branches showed approximately 80% and 70% more E-E breaks than BGB breaks, respectively.

At the first level of exercise (0.66m/s), the difference between the two types of breaks in all the areas supplied by the four branches of the pulmonary artery are considerably lower than values obtained at rest. At this level of exercise intensity, the area supplied by the cranial branch still shows highest difference and the caudomedial the lowest.

At 0.98m/s, the differences between the E-E- and the BGB breaks in all the branches are approximately the same. At increasing exercise intensity, the difference between the two types of breaks decreased while differences between branches did not show much variation.

3.2.6 Justification for use of percentage difference in comparing number of failure in the different vascular regions of the lung

Extremely thin BGB (Maina and King, 1982), high blood pressure (Seymour and Blaylock, 2000), energetic lifestyle (Tucker, 1972a, b) are thought to predispose avian BGB to failure because red blood cells are frequently reported to occur in their lavage fluid (e.g. Maina and Cowley, 1998; Nganpiep and Maina, 2002). The need to establish a relationship between factors that are thought to predispose and the observable effects is imperative. This experiment is therefore designed to test the vulnerability of the avian BGB at rest and during intense activity. The organization of the pulmonary arterial vasculature divides the avian lung into four vascular territories which usually overlaps but the vessels do not anastomose. The natural division simplifies analyses and allows pressure or flow profile in the four vascular regions to be drawn based on the number of failures – the observable effect of intervention. According to Abdalla and King (1975, 1976a, b, 1977) and Abdalla (1989) the four vascular branches besides subtending different angles to pulmonary artery within the lung, they have different internal diameters. These two parameters are known to affect physics of flow (Lindsay and John, 2009), hence the need to estimate number of failures in each of the vascular regions within a group. However, for inter group comparison; total number of failure in the lung need to be estimated. Furthermore, number of failure as a function of intervention (exercise/perfusion) in each of the vascular region in relation to total number of failure is

indicative of pressure in each vessels which can be related to their internal diameter and branching angle. For easy data handling, percentage contribution from each of the four branches to total number of failure in a lung was estimated. Because two components of the exchange tissue (air and blood capillaries), reported to strengthen each other, were observed to fail. Relationship between these two types of failure with increases in intervention was calculated as percentage difference.

Figure 3. 12: Difference between epithelial-epithelial- and blood-gas barrier breaks in the four vascular region of the lung at different exercise intensity

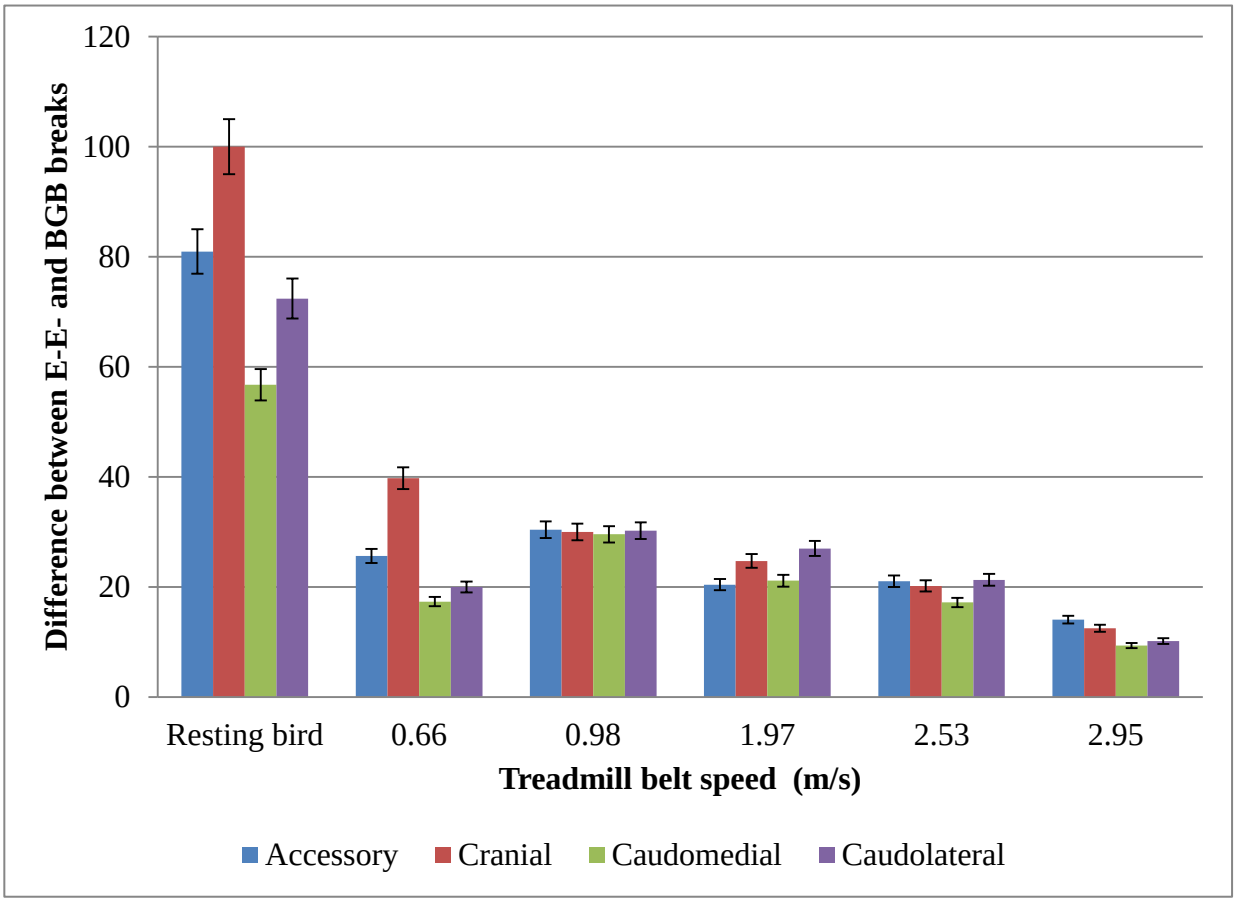

Figure 3.12 legend:

The difference between the two types of breaks decreased progressively with increasing exercise intensity. In the resting chicken, the air capillaries are more susceptible to failure than the blood capillaries. The drop in the number of breaks in the first exercise regimen, which made the difference in this group to fall below the next higher exercise regimen, could be the effect of pulmonary hemodynamic shift in response to exercise. Wide differences between vascular branches in the resting chicken and in the first exercise regimen are probably indicative of perfusion inequality, which disappears with increasing exercise intensity. Data are expressed as means ± SE (see appendix X).

3.2.7 Comparison of blood-gas barrier breaks in different regions of the lung

Comparison of BGB breaks in the different parts of the lung supplied by the main branches of the pulmonary artery gives relative contribution to total number of BGB breaks in the whole lung by each of the four areas supplied by the branches. This comparison shows the area with highest number of BGB breaks at each level of exercise intensity (Fig. 3.13). Regional comparison at a particular level of exercise intensity was calculated as follows:

> *Total number of breaks in a particular region branch of the pulmonary artery divided by the total number of breaks in the regions supplied by all the four branches of the pulmonary artery multiply by one hundred (100).*

In the resting chicken, the caudomedial branch had the highest number of BGB breaks compared to other branches while no BGB break were observed in the cranial branch area. The numbers of BGB breaks in the accessory- and caudolateral branches are similar.

At the level of exercise of 0.66m/s, the cranial branch had the lowest number of BGB breaks and the caudomedial one the highest number of breaks. The numbers of BGB breaks in areas supplied by the accessory- and caudolateral are similar.

At 0.98 m/s and higher, the numbers of BGB breaks in all the main branches of the pulmonary artery showed no significant difference ($P < 0.05$).

Figure 3. 13: Comparison of blood-gas barrier breaks in the four vascular region of the lung at different exercise intensity (treadmill speed)

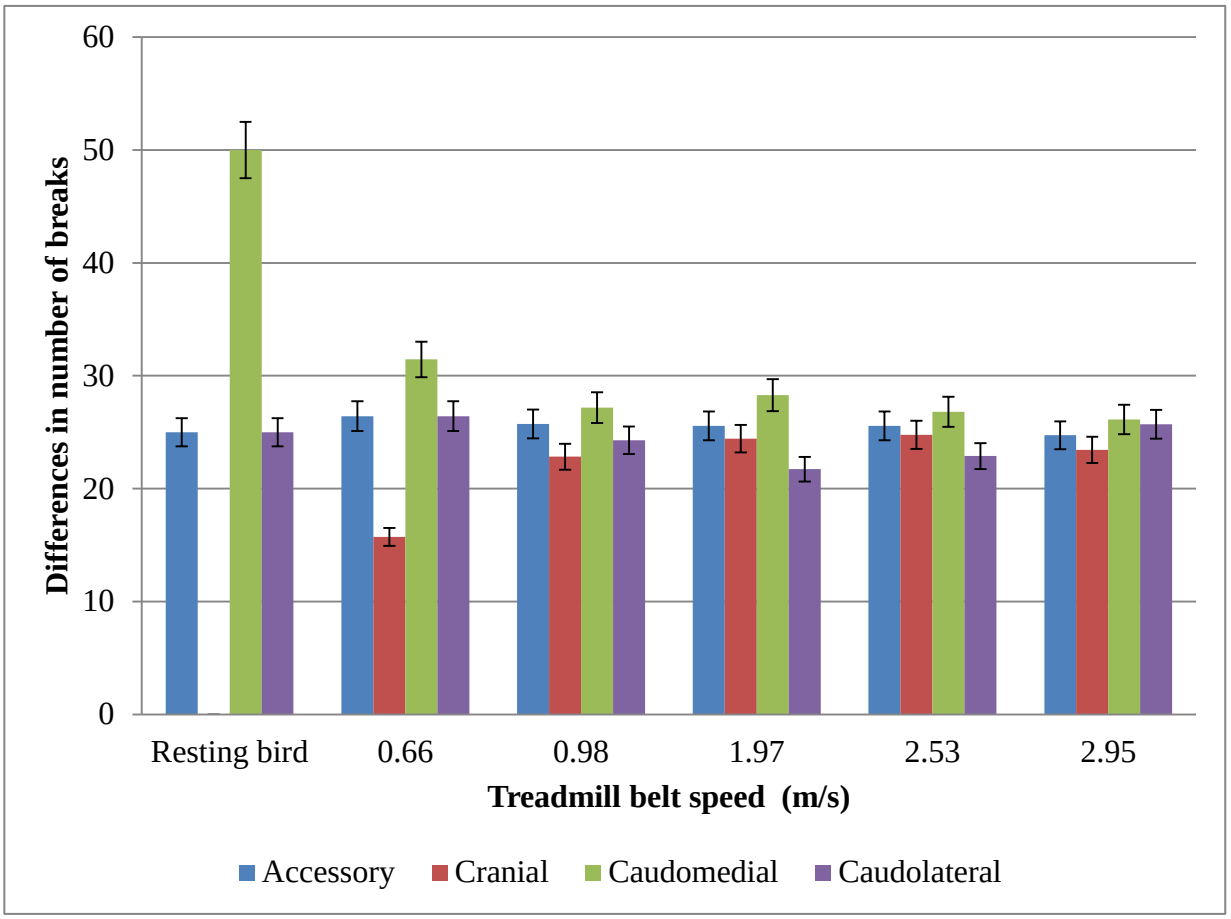

Figure 3.13 legend:

Comparison of number of breaks in all the four territories supplied by the pulmonary artery indicated contribution of each vascular territory to the total number of BGB breaks in the lung. Except in the resting chickens and those subjected to lowest exercise regimes, all the exercised chicken showed no significant difference in the distribution of numbers of breaks. In the resting chicken number of breaks in the caudomedial branch is significantly higher ($P < 0.05$) while no break was recorded in the cranial branch. Numbers of breaks in the accessory- and caudolateral branches of the pulmonary artery showed similar values in the resting chickens and those that ran at 0.66 m/s. In the different vascular territories of those chickens subjected to speed of 0.98 m/s and above, the lowest- and highest numbers of breaks were between 22 and 28, respectively. Data are expressed as means ± SE.

3.2.8 Comparison of epithelial-epithelial breaks in different parts of the lung

Regional comparison of the E-E breaks gave relative contribution by each of the four areas supplied by the four branches of the pulmonary artery to total E-E breaks in the whole lung. This comparison indicates the area with highest number of E-E breaks at each level of exercise intensity (Fig. 3.14). Regional comparison at a particular level of exercise intensity was calculated as stated for the BGB breaks (section 3.26).

In the resting chicken, highest numbers of E-E breaks occurred in the region supplied by the accessory branch and the lowest in the region supplied by the caudolateral branch while the values for the regions supplied by the cranial- and caudomedial branches were comparable, differences in all the branches, however, were not statistically significant ($P < 0.05$). Although, at the level of exercise of 0.66 m/s and 0.98 m/s, the numbers of E-E breaks in the accessory and caudomedial regions are the same but both are higher than in those regions supplied by the cranial- and the caudolateral branches both of which are also close, with no significant differences ($P < 0.05$). At 1.97 m/s and beyond values in all the branches showed no significant difference.

Figure 3. 14: Comparison of epithelial-epithelial breaks in different regions of the lung at different treadmill speed

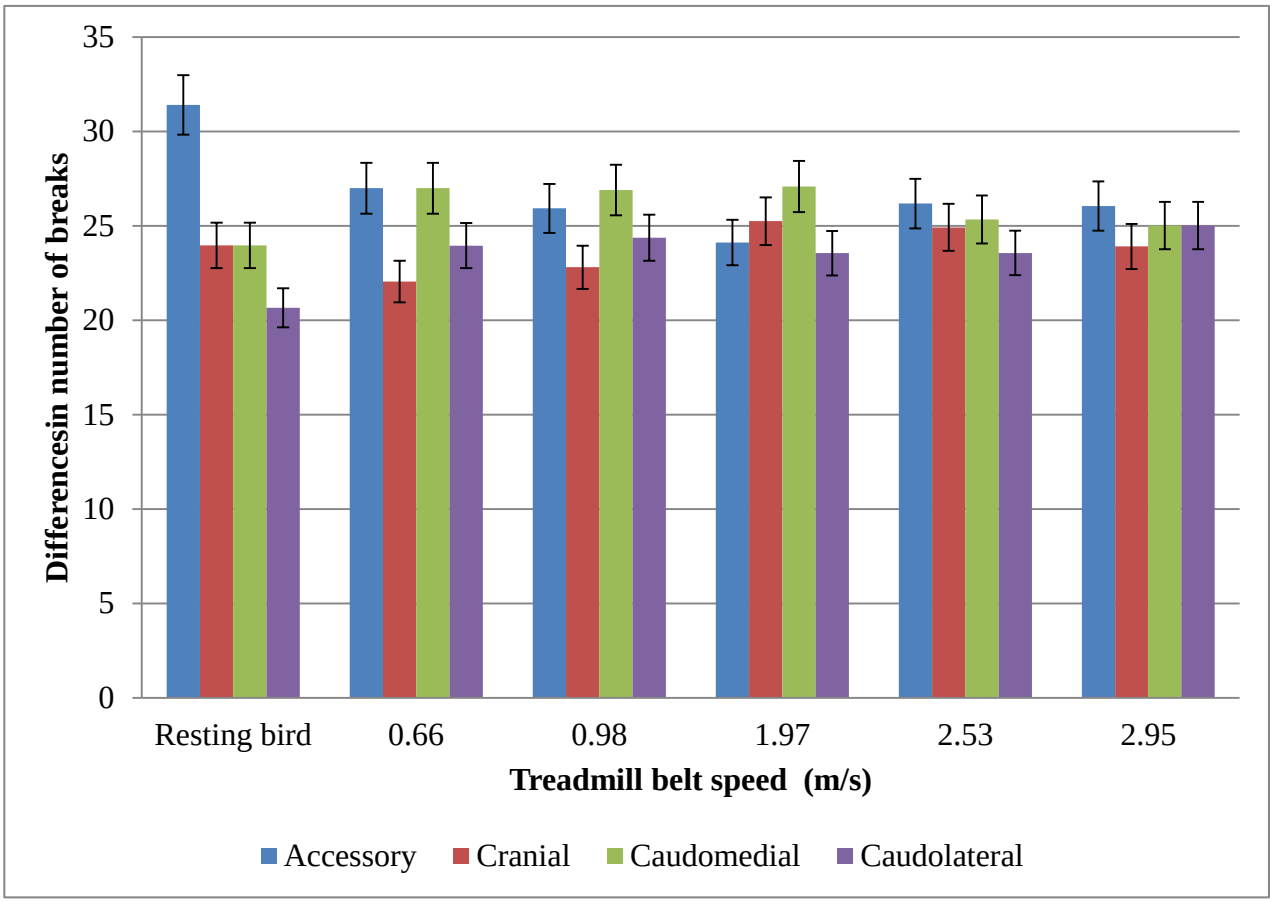

Figure 3.14 legend:

Comparison of number of E-E breaks in all the four vascular territories of the pulmonary artery indicates contribution of each vascular territory to the total number of breaks in the lung. In the resting chicken, the regions supplied by the accessory- and caudolateral branches of the pulmonary artery showed the highest and the lowest number of E-E breaks respectively, whereas, numbers of breaks are similar in the regions supplied by the cranial and caudomedial branches of the pulmonary artery. At speeds of 0.66- and 0.98 m/s, numbers of breaks in the regions supplied by the accessory- and caudomedial branches of the pulmonary arteries are similar and higher than values from the regions supplied by the cranial- and caudolateral branches of the pulmonary artery. From speed of 1.97 m/s and above, difference in numbers of breaks are similar. While there are differences in the numbers of breaks in the different arterial regions, the values are not significantly different. Data are expressed as means ± SE.

3.3 PERFUSION EXPERIMENT

3.3.1 Numbers of complete blood-gas barrier and epithelial-epithelial breaks in the terminal exchange units

Toluidine blue stained sections of the areas supplied by the four main branches of the pulmonary artery namely the accessory, the cranial, the caudomedial and the caudolateral branches were analyzed in the same manner as was done for exercise experiment. Complete BGB- and E-E breaks in randomly selected areas of 100 μm^2 at a magnification of x1000 were counted. The numbers of BGB- and E-E breaks in each of the four regions supplied by the main branches of the pulmonary artery were determined at different perfusion pressures (see appendix IX-X).

Using Toluidine blue stained photo micrographs similar to the one used for counting number of breaks in the exercise experiments, average number of E-E- and BGB breaks in randomly selected areas of supply of the four branches of the pulmonary artery were counted. Number of breaks increased with increasing perfusion pressure (Fig. 3.15). The fact that E-E contacts were more vulnerable than the BGB ones is evident at all perfusion pressures. There is a linear relationship between the perfusion pressure and number of both E-E and BGB breaks. In addition, there are more E-E breaks at any particular pressure than BGB.

Figure 3. 15: Average number of epithelial-epithelial- and blood-gas barrier breaks at different perfusion pressures

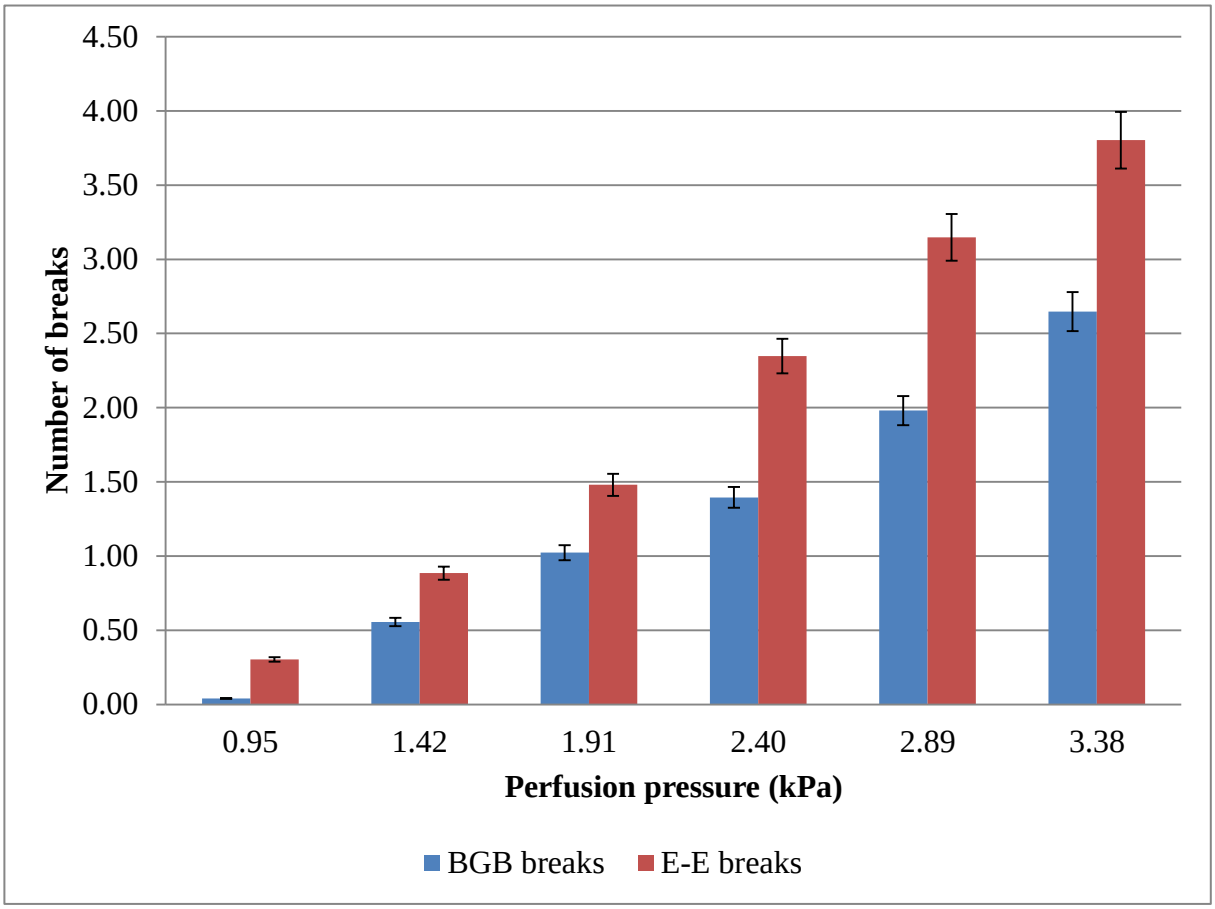

Figure 3.15 legend:

Numbers of blood-gas barrier- and epithelial-epithelial breaks counted in the whole lung increased progressively at different perfusion pressures. The lowest perfusion pressure, established during pilot study as the pressure that gave reasonable flow of perfusion fluid and the one that caused smallest number of failure, also registered both types of breaks. The two types of breaks increased with increasing perfusion pressure and at any pressure, there are more epithelial-epithelial breaks than blood-gas barrier ones. Data are expressed as means ± SE (see appendix V - VII).

3.3.2 Differences between blood-gas barrier and epithelial-epithelial breaks

In the resting chicken perfused at the lowest pressure (0.95 kPa), E-E breaks in the areas supplied by each of the four branches of the pulmonary artery are all 50% more than BGB breaks. At this perfusion pressure, no BGB break was recorded in the area supplied by the cranial branch of the pulmonary artery hence the difference was 100% (Fig. 3.16). At 1.42 kPa perfusion pressure, the difference in the areas supplied by each of the four branches of the pulmonary artery were considerably different and lower than values obtained for the lowest perfusion pressure (0.95 kPa). At 1.42 kPa perfusion pressure, the number of E-E breaks in the cranial region was about 40% higher than BGB breaks while the number of E-E breaks in the area supplied by the caudomedial branch was just 4% above the BGB breaks. Compared to the values obtained for the areas supplied by the cranial- and caudomedial branches, the difference in the accessory- and the caudolateral areas were comparable. At 1.91 kPa perfusion pressure, the differences between E-E and BGB breaks in all the branches were about 20% except for those area supplied by the caudomedial branch which was 12% greater than the BGB breaks. At 2.40 kPa perfusion pressure and above, more E-E than BGB breaks still occurred but the difference tended to decrease with increasing pressure.

Figure 3. 16: Differences between epithelial-epithelial and blood-gas barrier breaks in the four vascular region of the lung at different perfusion pressure

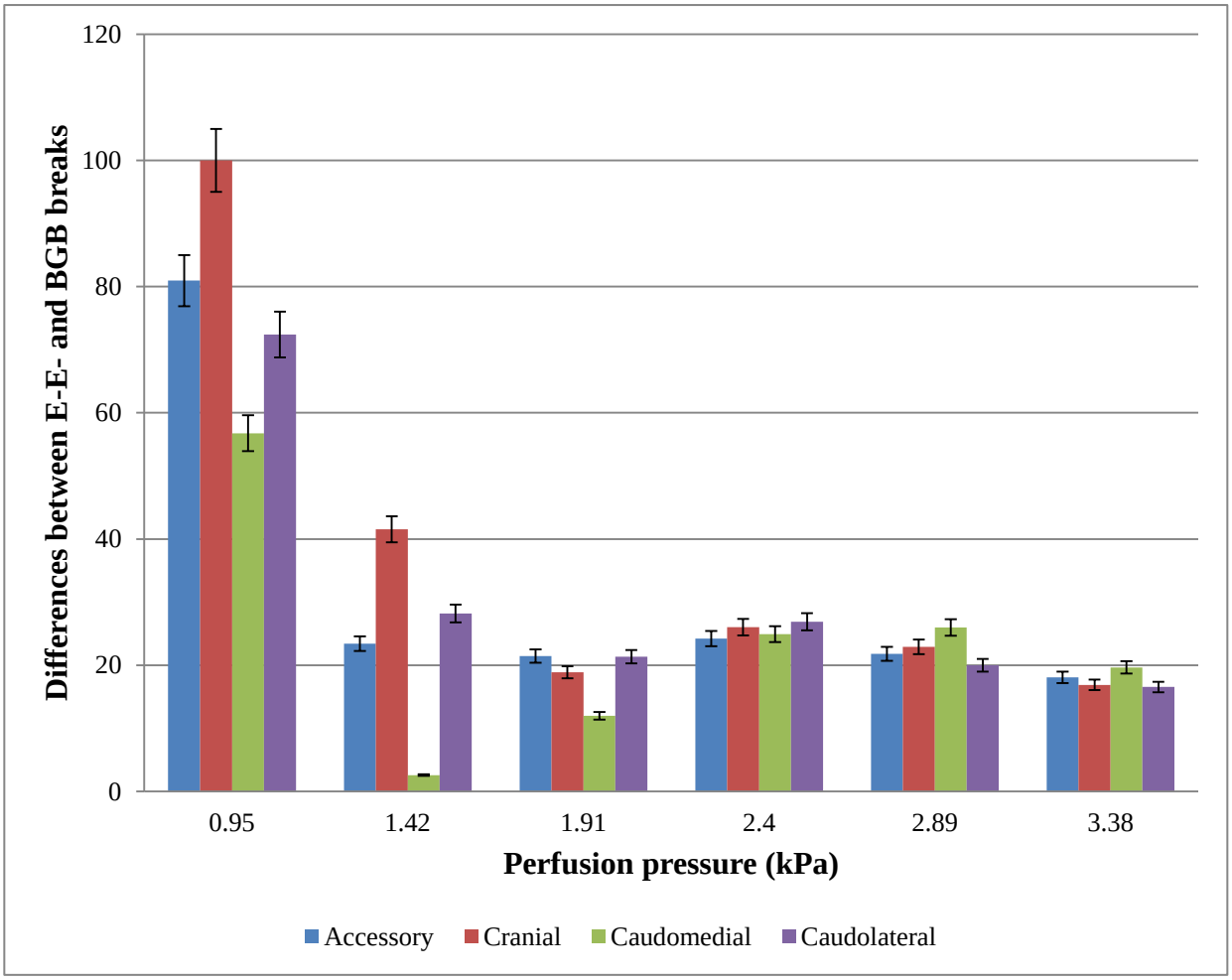

Figure 3.16 legend:

The difference between the two types of breaks decreased progressively with increasing perfusion pressure. At the lowest perfusion pressure (0.95 kPa), there were more E-E breaks (over 50%) in each of the vascular territories than the BGB ones. At the perfusion pressure of 1.42 kPa, the highest E-E break over BGB ones (41%) was in the region supplied by the cranial branch, while the lowest (4%) was in the caudomedial branch. At the perfusion pressure of 0.95 kPa, the differences between E-E and BGB in all the vascular territories are about 20% except for caudomedial branch, which was just 12%. From the perfusion pressure of 2.40 kPa and above, differences between E-E and BGB were almost similar in all the vascular territories and appear to drop slightly with increasing perfusion pressure. Data are expressed as means ± SE (see appendix X).

3.3.3 Comparison of BGB breaks in different regions of the lung after perfusion

No BGB break was recorded in the area of the lung supplied by the cranial branch of the pulmonary artery at the lowest perfusion pressure of 0.95 kPa. Fifty percent of the total failures in the lung occurred in the area of the lung supplied by the caudomedial branch at the lowest perfusion pressure while in the areas of the lung supplied by the accessory- and the caudolateral branches accounted for 25% each. At a perfusion pressure of 1.42kPa, the areas supplied by the accessory- and the caudomedial branches of the pulmonary artery had the highest number of BGB breaks in the whole lung (Fig. 3.17). At this pressure, the regions supplied by the accessory- and the caudomedial branches respectively accounted for 30% and 34% of the total BGB breaks in the lung while cranial and caudolateral areas of blood supply accounted for 17% and 19% respectively. At 1.91kPa and above, each areas supplied by the four pulmonary arterial branches contributed between 20% - 30 %. The accessory and the caudomedial branches, however, had the highest contribution.

Figure 3. 17: Comparison of blood-gas barrier breaks in the four vascular region of the lung at different perfusion pressure

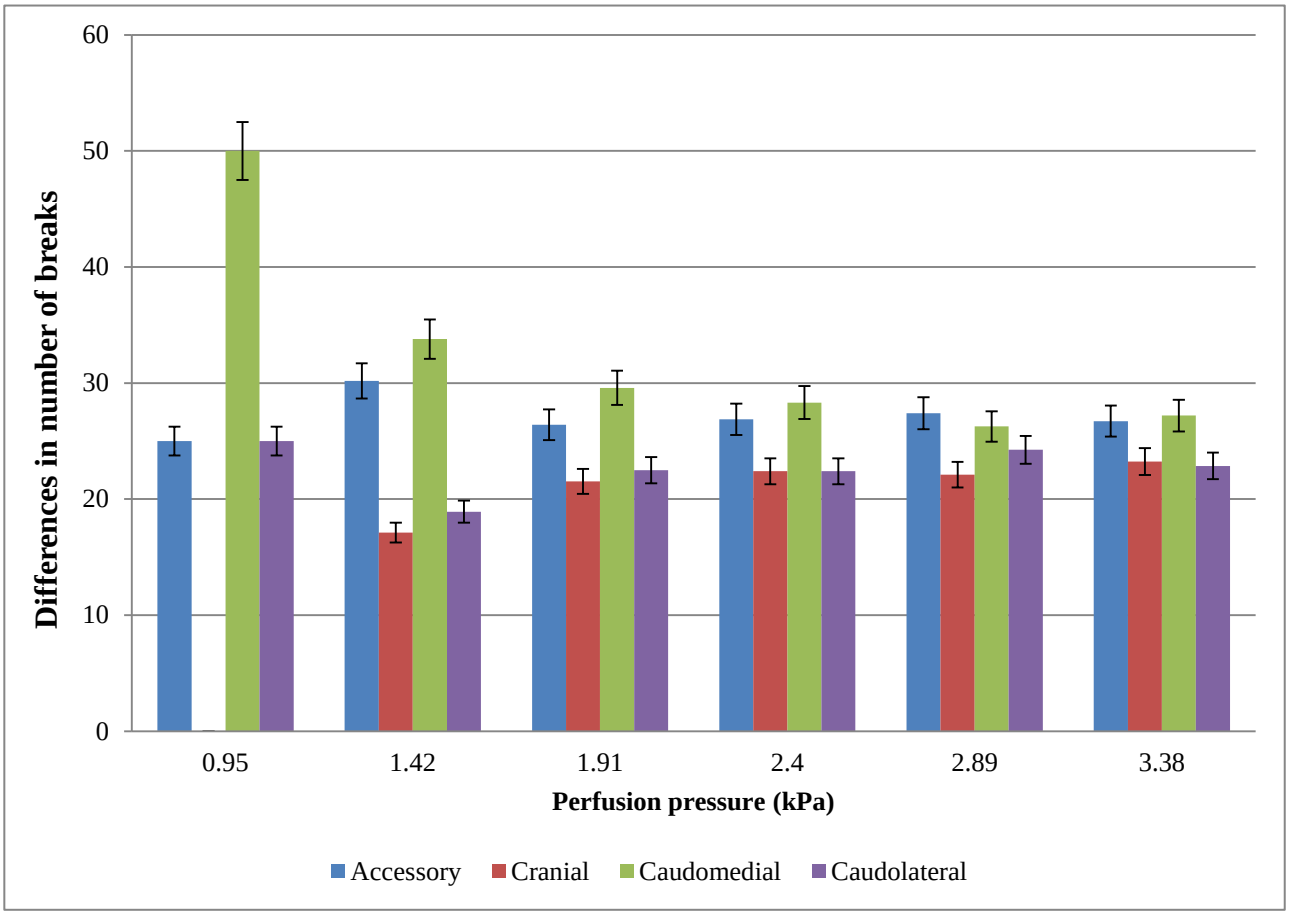

Figure 3.17 legend:

Except at the lowest perfusion pressure (0.95 kPa), the number of BGB breaks in all the branches of the pulmonary artery are not significantly different at all perfusion pressures although the values are different. Data are expressed as means ± SE.

3.3.4 Comparison of E-E breaks in different regions of the lung after perfusion

The highest number of E-E breaks (31.5% of the total E-E breaks) at the lowest perfusion pressure (0.95 kPa) occurred in the area of the lung supplied by the accessory branch of the pulmonary vessel (Fig. 3.18). On the other hand, the least number of breaks (20.5%) occurred in the area supplied by the caudolateral branch. Areas supplied by the cranial- and caudomedial branches contributed 24% each to the total E-E breaks in the lung. At 1.42 kPa perfusion pressure, the area supplied by the accessory branch still had the highest number of breaks (31%) while the lowest occurred in the area supplied by the caudolateral branch. The areas supplied by the cranial- and the caudomedial branches of the pulmonary artery contributed 26% and 22% respectively. At perfusion pressures of 1.91 kPa and higher, contribution to total E-E breaks from areas supplied by the accessory- and the caudomedial branches were both between 25 and 30% while contribution from areas of supply of cranial and caudolateral branches were between 20 and 25%.

Figure 3. 18: Comparison of epithelial-epithelial breaks in different regions of the lung at different perfusion pressure

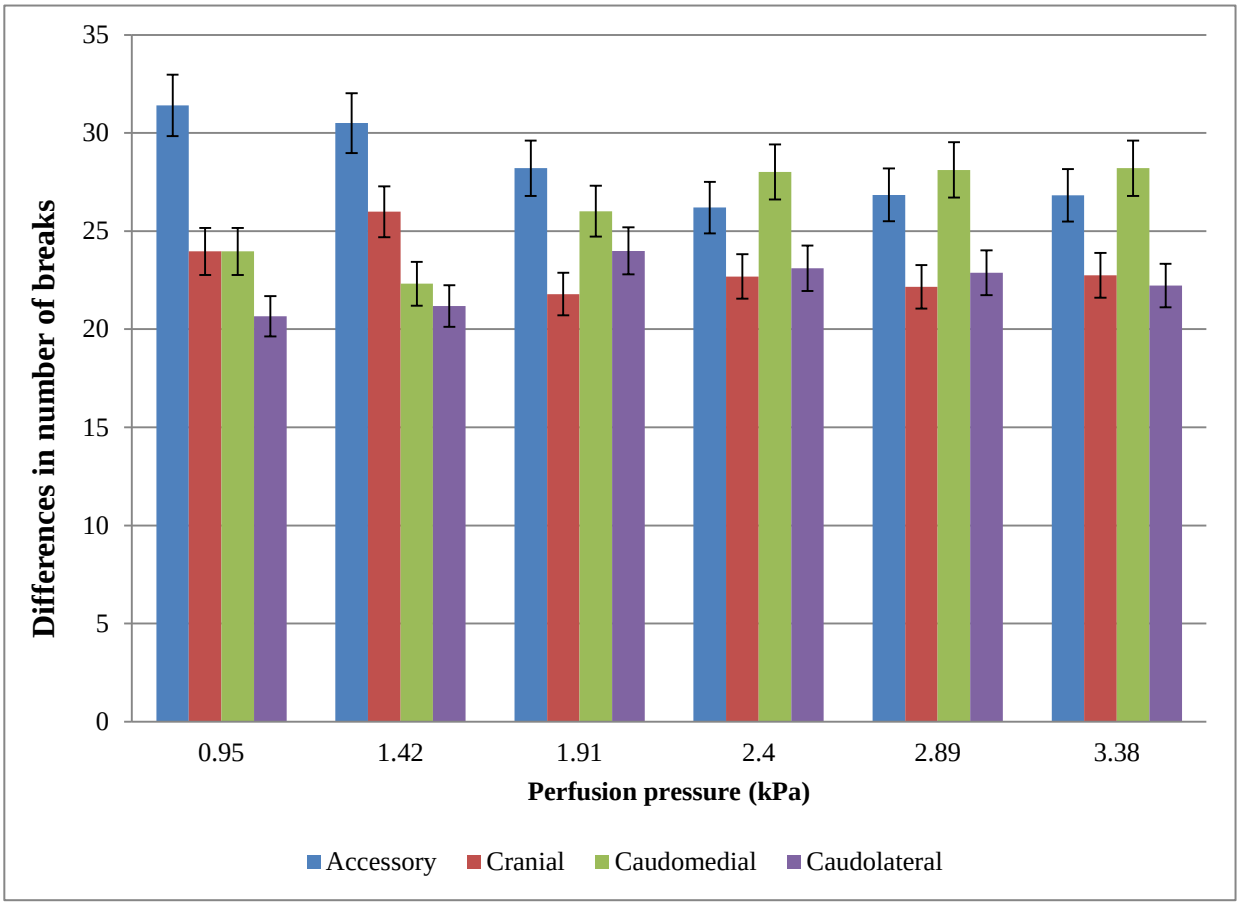

Figure 3.18 legend:

The area supplied by the accessory branch had the highest numbers of E-E breaks at perfusion pressures of 0.95, 1.42, and 1.91 kPa after which the highest number occurred in the area supplied by the caudomedial branch. At 1.91 kPa perfusion pressure and above, numbers of E-E breaks in the areas supplied by the accessory- and caudomedial branches showed higher values than in the areas supplied by the cranial and caudolateral branches however, the differences are not statistically significant. Data are expressed as means ± SE.

3.3.5 Scanning- and transmission electron microscopic observations of BGB and E-E breaks

The failure of the BGB and the E-E contacts of the air capillaries of the exchange tissue were confirmed using both scanning- and transmission electron microscopic studies. Both exercise- and perfusion-induced failure at corresponding sites are similar in most cases. Failures associated with exercise were often characterized by presence of fibrillary structures presumed to be fibrin because of the proximity to site of failure (Fig. 3.19), presence of white blood cells near the site of failure (Fig. 3.21B) and flaps. Failure of E-E contacts appears to start at the centre as small perforation (Fig. 3.20A-C) which probably joined to form a large defect without a flap (Fig. 3.20D-F). Failure of E-E contact is often seen with bulbous rollup ends (Fig. 3.22). Perfusion induced failure is characterized by tearing of the BGB, giving rough ends of break site (Fig. 3.21C and D).

Figure 3. 19: Blood-gas barrier breaks – scanning electron microscopy

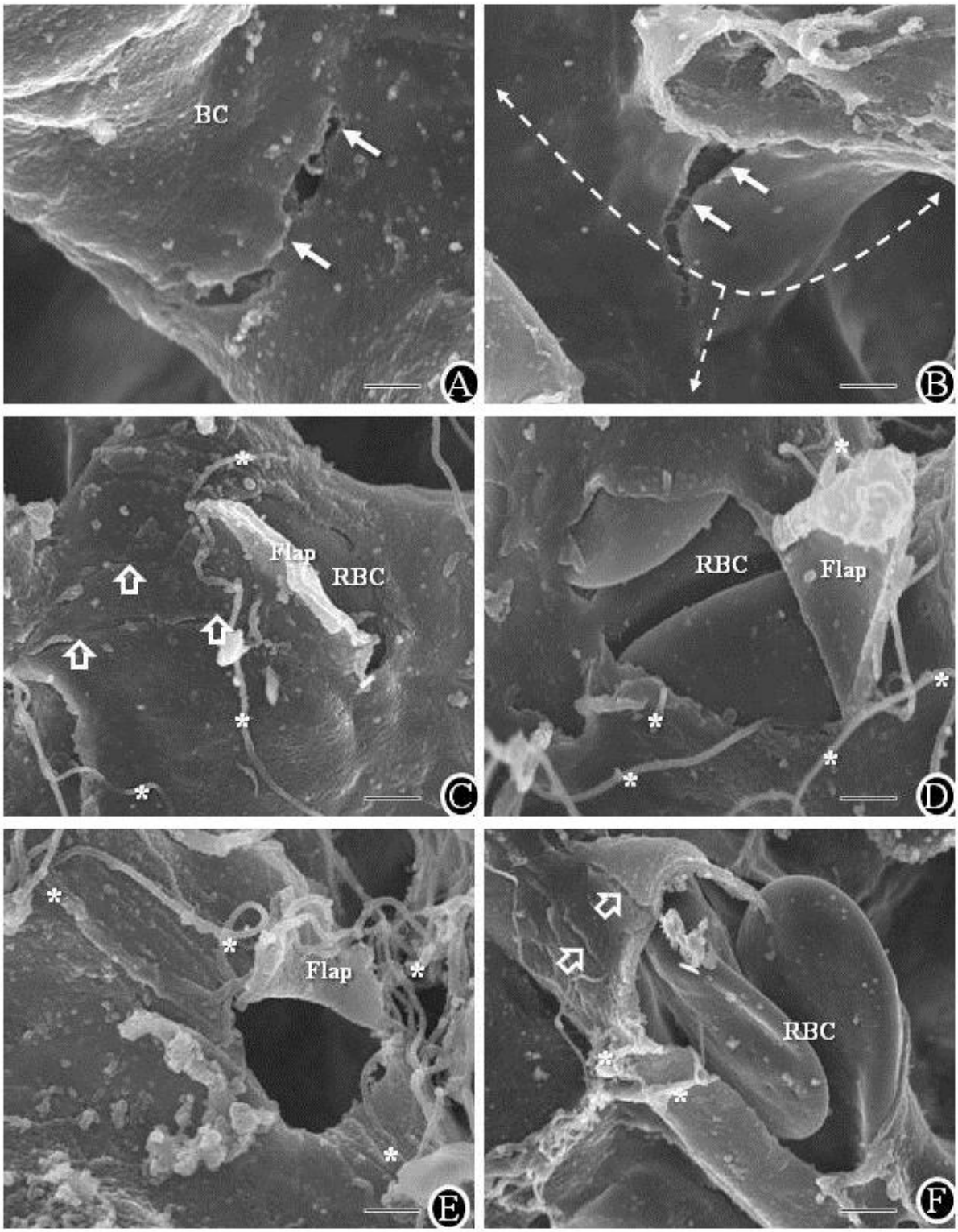

Figure 3.19 legend:

Scanning electron micrographs of the BGB breaks. **A, B:** Incomplete breaks involving mainly the epithelial cells (solid arrows). The dotted arrows in B indicate continuation into the air capillaries. Scale bars, 1μm. **C- E:** Complete breaks with flaps pushing into the air space. Open arrows in C and F are breaks affecting epithelial cells only. Scale bars, 1μm. **F:** Complete break with red blood cells (RBC) protruding out. Associated with BGB failure are fibrillary (*) structures which are probably fibrin. Scale bar, 2μm.

Figure 3. 20: Epithelial-epithelial breaks – scanning electron microscopy

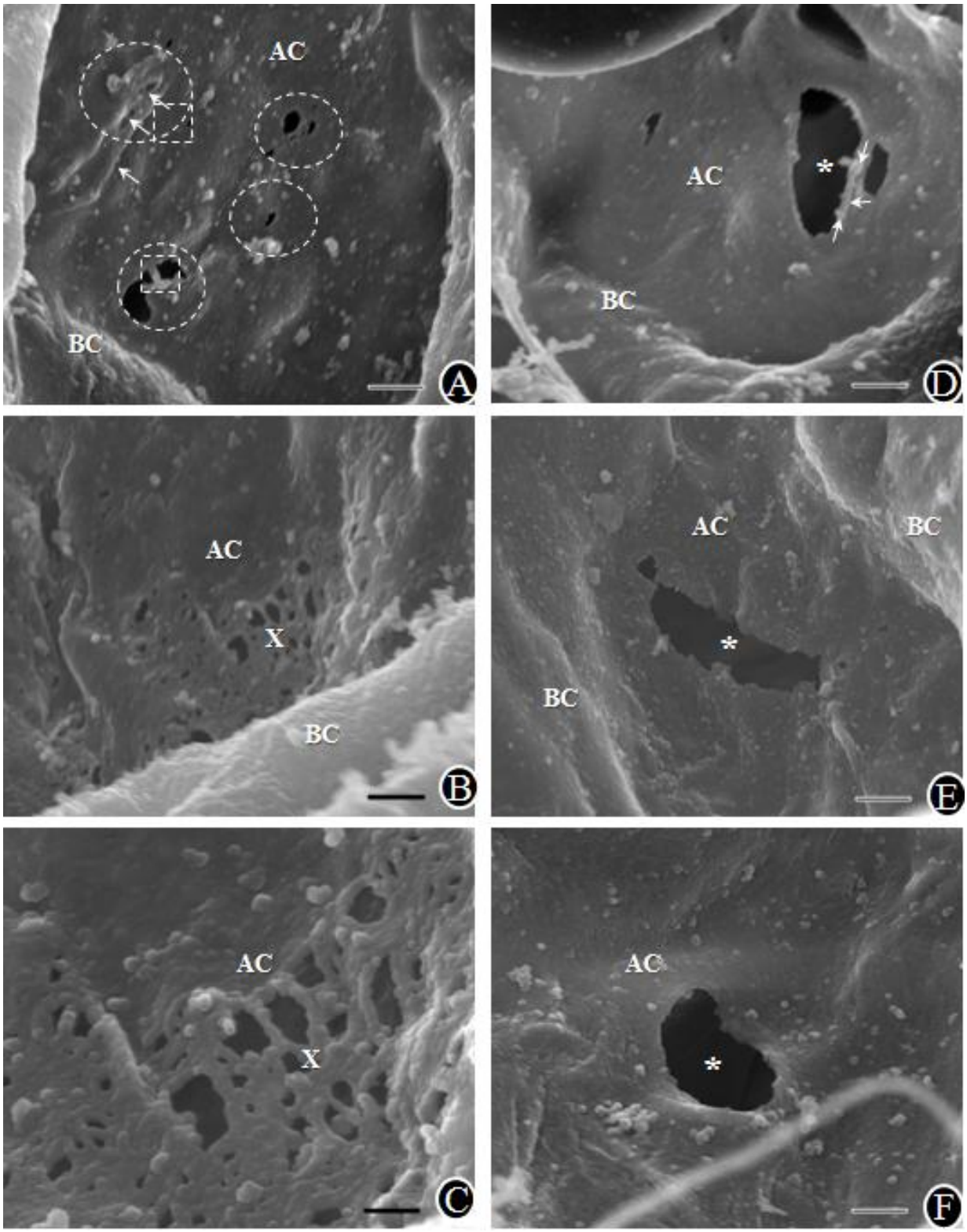

Figure 3.20 legend:

Scanning electron micrographs of E-E breaks. **A:** The opening in this micrograph represent initiation of failure which started as tiny perforations (dotted circles) that spread and join together to form bigger breaks shown as (x) in the **B** and **C**. Scale bar, 1 and 0.5 μm respectively. One unique feature of the E-E breaks is the absence of flap but a rollup (arrows) of cytoplasm as in **D** (Scale bar, 1μm). This observation indicates that E-E contacts are taut. **E** and **F** (Scale bar, 0.5μm) are E-E breaks without flap.

Figure 3. 21: Blood-gas barrier and epithelial-epithelial breaks – transmission electron microscopy

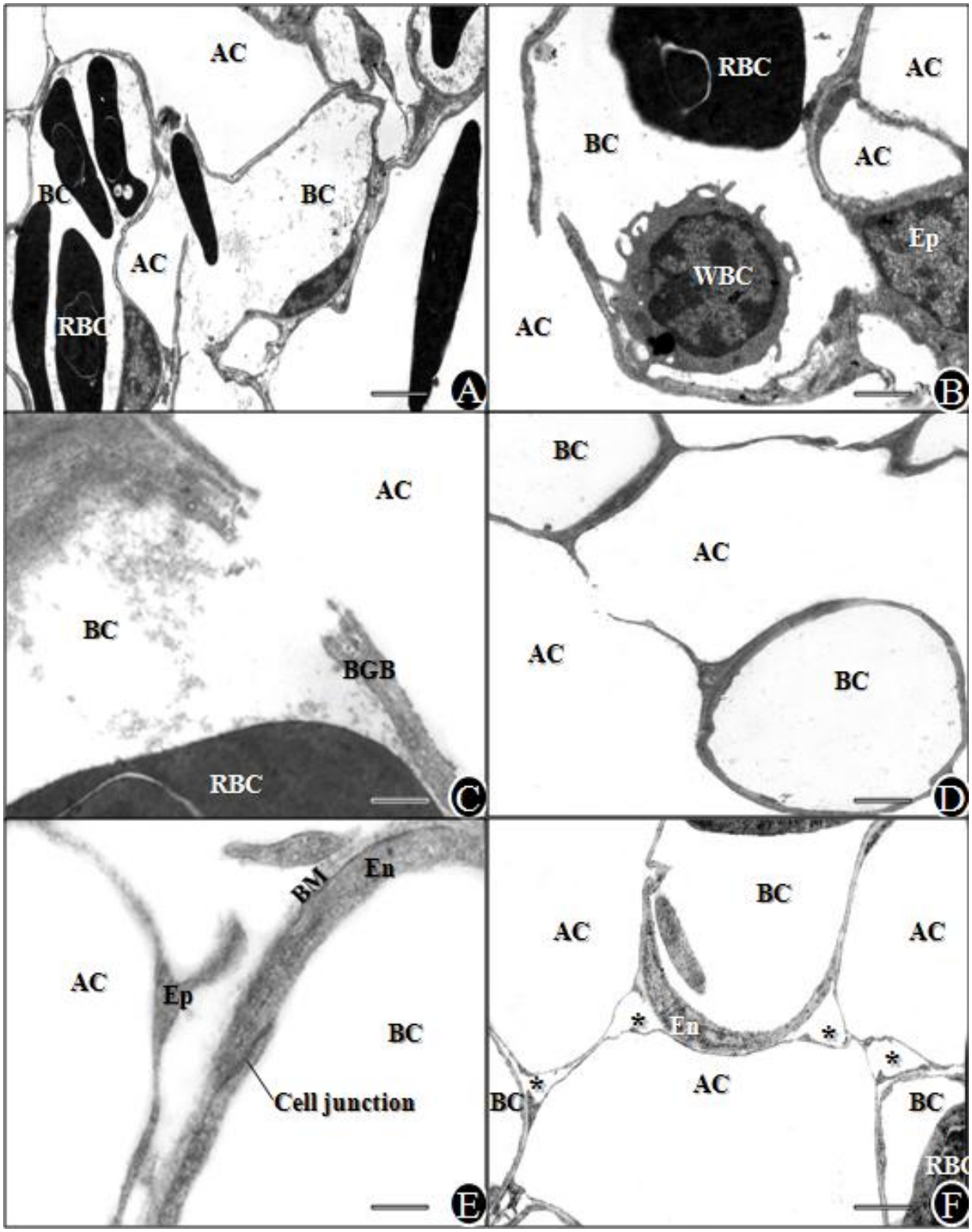

Figure 3.21 legend:

Figure A: Red blood cell **(**RBC) pushing through BGB which separates blood capillary (BC) from an air capillary (AC). Scale bar, 5µm. **B:** White blood cell (WBC) within a blood capillary (BC) is seen attached with its filopodia to the endothelial cell process of the endothelial side of the BGB close to a break region. Red blood cell (RBC) with its halo nucleus is seen close to the white blood cell (WBC). Epithelial cell nucleus (Ep) sends processes that surround an air capillary (AC). Scale bar, 5µm. **C:** A red blood cell (RBC) within a blood capillary (BC) seen close to rough ends of a break characteristic of perfusion-induced failure. Scale bar, 0.5µm. **D:** Break of epithelial-epithelial (E-E) contact which separates two air capillaries (AC) and connects two blood capillaries (BC). Scale bar 2µm. **E:** Separation of the component of the blood-gas barrier (BGB); epithelial cell process (Ep) separated from the basement membrane (BM). The basement membrane is still attached to the endothelial cell process (En). Scale bar, 0.5µm. **F:** Part of three blood capillaries (BC) two of which contain red blood cells (RBC). They are connected by two epithelial-epithelial (E-E) cell contacts, which separate three air capillaries (AC). One of the BC presented the nuclear side of the endothelial cell (En) for contact with the thin back-to-back epithelial cells processes separating two air capillaries (AC). The two E-E contacts connecting the BCs are seen here separated by wide intercellular spaces (*) near their connection to the BC. The mid-points of the E-E contacts, however, remain firmly apposed. Scale bar, 2µm.

Figure 3. 22: Epithelial-epithelial breaks – transmission electron microscopy

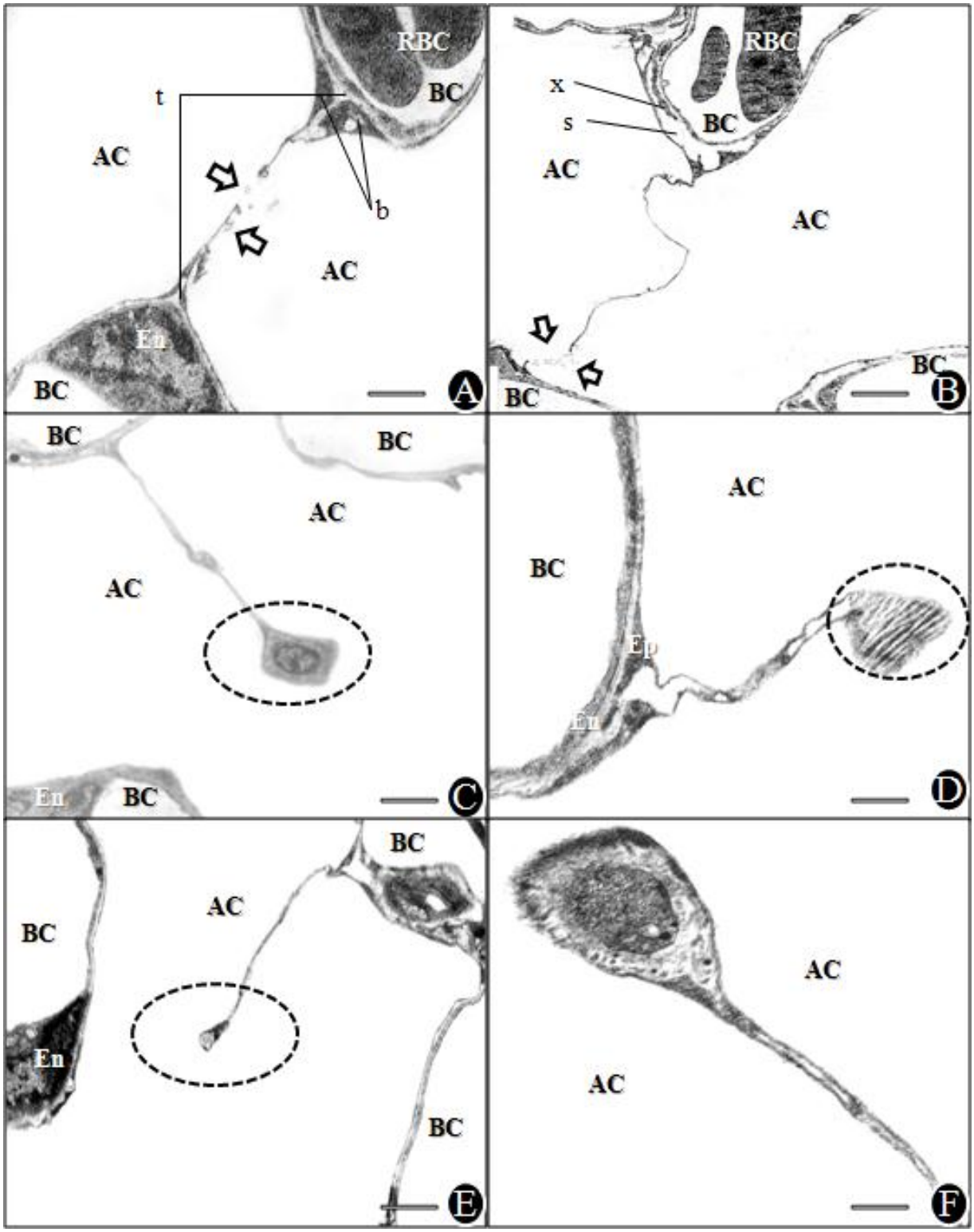

Figure 3.22 legend:

A: Two blood capillaries (BC), one of which contains red blood cells (RBC). Thin plates of back-to-back epithelial cells separating two air capillaries (AC) connect these blood capillaries. Epithelial-epithelial break (open arrows) is commonly initiated at the midpoint between the two capillaries. At the meeting point of one end of the epithelial-epithelial cell plate with blood capillary are bulges/dilations (b) of the two epithelial cells. The bulges/dilations contain most of the intracellular structures, especially cytoskeleton. The meeting points of the epithelial cell plate and blood capillaries enclosed areas (t) of basement membrane continuity – the 'triple point'. One of the blood capillaries (BC) presented the nuclear side of the endothelial cell (En) for connection with the epithelial plate. Scale bar, 2μm. **B:** Epithelia cell plate separating two ACs and connecting two BCs. RBCs are present in one of the blood capillaries. Epithelial-epithelial cell break (open arrows) near meeting point with the BC is rare. Epithelial cell is separated from the endothelial cell by wide space (S) containing cellular extension (x) of adjacent epithelial cell. Scale bar, 5μm. Break ends of epithelial cell plate are often associated with bulbous free with serrated (**C**) or core of dense material (**D**-**F**). Scale bars: C and D, 0.5μm; E and F, 1μm.

CHAPTER IV

4. DISCUSSION

4.1 ORGANIZATION OF COLLAGEN FIBERS IN THE EXCHANGE TISSUE OF THE AVIAN LUNG

4.1.1 The collagen scaffold

Collagens are a closely related family of proteins with similar amino acid sequences and similar chemical and physical properties (e.g. Hudson *et al.*, 1993). They form an integral part of a complex structural entity in the form of extracellular matrix (ECM) which surrounds and supports cells in a tissue. The ECM contains three major classes of molecules (e.g. Alberts *et al.*, 1989): (a) structural proteins made up of collagen and elastin, (b) specialized proteins consisting of laminin, fibrillin, and fibronectin, and (c) proteoglycans. Morphologically, collagen strands are arranged in the form of cord or tape shaped fibers (1-20µm wide) that run a wavy course in tissues. Collagen fibers are made up of thin and closely packed fibrils that split and join to alter number of its fibrils and thickness of its fibers while also forming a three-dimensional interconnecting network (e.g. Ushiki, 2002).

The parabronchial collagen fibers in this study are condensed into two distinctive rings/pillars - the central (axial) and peripheral collagen condensation. Stretching between these two collagen condensations are networks of thin collagen fibers that support the terminal respiratory units – the air- and the blood capillaries. The intensely red central (luminal) and peripheral (interparabronchial) parts in the transverse section of a parabronchus (Fig. 3.1B) indicates high collagen density while in between are less stained thin diffused collagen fibers. The outermost (peripheral) part of the hexagonal shaped parabronchus, the interparabronchial connective tissue septum, most likely form a sleeve around a parabronchus which is reinforced at intervals by blood vessels running parallel or circumferentially to the parabronchus.

Because the septum is located between parabronchi which are mechanically interconnected via collagen fibers in the tunica adventitia of vascular branches of the interparabronchial vessels entering the exchange tissues, the septum is probably strong. The collagen fibers entering the exchange tissues from the septum ultimately connect to luminal smooth muscles through the thin diffuse collagen of the exchange tissue (Fig. 4.1). Dynamic contractions of the neural stimulated parabronchial smooth muscles (King and Cowie, 1969; cook and King, 1970; King and Molony, 1971) of two adjacent parabronchi probably create zero net pull since their lines of contraction are directly opposite and most likely to generate equal force (Fig. 4.2). The parabronchial septum situated midway between the contracting muscles is subjected to zero net pull. Zero net pull in this part of the exchange tissue confers rigidity and thus behaves like a firm pillar. The high collagen density towards the parabronchial lumen forms the central condensation of connective tissue fibers. The collagen bundle interfaces with the atrial and the parabronchial smooth muscles to form the mobile (contractile) central pillar.

The part of the parabronchus between the two condensations of collagen fibers (the outer and the inner pillars/rings) comprises mainly of thin collagen fibers between the terminal exchange units - the air and the blood capillaries. This part is unlike the peripheral- or the central part; it does not contain thick collagen bundle wrapped around interparabronchial blood vessels, a characteristic feature of the peripheral part nor a condensation of collagen fibers around parabronchial and atrial muscles seen in the central part. The intermediate part is made up of terminal divisions of both the airways and blood vessels. Complex three-dimensional intertwining of the two terminal respiratory units, the air- and the blood capillaries, produce three types of contacts seen in the avian gas exchange tissue, namely epithelial-epithelial-, epithelial-endothelia-, and endothelial-endothelial contacts (Fig. 1.3). Dense collagen fibers

around the interparabronchial blood vessels enter the intermediate part (exchange tissue mantle) directly or indirectly via intraparabronchial blood vessels and travel in the basement membrane between these contacts. Existence of basement membrane in the contacts between two blood capillaries and between air and blood capillaries are well-established (Martin *et al*., 1988, Timpl *et al*., 1989; Leblond and Inoue, 1989), but presence of basement membrane between epithelial-epithelial cell contact is, until now, controversial. Immunolocalization of type-IV collagen, an important component of the basement membrane, between epithelial-epithelial contacts in this study established presence of basement membrane in this type of contact. Type-IV collagen forms a three-dimensional planar network of fibers surrounding the air and the blood capillaries. This network of fibers probably forms a suspensory cable that connects the central and the peripheral pillars of collagen while also supporting the terminal gas-exchange units. The suspensory collagen cable constitutes the tensional components that connect the compression components formed by the central- and peripheral pillars in a tensegrity arrangement as proposed by Maina (2007 a, b).

Large spiral and small irregular bands of smooth muscles bundles (King and Cowie, 1969; Cook and King, 1970) guard entrances to the atria from the parabronchial lumen. Dense collagen fibers formed from aggregation of fibers that course through the exchange tissue and run towards the atrial septa interfaced with the elastic tissue fibers (King et al 1967; King and Cowie, 1969; King and Molony, 1971). The collagen and the elastic tissues constitute core connective tissues of the interatrial septa. The collagen fibers are connected to the surface membrane of the atrial/parabrobronchial smooth muscle cells (Fig. 3.1F). The atrial smooth muscle, the elastic and collagen fibers connected in series. They probably work in concert to transmit tension generated by smooth muscle contraction to the thin diffuse collagen network

of the exchange tissue mantle. King and Cowie (1969) demonstrated atria smooth muscle contraction, which generates an intrinsic tone that tenses the collagen fibers. Close association or continuity between smooth muscle cells and elastic fibers has lead to suggestion of complex integration of smooth muscle action and elastic forces (King and Molony, 1971). The elastic fibers are thought to act like springs which stores energy to oppose the tone of the smooth muscle when it contracts to constrict the parabronchial lumen (Fig. 4.2). It is here proposed that the collagen fibers run uninterruptedly from the interparabronchial septa, where it is abundant, through the exchange tissue mantle, where it is thin and diffuse, to the interatrial septa where it becomes abundant again. The collagen fibers connect with the elastic tissue fibers and atrial smooth muscles. This network of collagen fibers is complexly distributed throughout the parabronchus to form a structure that exist in a state of continuous tension regulated by the smooth muscle action and elastic forces.

Figure 4. 1: Conceptual sequential stripping of a parabronchus in transverse section to show the three main arrangements of the collagen fibers that form mechanical support of a parabronchus

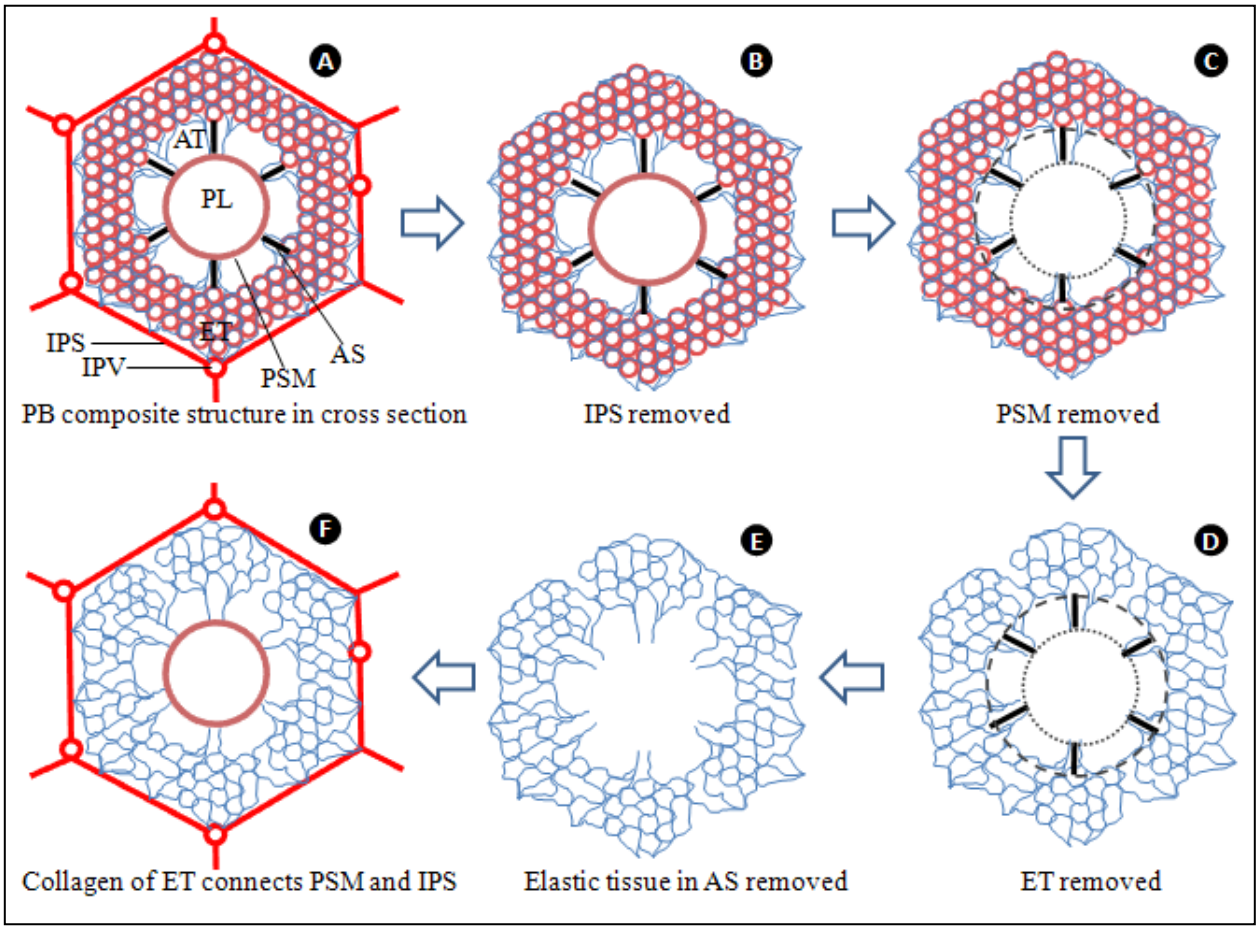

Figure 4.1 legend:

Composite structure of a parabronchus (**A**) (from inside out): Central ring of parabronchial and atrial/parabronchial smooth muscles (PSM) surround the parabronchial lumen (PL). Atrial septa (AS) containing elastic-, collagen, and other connective tissue cells surround the atria (AT). Exchange tissue mantle (ET) consisting mainly of blood and air capillaries and their extracellular connective tissue containing collagen fibers. Outer ring of interparbronchial connective tissue (IPS) containing blood vessels (IPV)

Removal of the outer ring of interparabronchial septum (**B**) and the central ring of smooth muscles (**C**) leaves the exchange tissue mantle, the atria walls and its contents (**D**). The exchange tissue mantle is supported by thin diffuse collagen fibers that permeate it. Removal of respiratory units (air- and blood capillaries) and content of atrial septa reveals the diffuse collagen (**E**). Diffuse collagen fibers of the exchange tissue mantle that support the respiratory units. Collagen fibers in this region follow the blood and the air capillaries in a complex three-dimensional arrangement. The diffuse collagenous support of the exchange units is suspended between the two rings shown in red (**F**). The dense collagenous fibers of the two rings (the interparabronchial septum (IPS) and the atrial septal (AS) ones and the diffuse collagen of the mantle probably form a continuum with different fiber arrangement and density and are under continuous tension generated by the contraction of the smooth muscle.

Figure 4. 2: Envisaged interplay of forces between and within parabronchi based on the arrangement of collagen fibers

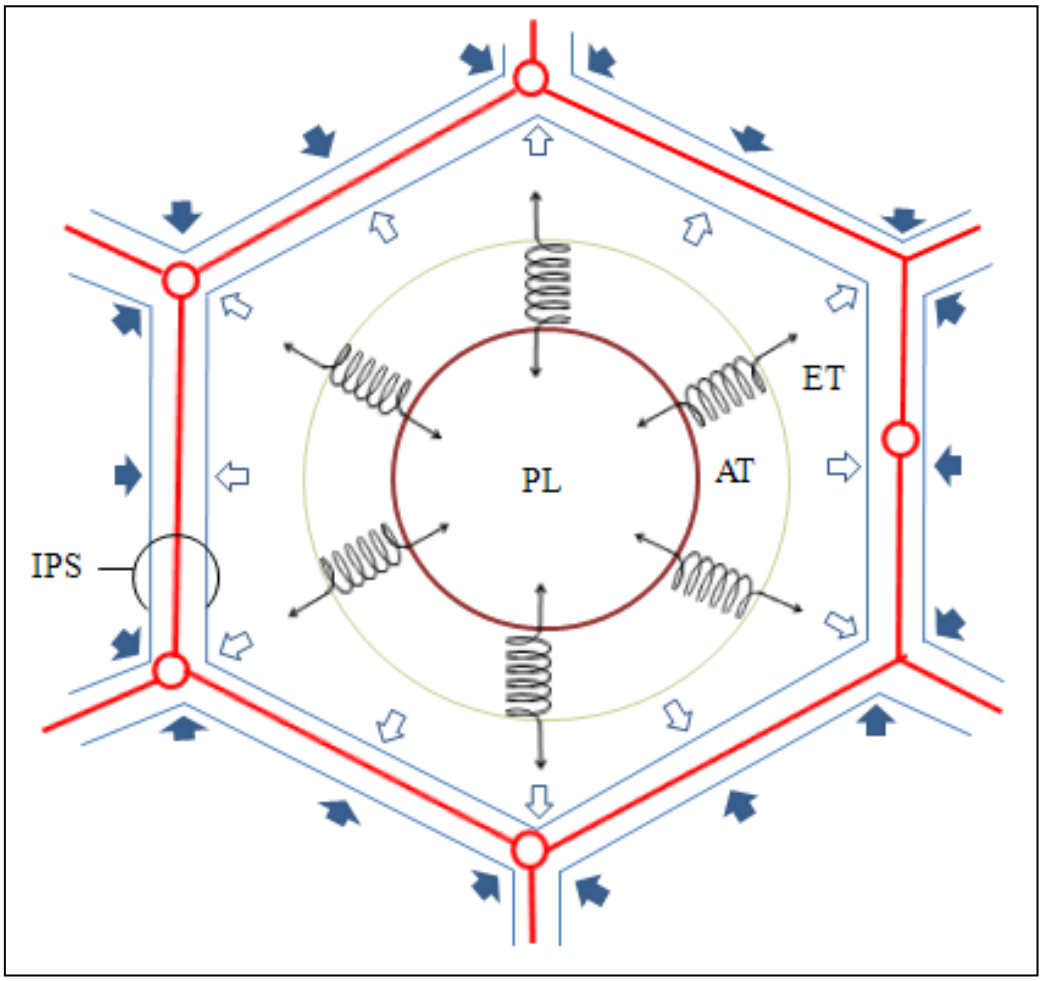

Figure 4.2 legend:

Schematic illustration to explain interplay of forces that may exist within a parabronchus and between two adjacent ones. Surrounding the parabronchial lumen (PL) is the mobile central pillar of neurogenically controlled atrial smooth muscle which is under continuous slow contraction and relaxation. Tension created by contraction of the smooth muscle (inner brown circle) is transmitted to the collagen fibers through the elastic tissue in the atria septa (springs) which surround atria (AT). The elastic tissue stores energy of smooth muscle contraction and releases the energy during smooth muscle relaxation to maintain tension in the collagen fibers in the exchange tissue mantle (ET). Because the collagen fibers of the exchange tissue are connected to the peripheral pillar (open arrows), it resists the pull of the smooth muscle thereby checking excessive pull. Existence of similar arrangement in adjacent parabronchi creates equal but opposite pull (closed arrows) on the peripheral pillar (interparabronchial septum, IPS). The net pull on the interparabronchial septum is therefore zero and so it behaves like a rigid pillar.

4.1.2 Functional organization of the components of a parabronchus

Maina (2007a, b) attributed the strength of the avian lung and particularly the air- and the blood capillaries to the mechanism of tensegrity. The American architect, engineer and philosopher, Richard Buckminster Fuller (1895-1983) first coined the term *tensegrity* (Fuller, 1961). Tensegrity is a word contraction that combined "tension" and "integrity". Tensegrity describes a structure that is held in place by a continuous system of tensional elements and a discontinuous system of compression elements (Ingber, 1997, 1998, 2003). Within a parabronchus, graded collagen condensation (thick and thin), the elastic tissue fibers and the smooth muscles are organized into an intricately interconnected unit that operates most likely on the principle of tensegrity. Bordering the parabronchial lumen, a circumferential band of dense atrial collagen fibers is coupled to smooth muscle and elastic tissue fibers. The three components are arranged into closely weaved helical structure. The long spiral and the short atrial bundles of smooth muscles described by King and Cowie (1969) can be seen as struts (compression components) while the abundant connective tissues (collagen and elastic), which connect to the muscles, as strings- the tensional components. Each short bundle of smooth muscle connects individually to the ends of two long bundles to form a closed system of compression part. The intrinsic tone maintained by the muscles (King and Cowie, 1969; Cook and King, 1970) may keep the tensional components taut so that they bind the struts, pressing on them as a continuous tensional network to maintain a pre-stressed state. The short atrial muscle component gives attachment to septal collagen and elastic tissues and the resultant woven column of smooth muscles forms the axial pillar. The whole arrangement resembles Snelson 'tensegrity column' or 'Kellem grip', a woven wire rope that absorbs tension during mechanical pulling of a cable. The dense collagen fibers in the interparabronchial septum and

those associated with the walls of the interparabronchial blood vessels form the external (peripheral) supporting column: the exchange tissue appears to be effectively ’suspended’ between the two columns (pillars) (Figs. 4.1- 4.3) and supported by thin diffuse collagen fibers that permeate the gas exchange tissue mantle. Tension generated by contraction of the smooth muscles is transmitted to and stored in the elastic tissue fibers. The elastic tissue ensures a constant tension in the suspended collagen cables between the two pillars.

Figure 4. 3: Distribution of collagen fibers in the various parts of the parabronchus

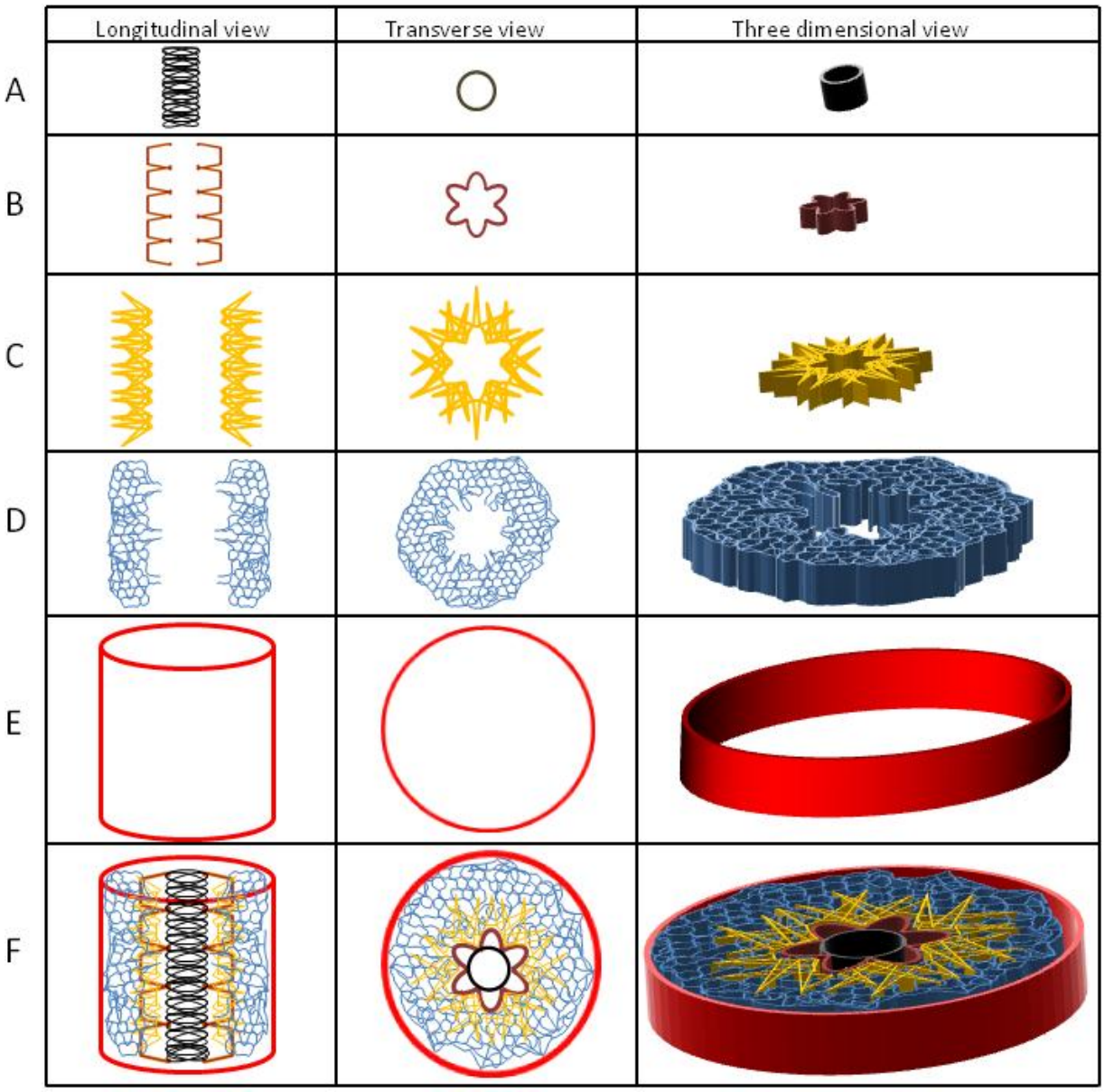

Figure 4.3 legend:

Schematic illustration of the arrangement of collagen fibers in the parabronchus in *longitudinal* (first column), *transverse* (middle column), and *three-dimensional* views (last column). From inside out, the division of the collagen fibers can be followed from the inside to the outside along the branching air spaces (from the parabronchial lumen to the interparabronchial septum) or inwards along the branches of the blood vessels (from the interparabronchial septum to the parabronchial lumen). In this illustration, the division of the air spaces is shown from the parabronchial lumen into the exchange tissue to the parabronchial outer limit at the interparabronchial septum. **A:** Complexly weaved collagen fibers, elastic tissues and the atrial smooth muscles. This is the most mobile part of a parabronchus; it is under neurogenic control to maintain tension in the network of collagen fibers within the exchange tissue. **B:** Bundle of collagen fibers from the atrial muscle split by following the division of the atria to give rise to the infundibula. **C:** Collagen fibers around the infundibulum become thin fibers as the infundibulum branches to become air capillaries. **D:** Thin support collagen fibers in the exchange tissue are sandwiched between the epithelial cell of the air capillaries and the endothelial cells of the blood capillaries. From the exchange tissue, collagen fibers follow the intraparabronchial blood vessels to where it becomes a significant bundle as the tunica adventitia of the interparabronchial blood vessels (**E**), which is located in the interparabronchi septa. **F:** Putting all the components (A-E) together form a composite structure of a parabronchus which is based on differential thickness of collagen fibers.

4.1.3 The basis of the strength of the parabronchial exchange tissue

Since the account by Macklem *et al*. (1979) and Powell *et al*. (1985), efforts have been directed at explaining the basis of the strength of the deceptively fragile but mechanically robust avian terminal gas exchange units (Klika *et al*., 1997; Scheuermann *et al*., 1997; West *et al*., 2006, 2007a; Watson *et al*., 2007, 2008; Maina, 2007a, b, 2008). However, the particular structures and/or mechanisms that can explain their remarkable strength have remained elusive. Very few studies have directly investigated the role of components of the basement membrane in the strength of the blood-gas barrier, in spite of numerous indications that the basement membrane and not the overlying (epithelial) - nor lining (endothelial) - cells is responsible for the mechanical strength in most tissues (e.g. Williamson *et al.*, 1971; Welling and Grantham, 1972; Fisher and Wakely, 1976; Brenner and Humes, 1977; Wieslander and Heinegard, 1985; Swayne *et al.*, 1989). While some investigators have attributed the remarkable strength to the hexagonal geodesic shape and the arrangement of the parabronchi, the mechanisms have not been fully explained. Recently, Maina (2007a, b) argued for the principle of tensegrity (first described by Fuller, 1961) to explain the reported remarkable strength of the air- and blood capillaries. He suggested that the arrangement of collagen connective tissue fibers, their topographical locations, and their known physical- and mechanical properties and behavior, portend existence of a tensegrity system in the avian lung.

Collagen- and elastic tissue fibers, proteoglycans, and other glycoproteins are the main structural macromolecules of the mammalian lung's connective tissue elements (e.g. Hance and Crystal, 1975; Hopkins *et al*., 1986; Crouch *et al*., 1997; Toshima *et al*., 2004). Collagen fibers, which constitute 6 to 20% of the matrix proteins of the dry lung weight (Bradley *et al*.,

1980), are responsible for the tissue tensile strength and relative inextensibility. Collagen fiber of a diameter of 1 mm can support a 0.5 kg weight before breaking (Elden, 1968) and only fails at strains of between 6 and 22% volume fraction (vf) (Liao and Belkoff, 1999). Collagen- and elastic tissue fibers are commonly found in close topographical relationship (Elden, 1968; Gosline, 1976; Gosline and French, 1979; Alter, 2004), forming a connective tissue framework that supports and maintains normal tissue architecture. Depending on their function, collagen- and elastic tissue fibers occur in a particular ratio in different organs (Weibel, 1984). Elastic tissue fibers have much lower tensile strength but high extensibility: they can stretch by as much as ~150% of their original (relaxed) length before breaking (Gosline, 1976; Gosline and French, 1979; Robins, 1988; Alter, 2004). In spite of their close proximity when they occur together in tissue, they have different functions. At all lung volume and within normal physiological range, collagen limits lung expansion while elastin brings about its recoil (Mead, 1961; Senior *et al*., 1975).

The connective tissue scaffold that forms part of mammalian lung fibroskeleton (Wang and Ying, 1977; Gil and Hernandez, 1984; Matsuda *et al*., 1987; Amenta *et al*., 1988; Mercer and Crapo, 1990, 1992; Mercer *et al*., 1994; Ohtani and Nakatani, 1994; Gonçalves *et al*., 1995; Maina, 2002a, b; Toshima *et al*., 2004) includes a dedicated type-I collagen cable that courses along the thick side of the polarized interalveolar septum (IAS) (Weibel, 1973, 1984, 2009). The relatively uniformly thin BGB in the avian lung (Maina and King, 1982; Maina *et al*., 1989; Maina and West, 2005; Watson *et al*., 2007) lacks the 'strong' supporting thick side found in mammalian IAS (e.g. Maina and West, 2005; Maina, 2005; Maina, 2007a). Type-I collagen, essential for maintaining integrity of the IAS (Weibel, 1973, 1984, 2009), is lacking in the avian BGB. The only collagen in the avian BGB is the basement membrane collagen

type-IV. In this study, it was observed that in the exchange tissue, gold conjugated secondary antibody targeted against primary antibody raised against type-IV collagen are found in the basement membrane between two blood capillaries (endothelial-endothelial contact), two air capillaries (epithelial-epithelial contact) and blood and air capillaries (endothelial-epithelial contact, BGB). The dense collagen in the interparabronchial septa teased out to enter the exchange tissue as thin diffuse fibers to become part of the sparse extracellular matrix of the exchange tissue. The sparse extracellular matrix is constituted mainly by the basement membrane sandwiched between the exchange units (air- and blood capillaries) therefore; collagen here is the basement membrane collagen type-IV. Within the lamina densa of the basement membrane, type-IV collagen is arranged to form a continuous two-dimensional cable (Alberts *et al*., 1989; Widnell and Pfenninger, 1990; Crouch *et al*., 1997). Other components of the basement (fibronectin, laminin, proteoglycan) bind type-IV collagen to cells (Lallemand *et al.,* 1995; Senior *et al.,* 1996). Because of the two-dimensional arrangement and the unique property of type-IV collagen, it can lengthen when pulled (Timpl *et al*., 1989; West and Mathieu-Costello, 1999).

Because of the fact that surface tension need not be overcome in the non-expansible volume constant terminal respiratory units (air-capillaries) in the rigid avian lung, limitation is not strictly imposed on the ultimate size of the terminal gas exchange units in the avian lung (Maina, 2000a, b; Maina and West, 2005; Maina, 2007a). The gas exchange tissue of the avian lung is therefore highly compartmentalized and subdivided to give rise to extremely small (e.g. Duncker, 1972; Maina, 1982; Maina and King, 1982) uniformly thin-walled air- and blood capillaries (Maina and King, 1982; Watson *et al*., 2007). The type-I epithelial cells are so thin that a basement membrane was reported to be lacking between the epithelial-epithelial

cell contacts (Maina and King, 1982). Though sparsely distributed, collagen type-IV, a major component of the basement membrane, was unequivocally demonstrated by imunocytochemical localization between epithelial-epithelial contacts in this study. Type-IV collagen alone does not constitute the entire basement membrane and appears only after deposition of laminin (Leivo, 1983; Lallemand *et al*., 1995), another major component of the basement membrane. Other components are incorporated to form a definitive plainer basement membrane structure (Leivo, 1983; Leblond and Inoue, 1989) after type-IV collagen molecules self assemble into a chicken wire-like mesh (Yurchenco and Ruben, 1988). Identification of type-IV collagen in this study unequivocally established presence of a basement membrane between the epithelial-epithelial cell contacts. Although, West *et al.* (2010) suggested extension of extracellular matrix containing type-IV collagen into the space between epithelial cells, they did not directly demonstrate it.

The arrangement of the respiratory units in the gas exchange tissue of the avian lung is characterized by three-dimensional intertwining, branching and anastomoses of the air- and blood capillaries (Woodward and Maina, 2005, 2008; Maina, 2007a; b; Maina and Woodward, 2009). Plane of section through any orientations of the avian exchange tissue may show a view where blood capillaries are completely surrounded by air capillaries. In such a case, back-to-back epithelial-epithelial (E-E) contacts, which look like spokes of a bicycle wheel (Fig. 1.3), interconnect blood capillaries. Klika *et al*., 1997, Watson *et al*. (2007) and West *et al*. (2007a,b) suggested that these E-E cells interconnections strengthen blood capillaries by forming what they termed ‘bridges’, ‘cross-braces’, ‘paired retinacula’ and ‘struts’. In another plane of section, E-E cells interconnections may not be as conspicuous such as where an air

capillary is completely surrounded by blood capillaries (e.g. Maina *et al*., 1989). Air capillaries that are completely surrounded by blood capillaries at a particular plane of section showing no E-E cells interconnections will show different arrangement 'above' and 'below' that particular plane because both the air and the blood capillaries anastomose and intertwine in three dimensions (Woodward and Maina, 2005, 2008; Maina, 2007a; b; Maina and Woodward, 2009). Although not directly confirmed, according to West *et al*. (2007a, b) and Watson *et al*. (2007), E-E cells interconnections together with the endothelial-endothelial contacts may provide robust mechanical support to the avian terminal gas-exchange units. These contacts probably function to absorb and redistribute tension from and across the BGB (Maina *et al.,* 2010). The presence of type-IV collagen in the E-E contact, established in this work, confirm occurrence of basement membrane between the contacts, which in all likelihood, form a continuum with the conspicuous basement membrane of the BGB, and that of the endothelial-endothelial contacts. A continuous system of collagen fibers running around the air- and the blood capillaries is indirectly connected to the peripheral and central pillars of the parabronchus, supporting the gas exchange tissue mantle. Maina (2007a) questioned the role of the strengthening of the lung by such E-E cells interconnections by pointing out that folds occur in such sites (Maina, 1984). Powell and Mazzone (1985) observed similar folds in the air and blood capillaries in rapidly frozen lungs. As pointed out by Maina (2007a), the observed pleats in the lung tissue could be the result of the caustic treatments and conditions that tissues are subjected to for microscopic viewing. Besides, such folds cannot be natural since pulmonary surfactant has been reported to function as an anti-adhesive which reduces the work required to separate apposed epithelial surfaces (Sanderson *et al*., 1976; Reinfenrath, 1983; Daniels and Orgeig, 2003) such as folds and pleats. In addition, pulmonary surfactant has also been reported to act as a boundary lubricator (Hills *et al*., 1982). Therefore, the

incidence of such folds needs to be determined before a meaningful conclusion can be drawn on their significance. Furthermore, since micrographs are in two dimensional representation, three-dimensional reconstruction of serial sections would provide more information concerning the morphologies of the pleats.

4.1.4 Cell shape generation and maintenance – role of basement membrane

It is still not yet clear how shapes are generated and maintained at the cellular level (e.g. Keren *et al*., 2008) but, interaction of intracellular cytoskeleton, the cell membrane and cellular substratum have been suggested (Pollard *et al*., 2000; Zaidel *et al*., 2004; Carlier and Pantaloni, 2007). The complexity of the interactions and the minuscule components involved in shape generation at cellular scale impose extreme challenge to precise understanding of the process (Keren *et al*., 2008). One explanation holds that extracellular matrix actively binds to growth factors in the micro-environment (e.g. Erickson and Couchman, 2000; Hagedorn *et al*., 2001) and through the cell membrane, the matrix influence intracellular assembly and arrangement of cytoskeletal structure to determine shape (Ingber *et al*., 1986; Bussey, 1996; Keren *et al*., 2008; Zemel *et al*., 2010). At the gas exchange level, extreme thinning of the pulmonary epithelium as well as pulmonary endothelium is vital to gas exchange function. Lack of cell organelles, especially in the cytoplasmic extensions of the type-I cells, minimizes oxygen consumption by the tissues and cells of the lung, generally promoting delivery of oxygen to the rest of the body. Thinning is so intense in pulmonary architecture that the type-I epithelial cell with a volume of 1,764 μm^3 covers an area of 5,098 μm^2 (Crapo *et al*., 1982). In birds the delicately thin pulmonary type-I epithelial cells, 0.086 μm (Watson *et al*., 2007),

spread over a large surface area and constitute only 12% of total BGB thickness (Maina and King, 1982; Watson *et al*., 2007). Attainment and maintenance of such shape and size is determined by mechanical balance of forces between the cell and its extracellular matrix (e.g. Ingber, 2006; Zemel *et al*., 2010).

The type-I epithelial cell has been reported to expresses type-I cell marker T1α (McElroy *et al*., 1995; Newman *et al*., 2000; McElroy and Kasper, 2004; DeBiase *et al*., 2006) and any cells that expresses T1α also deposit fibers of laminin-311 in their matrix (DeBiase *et al*., 2006). Laminin, a large family of heterotrimeric matrix proteins made up of α, β, γ subunits (Yurchenco and Cheng, 1994; Aumailley and Smyth, 1998; Tunggal *et al*., 2000; Aumailley *et al*., 2005), are very important in the organization and the stabilization of cell-basement membrane interactions (Aumailley and Rousselle, 1999; McGowan and Marinkovich, 2000; Miner and Yurchenco, 2004; Hamill *et al*., 2009). Laminin is also involved in mechanical-signal transduction initiated by stretching which in turn activates certain pathways in the attached epithelial cells (Jones *et al*., 2005). Furthermore, it has been proposed that cells are in a state of continuous isometric tension because of micromechanical interactions with the extracellular matrix (Ingber and Jamieson, 1985; Huang and Ingber, 1999) and shape modulation can alter cell fate (Ingber, 1990; Mooney *et al*., 1992; Chen *et al*., 1997). Definitive shape granted by regional variations in mechanical compliance of the extracellular matrix caused by local thinning of the basement membrane in turn stretches the associated adherent cells (Ingber, 2006). Modulated thinning of the pulmonary basement membrane may explain the organization and the stabilization reported in the transformation of type-II to type-I cells during the process of epithelial cell repair. The process involves adhesion, spreading and migration (Adamson and Bowden, 1974; Adamson *et al*., 1990; Kheradmand *et al*., 1994; Kim

et al., 1997) of the pulmonary type-II cells to form type-I cells (Adamson *et al*., 1988, 1990). In other words, changes in the intracellular balance of mechanical forces alter cellular responses to hormones and growth factors, which may lead to variation in cell form and function (Ingber, 2006). Loss of thickness in the formation of the BGB and E-E cells contacts during avian lung development as observed by Maina (2003) may involve modulated thinning of the extracellular matrix (secreted by mesenchyme) as suggested by Ingber (2006). Composition of the extracellular matrix has been reported to change with development (e.g. Miner *et al*., 1997; Pierce *et al*., 2000). Differences exist in the basement membrane on which both type-I- and II pneumocytes are resting despite being continuous and within the same tissue. For instance, the basement membrane anionic sites in relation to type I - and type II pneumocytes are different (Brody *et al*., 1984; Sannes, 1984). Unlike the basement membrane associated under type-I pneumocyte, disruption exist in the basement membrane under type-II pneumocyte through which it extends cytoplasmic processes to contact neighboring type-II pneumocyte cells (Brody *et al*., 1982). This may indicate cell specific extracellular composition, which in turn may dictate shape and function. Cellular function is dependent on shape (Singhvi *et al*., 1994; Shah, 2010) and shape is granted by the basement membrane (Ingber *et al*., 1986). Presence of basement membrane between E-E cells contacts is essential since the physical environment, dictated by the basement membrane (Ingber *et al*., 1986) influences cellular internal organization (Ingber *et al*., 1986; Huang and Ingber, 2000) and shape is determined by arrangement of intracellular cytoskeleton (Keren *et al*., 2008; Zemel *et al*., 2010). The particular barrier function that is performed by the epithelial cells in the gas exchange tissue of the avian lung is granted by its characteristic shape which is thin and extensive and determined by its basement membrane.

Figure 4. 4: Envisaged schematic illustration of formation of blood-gas barrier, epithelial-epithelial contacts, and possible explanation of thinning of the extracellular matrix in the contacts

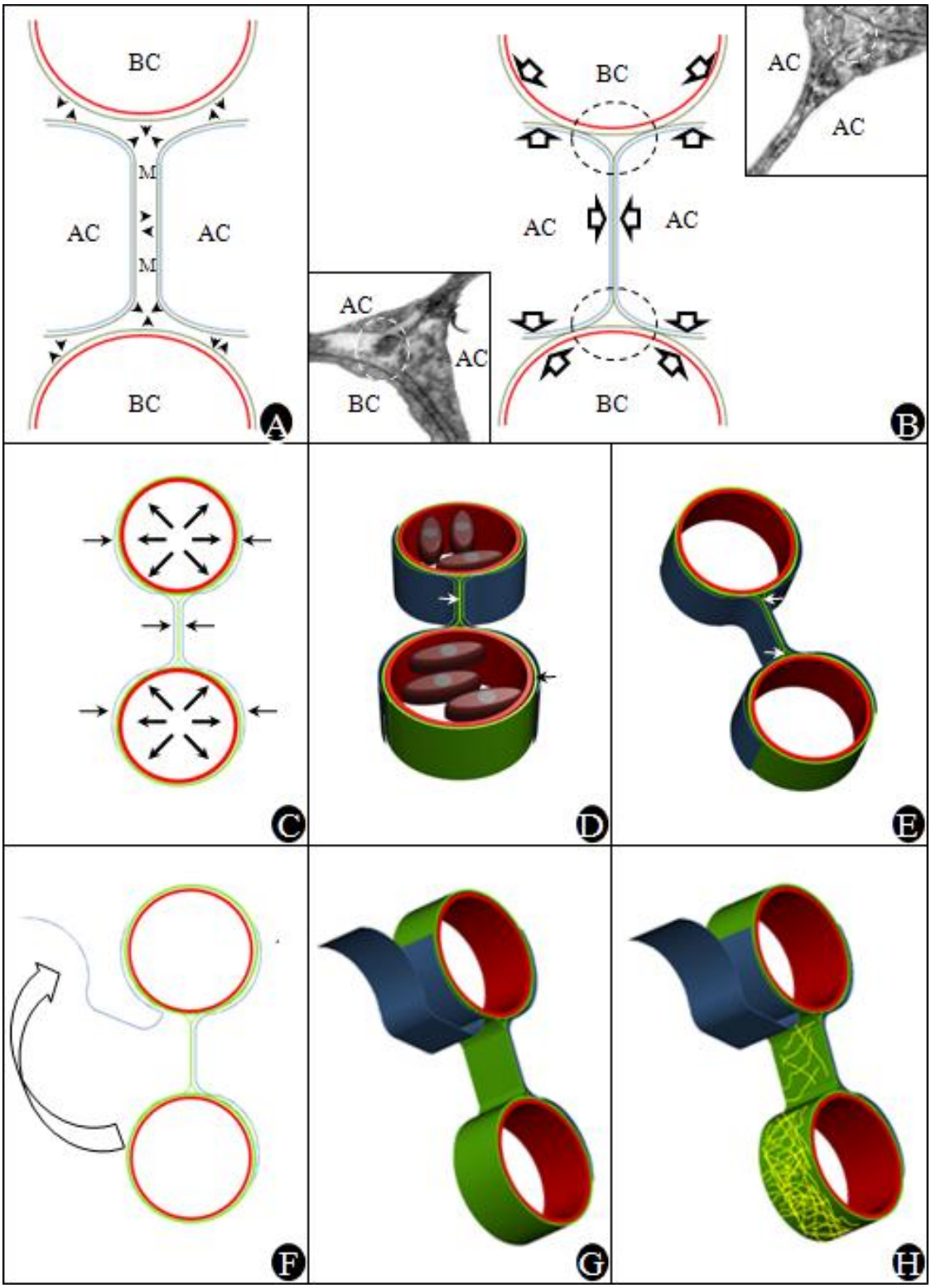

Figure 4.4 legend:

A: Developing air capillaries (AC) lined by epithelial cells project into the surrounding mesenchymal tissue (M) which in turn surround the outer surfaces of developing air capillaries. Mesenchymal tissue (M) trapped between projecting air capillaries and blood capillary (arrowheads) secretes components of extracellular matrix. Trapped mesenchymal tissue/cell degenerate and are replaced by the extracellular matrix. **B**: Factors in the microenvironment probably guide and govern arrangement of extracellular fibers and intracellular cytoskeleton to produce contacts that allow basement membrane continuity at the triple point (insert). **C**: Perhaps depending on mechanical stresses in the air- or blood capillaries (arrows), interaction between extracellular matrix and intracellular cytoskeleton produce difference in thickness of extracellular matrix through modulated thinning to form different basement associated with the BGB and the E-E cell contacts. **D**: When viewed in three dimensions, relatively high-pressure blood capillary have a significant basement membrane (black arrow) while low-pressure air capillary possess less significant basement membrane (white arrow). E: Three-dimensional view shows basement membrane continuity between BGB and E-E contact. Supposing the epithelial cell process is stripped away from the blood-gas barrier on one side of the terminal exchange units as in **F** and view in three dimension, **G**, collagen density in the comparatively high-pressure 'blood filled' blood capillary will be greater than in low-pressure 'air filled' air capillary **H**. This assumption is supported by the results of the experiment on selective alkali digestion that spared collagen connective tissue fibers and the experiment that immuno-localized type- IV collagen.

4.1.5 Interdependence between parabronchi and structural components within a parabronchus

Mutual structural relationships between adjoining parabronchi appear to exist across the interparabronchial septum in the avian lung. The 'honeycomb-like arrangement' of the air and the blood capillaries described by West *et al*. (2006) may be part of this interdependence. Interparabronchi septa conceivably transmit and distribute mechanical tension generated within or outside a parabronchus. Levitzky (2007) attributed similar role to the alveoli septa to explain structural interdependence in the mammalian lung. The hexagonal shape of the parabronchi is maintained by tension in the interparabronchi septa, which is connected to the fused pleurae (Duncker, 1978; King and McLelland, 1984; McLelland, 1989), to the oblique and horizontal septa (Duncker, 1971, 1978; McLelland, 1989), and ultimately to the body wall (Maina, 2005). The flat walls of interparabronchial septum and shared by adjacent hexagonal shaped parabronchi provided a firm plate of fibrous connective tissue to which the exchange tissues of individual parabronchi are attached. The luminal aspect of the exchange tissue is attached to the column of crisscrossing parabronchial smooth muscle, which 'parallel' the peripheral plate of interparabronchial connective tissue septa. Tension generated by the rhythmic contraction of the parabronchial smooth muscle and maintained by recoil of elastic tissue between phases of contraction and relaxation create mechanical interdependence across the interparabronchi septa. This arrangement prevents spontaneous collapse of any of the parabronchi and by default the exchange tissue of the avian lung. Prominent interparabronchial septa in the lung of poor flyers limit the gas exchange tissues externally (e.g. Maina *et al*., 1982; 2000a). Collagen and other connective tissue fibers surround the interparabronchial vessels and fill up spaces between parabronchi. Collagen connective tissue

fibers around intraparabronchial vessels successfully demonstrated in this study enter the exchange tissue directly and indirectly. The collagen fibers entering the exchange tissue from the interparabronchial septa are in continuity with the collagen fibers within the interatrial septa and those that surrounds the parabronchial muscles. Because adjacent parabronchi receive collagen fibers from the same section of the interparabronchial septum, they are directly interconnected. Collagen fibers from the interparabronchial septum enter adjacent parabronchi travel centrally and in opposite direction towards their respective parabronchial lumina. Contraction of the neurogenically controlled parabronchial smooth muscles (King and Cowie, 1969) pull on the diffuse collagen fibers that originate in the interparabronchial septa. Because the pulling is in the opposite direction and most likely with equal force (because of similarity in structure and dimension), the net effect on the septa is zero. Apparently, parabronchi surrounded on all sides by other parabronchi and subjected to such pull on all sides, are greatly stable. As suggested by West *et al*. (2006) similar interactive relationship may also exist between the terminal exchange units - air - and blood capillaries. Within avian exchange tissue, pulmonary blood capillary is surrounded by air capillaries or vice versa (Fig. 4.5, inset). Where two air capillaries exist side by side, a 'strut' (epithelial-epithelial cells plate) (E-E) connects two blood capillaries (Klika *et al*., 1997; West *et al*., 2007a; Watson *et al*., 2007, 2008; West 2009). These 'struts' appear to be arranged like spokes of a bicycle wheel around a blood capillary when the plane of section is across the long axis of the blood capillary. The space between the contacting epithelial cells was formerly thought to lack an extracellular component (Maina and King, 1982). Recently, West *et al*. (2010) reported that space between the contacting epithelial cells contains an extension of BGB basement membrane but that the contacting cells lack intercellular junctions. Presence of component of the basement membrane (Figs. 3.5A-E), contacts that appear to be intercellular junction (Figs.

3.21F and 3.6F,G) and abundant intracellular fibrilary structure (Figs. 3.6H-L) suggests that E-E contacts are important anatomical part of an integrated hierarchical support structure within the avian exchange tissue. Basement membrane in all the three contacts within avian exchange tissue form a continuum that ultimately connect to the mobile central part which regulates tension and the rigid peripheral part which resists tension. This hierarchical reciprocal interdependence within the exchange tissue mantle and between parabronchi provides robust mechanical stability to the exchange units, the parabronchi and the lung as a whole. Tensegrets (as applied to a parabronchus) are stabilized by balancing of opposing forces of tension and compression (e.g. Fuller, 1961). The states of push and pull that are often assumed to be simple opposites, do not in reality oppose each other but rather, complement each other to impart stability/strength (e.g. Wilken, 2001). In the lungs of those species of birds that lack interparabronchial septa like the nongalliform species (e.g. Duncker, 1971; Maina *et al*., 1982; McLelland, 1989), the tensegrity system may, to a greater extent, include features like the solidity of the lung, robust structures like the intrapulmonary primary bronchus which possesses cartilaginous support, the thick-walled secondary bronchi and large blood vessels. These structures form compression islands in a tensional sea of collagen.

Figure 4. 5: Envisaged structural interdependency between parabronchi

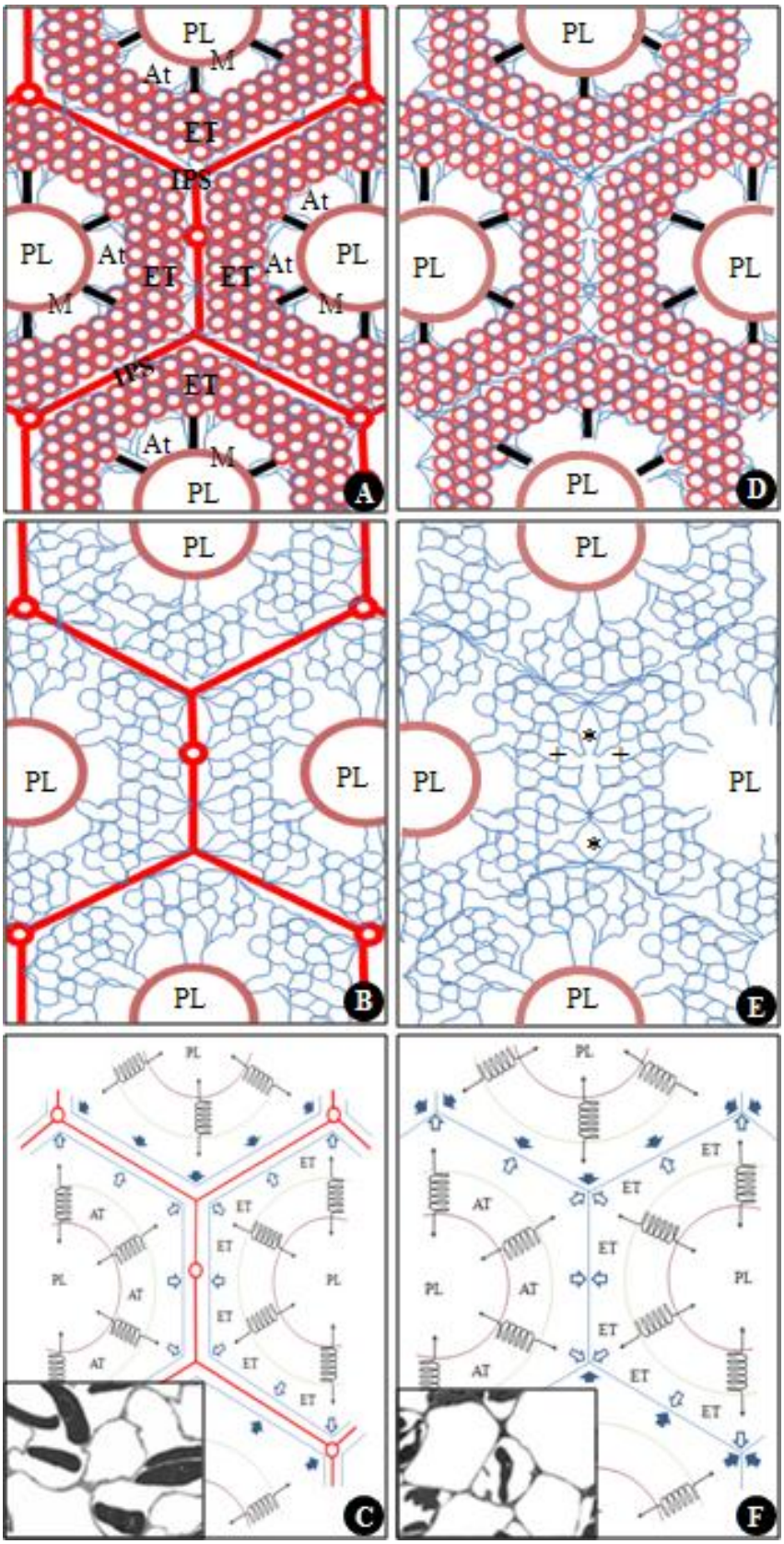

Figure 4.5 legend:

Schematic illustrations of four adjacent and connected parabronchi in cross sectional view. The lumina (PL), separated by the exchange tissue mantle (ET), are equidistant. Each lumen is surrounded by parabronchial smooth muscle (M) and separated from the exchange tissue mantle (ET) by the atria (At) but are connected to it by atrial septum separating two atria. The air- and blood capillaries (ET) are removed to leave only the envisaged support structure in galliform species (Figs. A-C) and in non-galliform species (Figs. D-F). **A:** Prominent interparabronchial vessels occupy the interparabronchial septa in the galliform species. This prominent feature marked the outer limit of the exchange tissue and serves as anchoring point for collagen fibers entering the exchange tissue. The less dense collagen (mainly type-IV) of the exchange tissue run and converge towards the parabronchial lumen where they become aggregated to form a prominent bundles that interface with elastic tissue within atria septa and attached to the parabronchial smooth muscle. **B:** The prominent centrally and peripherally aggregated collagen fibers are envisaged to be more firm and the two are connected by the exchange tissue collagen which is thin and less prominent. **C:** Contraction of the smooth muscles associated with the central prominent part pulls on the thin less prominent fibers within the exchange tissue which in turn pull on the interparabronchial septa to which it is attached. Because interparabronchial septa are situated between parabronchi, adjacent parabronchi are connected across it. Pulling caused by contraction of two adjacent parabronchi cancelled out at the septa where the two are connected. This may imply that parabronchial structure cannot be maintained without mechanical interconnection with adjacent parabronchi. **D:** Similar conceptual arrangements also exist in non-galliform species but instead of a prominent interparabronchial septa across which adjacent parabronchi are attached in galliform species, the exchange tissue collagen interconnect directly. **E:** Although dense

collagen fibers around blood vessels occupying the interparabronchial septum are rarely seen in lungs of non-galliform birds it does not mean they do not exist, only that the thin collagen fiber dominate. The '*' represent the position of the less seen interparabronchial vessel and + represent path followed by intraparabronchial vessel into the exchange tissue mantle in non-galliform species. **F: S**imilar interplay of forces and mechanical interdependency may exist much like in the galliform species.

Figure 4. 6: Three-dimensional and line schematic representation of epithelial-epithelial contact and its association with blood capillaries.

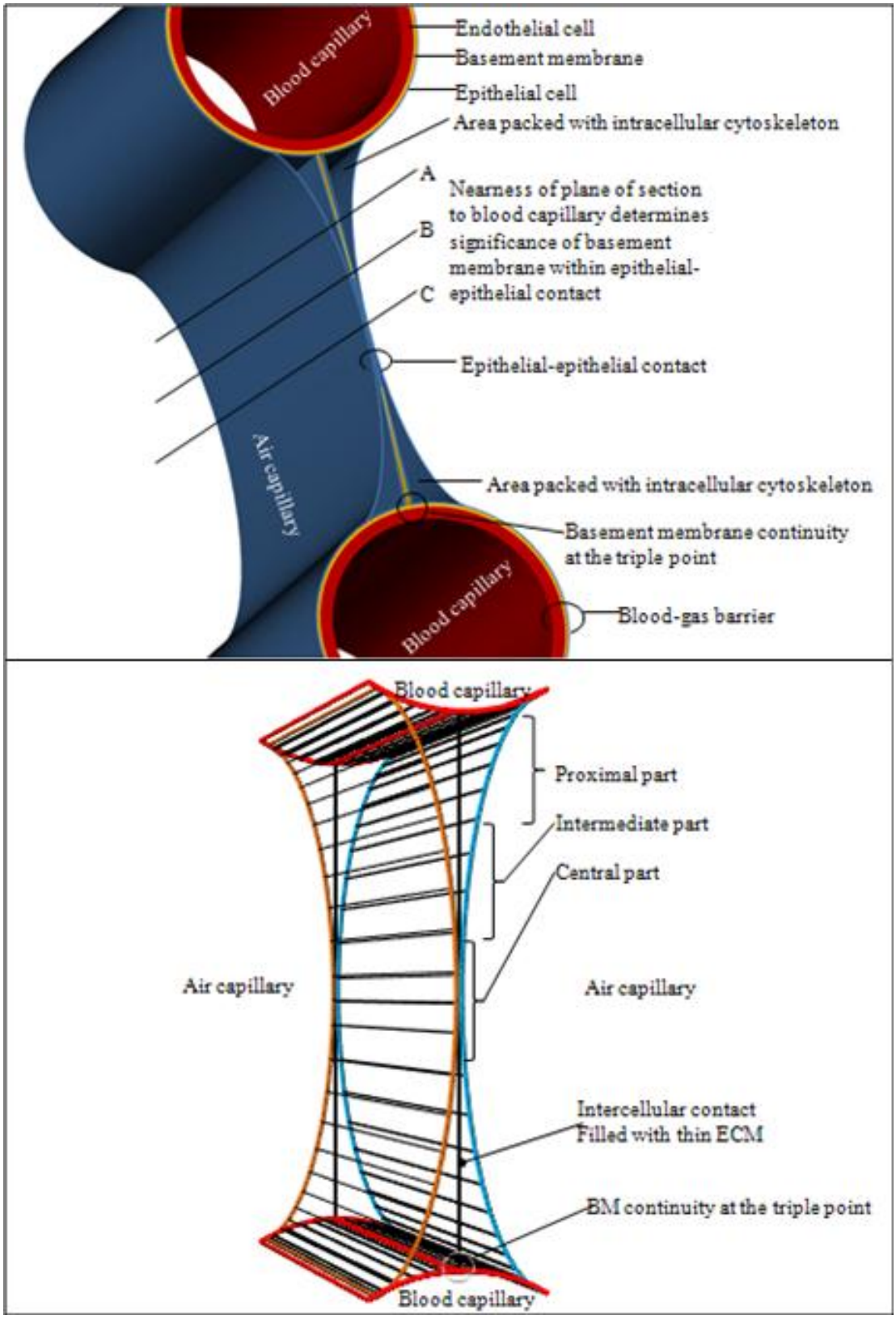

Figure 4.6 legend:

A: The blue colour represents the epithelial cell process of the air capillary (AC); red colour, the endothelial cell process of the blood capillary (BC) and yellow represent the basement membrane (BM) between the two cells processes. Cell-cell contact between the two epithelial cells processes span the distance between the two BC they bridge. Throughout the length, the BM between the two epithelial processes ensures that they are held together. The epithelial cell process is thinnest midway between the capillaries. Gentle curvature of the air-fronting plasma membrane away from the cell-fronting plasma membrane towards the BC increase the width of the process as the BC is approached. The widest portion of the cell created intracellular space that accommodates intracellular structures, i.e., cytoskeleton. **B**: Skeletal diagram of E-E contact showing firm back-to-back apposition of the cell processes (central straight line). The E-E contact is divisible into three parts: the *central*, *intermediate* and the *proximal* relative to the blood capillaries. The *proximal* part is close to the blood capillary and represents the widest intracellular space containing most of the intracellular structures. This part forms the base that supports the intermediate and the central parts. The intracellular space of the intermediate part contains few or no cytoskeleton. The central part is where the air- and cell- fronting plasma membrane are closest with barely noticeable cytoplasm between them.

4.2 RESTING AND EXERCISE EXPERIMENTS – THE OUTCOMES

4.2.1 Assessment of treadmill exercise

Because of morphological and functional differences mainly of the respiratory systems and the heart, the effect of exercise on pulmonary hemodynamic in bird may be different from that in mammal. For instance, separation of the mechanical pulmonary ventilator (air sacs) from the gas exchanger (lung) transferred expansible function, which stretches the lung to the thin walled air sacs (e.g. Piiper and Scheid, 1989) and birds have relatively larger hearts with a huge cardiac output (Hartman, 1955; Snyder, 1976; Jurgens *et al.* 1981). Compliance in mammalian lung creates longitudinal tension which contributes to stresses on the BGB (West *et al.*, 1991). The consequence of the separation of the exchanger from the ventilator in the avian respiratory system is that the avian lung only changes in volume by mere 1.4% during a respiratory cycle (Jones *et al.*, 1985). The reported maximum compliance of the avian respiratory system is: domestic fowl, 0.0096 L/cm H_2O (Scheid and Piiper, 1969); in the duck 0.03L/cm H_2O (Gillespie *et al*., 1982) and in the anesthetized pigeon 0.0028 L/cm H_2O (Kampe and Crawford, 1973). Whereas in mammals, maximum lung compliance are reported to be 0.24 L/cm H_2O in rat, 13.4 L/cm H_2O in cat, 71 L/cm H_2O in dog and 200 L/cm H_2O in man (Spells, 1969/70). Because of the small compliance in the avian lung, tension on the exchange tissue associated with inflation may be considered insignificant. If compliance is negligible in the avian lung, it is probable that out of the three forces (*surface tension force, circumferential wall tension, and longitudinal tension*) (see Fig. 1.3) reported to act on mammalian BGB (West *et al*., 1991), only circumferential wall tension and surface tension force, meaningfully act on the avian BGB. Although, the surface tension at the air-water

interface of the ACs that range in diameter between 3 and 20 μm (e.g. Duncker, 1972; Maina and Nathaniel, 2001; Woodward and Maina, 2008) should, in all likelihood, be much greater than in mammalian alveolus. The less efficient surfactant with little palmitoylmyristoylphosphatidylcholine that lack surfactant proteins (SP)-A and SP-C (Bernhard *et al*., 2001) may reduce surface tension to the same extent as that of mammalian lung because volume change in avian lung is small (Jones *et al*., 1985) even though parabronchial diameter may change (King and Cowie, 1969; Macklem *et al*., 1979). It is most likely that surfactant proteins in bird lungs primarily serve as antimicrobials and provide a thin lining layer that prevents exudation of plasma protein on to the respiratory surface. The surfactant in the bird lungs may also function as an anti-adhesive (Sanderson *et al*., 1976; Reinfenrath, 1983; Daniels and Orgeig, 2003) and as a boundary lubricator (Hills *et al*., 1982) than as a tension diffuser. In some species, the space between parietal and visceral pleurae is bridged by dense connective tissue fibers (King and McLelland, 1984) or is completely obliterated (Duncker, 1978; McLelland, 1989). Since surface tension force at the air-tissue interface did not have to be overcome in a volume constant avian lung because ventilation does not cause inflation/deflation of the terminal gas exchange unit – the air capillaries could become extremely small (Maina, 2007b). Increase in intramural pressure, caused by exercise-induce cardiac response, is probably the only significant force that acts on the BGB.

Lactate is a dynamic metabolite with a rapid turnover which can participate in a number of processes during rest, exercise, and recovery from exercise (Brooks, 1985). Depending on the level of energy demand and prevailing conditions, pyruvate, the end product of glycolysis can either be reduced to form lactate or oxidized to CO_2 and H_2O (Cabrera *et al*., 1999). A lactate pool serves as a critically important oxidizable substrate which is produced at some sites

during exercise and serves as raw material for energy production at other sites (Brooks, 1985). During exercise, the time lags that exist between supply of substrates for aerobic metabolism and removal of metabolites with increasing workload appear as high concentration of circulating lactate (Baudinette *et al*., 1982). Under resting conditions, the level of circulating lactate remains constant because the rate of production equals the rate of utilization (Brooks, 1985). At the start of exercise, lactate production increases rapidly to a value higher than resting one after which it starts to decrease slowly towards a new steady value after 3 minutes (Cabrera *et al*., 1999). Appearance of lactate in the blood during exercise has been described to occur in three phases (Roston *et al*., 1987; Cabrera and Chizeck, 1996). The first phase, which corresponds to less than 60% maximal rate of oxygen consumption, is described as mild to moderate exercise level. During this phase, the rate of glycolysis increases several times with no significant lactate accumulation. The second phase is described as heavy exercise; it corresponds to 60 – 80 % maximal rate of oxygen consumption (VO_2). During this phase, blood lactate reaches a higher steady state than at rest. The third phase occur in severe exercise when VO_2 is greater than 80% during which anaerobic glycolysis supplements the energy derived from aerobic production causing progressive accumulation of lactate in the blood (Cabrera *et al*., 1999). Because lactate pool serves as a critically important oxidizable substrate, blood lactate concentration during exercise has been used in prescribing and designing training programs and predicting endurance performance (Cabrera *et al*., 1999). Here, after the treadmill exercise, in the chickens, blood lactate concentration rose from 1.27±0.05 (SE) mmol L^{-1} in the resting bird to 5.14±0.35 (SE) mmol L^{-1} in the group subjected to the highest treadmill exercise. Because none of the birds were trained to exercise prior to the experiment, it is assumed that post-exercise blood lactate concentration correspond to exercise intensity. While pre-exercise lactate concentrations remain relatively constant, the

post-exercise lactate concentration increased as exercise intensity increased. However, the rate of increase gradually decreases at higher exercise intensity. Treadmill running is a highly aerobic exercise with a considerable anaerobic component requiring a lot of energy expenditure (Roston *et al*., 1987; Cabrera *et al*., 1999). Increase in energy demand that is caused by the exercise elicits coordinated and controlled responses which affect the heart rate and stroke volume, increasing the cardiac output (e.g. Raven and Potts, 2000). Simultaneously, the rate and depth of breathing are adjusted to accommodate energetic demands with exercise intensity (Whipp and Ward, 1982). The exercise intensity observed by the linear increase in blood lactate concentration corresponded with the number of failures of the BGB. Although the birds were handled as gently as possible and held in a cage one hour before the experiment to calm down, they still reacted to handling. The difference (not significant, $P < 0.05$) between the first and second measurement of blood lactate concentration in the resting birds can be explained by such reaction.

The event leading to structural failure of the BGB is normally a gradual process that stretches the tissue and cellular components beyond their physiological limits when they start to fail and then break. Failure is the last stage of series of events: it does not occur instantaneously Protein estimation and red blood cell (RBC) counts were carried out in order to understand the events that precede failure. In normal conditions, the airway should be free of RBC and does not contain unlimited amount of protein. Other than the limited concentration of surfactant proteins lining the air capillaries (e.g. Pattle, 1978), the pulmonary airways do not contain vast amount of proteins in the lining fluid. Most of the protein in the lavage fluid, which increased with increasing exercise intensity, is indicative of failure of BGB. Proteins lining the tissue-air interface (within the exchange tissue) should be limited in concentration and not increase with

increasing exercise intensity, unless there is communication with the vascular space. Here, increase in protein concentration with increases in exercise intensity shows that there was a gradual build-up of proteins on the respiratory surface with increase in activity. The extremely thin avian BGB is probably leaky, since proteins and RBCs have been reported (e.g. Maina and Cowley, 1998; Nganpiep and Maina, 2002) and confirmed in this study to be present in the lavage fluid even in the resting birds. Leakage of plasma and blood cells into the air capillaries possibly interfere with exercise performance. Build-up of blood cells and plasma in the air capillaries resulting from failure of the BGB may have contributed to collapse of some of the birds on the treadmill. Failure of the BGB and the resultant leakage of blood cells and plasma into the air capillaries, most likely, compromise respiratory function and affect endurance.

4.2.2 Pulmonary blood pressure in exercise

For exercise performance to be optimally maintained, coordinated and controlled responses to manage the immense stresses imposed on many physiological systems of the body keep arterial partial pressures of carbon dioxide (PCO_2) and oxygen (PO_2) optimal (Turner 1991). It is reported that when work rate is below the anaerobic threshold, ventilatory and cardiovascular responses maintain PCO_2 and PO_2 at or close to the resting levels (Whipp and Ward, 1982). As work rate rose above anaerobic threshold, cardiopulmonary responses mediated by neural and humoral mechanism via feed forward ventilator control of cardiac origin increases the rate and depth of breathing (Whipp and Ward, 1982). At the same time, increase in heart rate and stroke volume lead to increase in cardiac output (Raven and Potts,

2000) which increases perfusion of the lung. During treadmill exercise, Thomas and Fregin (1981) observed that in the horse, maximum exercise lead to six-fold increase in cardiac output and a 41% increase in stroke volume over resting values. For an untrained rat exercising on a treadmill, Gleeson and Baldwin (1981) observed that oxygen consumption rate (VO_2) increased linearly as a function of running speed. In marabou stork, *Leptoptilos crumeniferus*, exercising on a treadmill, Bamford and Maloiy (1980) noted a direct relationship between VO_2 and heart rate. At the beginning of exercise, birds flying in wind tunnel showed a dramatic rise in the respiratory - and cardiac frequencies (Butler *et al*., 1977). During flight, Eliassen (1963) reported that in gulls, pulse pressure about doubled from rest. Hart and Roy (1966) reported 3-4 times increases in heart rate over the resting level in exercising pigeon. As suggested previously (Pg. 169), longitudinal tension associated with inflation is considered insignificant in a volume constant avian lung and surface tension force at air-tissue interface need not be overcome during ventilation, if that is the case, the number of both BGB and E-E breaks observed in this study are the direct consequence of exercise induced increase in cardiac output.

Due to technical challenges of accessing such small and deeply situated structures, direct determination of pulmonary capillary pressure is not currently possible. It is generally taken to be the average between the arterial - and venous pressures in the pulmonary artery and vein (e.g. Bhattacharya *et al*., 1982; West, 2000b). Significant pressure drop in pulmonary circulation has been reported to occur in the capillary bed (Bhattacharya *et al*., 1982) but at high blood flow, pressure in the capillary bed is closer to arterial than venous pressure (Younes *et al*., 1987). Very high pulmonary capillary pressures have also been recorded in exercising animal using an implantable device which directly measured left atrial and

pulmonary arterial pressure (Jones *et al*., 1992). Susceptibility of the BGB to pressure induced failure is attributed to its extreme attenuation: the threshold pressure at which failure starts to appear is largely dependent on the thickness (Bhattacharya, 2003). Based on a theoretical estimation reported by West and Mathieu-Costello (1999) on a mammalian lung, all other factors being constant, theoretically, the BGB in the avian lung should fail at much lower pressure than in any mammal of comparable body mass. In this study, presence of RBCs in the lavage fluid of resting birds, which confirms the observation made by Nganpiep and Maina (2002) and Maina and Cowley (1998) shows that failure of the BGB in resting birds is a normal inconsequential occurrence. Here, white cells with their filopodia attaching to the plasma membrane of an endothelial cell were, in most instances, found very close to most of the breaks (Fig. 3.21B), a feature that may display an early stage of repair and/or defense process. Furthermore, fibrillary structures seen close to the break sites (Fig. 3.19C-E) are probably initiated by the activation of small GTPases Rho and Cdc42, which are known to stimulate actin cable formation that will possibly secure the break (Wood *et al*., 2002). Vlahakis *et al*. (2002) reported repair of the BGB to occur if pressure is increased to injurious levels and then returned to non-injurious levels.

4.2.3 Effect of exercise on epithelial-epithelial and blood-gas barrier breaks

The extremely high pulmonary artery and left atrial pressure recorded in galloping racehorses suggests that capillary pressures approach 100 mm Hg (13.33 kPa) (Jones *et al*., 1992). Although such high pressure may not occur in chicken during intense activity, this study shows BGB disruptions consistent with findings of other investigators (West *et al*., 1991).

Different types of failure (complete and incomplete) were observed but the focus of this study was on complete break of the barriers. Failure appears to be a common occurrence in the avian lung and BGB breaks were observed at all levels of exercise and in resting chicken. Increase in number of breaks, which show a relationship with exercise intensity, could be attributed only to increase in intramural pressure. Direct association between numbers of breaks and exercise intensity could be because intramural pressure is the only force acting on the BGB since other forces (longitudinal tension due to volume change and surface tension) appear to be well contained in the avian lung. For instance, lung volume change during respiration is insignificant (Jones *et al*., 1985) and surface tension force is probably opposed by firm attachment of the lung as a whole to the ribs. Furthermore, the dynamic integrated hierarchical neurally controlled mechanism of continuous tension and discontinuous compression confer strength by coupling adjacent parabronchi via the interparabronchial septum (Fig. 4.2) and prevent collapse of the air capillaries. Higher number of E-E cell breaks compared to BGB breaks in both exercise and perfusion experiments are indicative of the weakness of the air capillary-air capillary (E-E) contacts. The relatively frail construction of the E-E cell contact is evident because unlike the BGB it does not separate media (air and blood) of different densities operating at different pressure. Air capillaries are not designed for load bearing, as such bulk airflow, which requires pressure gradient (force), is confined to the parabronchial lumen. Air pressure is constant within and across air capillaries where air movement is by diffusion (Scheid, 1978). Different load bearing capacities of the BGB compared to E-E cell contact may be consistent with the observed difference in the density of collagen fibers around blood- and air capillaries (Figs. 3.2, 3.3 and 3.5). When BGB fails, blood and plasma from blood capillary ooze or flow into air capillaries, depending on the degree of failure. The weight of the denser blood and plasma on the extremely thin air capillary, especially on the E-

E cell contacts, probably stretches the contact beyond limit causing strain and eventual failure of the contact. More E-E cell failure compared to BGB may explain susceptibility of this type of contact. Moreover, a single blood capillary leak probably affects multiple air capillaries since the later are only separated by weak partition. Stretching of the blood capillaries caused by raised intramural pressure is also noted to cause separation of the E-E cell contacts (Fig. 3.21F). Although avian pulmonary capillaries have been reported to behave like a rigid tube (Powell *et al*., 1985), separation of E-E cell contacts that form "bridges" between blood-capillaries were observed here. Such separation may compromise integrity of the E-E cell contacts and render it susceptible to failure well before BGB fails. Determination of the numbers of BGB and E-E cell breaks in the whole lung for each exercise level and estimation of the percentage difference between the two shows that more E-E cell contacts fail well before BGB failure. While it cannot be ascertained yet, it is plausible that "epithelial bridges" serve as an absorber of capillary distension.

4.2.4 **Effect of exercise on structural failure in the vascular territories of the pulmonary arterial branches**

Based on the four main branches of the intra-pulmonary artery (IPA), the lung of the domestic fowl is divided into four regions of blood supply (Abdalla and King, 1975; Abdalla, 1989). The number of breaks in these regions divided by the total number of breaks in the entire lung in an exercise regimen gives the fractional failure contributed by a branch of the IPA. The number of breaks were significantly higher ($P < 0.05$) in the accessory- and caudomedial branches of the IPA at all levels of exercise intensity but, the differences in the numbers of BGB and E-E cell breaks were not significant ($P < 0.05$) except in the resting bird and the

lowest treadmill speed (Figs. 3.12 and 3.13). While there is need for more investigation to conclusively explain why more failure occur in the accessory and caudomedial vascular region, it may be suggested, based on the data available from this study, that the number of failure obtained for a given vascular area may give rough estimation of the blood pressure in the branches. Although determination of what the effect will be at the capillary bed is beyond the scope of this investigation and it is impossible to estimate with the present technology. More blood should flow in the caudomedial branch because it has the largest internal diameter of all the branches (Abdalla and King, 1975; Abdalla, 1989) and it is the direct continuation of the intra-pulmonary artery (see section 1.4.6). Higher pressure may exist in the accessory branch because it is the first and the narrowest branch of intra-pulmonary artery. This may explain the larger number of breaks in the areas supplied by these branches.

4.2.5 **Effect of perfusion on the number of epithelial-epithelial cell and blood-gas barrier breaks**

The air sacs were unavoidably punctured during the process of opening the thorax for isolation pulmonary circulation and cannulation for perfusion fixation of the lung. This made it impossible to maintain airway pressure. Since the airways opened to the outside through the punctured air sacs, the pressure in the airways was taken to be atmospheric in this experiment and the transpulmonary pressure was therefore taken to be equivalent to the perfusion pressure. In this state, the natural balance of force as should occur across the BGB is compromised and consequently, resistance within the air capillary (normally induced by air to oppose the push by intramural blood pressure) is removed. While it is generally believed that avian pulmonary blood capillary behaves like rigid tube which do not expand (Powell *et al*.,

1985), separations of the E-E contacts that started to appear at 2.89 kPa perfusion pressure (Fig. 3.21F) showed that the avian pulmonary capillaries do expand and follow mechanism of failure described by West *et al.* (1991) (see figure 1.4). The process of this separation can be likened to two points on a moderately inflated balloon. The points represent the two apposed epithelial cell processes in contact with the blood capillary (the balloon). Increase in blood pressure caused the blood capillary to expand leading to separation of the E-E contacts just like the two points on the balloon; s*econdly*, it was obvious from the micrographs that the middle parts of the E-E contacts remained connected while the parts closest to the BC were widely separated. This observation only points to presence of intercellular materials holding the two plates of cells together; *thirdly*, the ballooning leading to epithelial-epithelial cell separation may represents a prelude to frank failure of the BGB. In this study, the pressure (2.89 kPa) at which this separation were frequently observed is likely the pressure at which the BGB in the domestic fowl starts to fail.

The structural arrangement of the blood- and the air capillaries in the parabronchial lungs confers high gas transfer efficiency (Piiper and Scheid, 1975). The multicapillary serial arterialization system optimizes parabronchial perfusion (e.g. Abdalla and King, 1976a; Maina, 1988; Maina and Woodward, 2009) and maximizes oxygen extraction (Lasiewski and Calder, 1971; Scheid and Piiper, 1972; Bernstein and Schmidt-Nielsen, 1974). Unlike the homogenously ventilated and uniformly perfused dichotomously branching mammalian lung (e.g. Maina and van Gils, 2001), the serial-multicapillary arterialization system of the exchange tissue of the avian lung extract oxygen along the parabronchial length causing concentration differences of the gas (Holle *et al.*, 1978; Scheid, 1978). In mammals, regional

hypoxia affects regional lung perfusion (Folkow and Neil, 1971; Hughes, 1975; Fishman, 1976). In spontaneously breathing unanesthetized bird, the neopulmonic region was reported to be slightly better perfused than the paleopulmonic one (Holle *et al.,* 1978). Regional pulmonary blood flow has been reported to be affected by the position of the body. For instance, Nyren *et al.* (1999) used radiolabelled microaggregates of albumin, which are rapidly trapped by pulmonary capillaries in proportion to blood flow, to study postural effect on regional pulmonary blood flow. Their results showed that lung perfusion was more uniformly distributed in the prone than in the supine position. In birds, the first, the smallest and the narrowest branch of the intrapulmonary artery is the accessory branch; accordingly, it supplies the smallest area of the lung ventral to the hilum (Abdalla, 1989). The caudolateral part of the lung, which is dominated by neopulmonic parabronchi (Duncker, 1974), is supplied by the second largest branch of the intrapulmonary artery, the caudolateral branch. It is expected that more blood (perfusate) flow through the two largest branches of the intrapulmonary artery, the caudomedial- and caudolateral branches, which should translate to higher intramural pressure and consequently more failure in their capillary beds. However, the outcome of this investigation was not in accord with this expectation. It is possible and as reported by Nyren *et al.* (1999) on the human lung, that the supine position in which the birds were placed in this study during perfusion might have affected the natural flow of blood in the pulmonary circulation. At all perfusion pressures in this study, more flow (high pressure), seen as more breaks, occurred in the caudomedial- and the accessory branches of the intrapulmonary artery (Figs. 3.17 and 3.18). More perfusate flow in the caudomedial branch, a direct continuation of the intra-pulmonary artery, may explain the higher number of failures of the BGB which almost equaled the number recorded for E-E contact. This is reflected in the comparatively low value for percentage difference between the two types of breaks recorded in this region.

At 2.4 kPa perfusion pressures and above, the percentage differences in all the arterial regions showed no difference. The lowest difference between the BGB and the E-E breaks for the caudomedial region at 1.42 and 1.91 kPa show that failure of both types are greatest in this region. Difference between the BGB and the E-E cell contacts in all the arterial regions progressively decreased from 2.4 kPa and above. Progressive decrease is indicative of vulnerability of the E-E cell contacts even at lower pressure while the robustly built BGB effectively tolerated higher pressure. Alternatively, the air capillaries that surround blood capillary may provide a cushion more like the air bubble sheet use in packaging of delicate materials.

4.3 CONCLUSION

The parabronchi, the structural unit that support the gas exchange tissue, are interconnected to form integrated structural interdependency. The configuration and the interconnectedness of the parabronchi allow distribution, sharing, and dissipation of force applied to any part of the lung. Within the parabronchus, rhythmic contraction of the neurogenically controlled smooth muscle fibers tenses the elastic tissue fibers, which store potential energy. The presence of elastic tissue between atrial smooth muscle and network of collagen in the exchange tissue is suggestive of continuous tension in the collagen network within the gas exchange tissue. During smooth muscle relaxation, the potential energy stored in the elastic tissue is converted to kinetic energy. Tension is maintained by the elastic tissue between waves of contractions. Excessive contraction of the muscle is checked by the inflexible collagen fibers. Counterbalance of forces between smooth muscles, which contract to produce tension, pulls on the gas-exchange tissue mantle towards the center of the parabronchial lumen. The various condensation of collagen (central- and peripheral dense collagen and thin loose collagen between them) that resist the generated tension, and those that may exert outward force, e.g., the interparabronchial arteries suggests that the parabronchus exists in a dynamically tensed state. Stating it differently, the morphology of the parabronchus and its constitutive parts strongly suggests existence of a tensegrity structure. The integrated hierarchical network of collagen fibers within the exchange tissue mantle, which connect the interparabronchial septum and the parabronchial smooth muscle, are present as basement membrane collagen type- IV to form a continuous network of fibers. Presence of a basement membrane in all the three contacts present in the avian gas exchange tissue (endothelial-endothelial, endothelial-

epithelial and epithelial-epithelial, see Fig. 1.3) is important to maintain shapes and support the terminal gas exchange units.

In the mammalian lung, the stress failure of the BGB and subsequent hemorrhage occur as a result of high transmural pressures in the pulmonary capillaries that occur during intense activity (e.g. West *et al.,* 1993; West *et al.,* 1994) as means of averting failure. Increase in pulmonary vascular pressure causes vascular distension that contributes to exercise-related fall in resistance (Borst *et al.,* 1956; Glazier *et al.,* 1969; Reeves *et al.,* 2005). But the mechanism of stress failure in birds where pulmonary blood capillaries behave like a rigid tube (West *et al.,* 2007a; Watson *et al.,* 2008) and where vascular resistance remain unchanged when blood flow is doubled (Powell *et al.,* 1985) should be different. As speculated by other investigators, avian pulmonary capillaries receive support from structure within the exchange tissue such as retinacula (Scheuermann *et al.,* 1997), trilaminar substance (Klika *et al.,* 1997), and epithelial bridges (West, 2009). Such support in the avian exchange tissue should prevent mammalian type of pulmonary capillary distension which usually precedes stress failure. Pulmonary capillary distension was however, observed in this study and appeared to be transmitted to epithelial-epithelial cell contacts causing it to separate. While the distension may not be as significant as in the mammalian pulmonary capillaries, this study showed that under unphysiological conditions, the avian pulmonary capillaries do distend before the failure of the BGB.

The evidence gathered in this study is not enough to explain the presence of RBCs in the lung lavage fluid of a resting bird. While such RBCs may indicate failure of the BGB in the mammalian lung, it may be an inconsequential occurrence in the avian lung. Presence of RBCs on the surface of the lungs of resting chickens, as reported by other investigators (Maina

and Cowley, 1998; Nganpiep and Maina, 2002), and confirmed in this study, may be a common phenomenon. The lung may have an inherent mechanism of repairing the few breaks, as observed here by aggregation of white blood cells in the damaged sites and deposition of fibrin. The red blood cells are removed by the epithelial cells of the lung, especially in the atria and the infundibula (Nganpiep and Maina, 2002). The relatively high systemic pressure and by extension pulmonary pressures in birds (e.g. Seymour and Blaylock, 2000) may explain the occasional failures of the BGB in resting birds.

Occurrence of more E-E breaks at low exercise intensity indicated that tensions in the blood capillaries are transferred to the air capillaries. One possible explanation for this occurrence is that besides interfacing with the environment, the air capillaries also serve as a cushion for the blood capillaries. For the blood capillaries, the air capillaries may act like a bubble-wrap which was invented in 1957 by Alfred Fielding and Marc Chavannes (Associated Press, 2010). Bubble wrap is commonly used to protect delicate products during shipment. Air pockets between laminated nylon serve as cushions which pop on impact (absorbing shock) to protect products. Basement membrane continuity established in this study between blood- and air capillaries allow tension generated by changes in intramural pressure to be transferred from the BGB to the E-E cell contacts.

4.4 CRITIQUE OF EXERCISE- AND PERFUSION INDUCED FAILURE

It is important to note that setting up pulmonary perfusion to reproduce the complex dynamic interaction between the two convective media (air and blood) operating naturally in the avian lung is practically impossible. Separation of the ventilator from the exchanger in the avian pulmonary structure further makes it unachievable. The ventilator, represented by extremely thin walled, complexly interconnecting air sac system is widely distributed within the thoracoabdominal cavity. It was not possible to avoid puncturing the diffuse air sacs in the process of exposing the heart. No matter how small the puncture of any of the air sacs, it will severely compromise natural balance of force across the blood-gas barrier. The thoracic air sacs are especially vulnerable when the thorax is opened to access the heart. Unlike the mammalian lung, which can be perfused at a known airway pressure by inflating the lung and plugging the only opening, the trachea, the avian lung cannot be treated like that.

Pattern of breaks in the BGB- and the E-E cell contacts in the exercised chicken differ from the pattern observed in the perfused chicken. The difference can be attributed to the following.

a. **Surgical manipulation:** opening of the thorax to access the heart and cannulate pulmonary vessels unavoidably compromised the integrity of some of the air sacs especially the thoracic air sacs. When any of the air sac is punctured, transcapillary pressure is affected and the balance of force across the capillary wall cannot be what exists in the natural condition.
b. **Perfusate:** the flow dynamics of the perfusion fluid is not the same as that of blood with suspended particulate like the red and white blood cells is a non-Newtonian fluid which does not quite follow Poiseuille's hydrodynamic law. Attempt to harvest the blood and use

it for initial perfusion was made. It was, however, impossible to harvest enough for any effective perfusion. Plasma expander (Dextran T70) was also use to increase the viscosity of the perfusate but the result obtained in a pilot study was the same as using PBS alone. Moreover, it was too expensive to use dextran because of the large number of chickens used in the perfusion experiments.

c. **Position:** The perfused chickens were held in supine position throughout the perfusion process. Although the effect may be negligible, the unphysiological position may affect normal blood distribution. It is also highly likely that absence of normal blood distribution associated with posture and hemodynamic changes relating to ambulation affect blood flow in the principal arterial branches. While problems associated with perfusion in supine position are recognized, other approaches were impracticable for accessing the heart and cannulating the pulmonary vessels. In other words, there is no alternative to perfusion in supine position.

4.5 RECOMMENDATIONS

Exposure of birds to stress is an unavoidable event. In poultry husbandry when stress crosses a certain threshold level it results in overt physiological and/or morphological changes in birds (Mohan, 2005). Stress, which causes detrimental effects on health and performance, is a deviation from normal maintenance of constant internal environment of the body physiological condition (Mohan, 2005). Stress causes redistribution of body resources (energy and proteins) at the detriment of growth, reproduction and health (Brake, 1987; Gross and Siegel, 1988; Beck, 1991). With limited body resources afforded for growth, reproduction, response to environmental changes, and defense mechanism (Rosales, 1994), a bird subjected to repeated or long-term stress became fatigued and weak (Mohan, 2005) leading to starvation and infections (Freeman, 1987; Dohms, 1990). It is important to identify factors that cause stress in poultry with the intention of minimizing their effects on performance and health of birds. Because of the vulnerability of the avian blood-gas barrier to failure (observed in this study), the following causes of stress should be avoided or lessened:

- Harsh caretaking
- Overcrowding
- Inadequate ventilation
- Rough handling, e.g., during weighing, vaccination, grading, and transport.

CHAPTER V

5. REFERENCES

REFERENCES

Abdalla, MA. The blood supply to the lung. In Form and Function in Birds, Vol. 4 (eds. A. S. King and J. McLelland). London: Academic Press, 1989, pp. 281-306.

Abdalla MA, King AS. The functional anatomy of the pulmonary circulation of the domestic fowl. Respir Physiol 1975; 23: 267–290.

Abdalla MA, King AS. Pulmonary arteriovenous anastomoses in the avian lung: do they exist? Respir Physiol 1976a; 27:187 – 191.

Abdalla MA, King AS. The functional anatomy of the bronchial circulation of the domestic fowl. J Anat 1976b; 121: 537-550.

Abdalla MA, King AS. The avian bronchial arteries: species variations. J Anat 1977; 123: 697 – 704.

Adamson IY, Bowden DH. The type 2 cell as progenitor of alveolar epithelial regeneration. Lab Invest 1974; 30:35-40.

Adamson IY, Hedgecock C, Bowden DH. Epithelial cell-fibroblast interactions in lung injury and repair. Am J Pathol 1990; 137: 385–392.

Adamson IY, Young L, Bowden DH. Relationship of alveolar epithelial injury and repair to the induction of pulmonary fibrosis. Am J Pathol 1988; 130:377–83.

Aird WC. Mechanisms of endothelial cell heterogeneity in health and disease. Circ Res 2006; 98:159-162.

Aird WC. Phenotypic heterogeneity of the endothelium I. structure, function, and mechanisms. Circ Res 2007a; 100:158-173.

Aird WC. Phenotypic heterogeneity of the endothelium II. representative vascular beds. Circ Res 2007b; 100: 174-190.

Alberts B, Bray D, Lewis J, Raff M, Roberts K, Watson JD. Molecular Biology of the Cell, 2nd edition. New York: Garland publications, 1989.

Alter MJ. Science of Flexibility, 3rd Edition. New York: Sheridan Books, 2004.

Amenta PS, Gil J, Martinez-Hernandez A. Connective tissue of rat lung. II. utrastructural localization of collagen types III, IV, and VI. J Histochem Cytochem 1988; 36: 1167-1173.

Aschoff J, Pohl H. Rhythmic variation in energy metabolism. Fed Proc 1970; 29: 1541-1552.

Associated Press. Bubble wrap celebrating its 50th birthday. 2010 msn.com/id/35046691

Aumailley M, Bruckner-Tuderman L, Carter WG, Deutzmann R, Edgar D, Ekblom P, Engel J, Engvall E, Hohenester E, Jones JC *et al*. A simplified laminin nomenclature. Matrix Biol 2005; 24: 326-332

Aumailley M, Rousselle P. Laminins of the dermo-epidermal junction. Matrix Biol 1999; 18:19-28.

Aumailley M, Smyth N. The role of laminins in basement membrane function. J Anat 1998; 193**:** 1–21.

Bamford OS, Maloiy GMO. Energy metabolism and heart rate during treadmill exercise in the marabou stork, J Appl Physiol 1980; 49: 491–496.

Bancroft JD, Steven A. Theory and Practice of Histological Techniques. London: Churchill Livingstone, 1996.

Banerjee SD, Cohn RH, Bernfield MR. Basal lamina of embryonic salivary epithelia: Production by the epithelium and role in maintaining lobular morphology. J Cell Biol 1977; 73:445-463.

Banzett RB, Nations CS, Wang N, Butler JP, Lehr JL. Mechanical interdependence of wing beat and breathing in starlings. Respir Physiol 1992; 89: 27-36.

Baudinette RV, Tonkin AL, Orbach J, Seymour RS, Wheldrake JF. Cardiovascular function during treadmill exercise in the turkey. Comp Biochem Physiol Part A: Physiology 1982; 72 (2): 327-332.

Beck JT. Understanding and minimizing stress in broilers and broiler breeders. Zootechnica international 1991; XIV (3): 30-38

Berger AJ. Bird Study. 1st edition. New York: Dover Publications, 1961.

Berger M, Hart JS. Physiology and energetics of flight. In Avian Biology, vol. 4 (ed. D. S. Farner and J. R. King). New York: Academic Press, 1974, pp. 415–477.

Bernhard W, Gebert A, Vieten G., Rau GA, Hohlfeld JM, Postle AD, Freihorst J. Pulmonary surfactant in birds: coping with surface tension in a tubular lung. J Appl Physiol 2001; 281: R327-R337.

Bernstein MH, Scmidt-Nielsen K. Ventilation and oxygen extraction in the crow. Respir Physiol 1974; 21:393-401

Bettex-Galland M, Hughes GM. Contractile filamentous material in the pillar cells of fish gills. J Cell Sci 1973; 13: 359–366.

Bhattacharya J. Pressure-induced capillary stress failure: Is it regulated? Am J Physiol Lung Cell Mol Physiol 2003; 284: L701-L702

Bhattacharya J, Nanjo S, Staub NC. Micropuncture measurement of lung microvascular pressure during 5-HT infusion. J Appl Physiol 1982; 52:634-637.

Birks EK, Mathieu-Costello O, Fu Z, Tyler WS, and West JB. Comparative aspects of the strength of pulmonary capillaries in rabbit, dog, and horse. Respir Physiol 1994; 97: 235–246.

Black CP, Tenney SM. Oxygen transport during progressive hypoxia in high altitude and sea level waterfowl. Respir Physiol 1980; 39: 217–239.

Black CP, Tenney SM, Kroonenberg MV. Oxygen transport during progressive hypoxia in bar-headed geese (Anser anser) acclimated to sea level and 5600 m. In: Respiratory Function in Birds Adult and Embryonic (ed J. Piiper), Berlin: Springer-Verlag, 1978, pp. 79-83.

Borst HG, McGregor M, Whittenberger JL, Berglund E. Influence of pulmonary arterial and left atrial pressures on pulmonary vascular resistance. Circ Res 1956; 4: 393–399.

Boulianne M, Hunter DB, Physick-Sheard PW, Viel L and Julian RJ. Effect of exercise on cardiac output and other cardiovascular parameters of heavy turkeys and relevance to the sudden death syndrome. Avian Diseases 1993; 37:98-106

Boute N, Exposito JY, Boury-Esnault N, Vacelet Jean, Noro N, Miyazaki K, Yoshizato K, Garrone R. Type IV collagen in sponges, the missing link in basement membrane ubiquity. Biol Cell. 1996; 88: 37-44.

Bradley KH, Kawanami O, Ferrans VJ, Crystal RG. The fibroblast of human alveolar structures: a differentiated cell with a major role in lung structure and function. In: Methods in Cell Biology, vol. 2. (eds Harris CC, Trump BF, Stoner GD), New York: Academic Press, 1980, pp. 37-64.

Brainerd EL. New Perspectives on the evolution of lung ventilation mechanisms in vertebrates, Exp Biol Online 1999; 4: 11-28.

Brake JT. Stress and modern poultry management. Annuals production highlights 1987. F. Hoffman-LaRoche & Co. Ltd. 4002. Basie, Switzerland

Brenner BM, Humes HD. Mechanisms of glomerular ultrafiltration. New Engl. J. Med. 1977; 297: 148.

Brody JS, Vaccaro CA, Gill PJ, Silbert JE. Alterations in alveolar basement membranes during postnatal lung growth. J Cell Biol 1982; 95:394–402.

Brody JS, Vaccaro CA, Hills NS, Rounds S. Binding of charged ferritin to alveolar wall components and charge selectivity of macromolecular transport in permeability pulmonary edema in rats. Circ Res 1984; 55: 155-167.

Brooks GA. Anaerobic threshold: review of the concept and directions for future research. Med Sci Sports Exerc 1985; 17 (1): 22-34.

Burri PH. Morphology and respiratory function of the alveolar unit. Int Archs Allergy Appl Immunol 1985; 76: 2–12.

Bussey H. Cell shape determination: A pivotal role for Rho. Science 1996; 272: 224-225.

Butler PJ, West, NH, Jones DR. Respiratory and cardiovascular responses of the pigeon. J Exp Biol 1977; 71: 7-26.

Cabrera ME, Chizeck HJ. On the existence of a lactate threshold during incremental exercise: a systems analysis. J Appl Physiol 1996; 80(5):1819–1828.

Cabrera ME, Saidel GM, Kalhan SC. Lactate metabolism during exercise: analysis by an integrative systems model. Am J Physiol Regul Integr Comp Physiol 1999; 277: R1522-R1536.

Carlier MF, Pantaloni D. Control of actin assembly dynamics in cell motility. J Biol Chem 2007; 282: 23005–23009

Carlson CW. Aortic rupture. Turkey Producer (January Issue), 1960.

Carpenter FL. Bird hematocrits: effects of high altitude and strength of flight. Comp Biochem Physiol 1975; 50A: 415-417.

Chen CS, Mrksich M, Huang S, Whitesides GM, Ingber DE. Geometric control of cell life and death. Science 1997; 276: 1425–1428.

Cook RD, King AS. Observations on the ultrastructure of the smooth muscle and its innervations in the avian lung. J Anat 1970; 106: 273-283.

Corbetta S, Bairati A, Vitellaro Zuccarello L. Immunohistochemical study of subepidermal connective of molluscan integument. Eur J Histochem. 2002; 46 (3):259-72.

Crapo JD, Barry BE, Gehr P, Bachofen M, Weibel ER. Cell number and cell characteristics of the normal human lung. Am Rev Respir Dis 1982; 126: 332–337.

Crapo JD, Young SL, Fram EK, Pinkerton KE, Barry BE, and Crapo RO. Morphogenetic characteristics of cells in the alveolar region of mammalian lungs. Am Rev Respir Dis 1983; 128: S42–S46.

Crouch EC, Martin GR, Jerome BS, Laurie GW. Basement membranes. In: The Lung: Scientific Foundations, vol. I. (eds Crystal RG, West JB, Weibel ER, and Barnes PJ). Philadelphia, Lippincott-Raven 1997, pp. 769–791.

Currie RJW. Ascites in poultry: recent investigations. Avian Path 1999; 28: 313-326.

Daniels CB, Orgeig S. Pulmonary surfactant: The key to the evolution of air breathing. News Physiol Sci 2003; 18:151-157.

DeBiase PJ, Lane K, Budinger S, Ridge K, Wilson M, Jones JCR. Laminin-311 (laminin-6) fiber assembly by type I-like alveolar cells. J Histo Cytochem 2006; 54: 665-672.

Dock DS, Kraus WL, McGuire LB, Hyland JW, Haynes FW, Dexter L. The pulmonary blood volume in man. J Clin Invest 1961; 40: 317–328.

Dodson JW, Hay ED. Secretion of collagenous stroma by isolated epithelium grown *in vitro*. Exp Cell Res 1971; 65: 215.

Dohms JE. Stress: Mechanisms of immune suppression. in: proc. 41st North Central Avian Dis. and Poultry immunosuppressive Dis. Symp. 1990, pp 22-42 Columbus. OH

Dreyfuss D, Basset G, Soler P, Saumon G. Intermittent positive-pressure hyperventilation with high inflation pressures produces pulmonary microvascular injury in rats. Am Rev Respir Dis 1985; 132: 880-884.

Dubach M. Quantitative analysis of the respiratory system of the house sparrow, budgerigar, and violet-eared hummingbird. Respir Physiol 1981; 46: 43–60.

Duncker HR. The lung air sac system of birds. Adv Anat Embryol Cell Biol 1971; 45:1-171.

Duncker HR. Structure of avian lungs. Respir Physiol 1972; 14: 44–63.

Duncker HR. Structure of the avian respiratory tract. Respir Physiol 1974; 22: 1 – 19.

Duncker HR. Functional morphology of the respiratory system and coelomic subdivisions in reptiles, birds, and mammals. Vehr Dtsch Zool Ges 1978; 99 - 132.

Elden HR. Physical properties of collagen fibers. Int Rev Connect Tissue Res 1968; 4: 283-348.

Eldridge MW, Braun RK, Yoneda KY, Walby WF. Effects of altitude and exercise on pulmonary capillary integrity: evidence for subclinical high-altitude pulmonary edema. J Appl Physiol 2006; 100: 972-980

Ellerby DJ, Cleary M, Marsh RL, Buchanan CI. Measurement of maximum oxygen consumption in Guinea fowl *Numida meleagris* indicates that birds and mammals display a similar diversity of aerobic scopes during running. Physiol Biochem Zool 2003; 76: 695-703.

Eliassen E. Preliminary results from new methods of investigating the physiology of birds in flight, Ibis 1963; 105: 234–237.

Elkins N. Weather and Bird Behaviour. Calton, Stoke on Trent, UK: T. & A. D. Poyser 1983.

Erickson AC, Couchman JR. Still more complexity in mammalian basement membranes J. Histochem Cytochem 2000; 48: 1291–1306.

Erickson BK, Erickson HH, Coffman JR. Pulmonary artery, aortic and oesophageal pressure changes during high intensity treadmill exercise in the horse: A possible relation to exercise-induced pulmonary haemorrhage. Equine Vet J Suppl 1990; 9: 47–52.

Exposito JY, Cluzel C, Garrone R, Lethias C. Evolution of collagens. Anat Rec. 2002; 268: 302-316.

Farmer CG. On the origin of avian air sacs. Resp Physiol Neurobiol 2006; 154: 89–106.

Fedde MR. The structure and gas flow pattern in the avian respiratory system. Poult Sci 1980; 59: 2642 -2653.

Figueroa D, Olivares R, Salaberry M, Sabat P, Canals M. Interplay between morphometry of the lungs and the mode of locomotion in birds and mammals. Biol Rev 2007; 40: 193-201.

Fisher RF, Wakely J. The elastic constants and ultrastructural organization of a basement membrane (lens capsule). Proc R Soc Lond B Biol Sci 1976; 193: 335-358.

Fishman AP. Hypoxia on the pulmonary circulation. How and where it acts. Circulation Res 1976; 38: 221- 231.

Fishman AP. Endothelium: a distributed organ of diverse capabilities. In: Endothelium, vol. 401. (ed Fishman AP). Ann N.Y. Acad Sci New York. 1982, pp. 1–8.

Folkow B, Neil E. Pulmonary circulation in: Circulation, London: Oxford Univ Press, 1971 pp. 379 – 398.

Freeman BM. The stress syndrome World's Poult Sci J 1987; 43:15-19

Fu Z, Costello ML, Tsukimoto K, Prediletto R, Elliot AR, Mathieu-Costello O, West JB. High lung volume increases stress failure in pulmonary capillaries. J Appl Physiol 1992; 73: 123–133.

Fuller B. Tensegrity. Portfolio Art News Annual 1961; 4: 112-127.

Fung YC, Zweifach BW, Intaglietta M. Elastic environment of the capillary bed. Circ Res 1966; 19: 441-461.

Gehr P, Bachofen M, Weibel ER. The normal human lung: Ultrastructure and morphometric estimation of diffusion capacity. Respir Physiol 1978; 32: 121–140.

Gehr P, Erni H. Morphometric estimation of pulmonary diffusion capacity in two horse lungs. Respir Physiol 1980; 41: 199-210.

Gehr P, Sehovic S, Burri PH, Classen H, Weibel ER. The lung of shrews: morphometric estimation of diffusion capacity. Respir Physiol 1980; 44: 61-68.

Gehr P, Mwangi DK, Amman A, Maloiy GMO, Taylor CR, Weibel ER. Design of the mammalian respiratory system. V. Scaling morphometric pulmonary diffusing capacity to body mass: Wild and domestic animals. Respir Physiol 1981; 44: 61–86.

Gil J, Martinez-Hernandez A. The connective tissue of the rat lung: electron immunohistochemical studies. J Histochem Cytochem 1984; 32: 230-238.

Gillespie JR, Sagot JC, Gendner JP, Bouverot P. Impendance of the lower respiratory system in ducks under four conditions: pressure breathing, anaesthesia, paralysis or breathing CO_2-enriched gas. Respir Physiol 1982; 47: 177-191.

Glazier JB, Hughes JMB, Maloney JE, West JB. Measurements of capillary dimensions and blood volume in rapidly frozen lungs. J Appl Physiol 1969; 26: 65-76.

Gleeson TT, Baldwin KM. Cardiovascular response to treadmill exercise in untrained rats. J Appl Physiol 1981; 50: 1206-1211.

Gonçalves CA, Figueiredo MH, Bairos VA. Three-dimensional organization of the elastic fibers in the rat lung. Anat Rec 1995; 243: 63-70.

Gosline JM. The physical properties of elastic tissue. Int Rev Connet Tissue Res 1976; 7: 211-249.

Gosline JM, French CJ. Dynamic mechanical properties of elastin. Biopolymers 1979; 18: 2091-2103.

Gross WB and Siegel PB. Environment-genetic influences on immunocompetenceJ Anim Sci 1988; 66; 2091-2094

Gyles NR. Poultry, people and progress. Poultry Sci 1989; 68: 1-8.

Hagedorn HG, Bachmeier BE, Nerlich AG. Synthesis and degradation of basement membranes and extracellular matrix and their regulation by TGF-β in invasive carcinomas. Int J Oncol 2001; 18: 669–681.

Hamill KJ, Langbein L, Jones JC, McLean WH. Identification of a novel family of laminin N-terminal alternate splice isoforms: structural and functional characterization. J. Biol Chem 2009; 284 (51): 35588-35596.

Hance AJ, Crystal RG. The connective tissue of lung. Amer Rev Respir Dis 1975; 112: 657-711.

Hart JS, Roy OZ. Respiratory and cardiac responses to flight in pigeons, Physiol Zool 1966; 39**:** 291–305.

Hartmann FA. Heart weight in birds. Condor 1955; 57**:** 221–238.

Haworth SG, Hall SM, Patel M. Peripheral pulmonary vascular and airway abnormalities in adolescents with rheumatic mitral stenosis. Int J Cardiol 1988; 18: 405–416.

Hills BA, Butler BD, Barrow RE. Boundary lubrication imparted by pleural surfactants and their identification. J Appl Physiol 1982; 53: 463-469.

Holle JP, Heisler N, Scheid P. Blood flow distribution in the duck lung and its control by respiration gases. Am J Physiol 1978; 234 (3): R146 – R154.

Hopkins FG, Stothert Jr, Greaves IA, Lai Y-L, Kildebrandt J. Lung recoil: elastic and rheological properties. In: Handbook of Physiology: The Respiratory System (ed Fishman AP). Bethesda: American Physiological Society, 1986 pp. 195-215.

Hopkins SR, Schoene RB, Henderson WR, Spragg RG, West JB. Sustained submaximal exercise does not alter the integrity of the lung blood-gas barrier in elite athletes. J Appl Physiol 1998; 84:1185-1189.

Hopkins SR, Schoene RB, Martin TR, Henderson WR, Spragg RG, West JB. Intense exercise impairs the integrity of the pulmonary blood-gas barrier in elite athletes. Am J Respir Crit Care Med 1997; 155: 1090–1094.

Huang S, Ingber DE. The structural and mechanical complexity of cell growth control. Nat Cell Biol 1999; 1: E131-138.

Huang S, Ingber DE. Shape-dependent control of cell growth, differentiation and apoptosis: switching between attractors in cell regulatory networks. Exp Cell Res 2000; 261: 91-103.

Hudson BG, Reeder ST, Tryggvason K. Type - IV collagen: structure, gene organization and role in human diseases. J Biol Chem 1993; 288: 26033-26036.

Hughes GM. The dimensions of fish gills in relation to their function. J Exp Biol 1966; 45: 177–195.

Hughes GM. Some features of gas transfer in fish. Bull Inst Math Appl 1978; 14: 39-43.

Hughes GM, Grimstone AV. The fine structure of the secondary lamellae of the gills of Gadus pollachius. J Microsc Sci 1965; 106: 343–353.

Hughes GM, Wright DE. A comparative study of the ultrastructure of the water/blood pathway in the secondary lamellae of teleost and elasmobranch fishes - benthic forms. Z Zellforsch Mikrosk Anat 1970; 104: 478–493.

Hughes JMB. Lung gas tension and active regulation of ventilation/perfusion ratios in health and diseases. Brit J Diseases Chest 1975; 69: 153 – 170.

Hultgren HN. High altitude pulmonary edema. In: Biomedicine of High Terrestrial Elevations, (ed Hegnauer AH). New York: Springer-Verlag, 1969 pp. 131–141.

Ingber DE. Fibronectin controls capillary endothelial cell growth by modulating cell shape. Proc Natl Acad Sci USA 1990; 87: 3579–3583.

Ingber DE. Tensegrity: the architectural basis of cellular mechanotransudation. Annu Rev Physiol 1997; 59: 575-599.

Ingber DE. The architecture of life. Sci Am 1998; 278: 18-57

Ingber DE. Mechanical control of tissue morphogenesis during embryological development. Int J Dev Biol 2006; 50: 255-266.

Ingber DE. Cellular tensegrity: revisited I. Cell structure and hierarchical systems biology. J Cell Sci 2003; 116: 1157-1173.

Ingber DE, Jamieson JD. Cell as tensegrity structure: architectural regulation of histodifferentiation by physical forces tranduced over basement membrane (eds Anderson LC, Gahmberg CG and Ekblom P). Orlando: Academic Press, 1985 pp 13–32

Ingber DE, Madri JA, Jamieson JD. Basement membrane as a spatial organizer of polarized epithelia: exogenous basement membrane reorients pancreatic epithelial tumor cells *in vitro*. Amer J Pathol 1986; 122: 129-139.

Jones JCR, Lane K, Hopkinson SB, Lecuona E, Geiger RC, Dean DA, Correa-Meyer E, *et al*. Laminin-6 assembles into multimolecular fibrillar complexes with perlecan and participates in mechano-signal transduction via a dystroglycan-dependent, integrin independent, mechanism. J Cell Sci 2005; 118: 2557–2565.

Jones JH, Effmann EL, Schmidt-Nielsen K. Lung volume changes during respiration in ducks. Respir Physiol 1985; 59: 15-25.

Jones JH, Smith BL, Birks EK, Pascoe JR, Hughes TR. Left atrial and pulmonary arterial pressures in exercising horses (Abstract). FASEB J 1992; 6: A2020.

Julian RJ, Wilson JB. Right ventricular failure as a cause of ascites in broiler and rooster chickens. Proc IVth Int Symp Vet Lab Diag 1986; 608-611.

Junqueira LC, Carneiro J. Basic Histology Text & Atlas. 10th ed. Lange Medical Books, McGraw Hill, 2003.

Jürgens, JD, Bartels H, Bartels R. Blood oxygen transport and organ weight of small bats and small non-flying mammals. Respir Physiol 1981; 45: 243–260.

Kalluri R. Basement membranes: structure, assembly and role in tumour angiogenesis. Nat Rev Cancer; 2003; 3: 422-433.

Kampe G, Crawford EC. Oscillatory mechanics of the respiratory system of pigeons. Respir Physiol 1973; 18: 188-193.

Keren K, Pincus Z, Allen GM, Barnhart EL, Marriot G, Mogilner A, Theriot JA. Mechanism of shape determination in motile cells. Nature 2008; 453: 475-480.

Kheradmand F, Folkesson HG, Shum L, Derynk R, Pytela R, Matthay MA. Transforming growth factor- α enhances alveolar epithelial cell repair in a new *in vitro* model. Am J Physiol 1994; 267: L728-38.

Kim HJ, Henke CA, Savik SK *et al*. Integrin mediation of alveolar epithelial cell migration on fibronectin and type I collagen Am J Physiol 1997; 273: L134-41.

King AS. Structural and functional aspects of the avian lungs and air sacs. Int Rev Gen Exptl Zool 1966; 2: 171-267.

King AS, Molony V. The anatomy of respiration. In: Physiology and Biochemistry of the Domestic Fowl, vol. 1. (eds Bell DF, Freeman BM). London, Academic Press, 1971, pp 347-384.

King AS, Cowie AF. The functional anatomy of the bronchial muscle of the bird. J Anat 1969; 105: 323-336.

King AS, Ellis RNW, Watts, SMS. Elastic fibers in the avian lung. J Anat 1967; 101: 607.

Klika E, Scheuermann DW, De Groodt-Lasseel MHA, Bazantova I, Switka A. Anchoring and support system of pulmonary gas exchange tissue in four bird species. Acta Anat 1997; 159: 30–41.

Klika E, Scheuermann DW, De Groodt-Lasseel MHA, Bazantova I, Switka A. An SEM and TEM study of the transition of the bronchus to the parabronchus in quail (*Coturnix cortunix*). Ann Anat 1998; 180: 289-297.

Kobayashi T, Koyama S, Kubo K, Fukushima M, Kusama S. Clinical features of patients with high-altitude pulmonary edema in Japan. Chest 1987; 92 (5):814-821.

Koitzumi T, Kawashima A, Kubo K, Kobayashi T, Sekiguchi M. Radiographic and hemodynamic changes during recovery from high altitude pulmonary edema. Intern Med 1994; 33: 525–528.

Kramer JM. Structures and functions of collagens in Caenorhabditis elegans. FASEB J. 1994; 8: 329-336

Krista LM,Waibel PE, Shoffner RN, Soutter JH. A study of aortic rupture and performance as influenced by selection for hypertension and hypotension in turkey. Poultry Sci 1970; 49: 405-411.

Kuhl U, Ocalan M, Timpl R., Mayne R, Hay E, Von Der Mark K. Role of muscle fibroblasts in the deposition of type-IV collagen in the basal lamina of myotubes. Differentiation 1984; 28: 164-172.

Kuhn K. Basement membrane (type IV) collagen. Matrix Biol. 1994; 14: 439-445.

Lallemand AV, Ruocco SM, Gaillard DM. Synthesis and expression of laminin during human foetal lung development. Anat Rec 1995; 242(2): 233-241.

Lasiewski RC. The energetic of migrating hummingbirds. Condor 1962; 64: 324–335.

Lasiewski RC, Calder WA. A preliminary allometric analysis of respiratory variables in resting birds. Respir Physiol 1971; 11: 152-166.

Laybourne RC. Collision between a vulture and an aircraft at an altitude of 37,000 ft. Wilson Bull 1974; 86: 461-462.

Leblond CP and Inoue S. Structure, composition, and assembly of basement membrane. Am J Anat 1989; 185: 367–390.

Leivo I. structure and composition of early basement membranes: Studies with early embryos and teratocarcinoma cells. Med Biol 1983; 61: 1-30.

Lemanski LF, Paulson DJ, Hill CS, Davis LA, Riles LC, Lim SS. Immunoelectron microscopic localization of a-actin on Lowicryl embedded thin sectioned tissues. J Histochem Cytochem 1985; 33: 515-22.

Levitzky MG. Pulmonary Physiology, 7th edition. Lang physiology series: The McGraw-Hill Companies, Inc., 2007.

Liao H, Belkoff SM. A failure model for ligaments. J Biomechanics 1999; 32: 183-188.

Lindsay CH, John MD. Biomechanics of coronary artery and bypass graft disease: potential new approaches Ann Thorac Surg 2009; 87:331-338

Lockley RM. The most aerial bird in the world. Animals 1970; 13: 4 – 7.

Lopez J, Gomez E, Sesma P. Anatomical study of the bronchial system and major blood vessels of the chicken lung (*Gallus gallus*) by means of a three-dimensional scale model. Anat Rec 1992; 234: 234-240

Lowry OH, Rosbrough NJ, Farr AL, Randall RJ. Protein measurement with the Folin phenol reagent. J Biol Chem 1951; 193: 265-275.

Ludwig BB, Mahon RT, Schwartzman EL. Cardiopulmonary function after recovery from swimming-induced pulmonary edema. Clin J Sport Med 2006; 16: 348-351

Maarek JMI and Chang HK. Pulsatile pulmonary microvascular pressure measured with vascular occlusion techniques. J Appl Physiol 1991; 70: 998–1005.

Macklem P, Bouverot P, Scheid P. Measurement of the distensibility of the parabronchi in duck lungs. Respir Physiol 1979; 33: 23 – 35.

Maina JN. A scanning electron microscopic study of the air- and blood capillaries of the lung of the domestic fowl (*Gallus domesticus*). Experientia 1982; 35: 614-616.

Maina JN Morphometrics of the avian lung. 3. The structural design of the passerine lung. Respir Physiol 1984; 55: 291-309.

Maina JN. A scanning and transmission electron microscopic study of the bat lung. J Zool, Lond 1985; 205: 19-27.

Maina JN. The structural design of the bat lung. Myotis 1986; 23: 71-77.

Maina JN. The morphometry of the avian lung. In: Form and Function in Birds, vol. 4. (ed King AS, McLelland J). London: Academic Press, 1989, pp. 307-368.

Maina JN. Perspectives on the structure and function in birds. In: Diseases of Cage and Aviary Birds, (ed Rosskoff E.). Baltimore: Williams and Wilkins, 1996, pp. 163-256.

Maina JN. The Gas Exchangers: Structure, Function and Evolution of the Respiratory Processes. Heidelberg: Springer-Verlag, 1998.

Maina JN. What it takes to fly: The novel respiratory structural and functional adaptations in birds and bats. J Exp Biol 2000a; 203: 3045-3064.

Maina JN. Comparative respiratory morphology: themes and principles in the design and construction of the gas exchangers. Anat Rec 2000b; 261: 25-44.

Maina JN. Structure, function and evolution of the gas exchangers: comparative perspectives. J Anat 2002a; 201: 281–304.

Maina JN Functional Morphology of the Vertebrate Respiratory Systems. Enfield (NH): Science Publishers Inc. 2002b.

Maina JN. A systemic study of the development of the airway (bronchial) system of the avian lung from days 3 – 26 of embryogenesis: a transmission electron microscopic study on the domestic fowl, *Gallus gallus* variant *domesticus*. Tissue & Cell 2003; 35: 375-391.

Maina JN. Morphogenesis of the laminated, tripartite cytoarchitectural design of the blood-gas barrier of the avian lung: a systemic electron microscopic study on the domestic fowl, *Gallus gallus* variant *domesticus*. Tissue Cell 2004; 36: 129-139.

Maina JN. The Lung-Air Sac System of Birds: Development, Structure, and Function. Heidelberg, Springer-Verlag, 2005.

Maina JN. Minutialization at its extreme best! The underpinnings of the remarkable strengths of the air- and the blood capillaries of the avian lung: A conundrum. Respir Physiol Neurobiol 2007a; 159: 141-145.

Maina JN. Spectacularly robust! Tensegrity principle explains the mechanical strength of the avian lung. Respir Physiol Neurobiol 2007b; 155: 1-10.

Maina JN. Structure of the air- and blood capillaries of the avian lung and the debate regarding the basis of their astounding strengths. In: The 4th Comparative Physiology and Biochemistry in Africa. Molecules to Migration: The Pressure of Life, Morris S and Vosloo A. (eds), 2008, pp. 313-324

Maina JN, Abdalla MA, King AS. Light microscopic morphometry of the lungs of 19 avian species. Acta Anat 1982; 112: 264-270.

Maina JN, Cowley HM. Ultrastructural characterization of the pulmonary cellular defenses in the lung of a bird, the rock dove, *Columba livia*. Proc R Soc Lond B Biol Sci 1998; 265: 1567–1572.

Maina JN, P. van Gils. Morphometric characterization of the airway and vascular systems of the lung of the domestic pig, Sus scrofa: comparison of the airway, arterial and venous systems. Compar Biochem and Physiol 2001; 130: 781-798.

Maina JN, Jimoh SA, Hosie M. Implicit mechanistic role of the collagen, smooth muscle, and elastic tissue components in strengthening the air and blood capillaries of the avian lung. J Anat 2010; 217: 597-608.

Maina JN, King AS. The thickness of the avian blood-gas barrier: Qualitative and quantitative observations. J Anat 1982; 134: 553-562.

Maina JN, King AS. The structural functional correlation in the design of the bat lung. A morphometric study. J Exp Biol 1984; 111: 43-63.

Maina JN, King AS, Settle JG. An allometric study of the pulmonary morphometric parameters in birds, with mammalian comparison. Philos Trans R Soc Lond B Biol Sci 1989; 326: 1–57.

Maina JN, Thomas SP, Dalas DM. A morphometric study of bats of different size: correlation between structure and function of chiropteran lung. Philos Trans R Soc Lond B Biol Sci 1991; 333: 31-50

Maina JN, Maloiy GMO, Makanya AN. Morphology and morphometry of the lungs of two East African mole rats, *Tachyoryctes splendens* and *Heterocephalus glaber* (Mammalia, Rodentia). Zoomorphology 1992; 112: 167-179.

Maina JN, Nathaniel C. A qualitative and quantitative study of the lung of an ostrich, *Struthio camelus*. J Exp Biol 2001; 204: 2313-2330.

Maina JN, Nicholson T. The morphometric diffusing capacity of a bat *Epomophorus wahlbergi*. J Physiol, Lond 1982; 325: 1-57.

Maina JN, West JB. Thin and Strong! The bioengineering dilemma in the structural and functional design of the blood-gas barrier: Comparative and evolutionary perspectives. Physiol Rev 2005; 85: 811-844.

Maina JN, Woodward JD.three-dimensional serial section computer reconstruction of the arrangement of the structural components of the parabronchus of the ostrich,*Struthio camellus* lung. Ana Rec 2009; 292:1685-1698

Makanya AN, Djonov V. Development and spatial organization of the air conduits in the lung of the domestic fowl, *Gallus gallus* variant *domesticus*. Microsc Res Tech 2008; 71: 689-702

Manohar M. Pulmonary artery wedge pressure increases with high-intensity exercise in horses. Am J Vet Res 1993; 54: 142–146.

Martin GR, Timpl R, Kuhn K. Basement lamina proteins: molecular structure and function. Adv Protein Chem 1988; 39:1 – 50.

Matsuda M, Fung YC, Sobin SS. Collagen and elastin fibers in human pulmonary alveolar mouths and ducts. J Appl Physiol 1987; 63: 1185-l 194.

McElroy MC, Kasper M. The use of alveolar epithelial type I cell-selective markers to investigate lung injury and repair. Eur Respir J 2004; 24**:** 664–673.

McElroy MC, Pittet JF, Hashimoto S, Allen L, Wiener-Kronish JP, Dobbs LG. A type I cell-specific protein is a biochemical marker of epithelial injury in a rat model of pneumonia. Am J Physiol 1995; 268**:** L181–L186.

McGowan KA, Marinkovich MP. Laminins and human disease. Micro Res Tech 2000; 51:262–279.

McLelland J. Anatomy of the lungs and air sacs. In: Form and Function in Birds, vol 4. (Eds King AS, McLelland J). London: Academic Press, 1989, pp 221-279.

Mead J. Mechanical properties of lungs. Physiol Rev 1961; 41: 281-328.

Meban C. Thicknesses of the air-blood barriers in vertebrate lungs. J Anat 1980; 131: 299–307.

Mercer RR, Crapo JD. Spatial distribution of collagen and elastin fibers in the lungs. J Appl Physiol 1990; 69: 756-765.

Mercer RR, Crapo JD. Structural changes in elastic fibers after pancreatic elastase administration in hamsters. J Appl Physiol 1992; 72: 1473-1479.

Mercer RR, Russell ML, Crapo JD. Alveolar septal structure in different species. J Appl Physiol 1994; 77: 1060-1006.

Milnor WR. Hemodynamics. Baltimore, Williams & Wilkins, 1982.

Miner JH, Patton BL, Lentz SI, Gilbert DJ, Snider WD, Jenkins NA, Copeland NG, Sanes JR The laminin α chains: expression, developmental transitions, and chromosomal locations of α1–5, identification of heterotrimeric laminins 8–11, and cloning of a novel α3 isoform. J Cell Biol 1997; 137:685–701.

Miner, JH and Yurchenco PD. Laminin function in tissue morphogenesis. Annu Rev Cell Dev Biol 2004; 20:255-284.

Mohammed H, Hassan G, Saied C, Johan B, Eddy D. Anatomical parameters of cardiopulmonary system in three different lines of chickens: Further evidence for involvement in ascites syndrome. Avian Path 2005; 34: 188-193.

Mohan J. Physiology of stress in poultry 2005 IPSACON

Mooney DJ, Hansen L, Vacanti J, Langer R, Farmer S, Ingber DE. Switching from differentiation to growth in hepatocytes: control by extracellular matrix. J Cell Phys 1992; 151: 497–505.

Negrini D, Passi A, de Luca G, Miserocchi G. Pulmonary interstitial pressure and proteoglycans during development of pulmonary edema. Am J Physiol 1996; 270: 2000-2007.

Newman V, Gonzalez RF, Matthay MA, Dobbs LG. A novel alveolar type I cell-specific biochemical marker of human acute lung injury. Am J Respir Crit Care Med 2000; 161: 990–995.

Nganpiep L and Maina JN Composite cellular defense stratagem in the avian respiratory system: functional morphology of the free (surface) macrophages and specialized pulmonary epithelia. J Anat 2002; 200: 499-516.

Nyren S, MureM, JacobssonH, Larson SA, Lindahl SGE. Pulmonary perfusion is more uniform in the prone than in the supine position: scintigraphy in healthy humans. J Appl Physiol 1999; 86 (4): 1135- 1141.

Ochs M, Nyengaard JR, Jung A, Knudsen L, Voigt M, Wahlers T, Richter J, Gundersen HJ. The number of alveoli in the human lung. Am J Respir Crit Care Med 2004; 169: 120-4

Ohtani O. Three-dimensional organization of the connective tissue fibers of the human pancreas. A scanning electron microscopic study of NaOH treated tissues. Arch Histolol Jap 1987; 50: 557-566.

Ohtani O. The maceration technique in scanning electron microscopy of collagen fiber frameworks. It's application in the study of human livers. Arch Histol Cytol 1992; 55: 225-32.

Ohtani O, Nakatani T. Spatial organization of the collagen and elastin fibers of the lung in the Japanese monkeys, *Macaca fascata*. Anthropol Sci 1994; 102: 181-187.

Pattle RE. Lung surfactant and lung lining in birds. In: Respiratory Function in Birds, Adult and Embryonic (ed Piiper J). Springer, Berlin, Heidelberg: 1978, pp 23 – 32.

Pennycuick CJ. Animal Flight. London: Edward Arnold, 1972.

Perry SF. Mainstreams in the evolution of vertebrate respiratory structures. In: Form and Function in Birds, vol 4. (eds King AS, McLelland J). London: Academic Press, 1989, pp. 1-67.

Perry SF, Duncker HR. Interrelationship of static mechanical factors and anatomical structure in lung ventilation. J Comp Physiol 1980; 138: 321 – 334.

Pierce RA, Griffin GL, Miner JH, Senior RM. Expression patterns of laminin α1 and α5 in human lung during development. Am J Respir Cell Mol Biol 2000; 23: 742–747.

Piiper J, Scheid P. Gas transport efficacy in gills, lungs and skin: theory and experimental data. Respiration Physiol 1975; 23:209- 221.

Piiper J, Scheid P. Respiratory mechanics and air flow in birds. In: Form and Function in Birds, vol. 4 (eds King AS, McLelland J), London: Academic Press, 1989 pp. 369-391.

Pollard TD, Blanchoin L, Mullins RD. Molecular mechanisms controlling actin filament dynamics in nonmuscle cells. Annu Rev Biophys Biomol Struct 2000; 29: 545–576.

Powell FL, Hastings RH, Mazzone RW. Pulmonary vascular resistant during unilateral pulmonary arterial occlusion in ducks. Am J Physiol 1985; 249: R39 – R43.

Powell FL, Hopkins SR. Comparative physiology of lung complexity: Implications for gas exchange. News Physiol Sci 2004; 19: 55-60.

Powell FL, Mazzone RW. Morphometrics of rapidly frozen lungs. Respir Physiol 1985; 31: 319-332.

Raven PB, Potts JT, Cardiovascular responses to exercise and training. In: Oxford Textbook of Sport Medicine, 2nd edition (eds Mark Harries, Clyde Williams, William D Stanish, Micheli Micheli). Oxford University Press, USA. 2000, pp. 32-45.

Reeves JT, Linehan JH, Stenmark KR. Distensibility of the normal human lung circulation during exercise. Am. J Physiol. Lung Cell Mol Physiol 2005; 288: L419-L425.

Reifenrath R. Surfactant action in bronchial mucus transport. In: Pulmonary Surfactant System, (eds Cosmi EV, Scarpelli EM). Amsterdam: Elsevier 1983 pp. 334-347.

Richardson J. Autumnal migration over Puerto Rico and the Western Atlantic: A radar study. Ibis 1976; 118: 309–332.

Riedesel ML. Blood physiology: In: Biology of Bats, vol. II (ed. WA Wimsatt), New York: Academic Press, 1977, pp. 485–517.

Ringer RK, Rood K. Hemodynamic changes associated with aging in the broad-breasted Bronze turkey. Poultry Sci 1959; 38**:** 395–397.

Robins SP. Functional properties of collagen and elastin. Beillieres Clin Rheumatol 1988; 2: 1-36.

Rosales AG. Managing stress in broiler breeders: a review. J Appl Poult Res 1994; 3:199-207

Roston WL, Whipp BJ, Davies JA, Cunningham DA, Effros RM, Wassermann K. Oxygen uptake kinetics and lactate concentration during exercise in humans. Am Rev Respir Dis 1987; 135: 1080-1084.

Rowell LB. Human cardiovascular adjustments to exercise and thermal stress. Physiol Rev 1974; 54: 75-159.

Salomonsen F. Migratory movements of the Arctic tern (Sterna paradisea pontoppidan) in the Southern Ocean. Det Kgl Danske Vid Selsk Biol Med 1967; 24: 1-37.

Sanderson RD, Fitch JM, Llnsenmayer TR, Mayne R. Fibroblasts promote the formation of a continuous basal lamina during myogenesis *in vitro*. J Cell Biol 1986; 102: 740-747.

Sanderson RJ, Paul GW, Vatter AE, Filley GF. Morphological and physical basis for lung surfactant action. Respir Physiol 1976; 27: 379-392.

Sannes PL. Differences in basement membrane-associated microdomains of type 1 and type 2 pneumocytes in the rat and rabbit lung. J Histochem Cytochem 1984; 32: 827–833.

Scheid P. Mechanisms of gas exchange in bird lungs. Rev Physiol Bioch Pharm 1979; 86:136-186.

Scheid, P. Analysis of gas exchange between air capillaries and blood capillaries in avian lungs. Respir Physiol 1978; 33: 27-49.

Scheid P (1990) Cited in Maina JN. The Lung-Air Sac System of Birds: Development, Sructure, and Function. Heidelberg, Springer-Verlag, 2005.

Scheid P, Piiper J. Volume ventilation and compliance of the respiratory system in the domestic fowl. Respir Physiol 1969; 6: 298-308.

Scheid P, Piiper J. Cross-current gas exchange in the avian lungs: effects of reversed parabronchial air flow in ducks. Respir Physiol 1972; 16: 304-312.

Scheuermann DW, Klika E, De Groodt-Lasseel MHA, Bazantova I, Switka A. An electron microscopic study of the parabronchi epithelium in the mature lung of four bird species. Anat Rec 1997; 249: 213-225.

Schmidt-Nielsen K. Locomotion: energy cost of swimming, flying and running. Science 1972; 172: 222-228.

Schmidt-Nielsen K. Recent advances in avian respiration. In: Avian Physiology (ed Peaker M). London: Academic Press 1975, pp. 33-47.

Schoene RB, Hackett PH, Henderson WR, Sage EH, Chow M, Roach RC. High-altitude pulmonary edema: Characteristics of lung lavage fluid. JAMA 1986; 256: 63-69.

Senior RM, Bielefeld DR and Abensohn MK. The effects of proteolytic enzymes on the tensile strength of human lung. Amer Rev Respir Dis 1975; 111: 184-188.

Senior RM, Griffin GL, Mudd MS, Moxley MA, Lonmore WJ, Pierce RA. Entactin expression by rat lung and rat alveolar epithelial cells. Am J Resp Cell Mol Biol 1996; 14: 239-247.

Seymour RS, Blaylock AJ. The principle of Laplace and scaling of ventricular wall stress and blood pressure in mammals and birds. Physiol Biochem Zool 2000; 73: 389-405.

Seymour RS, Runciman S, Baudinette RV,Pearson JT. Developmental allometry of pulmonary structure and function in the altricial Australian pelican *Pelecanus conspicillatus.* J Exp Biol 2004; 207:2663-2669.

Shah JV, Cells in tight spaces: the role of cell shape in cell function. JCB 2010; 191: (2) 233-236

Shimura S, Martin CJ, Boatman ES, Dhand R. A role for interstitial matrix in tissue tension of alveolar wall. Respir Physiol 1985; 62(3): 293-303.

Silversides FG, Lefrancois MR, Villeneuve P. The effect of strain of broiler on physiological parameters associated with the ascites syndrome. Poultry Sci 1997; 76: 663–667.

Simon-Assmann P, Bouziges F, Arnold C, Haffen K, Kedinger M. Epithelial-mesenchymal interactions in the production of basement membrane components in the gut. Development 1988; 102: 339-347.

Singhvi R, Kumar A, Lopez G, Stephanopoulos GN, Wang DIC, Whitesides GM, Ingber DE. Engineering cell shape and function. Science 1994; 264: 696-698.

Smith DG and Chamley-Campbell J. Localization of smooth muscle myosin in branchial pillar cells of snapper, *Chrysophys auratus*, by immunofluorescence histochemistry. J Exp Biol 1981; 215: 121–124.

Snyder GK. Respiratory characteristics of whole blood and selected aspects of circulatory physiology in the common short-nosed fruit bat, *Cynopterus brachyotes*. Respir Physiol 1976; 28: 239–247.

Speckman EW, Ringer RK. The cardiac output and carotid and tibia blood pressure of the turkey. Can J Biochem Physiol 1963; 41: 2337-2341.

Spells KE. Comparative studies in the lung mechanics based on a survey of literature data. Respir Physiol 1969/70; 8:37-57

Stevens T, Phan S, Frid MG, Alvarez D, Herzog E, Stenmark KR. Lung vascular cell heterogeneity: Endothelium, smooth muscle, and fibroblasts. Proc Am Thorac Soc 2008; 5(7): 783-791.

Swan LW. The ecology of the high Himalayas. Scient Am 1961; 205: 67–78.

Swan LW. Goose of the Himalayas. Nat Hist 1970; 79: 68–75.

Swayne GT, Smaje LH, Bergel DH. Distensibility of single capillaries and venules in the rat and frog mesentery. Int J Microcirc Clin Exp 1989; 8: 25–42.

Tatner P, Bryant DM. Flight cost of a small passerine measured using doubly labeled water: Implications for energetics studies. The Auk 1986; 103: 169-180

Taylor CR, Heglund NC, Maloiy GMO. Energetics and mechanics of terrestrial locomotion. I. Metabolic energy consumption as a function of speed and body size in birds and mammals. J Exp Biol 1982; 97: 1-22.

Tenney SM, Remmers JE. Comparative quantitative morphology of the mammalian lung: diffusing area. Nature 1963; 197: 54-56.

Tenney SM, Tenney JB. Quantitative morphology of cold-blooded lungs: Amphibia and Reptilia. Respir Physiol 1970; 9: 197 – 215.

Thomas DP, Fregin GF. Cardiorespiratory and metabolic responses to treadmill exercise in the horse. J Appl Physiol 1981; 50: 864-868.

Thomas SP. Metabolism during flight in two species of bats, *Phyllostomus hastatus* and *Pteropus gouldii*. J Exp Biol 1975; 63: 273–293.

Timmwood KT, Hyde DM, Plopper CG. Lung growth of the turkey, Meleagris gallopavo: II. Comparison of two genetic lines. Am J Anat 1987; 178: 158-169.

Timpl R. Structure and biological activity of basement membrane proteins. Eur J Biochem. 1989; 180: 487-502.

Tochima M, Ohtani Y, Ohtani O. Three-dimensional architecture of elastin and collagen fiber networks in the human and rat lung. Arch Histolol Jap 2004; 67: 31-40.

Torre-Bueno JR. The energetics of avian flight at altitude. In: Bird Flight, BIONA Report 3 (ed Nachtigall W). Stuttgart: Gustav Fischer Verlag 1985, pp. 45–87.

Tsukimoto K, Mathieu-Costello O, Prediletto R, Elliot AR, West JB. Ultrastructural appearances of pulmonary capillaries at high transmural pressures. J Appl Physiol 1991; 71: 573–582.

Tucker VA. Respiration during flight in birds. Respir Physiol 1972a; 14: 75–82.

Tucker VA. Metabolism during flight in the laughing gull, *Larus atricilla*. Am J Physiol 1972b; 222: 237–245.

Tucker VA. Gliding flight: speed and accelelation of ideal falcons during diving and pull out. J Exp Biol 1998; 201: 403-414.

Tunggal P, Smyth N, Paulsson M, Ott M-C. Laminins: structural and genetic regulation. Microsc Res Tech 2000; 51: 214–227.

Turner DL. Cardiovascular and respiratory control mechanisms during exercise: an integrated view. J Exp Biol 1991; 160**:** 309–340.

Ushiki T. Collagen fibers, reticular fibers and elastic fibers. A comprehensive understanding from a morphological viewpoint. Arch Histol Cytol 2002; 65: 109-126.

Vaccaro CA, Brody JS. Structural features of alveolar wall basement membrane in the adult rat lung. J Cell Biol 1981; 91: 427–437.

Vlahakis NE,Schroeder MA, Pagano RE, Hubmayr RD. Role of deformation-induced lipid trafficking in the prevention of plasma membrane stress failure. Am J Respir Crit Care Med 2002; 166: 1282-1289.

Voigt CC, Winter Y. Energetic cost of hovering flight in nectar-feeding bats (Phyllostomidae: Glossophaginae) and its scaling in moths, birds and bats. J Comp Physiol B. 1999; 169: 38-48

Wagner PD. Why doesn't exercise grow lungs when other factors do? Exerc Sport Sci Rev 2005; 33: 3-8

Wang NS, Ying WL. A scanning electron microscopic study of alkali-digested human and rabbit alveoli. Am Rev Respir Dis 1977; 115: 165-173.

Watson RR, Fu Z, West JB. Morphometry of the extremely thin pulmonary blood-gas barrier in the chicken lung, Am J Physiol Lung Cell Mol Physiol 2007; 292**:** L769–L777.

Watson RR, Fu Z, West JB. Minimal distensibility of pulmonary capillaries in avian lungs compared with mammalian lungs. Respir Physiol Neurobiol 2008; 160: 208-214.

Weibel ER. Morphometry of the Human Lung. Springer-Verlag, Berlin, Heidelberg, New York 1963.

Weibel ER. Morphometric estimation of pulmonary diffusion capacity. V. Comparative morphometry of alveolar lungs. Respir Physiol 1970/1971; 14: 26-43.

Weibel ER.Morphometric estimation of pulmonary diffusing capacity. V. Comparative analysis of mammalian lungs. Respir Physiol 1972; 14: 26-43

Weibel ER. Morphological basis of the alveolar-capillary gas exchange. Physiol Rev 1973; 53: 419–495.

Weibel ER. The Pathway for Oxygen: Structure and function in the mammalian respiratory system. Harvard, Harvard University Press 1984.

Weibel ER. Lung morphometry and models in respiratory physiology. In: Respiratory Physiology: An Analytical Approach, (eds Chang HK, Paiva M.) New York: Dekker, 1989, pp. 1–55.

Weibel ER. What makes a good lung? Swiss Med Wkly 2009; 139: 375-386.

Weibel ER, Knight BW. A morphometric study on the thickness of the pulmonary air-blood barrier. J Cell Biol 1964; 21: 367 – 384.

Weislander J, Heinegard D. The involvement of type IV collagen in Goodpasture's syndrome. Ann NY Acad Sci 1985; 460: 363-374.

Welling LW, Grantham JJ. Physical properties of isolated perfused renal tubules and tubular basement membranes. J Clin Invest 1972; 51: 1063–1075.

Welty JC. The Life of Birds, 3rd edition. Philadelphia, Saunders, 1982.

Welty JC. The Life of Birds, 2nd edition. Philadelphia, Saunders, 1979

West, JB. Climbing Mt Everest without oxygen: an analysis of maximal exercise during extreme hypoxia. Respir Physiol 1983; 52: 265–274.

West JB. Cellular responses to mechanical stress: pulmonary capillary stress failure. J Appl Physiol 2000a; 89: 2483–2489.

West JB. Respiratory Physiology - The Essentials, 6th edition. Lippincott Williams and Wilkins, 2000b.

West JB. Vulnerability of pulmonary capillaries during exercise. Exerc Sport Sci Rev 2004; 32: 24-30

West JB. Comparative physiology of the pulmonary blood-gas barrier: The unique avian solution. Am J Physiol Regul Integr Comp Physiol 2009; 297: R1625-R1634.

West JB, Mathieu-Costello O. Strength of pulmonary blood-gas barrier. Respir Physiol 1992; 88: 141-148.

West JB, Mathieu-Costello O. Vulnerability of pulmonary capillaries in heart disease. Circulation 1995; 92: 622-631.

West JB, Mathieu-Costello O. Structure, strength, failure, and remodeling of the pulmonary blood-gas barrier. Annu Rev Physiol 1999; 61: 543–572.

West JB, Mathieu-Costello O, Jones JH, Birks EK, Logerman RB, Pascoe JR, Tyler WS. Stress failure of pulmonary capillaries in racehorses with exercise-induced pulmonary hemorrhage. J Appl Physiol 1993; 75: 1097–1109.

West JB, Tsukimoto K, Mathieu-Costello O, Prediletto R. Stress failure in pulmonary capillaries. J Appl Physiol 1991; 70: 1731–1742.

West JB, Watson RR, Fu Z. The honeycomb-like structure of the bird lung allows a uniquely thin blood–gas barrier, Respir Physiol Neurobiol 2006; 152**:** 115–118.

West JB, Watson RR, Fu Z. Major differences in the pulmonary circulation between birds and mammals. Respir Physiol Neurobiol 2007a; 157: 382–390.

West JB, Watson RR, Fu Z. The human lung: did evolution get it wrong? Eur Respir J 2007b; 29: 11-17.

West JB, Zhou BW. Did chickens go North? New evidence for domestication. J Archeol Sc 1988; 15: 515-533.

West JB, Fu Z. Deerinck TJ, Mackey MR, Obayashi JT, Ellisman MH. Structure-function studies of blood and air capillaries in chicken lung using 3D electron microscopy. Respir Physiol Neurobiol 2010; 170: 202-209

West NH, Bamford OS, Jones DR. A scanning electron microscope study of the microvasculature of the avian lung. Cell Tissue Res 1977; 176: 553-564.

Whipp BJ, Ward SA. Cardiopulmonary coupling during exercise. J Exp Biol 1982; 100: 175-193.

Whitwell KE, Greet TR. Collection and evaluation of tracheobronchial washes in the horse. Equine Vet J 1984; 16: 499–508.

Wideman RF. Pathophysiology of heart/lung disorders: pulmonary hypertension syndrome in broiler chickens. World's Poult Sci J 2001; 57**:** 289–307.

Wideman Jr RF, Chapman ME, Hamal KR, Bowen OT, Lorenzoni AG, Erf GF, Anthony NB. An inadequate pulmonary vascular capacity and susceptibility to pulmonary arterial hypertension in broilers. Poult Sci 2007; 86**:** 984–998.

Widnell CC, Pfenninger KH. Essential Cell Biology, Baltimore: Williams and Wilkins, 1990.

Wienner F, Morkin E, Skalak R, Fishman AP. Wave propagation in the pulmonary circulation. Circ Res 1966; 19: 834–850.

Wieslander J, Heinegard D. The involvement of type IV collagen in Goodpasture's Syndrome. Ann N.Y. Acad Sci 1985; 460: 363–374.

Williamson JR, Vogler NJ, Kilo C. Regional variations in the width of the basement membrane of muscle capillaries in man and giraffe. Am J Pathol 1971; 63: 359–370.

WilkenT. A gift tensegrity. http://www.synearth.net/Restricted-Confidential/Gift/Gift_Tensegrity.html 2001.

Wolk E, Bogdanowicz W. Hematology of the hibernating bat, *Myotis daubentoni*. Comp Biochem Physiol 1987; 88A: 637–639.

Wood W, Jacinto A, Grose R, Woolner S, Gale J, Wilson C, Martin P. Wound healing recapitulate morphogenesis in Drosophila embryo. Nat Cell Biol 2002; 4: 907-912.

Woodbury RA, Hamilton WF. Blood pressure studies in small animals. Am J Physiol 1937; 119 (4): 663 – 674.

Woodward JD, Maina JN. A 3D digital reconstruction of the components of the gas exchange tissue of the lung of the Muscovy duck Cairina moschata. J Anat 2005; 206**:** 477–492.

Woodward JD, Maina JN. Study of the structure of the air- and blood capillaries of the gas exchange tissue of the avian lung by serial section three-dimensional reconstruction. J Microsc 2008; 230: 84-93.

Yalden DW and Morris PA. The lives of bats. New York: The New York Times Book Co, 1975.

Younes M, Bshouty Z, Ali J. Longitudinal distribution of pulmonary vascular resistance with very high pulmonary blood flow. J Appl Physiol 1987; 62:344-358.

Yurchenco PD, Cheng YS. Laminin self-assembly: a three-arm interaction hypothesis for the formation of a network in basement membranes. Contrib Nephrol 1994; 107: 47-56.

Yurchenco PD, Ruben GC. Type IV collagen lateral associations in the EHS tumor matrix. Comparison with amniotic and *in vitro* networks. Am J Pathol 1988; 132: 278-291.

Zaidel-Bar R, Cohen M, Addadi L, Geiger B. Hierarchical assembly of cellmatrix adhesion complexes. Biochem Soc Trans 2004; 32: 416–420.

Zavorsky GS, Saul L, Decker A, Ruiz P. Radiographic evidence of pulmonary edema during high-intensity interval training in women. Respir Physiol Neurobiol 2006; 153: 181-190.

Zemel A, Rehfeldt F, Brown AEX, Discher DE, Safran SA. Cell shape spreading symmetry and the polarization of stress-fibers in cells. J Phys Condens Matter 2010; 22: 1-11.

APPENDIXES

Appendix I: Lowry reagent

1. Bovine serum albumin (BSA) stock solution (500µg/ml)
2. Analytical reagents:
    a. 2% sodium carbonate (w/v) in 0.1M sodium hydroxide
    b. 1% copper sulphate solution
    c. 2%sodium potassium tartrate solution
    d. Folin-Ciocalteau reagent solution
3. **Reagent A** is prepared by adding 25 ml of analytical reagent 2a to 250 µl each of analytical reagent 2b and 2c
4. **Reagent B** is made by diluting Folin reagent in distilled water in ratio 1:4
5. Triplicate of graded concentration of 50 µl BSA standard working solutions were made as shown in the table below:
6. Graded dilution of BSA standard working solution

BSA conc. (µg/ml)	Volume of BSA solution (µl)	Volume of PBS (µl)
100	50	0
100	50	0
100	50	0
80	40	10
80	40	10
80	40	10
60	30	20
60	30	20
60	30	20
40	20	30
40	20	30
40	20	30
20	10	40
20	10	40
20	10	40
0	0	50
0	0	50
0	0	50

Spectrometer reading

	STANDARD					UNKNOWN				
	Spectrometer readings			Average	BSA Conc.					
Expt 1	0.000	0.000	0.000	**0.000**	0	Unperturb/Resting				
	0.398	0.422	0.431	**0.417**	20	CHKa	0.221	0.213	0.198	**0.211**
	0.698	0.743	0.751	**0.731**	40	CHKb	0.189	0.178	0.182	**0.183**
	1.515	1.486	1.459	**1.487**	60	CHKc	0.202	0.229	0.191	**0.207**
	1.885	1.921	1.853	**1.886**	80					
	2.431	2.382	2.426	**2.413**	100					
Expt 2	0.000	0.000	0.000	**0.000**	0	Exercise at 0.66 m/s				
	0.395	0.432	0.412	**0.413**	20	CHK1a	0.363	0.387	0.372	**0.374**
	0.755	0.710	0.759	**0.741**	40	CHK1b	0.337	0.351	0.349	**0.346**
	1.499	1.517	1.459	**1.492**	60	CHK1c	0.298	0.325	0.316	**0.313**
	1.794	1.855	1.806	**1.818**	80					
	2.434	2.423	2.408	**2.422**	100					
Expt 3	0.000	0.000	0.000	**0.000**	0	Exercise at 0.98 m/s				
	0.428	0.412	0.398	**0.413**	20	CHK2a	0.535	0.496	0.549	**0.527**
	0.778	0.839	0.769	**0.795**	40	CHK2b	0.515	0.562	0.498	**0.525**
	1.431	1.471	1.429	**1.444**	60	CHK2c	0.534	0.572	0.544	**0.550**
	1.919	1.869	1.897	**1.895**	80					
	2.393	2.421	2.390	**2.401**	100					
Expt 4	0.000	0.000	0.000	**0.000**	0	Exercise at 1.97 m/s				
	0.378	0.429	0.392	**0.400**	20	CHK3a	0.687	0.721	0.684	**0.697**
	0.678	0.731	0.704	**0.704**	40	CHK3b	0.734	0.675	0.714	**0.708**
	1.497	1.512	1.535	**1.515**	60	CHK3c	0.727	0.682	0.679	**0.696**
	1.840	1.913	1.895	**1.883**	80					
	2.424	2.418	2.389	**2.410**	100					
Expt 5	0.000	0.000	0.000	**0.000**	0	Exercise at 2.53 m/s				
	0.407	0.383	0.412	**0.401**	20	CHK4a	0.846	0.811	0.847	**0.835**
	0.736	0.694	0.687	**0.706**	40	CHK4b	0.788	0.781	0.809	**0.793**
	1.482	1.529	1.484	**1.498**	60	CHK4c	0.797	0.828	0.833	**0.819**
	1.789	1.869	1.808	**1.822**	80					
	2.386	2.395	2.415	**2.399**	100					
Expt 6	0.000	0.000	0.000	**0.000**	0	Exercise at 2.95 m/s				
	0.422	0.415	0.384	**0.407**	20	CHK5a	0.967	0.946	0.928	**0.947**
	0.729	0.767	0.683	**0.726**	40	CHK5b	0.883	0.912	0.896	**0.897**
	1.479	1.515	1.521	**1.505**	60	CHK5c	0.923	0.879	0.93	**0.911**
	1.886	1.914	1.907	**1.902**	80					
	2.406	2.380	2.404	**2.397**	100					

Appendix II: Standard curve for BSA determination

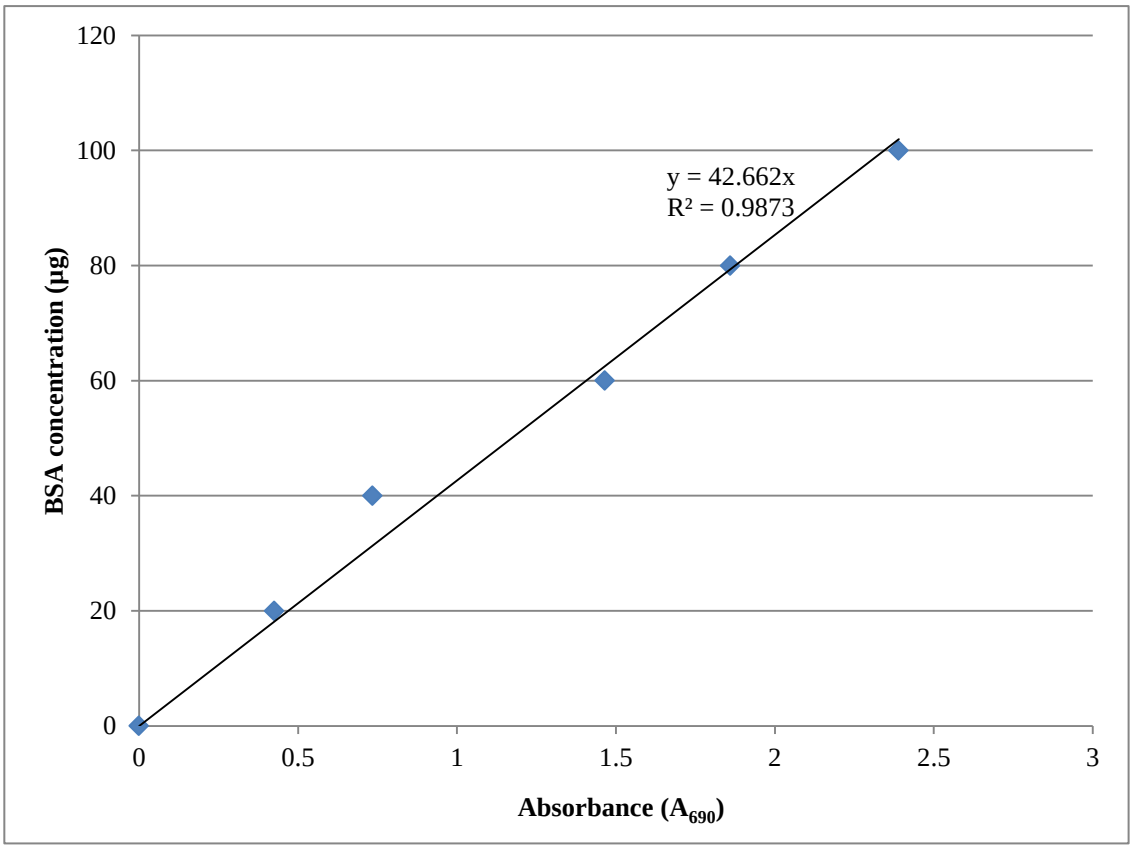

Protein concentration in the lavage fluid

CHKa:	8.85	14.75	24.33	34.06	37.75	37.64
CHKb:	9.10	14.19	24.25	34.41	36.05	39.52
CHKc:	8.61	14.39	25.26	33.62	37.11	38.20
AVE:	8.85	14.44	24.61	34.03	36.97	38.45
SEM	0.14	0.17	0.32	0.23	0.50	0.56

Appendix III: Blood lactate measurement

SPEED	TIME	WEIGHT	LACTATE BEFORE			AVE	LACTATE AFTER			AVE
Resting bird	0	2016	1.4	1.4	1.3	1.4	1.3	1.2	1.1	1.2
		2370	1.6	1.4	1.5	1.5	1.5	1.2	1.4	1.4
		2370	1.2	1.4	1.3	1.3	1.3	1.2	1.2	1.2
	Mean	2252.00			Mean	1.39			Mean	1.27
	SD	204.38			SD	0.10			SD	0.09
0.66 m/s	10 mins	1392	1.4	1.3	1.5	1.4	3.3	3.1	3.1	3.2
		1927	1.6	1.2	2.0	1.6	3.4	3.0	2.9	3.1
		1896	2.2	1.4	1.9	1.8	3.2	3.2	3.1	3.2
	Mean	1738.33			Mean	1.61			Mean	3.14
	SD	300.33			SD	0.22			SD	0.04
0.98 m/s	10 mins	1392	1.3	1.5	1.3	1.4	3.7	3.6	3.5	3.6
		1927	1.6	1.9	1.7	1.7	3.5	3.5	3.2	3.4
		2261	2.0	2.1	2.4	2.2	3.8	3.4	3.4	3.5
	Mean	1860.00			Mean	1.76			Mean	3.51
	SD	438.36			SD	0.40			SD	0.10
1.97 m/s	10 mins	2122	2.3	1.9	1.7	2.0	3.9	3.9	3.7	3.8
		1915	1.5	1.9	2.0	1.8	4.2	4.0	4.1	4.1
		2166	2.4	2.2	1.8	2.1	4.4	4.1	4.0	4.2
	Mean	2067.67			Mean	1.97			Mean	4.03
	SD	134.03			SD	0.17			SD	0.18
2.53 m/s	10 mins	1702	2.3	2.4	2.2	2.3	4.4	4.6	4.4	4.5
		1632	1.6	1.9	1.9	1.8	4.8	4.8	4.6	4.7
		2187	1.4	1.4	1.5	1.4	4.6	4.7	4.7	4.7
	Mean	1840.33			Mean	1.84			Mean	4.62
	SD	302.26			SD	0.44			SD	0.14
2.95 m/s	10 mins	2137	2.0	2.0	2.1	2.0	4.9	4.6	4.5	4.7
		1995	1.5	1.3	1.5	1.4	5.5	4.7	4.6	4.9
		1595	1.2	2.0	2.4	1.9	5.9	5.8	5.8	5.8
	Mean	1909.00			Mean	1.78			Mean	5.14
	SD	281.05			SD	0.31			SD	0.61

Appendix IV: Red blood cell counts

		Hemocytometer				Equivalent values					
		S1	S2	S3	S4	S1	S2	S3	S4	MEAN	SEM
Resting chicken	CHKa	6	5	8	9	300000	250000	400000	450000	350000	45643.55
	CHKb	5	6	4	6	250000	300000	200000	300000	262500	23935.68
	CHKc	7	7	6	8	350000	350000	300000	400000	350000	20412.41
										320833.33	
0.66m/s	CHK1a	8	6	7	9	400000	300000	350000	450000	375000	32274.86
	CHK1b	9	10	8	7	450000	500000	400000	350000	425000	32274.86
	CHK1c	8	5	8	8	400000	250000	400000	400000	362500	37500.00
										387500.00	
0.98m/s	CHK2a	12	9	8	10	600000	450000	400000	500000	487500	42695.63
	CHK2b	8	11	9	10	400000	550000	450000	500000	475000	32274.86
	CHK2c	8	10	9	11	400000	500000	450000	550000	475000	32274.86
										479166.67	
1.97m/s	CHK3a	10	12	11	12	500000	600000	550000	600000	562500	23935.68
	CHK3b	11	12	13	12	550000	600000	650000	600000	600000	20412.41
	CHK3c	14	11	12	12	700000	550000	600000	600000	612500	31457.64
										591666.67	
2.53m/s	CHK4a	13	11	14	12	650000	550000	700000	600000	625000	32274.86
	CHK4b	34	38	35	34	1700000	1900000	1750000	1700000		47324.24
	CHK4c	12	13	12	12	600000	650000	600000	600000	612500	12500.00
										618750.00	
2.95m/s	CHK5a	40	37	38	39	2000000	1850000	1900000	1950000		32274.86
	CHK5b	15	12	13	12	750000	600000	650000	600000	650000	35355.34
	CHK5c	12	14	14	11	600000	700000	700000	550000	637500	37500.00
										643750.00	

Summary:

Speed	RBC $x10^5$
0m/s	3.2E+05
0.66m/s	3.9E+05
0.98m/s	4.8E+05
1.97m/s	5.9E+05
2.53m/s	6.2E+05
2.95m/s	6.4E+05

Appendix V: Number of blood-gas barrier- and epithelial-epithelial breaks in the resting chicken

CHICK	ACCESSORY									CRANIAL									CAUDOMEDIAL									CAUDOLATERAL								
	I	II	III	IV	V	VI	VII	VIII	AVE	I	II	III	IV	V	VI	VII	VIII	AVE	I	II	III	IV	V	VI	VII	VIII	AVE	I	II	III	IV	V	VI	VII	VIII	AVE
A	0	0	0	0	0	0	0	0	0.00	0	0	0	0	0	0	0	0	0.00	0	0	0	0	0	0	0	0	0.00	0	0	0	0	0	0	0	0	0.00
B	0	0	0	0	0	0	0	0	0.00	0	0	0	0	0	0	0	0	0.00	0	1	0	0	0	0	0	0	0.13	0	0	0	0	1	0	0	0	0.13
C	0	0	0	0	0	0	1	0	0.13	0	0	0	0	0	0	0	0	0.00	0	0	0	1	0	0	0	0	0.13	0	0	0	0	0	0	0	0	0.00
								M	0.04								M	0.00								M	0.08								M	0.04

BGB

	ACC	CNN	CDM	CDL
	0.00	0.00	0.00	0.00
	0.00	0.00	0.13	0.13
	0.13	0.00	0.13	0.00
M	0.04	0.00	0.08	0.04
SEM	0.04	0.00	0.04	0.04

Epithelial-epithelial breaks

CHICK	ACCESSORY									CRANIAL									CAUDOMEDIAL									CAUDOLATERAL								
	I	II	III	IV	V	VI	VII	VIII	AVE	I	II	III	IV	V	VI	VII	VIII	AVE	I	II	III	IV	V	VI	VII	VIII	AVE	I	II	III	IV	V	VI	VII	VIII	AVE
A	0	1	0	1	0	0	1	0	0.38	0	0	0	1	0	0	1	0	0.25	0	1	1	0	0	0	0	0	0.25	0	0	1	0	0	1	0	0	0.25
B	1	0	0	1	0	1	0	0	0.38	1	0	1	0	0	1	0	0	0.38	0	0	1	0	0	0	1	0	0.25	0	0	0	1	0	0	1	0	0.25
C	1	0	0	1	0	1	0	0	0.38	0	0	0	1	0	0	0	1	0.25	1	0	0	0	2	0	0	0	0.38	0	1	0	0	1	0	0	0	0.25
								M	0.38								M	0.29								M	0.29								M	0.25

E-E

	ACC	CNN	CDM	CDL
	0.38	0.25	0.25	0.25
	0.38	0.38	0.25	0.25
	0.38	0.25	0.38	0.25
M	0.38	0.29	0.29	0.25
SEM	0.00	0.04	0.04	0.00

Appendix VI: Number of blood-gas barrier breaks in the exercised chicken

EXERCISE: BGB Breaks

Speed	CHICKE	ACCESSORY									CRANIAL									CAUDOMEDIAL									CAUDOLATERAL								
		I	II	III	IV	V	VI	VII	VIII	AVE	I	II	III	IV	V	VI	VII	VIII	AVE	I	II	III	IV	V	VI	VII	VIII	AVE	I	II	III	IV	V	VI	VII	VIII	AVE
0.66 m/s	A	0	0	0	1	0	0	1	1	0.38	0	1	0	0	1	0	0	0	0.25	0	1	0	0	1	0	1	0	0.38	0	0	1	0	2	0	0	0	0.38
	B	0	1	0	1	0	0	0	1	0.38	1	0	0	0	1	0	0	0	0.25	1	0	1	0	1	0	1	0	0.50	0	1	1	0	0	0	2	0	0.50
	C	1	0	1	0	1	1	0	0	0.50	0	0	0	0	1	0	1	0	0.25	0	1	1	1	0	0	0	2	0.63	0	0	2	0	0	0	0	1	0.38
									M	0.42								M	0.25								M	0.50								M	0.42
0.98 m/s	A	0	0	2	1	0	0	1	1	0.63	0	0	1	0	1	0	1	1	0.50	0	1	1	0	1	1	1	1	0.75	2	0	1	0	1	0	0	2	0.75
	B	0	1	1	1	1	1	0	1	0.75	1	0	0	0	1	2	0	1	0.63	0	1	1	0	2	0	1	1	0.75	0	0	2	0	1	1	0	1	0.63
	C	1	1	2	1	0	0	0	1	0.75	1	0	1	1	0	1	1	1	0.75	2	0	0	0	1	1	1	1	0.75	0	1	0	1	0	0	2	1	0.63
									M	0.71								M	0.63								M	0.75								M	0.67
1.97 m/s	A	1	1	2	1	1	1	1	1	1.13	0	1	1	1	1	1	2	1	1.00	2	1	2	1	1	1	1	1	1.25	0	1	2	2	1	0	1	1	1.00
	B	1	1	1	1	2	1	1	1	1.13	1	1	1	1	2	1	1	1	1.13	1	2	1	1	1	1	1	2	1.25	1	1	0	1	1	1	1	1	0.88
	C	2	1	1	1	2	1	0	1	1.13	1	1	1	2	2	1	1	0	1.13	1	1	2	1	1	2	1	1	1.25	1	1	1	1	1	2	1	0	1.00
									M	1.13								M	1.08								M	1.25								M	0.96
2.53 m/s	A	2	1	2	1	1	2	3	1	1.63	1	1	2	2	2	1	2	2	1.63	1	2	2	2	3	1	1	2	1.75	1	2	1	2	1	2	2	1	1.50
	B	3	2	2	1	2	1	1	1	1.63	1	2	1	1	2	2	2	2	1.63	1	2	2	1	2	3	1	2	1.75	1	1	2	1	3	1	1	2	1.50
	C	2	1	1	1	2	2	3	1	1.63	2	2	1	1	1	3	1	1	1.50	2	1	2	1	2	2	1	2	1.63	1	1	1	2	1	2	2	1	1.38
									M	1.63								M	1.58								M	1.71								M	1.46
2.95 m/s	A	4	2	2	2	3	2	2	2	2.38	2	2	2	2	3	2	2	2	2.13	2	2	2	2	3	2	4	2	2.38	2	3	2	2	2	2	3	2	2.25
	B	2	2	3	2	2	3	2	2	2.25	3	2	2	2	2	3	2	2	2.25	4	2	2	2	2	3	3	2	2.50	3	3	2	2	2	2	2	3	2.38
	C	2	2	2	2	3	2	3	2	2.25	2	2	2	2	3	2	2	2	2.13	2	3	2	3	3	2	2	2	2.38	2	3	3	3	2	2	3	2	2.50
									M	2.29								M	2.17								M	2.42								M	2.38

	ACCESSORY BGB (E)					CRANIAL BGB (E)				
S	0.66	0.98	1.97	2.53	2.95	0.66	0.98	1.97	2.53	2.95
C1	0.38	0.63	1.13	1.63	2.38	0.25	0.50	1.00	1.63	2.13
C2	0.38	0.75	1.13	1.63	2.25	0.25	0.63	1.13	1.63	2.25
C3	0.50	0.75	1.13	1.63	2.25	0.25	0.75	1.13	1.50	2.13
M	0.42	0.71	1.13	1.63	2.29	0.25	0.63	1.08	1.58	2.17
SEM	0.04	0.04	0.00	0.00	0.04	0.00	0.07	0.04	0.04	0.04

	CAUDOMEDIAL BGB (E)					CAUDOLATERAL BGB (E)				
S	0.66	0.98	1.97	2.53	2.95	0.66	0.98	1.97	2.53	2.95
C1	0.38	0.75	1.25	1.75	2.38	0.38	0.75	1.00	1.50	2.25
C2	0.50	0.75	1.25	1.75	2.50	0.50	0.63	0.88	1.50	2.38
C3	0.63	0.75	1.25	1.63	2.38	0.38	0.63	1.00	1.38	2.50
M	0.50	0.75	1.25	1.71	2.42	0.42	0.67	0.96	1.46	2.38
SEM	0.07	0.00	0.00	0.04	0.04	0.04	0.04	0.04	0.04	0.07

Appendix VII: Number of epithelial-epithelial breaks in the exercised chicken

Speed	CHICK	ACCESSORY									CRANIAL									CAUDOMEDIAL									CAUDOLATERAL								
		I	II	III	IV	V	VI	VII	VIII	AVE	I	II	III	IV	V	VI	VII	VIII	AVE	I	II	III	IV	V	VI	VII	VIII	AVE	I	II	III	IV	V	VI	VII	VIII	AVE
0.66 m/s	A	2	1	0	1	1	0	1	0	0.75	0	1	0	2	1	1	0	0	0.63	1	1	0	0	2	1	1	0	0.75	1	0	1	0	2	0	1	0	0.63
	B	0	1	0	2	0	1	0	1	0.63	1	0	2	0	1	0	0	0	0.50	1	0	1	0	1	0	2	0	0.63	1	1	1	0	0	0	2	0	0.63
	C	1	0	2	0	1	1	0	1	0.75	0	1	0	1	2	0	0	1	0.63	0	1	1	1	0	0	1	2	0.75	0	0	2	0	1	1	0	1	0.63
										0.71									0.58									0.71									0.63
0.98 m/s	A	1	2	1	1	2	1	2	1	1.38	1	1	1	1	2	1	1	1	1.13	1	1	1	2	1	1	3	1	1.38	2	1	0	2	2	2	1	0	1.25
	B	1	1	3	1	1	1	2	1	1.38	3	0	1	2	1	1	2	0	1.25	1	1	2	1	1	2	1	1	1.25	0	1	0	2	2	1	3	1	1.25
	C	1	1	2	1	1	2	1	1	1.25	0	1	1	1	2	1	1	2	1.13	3	1	1	1	2	1	2	1	1.50	2	0	2	0	1	2	2	1	1.25
										1.33									1.17									1.38									1.25
1.97 m/s	A	2	1	2	2	1	1	3	2	1.75	1	2	1	2	2	1	3	2	1.75	1	2	3	2	2	1	3	1	1.88	1	2	1	3	2	2	2	1	1.75
	B	1	3	2	1	3	2	0	1	1.63	3	1	2	1	3	2	1	2	1.88	3	1	2	1	3	2	1	3	2.00	2	1	2	1	1	1	2	3	1.63
	C	3	1	3	1	2	1	2	1	1.75	1	2	2	3	2	1	2	1	1.75	1	2	1	3	2	2	2	2	1.88	1	2	1	3	1	2	2	1	1.63
										1.71									1.79									1.92									1.67
2.53 m/s	A	2	2	3	2	2	4	3	2	2.50	2	2	2	3	2	2	3	2	2.25	4	2	3	2	2	2	3	1	2.38	2	2	2	3	3	2	3	1	2.25
	B	3	3	2	4	3	2	1	3	2.63	2	3	2	2	3	2	3	3	2.50	3	1	2	2	3	2	4	3	2.50	1	3	2	2	3	2	2	3	2.25
	C	4	2	1	3	2	2	3	2	2.38	2	2	3	3	2	3	2	2	2.38	2	2	4	3	2	2	2	2	2.38	2	2	3	2	2	3	2	2	2.25
										2.50									2.38									2.42									2.25
2.95 m/s	A	3	3	3	2	3	4	3	3	3.00	4	2	3	2	3	2	2	4	2.75	2	4	3	3	3	2	3	4	3.00	2	4	2	3	3	4	3	2	2.88
	B	3	3	3	4	3	2	4	3	3.13	3	4	2	3	2	2	4	3	2.88	3	3	3	3	3	3	2	3	2.88	2	3	2	4	3	3	4	3	3.00
	C	4	2	3	3	3	3	3	3	3.00	2	3	4	3	2	3	2	3	2.75	3	3	3	2	3	4	3	2	2.88	4	2	4	3	2	3	3	2	2.88
										3.04									2.79									2.92									2.92

	ACCESSORY E-E (E)				
S	0.66	0.98	1.97	2.53	2.95
C1	0.75	1.38	1.75	2.50	3.00
C2	0.63	1.38	1.63	2.63	3.13
C3	0.75	1.25	1.75	2.38	3.00
M	0.71	1.33	1.71	2.50	3.04
SEM	0.04	0.04	0.04	0.07	0.04

	CRANIAL E-E (E)				
S	0.66	0.98	1.97	2.53	2.95
C1	0.63	1.13	1.75	2.25	2.75
C2	0.50	1.25	1.88	2.50	2.88
C3	0.63	1.13	1.75	2.38	2.75
M	0.58	1.17	1.79	2.38	2.79
SEM	0.04	0.04	0.04	0.07	0.04

	CAUDOMEDIAL E-E (E)				
S	0.66	0.98	1.97	2.53	2.95
C1	0.75	1.38	1.88	2.38	3.00
C2	0.63	1.25	2.00	2.50	2.88
C3	0.75	1.50	1.88	2.38	2.88
M	0.71	1.38	1.92	2.42	2.92
SEM	0.04	0.07	0.04	0.04	0.04

	CAUDOLATERAL E-E (E)				
S	0.66	0.98	1.97	2.53	2.95
C1	0.63	1.25	1.75	2.25	2.88
C2	0.63	1.25	1.63	2.25	3.00
C3	0.63	1.25	1.63	2.25	2.88
M	0.63	1.25	1.67	2.25	2.92
SEM	0.00	0.00	0.04	0.00	0.04

Appendix VIII: Number of blood-gas barrier breaks in the perfused chicken

Press.	CHICK	ACCESSORY									CRANIAL								
		I	II	III	IV	V	VI	VII	VIII	AVE	I	II	III	IV	V	VI	VII	VIII	AVE
1.42 KPa	A	0	1	0	1	1	0	1	1	0.63	0	1	0	0	1	1	0	0	0.38
	B	0	1	0	2	2	0	0	1	0.75	1	0	0	0	1	0	0	0	0.25
	C	1	0	2	0	0	1	1	0	0.63	0	0	1	0	2	0	1	0	0.50
									M	0.67								M	0.38
1.91 KPa	A	0	1	2	1	2	1	1	1	1.13	0	0	1	2	1	1	1	1	0.88
	B	1	2	1	1	2	1	0	1	1.13	1	0	1	0	1	2	2	1	1.00
	C	1	1	2	1	1	0	1	1	1.00	1	0	1	1	0	1	1	1	0.75
									M	1.08								M	0.88
2.4 KPa	A	1	1	2	2	2	1	1	1	1.38	1	0	1	1	1	2	2	2	1.25
	B	1	2	3	1	2	1	2	1	1.63	1	1	0	2	1	2	1	1	1.13
	C	2	1	2	1	2	2	1	1	1.50	1	1	2	1	2	1	1	2	1.38
									M	1.50								M	1.25
2.89 KPa	A	2	3	2	2	2	2	3	2	2.25	1	1	2	2	1	2	2	3	1.75
	B	3	3	2	3	2	1	2	1	2.13	2	3	2	1	2	2	1	1	1.75
	C	2	1	2	2	2	2	3	3	2.13	2	2	1	2	1	2	3	1	1.75
									M	2.17								M	1.75
3.38 KPa	A	4	2	4	2	3	2	3	2	2.75	2	3	3	2	3	2	3	2	2.50
	B	2	4	3	2	4	3	4	2	3.00	3	2	2	2	2	3	4	2	2.50
	C	3	2	2	3	3	2	3	4	2.75	2	3	2	2	3	2	3	2	2.38

Press.	CHICK	CAUDOMEDIAL									CAUDOLATERAL								
		I	II	III	IV	V	VI	VII	VIII	AVE	I	II	III	IV	V	VI	VII	VIII	AVE
1.42 KPa	A	0	1	0	0	2	2	1	0	0.75	0	0	1	0	2	0	0	0	0.38
	B	1	0	1	0	1	2	2	0	0.88	0	1	1	0	0	0	2	0	0.50
	C	0	1	1	1	0	0	0	2	0.63	0	0	2	0	0	0	0	1	0.38
									M	0.75								M	0.42
1.91 KPa	A	0	1	0	2	1	2	1	2	1.13	0	0	1	0	1	2	1	2	0.88
	B	0	1	1	1	2	2	2	1	1.25	0	1	0	2	1	1	1	1	0.88
	C	2	1	2	0	1	2	1	1	1.25	0	2	0	1	1	2	1	1	1.00
									M	1.21								M	0.92
2.4 KPa	A	1	2	1	1	2	2	2	2	1.63	0	1	2	1	2	1	2	1	1.25
	B	1	2	1	1	3	2	1	2	1.63	1	1	2	1	1	2	1	1	1.25
	C	1	1	2	2	1	2	1	2	1.50	1	1	1	1	2	1	2	1	1.25
									M	1.58								M	1.25
2.89 KPa	A	2	2	2	3	2	2	2	2	2.00	1	2	1	2	2	3	2	3	2.00
	B	3	2	2	2	2	3	1	1	2.13	3	2	2	1	2	3	2	2	2.13
	C	2	1	2	3	3	2	2	2	2.13	2	1	3	2	2	2	1	2	1.88
									M	2.08								M	1.92
3.38 KPa	A	4	2	3	3	3	2	3	3	2.88	2	3	2	2	2	2	3	3	2.38
	B	3	3	2	2	2	2	2	4	2.88	3	3	2	2	2	2	2	4	2.50
	C	2	2	3	3	2	2	2	3	2.88	2	2	3	2	2	2	3	3	2.38

	ACCESSORY BGB (P)					CRANIAL BGB (P)				
P	1.42	1.91	2.40	2.89	3.38	1.42	1.91	2.40	2.89	3.38
C1	0.63	1.13	1.38	2.25	2.75	0.38	0.88	1.25	1.75	2.50
C2	0.75	1.13	1.63	2.13	3.00	0.25	1.00	1.13	1.75	2.50
C3	0.63	1.00	1.50	2.13	2.75	0.50	0.75	1.38	1.75	2.38
M	0.67	1.08	1.50	2.17	2.83	0.38	0.88	1.25	1.75	2.46
SEM	0.04	0.04	0.07	0.04	0.08	0.07	0.07	0.07	0.00	0.04

	CAUDOMEDIAL BGB (P)					CAUDOLATERAL BGB (P)				
P	1.42	1.91	2.40	2.89	3.38	1.42	1.91	2.40	2.89	3.38
C1	0.75	1.13	1.63	2.00	2.88	0.38	0.88	1.25	2.00	2.38
C2	0.88	1.25	1.63	2.13	2.88	0.50	0.88	1.25	1.88	2.50
C3	0.63	1.25	1.50	2.13	2.88	0.38	1.00	1.25	1.88	2.38
M	0.75	1.21	1.58	2.08	2.88	0.42	0.92	1.25	1.92	2.42
SEM	0.07	0.04	0.04	0.04	0.00	0.04	0.04	0.00	0.04	0.04

Appendix IX: Number of epithelial-epithelial breaks in the perfused chicken

		ACCESSORY									CRANIAL									CAUDOMEDIAL									CAUDOLATERAL								
Press.	CHICK	I	II	III	IV	V	VI	VII	VIII	AVE	I	II	III	IV	V	VI	VII	VIII	AVE	I	II	III	IV	V	VI	VII	VIII	AVE	I	II	III	IV	V	VI	VII	VIII	AVE
1.42 kPa	A	2	1	0	1	1	1	2	1	1.13	0	1	1	1	1	1	2	0	0.88	1	1	0	0	2	1	1	0	0.75	1	0	2	0	2	0	1	0	0.75
	B	1	1	1	2	1	1	1	1	1.13	1	0	2	1	1	1	2	0	1.00	1	0	1	0	1	2	2	0	0.88	1	2	1	0	0	0	2	0	0.75
	C	2	0	1	1	1	1	1	1	1.00	0	1	2	1	2	0	0	1	0.88	0	1	1	1	0	0	1	2	0.75	0	0	2	0	1	2	0	1	0.75
										1.08									0.92									0.79									0.75
1.91 kPa	A	2	2	2	1	2	1	2	2	1.75	1	1	2	1	2	1	2	1	1.38	1	1	1	2	1	2	3	1	1.50	2	2	0	2	2	2	1	1	1.50
	B	1	1	3	1	2	1	2	1	1.50	3	0	1	2	1	1	2	0	1.25	1	1	2	2	3	2	1	1	1.63	1	1	0	2	2	1	3	1	1.38
	C	2	1	2	2	1	2	2	2	1.75	0	1	1	2	2	1	1	2	1.25	3	1	1	1	2	1	2	1	1.50	2	0	2	2	1	1	2	1	1.38
										1.67									1.29									1.54									1.42
2.4 kPa	A	2	3	2	2	3	3	3	2	2.50	1	3	2	2	3	2	3	1	2.13	3	2	3	2	2	3	3	2	2.50	3	2	2	2	2	2	2	3	2.25
	B	2	3	2	2	3	2	3	2	2.38	3	1	2	2	2	2	2	2	2.00	2	3	3	3	3	2	3	3	2.75	2	2	2	3	2	2	2	2	2.13
	C	3	2	3	2	3	2	2	3	2.50	1	2	3	2	2	3	2	3	2.25	3	2	2	3	3	2	3	3	2.63	2	2	2	2	3	2	2	2	2.13
										2.46									2.13									2.63									2.17
2.89 kPa	A	2	3	5	3	3	4	3	4	3.38	4	2	2	2	2	3	3	4	2.75	4	4	3	2	4	3	5	4	3.63	2	4	2	2	3	3	3	4	2.88
	B	3	3	4	4	2	4	4	3	3.38	2	2	3	4	4	2	3	3	2.88	3	4	2	4	3	5	4	3	3.50	3	3	2	4	3	4	2	3	3.00
	C	4	3	3	5	4	3	3	2	3.38	3	2	4	2	2	3	3	3	2.75	4	4	4	3	3	4	3	3	3.50	2	4	3	2	3	4	2	2	2.75
										3.38									2.79									3.54									2.88
3.38 kPa	A	5	4	4	4	3	4	5	4	4.13	4	2	3	3	3	5	4	3	3.38	5	4	3	5	4	4	5	4	4.25	2	4	3	3	5	4	3	3	3.38
	B	3	4	5	4	3	5	4	4	4.00	3	5	2	4	4	3	4	3	3.50	4	5	4	4	5	4	4	5	4.38	2	3	4	4	3	4	4	3	3.38
	C	4	5	4	4	4	4	4	4	4.13	3	3	4	3	4	4	5	2	3.50	4	5	4	4	4	4	5	4	4.25	4	4	5	3	2	3	3	3	3.38
										4.08									3.46									4.29									3.38

	ACCESSORY E-E (P)				
P	1.42	1.91	2.40	2.89	3.38
C1	1.13	1.75	2.50	3.38	4.13
C2	1.13	1.50	2.38	3.38	4.00
C3	1.00	1.75	2.50	3.38	4.13
M	1.08	1.67	2.46	3.38	4.08
SEM	0.04	0.08	0.04	0.00	0.04

	CRANIAL E-E (P)				
P	1.42	1.91	2.40	2.89	3.38
C1	0.88	1.38	2.13	2.75	3.38
C2	1.00	1.25	2.00	2.88	3.50
C3	0.88	1.25	2.25	2.75	3.50
M	0.92	1.29	2.13	2.79	3.46
SEM	0.04	0.04	0.07	0.04	0.04

	CAUDOMEDIAL E-E (P)				
P	1.42	1.91	2.40	2.89	3.38
C1	0.75	1.50	2.50	3.63	4.25
C2	0.88	1.63	2.75	3.50	4.38
C3	0.75	1.50	2.63	3.50	4.25
M	0.79	1.54	2.63	3.54	4.29
SEM	0.04	0.04	0.07	0.04	0.04

	CAUDOLATERAL E-E (P)				
P	1.42	1.91	2.40	2.89	3.38
C1	0.75	1.50	2.25	2.88	3.38
C2	0.75	1.38	2.13	3.00	3.38
C3	0.75	1.38	2.13	2.75	3.38
M	0.75	1.42	2.17	2.88	3.38
SEM	0.00	0.04	0.04	0.07	0.00

Appendix X: Average number of blood-gas barrier- and epithelial-epithelial breaks in the perfused and exercised chicken

Exercise E-E

S(m/s)	n	ACC	CNN	CDM	CDL	AVE	SEM
0	3	0.38	0.29	0.29	0.25	0.30	0.03
0.66	3	0.71	0.58	0.71	0.63	0.66	0.03
0.98	3	1.33	1.17	1.38	1.25	1.28	0.05
1.97	3	1.71	1.79	1.92	1.67	1.77	0.06
2.53	3	2.5	2.38	2.42	2.25	2.39	0.05
2.95	3	3.04	2.79	2.92	2.92	2.92	0.05

Perfusion E-E

P(kPa)	n	ACC	CNN	CDM	CDL	AVE	SEM
0	3	0.38	0.29	0.29	0.25	0.30	0.03
1.42	3	1.08	0.92	0.79	0.75	0.89	0.07
1.91	3	1.67	1.29	1.54	1.42	1.48	0.08
2.4	3	2.46	2.13	2.63	2.17	2.35	0.12
2.89	3	3.38	2.79	3.54	2.88	3.15	0.18
3.38	3	4.08	3.46	4.29	3.38	3.80	0.23

Exercise BGB

S(m/s)	n	ACC	CNN	CDM	CDL	AVE	SEM
0	3	0.04	0	0.08	0.04	0.04	0.02
0.66	3	0.42	0.25	0.5	0.42	0.40	0.05
0.98	3	0.71	0.63	0.75	0.67	0.69	0.03
1.97	3	1.13	1.08	1.25	0.96	1.11	0.06
2.53	3	1.63	1.58	1.71	1.46	1.60	0.05
2.95	3	2.29	2.17	2.42	2.38	2.32	0.06

Perfusion BGB

P(kPa)	n	ACC	CNN	CDM	CDL	AVE	SEM
0	3	0.04	0	0.08	0.04	0.04	0.02
1.42	3	0.67	0.38	0.75	0.42	0.56	0.09
1.91	3	1.08	0.88	1.21	0.92	1.02	0.08
2.4	3	1.5	1.25	1.58	1.25	1.40	0.09
2.89	3	2.17	1.75	2.08	1.92	1.98	0.09
3.38	3	2.83	2.46	2.88	2.42	2.65	0.12

Percentage difference between E-E & BGB breaks (exercise)

S(m/s)	ACC	CNN	CDM	CDL
0	89.47	100.00	72.41	84.00
0.66	40.85	56.90	29.58	33.33
0.98	46.62	46.15	45.65	46.40
1.97	33.92	39.66	34.90	42.51
2.53	34.80	33.61	29.34	35.11
2.95	24.67	22.22	17.12	18.49

Percentage difference between E-E & BGB breaks (perfusion)

P(kPa)	ACC	CNN	CDM	CDL
0	89.47	100.00	72.41	84.00
1.42	37.96	58.70	5.06	44.00
1.91	35.33	31.78	21.43	35.21
2.4	39.02	41.31	39.92	42.40
2.89	35.80	37.28	41.24	33.33
3.38	30.64	28.90	32.87	28.40